JPRS-CST-86-040

29 SEPTEMBER 1986

China Report

SCIENCE AND TECHNOLOGY

FBIS FOREIGN BROADCAST INFORMATION SERVICE

NOTE

JPRS publications contain information primarily from foreign newspapers, periodicals and books, but also from news agency transmissions and broadcasts. Materials from foreign-language sources are translated; those from English-language sources are transcribed or reprinted, with the original phrasing and other characteristics retained.

Headlines, editorial reports, and material enclosed in brackets [] are supplied by JPRS. Processing indicators such as [Text] or [Excerpt] in the first line of each item, or following the last line of a brief, indicate how the original information was processed. Where no processing indicator is given, the information was summarized or extracted.

Unfamiliar names rendered phonetically or transliterated are enclosed in parentheses. Words or names preceded by a question mark and enclosed in parentheses were not clear in the original but have been supplied as appropriate in context. Other unattributed parenthetical notes within the body of an item originate with the source. Times within items are as given by source.

The contents of this publication in no way represent the policies, views or attitudes of the U.S. Government.

PROCUREMENT OF PUBLICATIONS

JPRS publications may be ordered from the National Technical Information Service, Springfield, Virginia 22161. In ordering, it is recommended that the JPRS number, title, date and author, if applicable, of publication be cited.

Current JPRS publications are announced in Government Reports Announcements issued semi-monthly by the National Technical Information Service, and are listed in the Monthly Catalog of U.S. Government Publications issued by the Superintendent of Documents, U.S. Government Printing Office, Washington, D.C. 20402.

Correspondence pertaining to matters other than procurement may be addressed to Joint Publications Research Service, 1000 North Glebe Road, Arlington, Virginia 22201.

JPRS-CST-86-040

29 SEPTEMBER 1986

CHINA REPORT

SCIENCE AND TECHNOLOGY

CONTENTS

PEOPLE'S REPUBLIC OF CHINA

APPLIED SCIENCES

Performance of Hybrid Tea CO_2 Laser Studied
(Xu Hualuo, et al.; GUANGXUE XUEBAO, No 6, Jun 86) 1

ABSTRACTS

APPLIED MATHEMATICS

YINGYONG SHUXUE HE LIXUE /APPLIED MATHEMATICS AND MECHANICS/, No 1, Jan 86 8

YINGYONG SHUXUE HE LIXUE /APPLIED MATHEMATICS AND MECHANICS/, No 2, Feb 86 11

YINGYONG SHUXUE HE LIXUE /APPLIED MATHEMATICS AND MECHANICS/, No 3, Mar 86 15

ASTRONOMY

TIANWEN XUEBAO /ACTA ASTRONOMICA SINICA/, No 2, Jun 86 20

ELECTRONICS

DIANZI KEXUE XUEKAN /JOURNAL OF ELECTRONICS/, No 5, Sep 86 25

ENGINEERING

NANJING GONGXUEYUAN XUEBAO /JOURNAL OF NANJING INSTITUTE OF TECHNOLOGY/, No 3, Jul 86 31

MICROBIOLOGY

WEISHENGWU XUEBAO /ACTA MICROBIOLOGICA SINICA7, No 2, Jun 86 35

NEUROLOGY

ZHONGHUA SHENJING-JINGSHENKE ZAZHI /CHINESE JOURNAL OF NEUROLOGY AND PSYCHIATRY7, No 3, 23 Jun 86 45

ONCOLOGY

ZHONGHUA ZHONGLIU ZAZHI /CHINESE JOURNAL OF ONCOLOGY7, No 4, 23 Jul 86 48

OPTICS

GUANGXUE XUEBAO /ACTA OPTICA SINICA7, No 7, Jul 86 50

PETROCHEMICALS

SHIYOU HUAGONG /PETROCHEMICAL TECHNOLOGY7, No 1, Jan 86 53

/9986

APPLIED SCIENCES

PERFORMANCE OF HYBRID TEA CO_2 LASER STUDIED

Shanghai GUANGXUE XUEBAO [ACTA OPTICA SINICA] in Chinese Vol 6 No 6, Jun 86 pp 501-505

[Article by Xu Hualuo [1776 5478 2867], Yi Jingrong [0122 2529 2837], and Cai Yingshi [5591 5391 2514] of the Shanghai Institute of Optics and Fine Mechanics, Chinese Academy of Sciences]

[Text] Abstract: The operating characteristics of a hybrid TEA CO_2 laser are analyzed based on a numerical model. We have found the possibility of single longitudinal mode oscillation in a low-pressure CW CO_2 tube operating below the lasing threshold. The results have been borne out by experiments.

I. Introduction

A number of techniques have been developed to operate a TEA CO_2 laser in the single longitudinal mode.[1] Examples are: 1) Adding a F-P etalon in the cavity, 2) adding a gas absorption cell in the cavity, 3) using an injection locking device, and 4) hybrid gain medium consisting of a high pressure region and low pressure region. The distinct advantages of the hybrid devices are that they are easy to tune and that their single longitudinal mode operation is stable. They can therefore be combined with an external electro-optic trigger to form a pulsed CO_2 laser generator.

Theoretical studies of the operating characteristics of a hybrid CO_2 laser have been reported.[2-3] Following the ideas advanced in Reference 3, we have introduced the role of a CW CO_2 tube and, starting from a numerical model, studied the operating characteristics of a hybrid TEA CO_2 laser under various conditions. Good agreements have been obtained between computed results and experimental test results.

The CW CO_2 tube serves two purposes: gain and intensity. When the small signal gain of the CW CO_2 tube is smaller than the threshold gain, the tube only provides amplification. When the small gain is greater than the threshold, the tube provides both gain and intensity.

II. Numerical Model

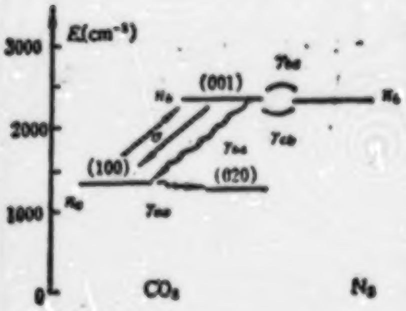

Figure 1. Energy-Level Diagram of CO_2 Transitions

Based on the four-level model of Gilbert shown in Figure 1, the multi-longitudinal mode rate equations of a CO_2 laser are:

$$\frac{dn_a}{dt}=(n_b-n_a)c\sum_{\nu}\sigma(\nu)q(\nu)+\gamma_{ba}n_b-\gamma_{a0}n_a-W_a, \tag{1}$$

$$\frac{dn_b}{dt}=-(n_b-n_a)c\sum_{\nu}\sigma(\nu)q(\nu)-\gamma_{ba}n_b+\gamma_{cb}n_c-\gamma_{bc}n_b+W_b, \tag{2}$$

$$\frac{dn_c}{dt}=-\gamma_{cb}n_c+\gamma_{bc}n_b+W_c, \tag{3}$$

$$\frac{dq(\nu)}{dt}=(n_b-n_a)\frac{l}{L}\,c\sigma(\nu)q(\nu)-\frac{q(\nu)}{t_c}+W_s(\nu)$$
$$+q(\nu)k(\nu)\exp\left[-\int Idt/E_s\right], \tag{4}$$

where n_a, n_b, and n_c are respectively the particle densities of the lower energy level of the CO_2 laser, the upper energy level of the CO_2 laser and the first excited vibrational state of the nitrogen molecule, $q(\nu)$ is the photon density of the longitudinal mode at frequency ν, l is the length of the activated medium, L is the cavity length,^{5} γ is the collision transition probability, $W_s(\nu)$ is the photon density radiated to each longitudinal mode in unit time via spontaneous emission, t_c is the photon lifetime, defined by:

$$t_c=\frac{2L}{c\ln(1/RT)}, \tag{5}$$

in which c is the speed of light, R is the reflectivity of the output mirror, and T is the transmissivity of the cavity. W_a, W_b, and W_c in (1), (2), and (3) are respectively the pumping rate for energy levels a, b, and c.

$$W_a=W_b=0.4W_c=W_0t\exp(-t/t_p), \tag{6}$$

Here t_p is the width of the pumping pulse, W_0 is determined by the small signal gain of the TEA device. $\sigma(\nu)$ in (1)-(3) is the stimulated radiation cross-section of the high pressure amplification tube and its relationship to frequency is given by

$$\sigma(\nu)=\sigma_0\frac{(\Delta\nu/2)^2}{(\nu-\nu_0)^2+(\Delta\nu/2)^2}, \qquad (7)$$

where $\Delta\nu$ is the full width at half maximum of the gain curve.

Since the factor $k(\nu)\exp\left[-\int I\,dt/E_s\right]$ in the last term on the right-hand side of (4) is of importance, we shall describe its origin in detail. Similar to the TEA portion, the particle density variation of the upper and lower energy levels of the CW CO_2 tube may be described by:

$$\frac{dn'_a}{dt}=(n'_b-n'_a)c\sum_{\nu}\sigma'(\nu)q(\nu)+\gamma'_{ba}n'_b-\gamma'_{a0}n'_a+W'_a, \qquad (1')$$

$$\frac{dn'_b}{dt}=-(n'_b-n'_a)c\sum_{\nu}\sigma'(\nu)q(\nu)-\gamma'_{ba}n'_b+\gamma'_{ab}n'_a+\nu'_{b0}n'_b+W'_b, \qquad (2')$$

Primed quantities in (1') and (2') represent quantities of the CW CO_2 laser tube, carrying similar definitions as their counterparts in (1) and (2). In fact, the operating process of the entire TEA CO_2 laser is the back-and-forth propagation process of the pulse generated in the TEA portion in the low pressure tube. The typical width of an output pulse from the TEA CO_2 laser is about 100 ns, far less than that of various relaxation process in the CW CO_2 gain medium. Also, in the 100 ns interval, the excitation of the particle number may be ignored. Furthermore, since the gain linewidth of the CW CO_2 medium is very narrow (about 75 MHz), usually only one longitudinal mode falls within the linewidth. Hence, (1') and (2') may be simplified to:

$$\frac{dn'_a}{dt}=(n'_b-n'_a)c\sigma'q, \qquad (8)$$

$$\frac{dn'_b}{dt}=-(n'_b-n'_a)c\sigma'q, \qquad (9)$$

From (8) and (9), we have

$$\frac{d\delta}{dt}=-2\delta c\sigma'q, \qquad (10)$$

$$\delta\equiv n'_b-n'_a,$$

Integrating (10) and making use of the relationships $I=ch\nu q$ and $=h\nu/2\sigma'$, we have

$$\delta=\delta_0\exp\left[-\int_{-\infty}^{t}I\,dt/E_s\right], \qquad (11)$$

where E_s is the saturation energy. From (11), we obtain the gain of the continuous tube:

$$k'=\sigma(\nu)\delta=\sigma'(\nu)\delta_0\exp\left[-\int_{-\infty}^{t}I\,dt/E_s\right]=k(\nu)\exp\left[-\int_{-\infty}^{t}I\,dt/E_s\right], \qquad (12)$$

where $k(\nu)$ is the small gain of the CW CO_2 tube. The frequency dependence of $k(\nu)$ is given by

$$k(\nu)=k_0\frac{(\Delta\nu_{CW}/2)^2}{(\nu-\nu_0)^2+(\Delta\nu_{CW}/2)^2}, \qquad (13)$$

where k_0 is the small signal gain of the central longitudinal mode, and $\Delta\nu_{CW}$ is the full width at half maximum of the gain curve of the continuous tube. When k_0 is greater than the threshold gain, k_0 itself becomes the threshold gain because a continuous tube in the steady state can only operate at the threshold. The initial condition of $q(\nu)$ is determined by the light intensity already existing in the cavity. It should be mentioned that the actual gain curve of the continuous tube should have a Voight lineshape but the error in using (13) as a substitute is very small. To explain the operation of the continuous tube, the author of Reference 2 added an extra constant excitation term on the right-hand sides of (1), (2), and (3). This approach is less than satisfactory for the following two reasons: 1) In an actual hybrid device the continuous tube is already in a stable state when the TEA part is discharge excited. The treatment of Reference 2 amounts to a simultaneous excitation of the TEA and the continuous tube, thus degrading the gain of the continuous tube, 2) this treatment ignores the saturation effect of the continuous tube. In our model the above two difficulties do not arise.

III. Results

Using the following parameters, calculations are performed on a Burroughs computer using the Runge-Kutta method:

l	L	V_m	R	T
0.5 m	2.23 m	70 cm^3	0.36	0.85

V_m

$P^{(cw)}_{CO_2}$	$P^{(cw)}_{N_2}$	$P^{(cw)}_{He}$	$\Delta\nu_{CW}$	E_s
2τ	1τ	8τ	74 MHz	1.61 mJ/cm^3

P_{CO_2}	P_{N_2}	P_{He}	$\Delta\nu$	σ_0
120τ	60τ	480τ	3.8 GHz	5.8×10^{-20} cm^2

γ_{ba}	γ_{a0}	γ_{bc}	γ_{c0}	W_0
0.0868 µs^{-1}	2.1 µs^{-1}	1.145 µs^{-1}	24.4 µs^{-1}	5.7×10^{18} cm^{-3}µs^{-1}

Our calculation takes into account the effects of TEA population inversion of 50 longitudinal modes and the contribution due to the saturation of the continuous tube. We also assume that the center frequencies of the high pressure gain curve and the low pressure gain curve coincide.

The results in Figures 2 and 3 are obtained under the condition that the deviation frequency Δf is equal to zero for the longitudinal mode frequency ν_c and the center frequency ν_0 of the gain curve. Curves (a), (b), and (c) in Figure 2 correspond respectively to the computed pulse waveform when the continuous tube is not operating, operating below the threshold, and operating above the threshold. These results are in good agreement with those in Reference 6. The experimental results of Reference 2 are also plotted here. The discrepancies in the pulse width are due to different cavity lifetime. In our calculation the output mirror reflectivity is 36 percent, whereas in the experiments of Reference 2, the reflectivity is 65 percent. Differences in the tail of the pulse are caused by different gas composition. In their experiment they used a high nitrogen content and hence had a greater intensity in the tail portion. Figure 2 shows that, under the three operating conditions of the continuous tube, the relative positions of the computer waveform agree fairly well with the relative positions of the experimental waveform. As we pointed out earlier, the theoretical treatment in Reference 2 assumed a simultaneous excitation of TEA and the continuous tube. As a result, the gain of the continuous tube was degraded and there was a considerable difference between the relative positions of the computer waveform and those of the experimental waveform.

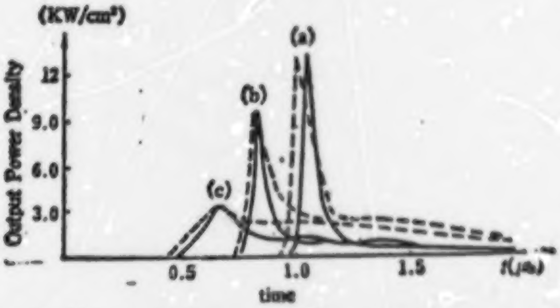

Figure 2. Calculated Output Pulse Shapes (The Broken Curves Represent Experimental Results of Reference [2])

(a) Low-pressure section not operating; (b) Low-pressure section operating below threshold; (c) Low-pressure section operating above threshold

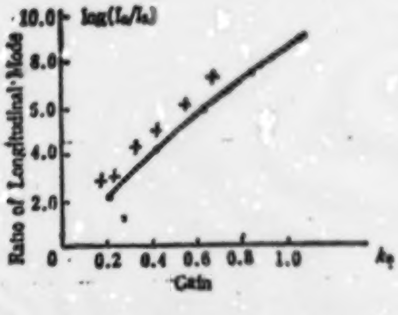

Figure 3. Dependence of the Ratio of I_c to I_s on the Gain of a Low-Pressure Section

I_c--density of center longitudinal mode; I_s--sum of the densities of other longitudinal modes k_0 represents threshold gain, crosses represent experimental results of Reference [7]

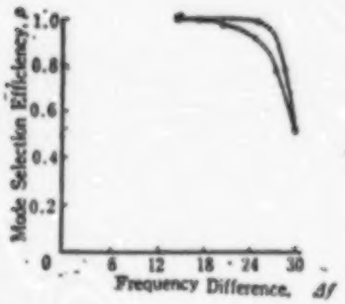

Figure 4. Relationship Between Mode Selection Efficiency and Frequency Difference, f is the Frequency Difference Between the Center of Gain Profile and the Closest Longitudinal Mode of the Resonator

Figure 3 shows the effect of the low pressure gain on the ratio of the central longitudinal mode intensity to the intensity of all the other longitudinal modes combined $(I_0/\sum I_i,\ i\neq 0)$. The results in Figure 3 are basically in agreement with the experimental results in Reference 7 (also plotted here). In our calculation the pressure in the continuous tube is 11 Torr, whereas in Reference 7 it is 2 Torr. That is, our $\Delta\nu_{cw}$ is greater than that in Reference 7. Considering this difference, the agreement between theory and experiment is quite good.

Figure 4 shows the relationship between the mode selection efficiency and Δf. The mode selection efficiency ρ is defined as

$$\rho = \frac{I_0}{I_0 + \sum_{i\neq 0} I_i}, \tag{14}$$

where I_o is the longitudinal mode intensity at frequency ν_c and Δf is the difference between ν_c and the center frequency of the gain curve. The calculated results show that the hybrid TEA CO_2 laser still operated in a single longitudinal mode even when the gain of the low pressure continuous tube is only 80 percent of the threshold gain and Δf is as high as 24 MHz. For a low pressure tube gain of 40 percent the threshold gain and a Δf of 18 MHz, the device operates in a single longitudinal mode. In the calculation the cavity length is 2.23 m and the corresponding longitudinal mode interval is 67.3 MHz. For a hybrid TEA CO_2 laser without a stable cavity length, we define a probability for a single longitudinal mode operation:

$$\rho = 2\ \frac{\text{Maximum} \quad \text{f for single longitudinal mode operation}}{\text{Longitudinal mode interval of cavity}}$$

Then, for the above two cases the probabilities are respectively 71 percent and 54 percent.

REFERENCES

1. S. L. Chin, "Opt & Laser Technol.," 1980, 12, No 2 (Apr), p 85.

2. A. Gondhalekar, "IEEE JQE," 1975, QE-11, No 3 (Mar), p 103.

3. V. V. Likhanskii, "Sov. JQE," 1978, 8, No 4 (Apr), p 512.

4. J. Gilbert, "Can. J. Phys.," 1972, 50, No 20 (Oct), p 2523.

5. P. H. Flamant, "IEEE JQE," 1983, QE-19, No 5 (May), p 821.

6. Cai Yingshi, et al., GUANGXUE XUEBAO [ACTA OPTICA SINICA], Vol 4, No 2, Feb 84, p 168.

7. N. R. Heckenberg, "Opt. Commun.," 1976, 16, No 1 (Jan), p 54.

8. J. L. Lachamber, "IEEE JQE," 1976, QE-12, No 12 (Dec), p 756.

9. E. R. Pike, "High-Power Gas Laser," (The Institute of Physics Bristol and London, 1975).

9698/9599
CSO: 4008/86

Applied Mathematics

ON A CLASS OF METHOD FOR SOLVING PROBLEMS WITH RANDOM BOUNDARY NOTCHES AND/OR CRACKS-(IV) COMPUTATIONS FOR DEEP BOUNDARY NOTCHES AND/OR CRACKS

Chongqing YINGYONG SHUXUE HE LIXUE [APPLIED MATHEMATICS AND MECHANICS] in Chinese Vol 7 No 1, Jan 86 pp 7-16

[English abstract of article by Ou Yangchang [2962 7122 7598], and Zhu Han [2612 3211] of Department of Applied Mechanics, Fudan University, Shanghai]

[Text] This paper continues the discussions to a class method for solving problems with random boundary notches and/or cracks in references by C. Ouyang in [1] (see also [2] and [3]). Using the basic method given in this reference as well as some further developments, we develop here a new effective computational method for solving random deep boundary notches and/or cracks. The actual numerical computations given in this paper show that the present method is quite workable and the results obtained have enlarged the contents of "Handbook of Stress Intensity Factors" given by G. C. Sih. (Paper received 26 Sep 84.)

REFERENCES

[1] 欧阳鬯. 应用数学和力学. 1, 2(1980), 156
[2] 欧阳鬯、朱涵, 应用数学和力学, 5, 2. (1984), 153
[3] 欧阳鬯、朱涵, 应用数学和力学, 6, 8(1985), 671—680.
[4] 斯米尔诺夫, <高等数学教程>. Vol. 3, №2.

THE COMPUTATION OF NONLINEAR INSTABILITY FOR MULTILAYER COMPOSITE CYLINDRICAL SHELLS

Chongqing YINGYONG SHUXUE HE LIXUE [APPLIED MATHEMATICS AND MECHANICS] in Chinese Vol 7 No 1, Jan 86 pp 17-23

[English abstract of article by Zhou Chengti [0719 2110 0232] of Dalian University, Dalian, and Zhou Jianping [0719 1696 1627] of Chansha Institute of Technology, Changsha]

[Text] In this paper, energy method and finite difference method are used to compute the instability behavior of multilayered fiber reinforced composite cylindrical shells under axial compression, hydrostatic pressure and torsion. The influences of initial imperfections, geometrical nonlinearities of shells and physical nonlinearities of the materials to the buckling and postbuckling behavior of the shells are considered. The effect of transverse shear is also discussed. The computational results of this paper are well agreed with the experimental data. (Paper received 11 Sep 84.)

REFERENCES

[1] 周承倜，《复合材料弹性力学》，应用数学和力学丛书，(1983).
[2] 周承倜，《薄壳弹塑性稳定性理论》，国防工业出版社，(1979).
[3] 周承倜，《弹性稳定性理论》，应用数学和力学丛书，四川人民出版社，(1981).
[4] Khot, N. S. and V. B., Venkaya, Effect of fiber orientation on initial postbuckling behavior and imperfection sensitivity of composite cylindrical shells, *AFFDL-TR*-70-125, (1970).
[5] Khot, N. S., Buckling and postbuckling behavior of composite cylindrical shells under axial pressure, *AIAA Journal*, 8, 2 (1970) 229—235.
[6] Khot, N. S., Postbuckling behavior of geometrical imperfection of composite cylindrical shells under axial compression, *AIAA Journal*, 8, 3 (1970), 579—581.
[7] Tennyson, R. C., Buckling of laminated composite cylinders: a review, *Composites*, (1975).
[8] Hahn, H. T., Nonlinear behavior of liminated composites, *Journal of Composite Materials*, (1973), 257—271.
[9] Jones, R. M., *Mechanics of Composite Materials*, Mc Graw-Hill Book Co. (1975).
[10] 周承倜，有初始缺陷的加肋薄壳的塑性稳定性理论，力学学报，特刊，(1981) 162—172.
[11] 周承倜、周建平，复合材料圆柱壳的非线性稳定性分析，大连大学，计算机科学和力学研究室，科研资料，编号：84-001，全国复合材料力学学术会议宣读论文，上海，(1984).
[12] Hahn, H. T. and S. Tsai, Nonlinear elastic behavior of unidirectional composites laminates, *Journal of Composite Materials*, (1973) 102—118.
[13] 周承倜、周建平，横向剪切对于复合材料迭层圆柱壳的非线性稳定性的影响，大连大学，计算机科学和力学研究室，科研资料，编号：84-003，(1984).

AN ESTIMATION METHOD OF BEARING STRENGTH OF BOLTED JOINTS IN FIBRE REINFORCED COMPOSITE

Chongqing YINGYONG SHUXUE HE LIXUE [APPLIED MATHEMATICS AND MECHANICS] in Chinese Vol 7 No 1, Jan 86 pp 95-101

[English abstract of article by Yang Jin [5017 1180] of Department of Aircraft Engineering Northwestern Polytechnical University, Xi'an]

[Text] Some researchers have estimated the strength of bolted joints in fibre reinforced composite, using simple and efficient engineering procedures. However, for these procedures the effect of clamping due to the strength of bolted joints is not considered. In this paper, a method is presented for predicating critical bearing strength of single-hole bolted joints in composite on the basis of observing and analysing the results of experiments. The clamping effect of bolts is considered. The calculated results correspond to the test data on Glaphic/Epoxy laminates. (Paper received 3 May 83.)

REFERENCES

[1] 羊羚，复合材料螺栓连接设计，西工大科研资料 SHJ 8050期，(1980)。

[2] Waszczak, J. P and T. A. Cruse., Failure mode and strength prediction of anisotropic bolt bearing specimens, *Composite Materials*, 5 (1971),. 421.

[3] Jong, Theo. De., Stresses around pin-loaded holes in elastically orthotropic or isotropic plates, *J. Composite Matriols*, 2, (1977). 313.

[4] Eisenmann, J. R., Bolted joint static strength model for composite materials, NASA-TM-X-3377 (1976).

[5] Hart-Smith, L. J., Bolted joints in grabhite epoxy composites, *Douglas Aircraft Compony NASA Contract Report*, No NASA CR-144899. (1976).

[6] Collings, T. A., The strength of bolted joints in multidirectional CFRP laminates, *Composies*, 8 (1977).

[7] Quinn, W. J. and P. L. Matthews, The effect of stacking sequence on the pin-bearing strength in glass fibre reinforced plastic, *I. Composite Materials*, 2, (1977). 139.

[8] Kim, R. Y and J. M. Whitney, Effect of temperature and moisture on pin bearing strength of composite laminates, *J. Composite Materials*, 10, (1976). 149.

[9] Wilson, D. W. and R. B. Pipes, Analysis of the shearout failure mode in composite bolted joints, *Composite Structure*, p34.

[10] Tang, S., Failure of composite joints under combined tension and bolt loads, *J. Composite Materials*, 15 (1981). 329.

[11] Soni, S. R., Failure analysis of composite laminates with a fastener hole, *Joining of Composite Materials*, p 145.

[12] Soni, S. R., Stress and strength analysis of bolted joints in composite laminates, *Composite Structure*, p 50.

[13] 吴金泉，碳纤维/环氧树脂复合材料迭层板螺栓接头强度试验及应力集中系数的研究，航空工业部625所。

[14] 陈绍杰等，复合材料连接试验报告，航空工业部601所。

[15] 杨炳章等，碳纤维/环氧复合材料迭层板挤压强度的实验研究，西工大科技资料 SHJ 8489期，(1982)。

[16] 羊羚，碳纤维复合材料迭层平板孔边应力分析，西工大科技资料 SHJ8217期，(1982)。

/7358
CSO: 4009/1003

THE RESPONSE ANALYSIS OF SEVERAL NONLINEAR ISOLATION SYSTEMS SUBJECTED TO RANDOM EXCITATION

Chongqing YINGYONG SHUXUE HE LIXUE [APPLIED MATHEMATICS AND MECHANICS] in Chinese Vol 7 No 2, Feb 86 pp 109-114

[English abstract of article by Zhuang Biaozhong [8369 5903 0022], et al. of Zhejiang University, Hangzhou]

[Text] The nonlinear isolation system is popular in modern isolation mounting. By using Fokker-Planck equation and the statistical linearization method and under the condition of random excitation, we discuss in this article the best damping selection of the dashpots of the stiffening nonlinear stiffness, the response characteristics of the single-degree-of-freedom isolation system of non-antisymmetrical and nonlinear stiffness, and the response analysis of two-degree-of-freedom nonlinear isolation systems. The selection of some parameters of the nonlinear isolation system is also dealt with by virtue of calculation examples. (Paper received 24 Mar 84.)

REFERENCES

[1] Светлицкий В. А., *Случайные Колебания Механических Систем*, Москва «МАШИНОСТРОЕНИЕ» (1975).

[2] Iwan, W. D., A generalization of the method of equivalent linearization, *International Journal of Nonlinear Mechanics*, 8 (1973), 279—287.

[3] Bover, D. C. C., Moment equation methods for nonlinear stochastic systems, *J. Math. Anal. Appl.*, 65 (1978), 306—320.

[4] 庄表中、陈乃立、秦瑞芬，非线性减振器的鉴别及其受白噪声激励时的响应分析，振动与冲击，2 (1984).

FIXED POINT THEOREMS FOR FUZZY MAPPING (II)

Chongqing YINGYONG SHUXUE HE LIXUE [APPLIED MATHEMATICS AND MECHANICS] in Chinese Vol 7 No 2, Feb 86 pp 133-138

[English abstract of article by Zhang Shisheng [1728 4258 3932] of Department of Mathematics, Sichuan University, Chengdu]

[Text] Some new fixed point theorems for fuzzy mappings are presented. The results given in this paper improve and extend some recent results of [1, 4, 5]. (Paper received 7 Dec 84.)

REFERENCES

[1] 张石生. Fuzzy 映象的不动点定理. 应用数学和力学. 5, 2 (1984) , 297—304.

[2] 张石生. 模糊映象的不动点定理. 科学通报. 29, 14 (1984), 833—836.

[3] 张石生、黄南京. 广义模糊映象的不动点定理. 工程数学学报. 2 (1984), 135—137.

[4] Heilpern, S., Fuzzy mapping and fixed point theorem, *J. Math. Anal. Appl.*, 83 (1981), 566--569.

[5] Butnariu, D., Fixed points for fuzzy mappings, *Fuzzy Sets and Systems*, 7 (1982), 191--207.

[6] 付文义. 压缩集值映象族的不动点定理. 江西大学自然科学学报. 9, 1 (1985), 5—10.

[7] Nadler, S. B., Jr., Multi-valued contraction mappings, *Pacific J. Math.*, 30 (1969), 475--488.

REPRESENTING GENERAL SOLUTION OF EQUATIONS IN THEORY OF ELASTICITY BY HARMONIC FUNCTIONS

Chongqing YINGYONG SHUXUE HE LIXUE [APPLIED MATHEMATICS AND MECHANICS] in Chinese Vol 7 No 2, Feb 86 pp 155-160

[English abstract of article by Nie Yiyong [5119 5030 0516] of Shenyang Institute of Computing Technology, Academia Sinica, Shenyang]

[Text] The general solution of the equations in the theory of elasticity is represented by seven harmonic functions, where there are only three harmonic functions independent of each other and every one of them has certain mechanics meaning. The examples applying the general solution to solve several simple inverse problems in elastostatics are presented. (Paper received 19 Dec 84.)

REFERENCES

[1] Timoshenko, S. and J. N. Coodier, *Theory of Elasticity* (sec. ed.), chapters 1 and 9, McGraw-Hill Book Company, Inc., New York (1951).

THE FINITE ELEMENT TECHNIQUE FOR PREDICTING THE NATURAL FREQUENCIES, MODE SHAPES AND DAMPING VALUES OF FILAMENTARY COMPOSITE PLATES

Chongqing YINGYONG SHUXUE HE LIXUE [APPLIED MATHEMATICS AND MECHANICS] in Chinese Vol 7 No 2, Feb 86 pp 181-196

[English abstract of article by Lin Dunxiang [2651 2415 4382] of Shanxi Institute of Mechanical Engineering, Xi'an, and Ni Ronggen [0242 2837 2704] of Institute 621, Ministry of Aeronautics Industry, Beijing]

[Text] This article presents the numerical method for predicting the natural frequencies, mode shapes and damping values of filamentary composite plates. This method is based on finite element technique, using damped element and allowing transverse shear deformation. For the example of this technique, the theoretical results comparing with experimental values of carbon fibre and glass fibre reinforced plastics plates (mid-plane symmetric) are provided. The dynamic properties of these laminates are discussed. Finally, a simple graphic technique to estimate the natural frequencies and damping values is suggested. (Paper received 27 May 83.)

REFERENCES

[1] Ashton, J. E. and M. E. Waddoups, Analysis of anisotropic plates, *J. Composite Materials*, 3 (Jan. 1969), 148.

[2] Ashton, J. E. and J. D. Anderson, The natural modes of vibration of boron-epoxy plates, *Shock and Vibration Bulletin*, 39 (1969).81.

[3] Cawley P. and R. D. Adams, The predicted and experimental natural modes of free-free CFRP plates, *J. Composite Materials*, 12 (Oct. 1978),336.

[4] Reddy, J. N., Free vibration of antisymmetric, angle-ply laminated plates including transverse shear deformation by finite element method, *J. Sound and Vibration*, 66.4 (1979), 565.

[5] Hashin, Z., Complex moduli of viscoelastic composite——2. Fibre reinforced materials, *Int. J. of Solids and Structures*, 6 (1970), 797.

[6] Bert, C. M.,Vibration of composite structures, *Recent Advances in Structural Dynamics*, Int. Conf. Univ. of Southampton (July 1980),7—11.

[7] Adams, R. D. and D. G. C. Bacon, Effect of orientation and laminated geometry on the dynamic properties of CFRP, *J. Composite Materials*, 7 (Oct.1973), 402.

[8] Ioannides, E. and P. Grootenhuis, Finite element analysis of the harmonic response of damped three-layer plates, *J. Sound and Vibration*, 67, 2 (1979).203.

[9] Lin Dun-xiang (林敦祥), Ni Rong-gen (倪荣根) and R. D. Adams, Prediction and measurement of the vibrational damping parameters of carbon and glass fibre-reinforced plastics plates, *J. Composite Materials*, 18 (March 1984), 132.

[10] Ni Rong-gen(倪荣根), Lin Dun-xiang(林敦祥) and R.D. Adams, The dynamic properties of carbon-glass fibre sandwich hybrid laminated composites, Theoretical, experimental and economic consideration, *Composites*, 15,4 (Oct. 1984),297.

[11] Yang, P. C., C. H. Norris and Y. Stavsky,Elastic wave propagation in heterogeneous plates, *Int. J. Solids and Structure*, 2 (1966).665.

[12] Ashton, J. E. and J. M. Whitney, *Theory of Laminated Plates*, Technomic Publishing Co., Inc. (1970).

[13] Cawley, P. and R. D. Adams, The location of defects in structures from measurements of natural frequencies, *J. Strain Analysis*, 14, 2 (1979), 49.

[14] Ni Rong-gen (倪荣根) and R. D. Adams, A rational method for obtaining the dynamic properties of laminae for predicting the stiffness and damping of laminated plates and beams, *Composites*, 15, 3 (July 1984), 193.

[15] Lin Dun-xiang (林敦祥) and R. D. Adams, Determination of damping characteristics of structures by transient testing using Zoom-FFT, *J. of Physics*, E. 18, 2 (1985), 161.

/7358
CSO: 4009/1104

THE METHOD OF MIXED BOUNDARY CONDITION FOR A KIND OF LINEAR AND NONLINEAR COMPOSITE STRUCTURE

Chongqing YINGYONG SHUXUE HE LIXUE [APPLIED MATHEMATICS AND MECHANICS] in Chinese Vol 7 No 3, Mar 86 pp 215-224

[English abstract of article by Chen Shanlin [7115 1472 2651] of Chongqing Institute of Architecture and Engr., Chongqing, and Zhang Liying [1728 4539 5391] of Chongqing Jiaotong Institute, Chongqing]

[Text] This paper deals with the axisymmetrical deformation of shallow shells in large deflection, which are in conjunction with linear elastic structures at the boundary. A method of mixed boundary condition for this problem is introduced, then the problem of a composite structure is transformed into a problem of a single structure and the integral equations are given. The perturbation method is used to obtain the solutions and an example of composite structure consisting of a shallow spherical and a cylindrical shell is presented. Calculations were carried via Cromemco System-III microcomputer. (Paper received 1 Sep 85.)

REFERENCES

[1] Феодосьев В. И., *Упругие Элементы Точного Приборостроения*, Оборонгиз(1949).
[2] 陈山林. 圆板大挠度的钱伟长解及其渐近特性. 应用数学和力学. 3, 4 (1982), 513—518.
[3] 陈山林. 板和扁壳大挠度问题摄动参数的最小二乘法选择. 上海国际非线性力学会议论文集. 上海. (1985).
[4] 刘人怀、陈山林. 椭球封头中心开孔接管的强度问题. 兰州大学科技专刊. 1 (1973), 14—28.

PLASTIC ANALYSIS OF THIN PLATES WITH ANISOTROPIC HARDENING

Chongqing YINGYONG SHUXUE HE LIXUE [APPLIED MATHEMATICS AND MECHANICS] in Chinese Vol 7, No 3, Mar 86 pp 225-234

[English abstract of article by Jing Yongjie [6855 3057 2638] of Department of Engineering Mechanics, Shanghai Jiaotong University, Shanghai]

[Text] In this paper we discuss the adoption of the anisotropic hardening model due to the existence of Bauschinger effect when thin plate is applied by repeated loading. The loading condition of thin plates for linear kinematic hardening has been deduced in terms of generalized forces and generalized plastic deformation. And it can be extended to nonlinear kinematic hardening and mixed hardening. Finally as an example the numerical results are obtained for a circular plate. (Paper received 10 Feb 85.)

REFERENCES

[1] Shield, R. T. and H. Ziegler, On Prager's hardening rule, *J. Appl. Math. Phys.* (ZAMP). 9a, 3 (1958), 260—276.

[2] Ziegler, H., A Modification of Prager's hardening rules, *Quarterly Appl. Math.*, 17 (1959), 55—65.

[3] Mroz, Z., On the description of anisotropic work-hardening, *J. Mech. Phys. Solids*, 15 (1967), 163—175.

[4] Axelsson, K. and A. Samuelsson, Finite element analysis of elasto-Plastic materials displaying mixed hardening, *Inter. J. Num. Meth. Engng.* 14 (1979), 211—225.

[5] Lamba, H. S. and O. M. Sidebottom, Cyclic plasticity for nonproportional paths, Part 2—comparison with prediction of three incremental plasticity models, *J. Engng Mat. Tech.* (Trans. ASME) 100, Jan. (1978). 104—111.

[6] Zenner, H., On life prediction in low cyclic-fatigue, *Proceedings of the International Symposium on Low-Cycle Fatigue Strength and Elasto-Plastic Behaviour of Materials*, (1979).

[7] Kachanov, L. M., *Foundation of the Theory of Plasticity* (1971).

[8] Hwang, Chintsun, Incremential Stress-strain law applied to work-hardening plastic materials, *J. Appl. Mech.*, (Trans. ASME) Dec. (1959). 594—598.

NONLINEAR OSCILLATION OF A TWO-DIMENSIONAL LIFT BODY

Chongqing YINGYONG SHUXUE HE LIXUE [APPLIED MATHEMATICS AND MECHANICS] in Chinese Vol 7, No 3, Mar 86 pp 235-238

[English abstract of article by Wang Maohua [3076 2021 7520] of Beijing Institute of Aeronautics and Astronautics, Beijing]

[Text] It is very difficult to obtain an exact analytical solution to a nonlinear ordinary differential equation, so till now analytical solutions are rare in this area. The author has obtained the exact analytical solutions of this type of nonlinear oscillations. In this paper as an example, the exact analytical solution of nonlinear oscillation of a two-dimensional lift body, which has attracted the attention of research workers for a long time, is given. (Paper received 29 Jan 85.)

REFERENCES

[1] Iyengar, R. N. and O. Mahrenholtz, Nonlinear oscillations of a vortex excited cylinder in wind, *Solid Mechanics Archives*, 7, 4 (1982), 411–432.

CONTACT PROBLEM OF RUBBER RINGS WITH LARGE DEFORMATION

Chongqing YINGYONG SHUXUE HE LIXUE [APPLIED MATHEMATICS AND MECHANICS] in Chinese Vol 7 No 3, Mar 86 pp 239-248

[English abstract of article by Lu Hexiang [0712 0735 4382] of Department of Engineering Mechanics, Dalian Institute of Technology, Dalian]

[Text] A combined problem with frictional contact between a rubber ring with large deformation and linear elastic thin plate is solved by means of the substructuring technique. A study of the influence of frictional coefficient and the influence of plate thickness is presented. (Paper received 13 Sep 84.)

REFERENCES

[1] Oden, J. T., *Finite Elements of Nonlinear Continua*, McGraw-Hill, (1972).

[2] Jankovich, E., F. Leblance and M. Durand, A finite element method for the analysis of rubber parts, experimental and analytical-assessment, *Computers Structures*, 14, 5—6 (1981), 385—391.

[3] Lü He-xiang, Superelement method for solution of nonlinear large deformation, Dalian Institute of Technology Dept. of. Appl. Mech. Research Report 83—306(1983).

[4] Lü He-xiang, Analysis of axisymmetric large deformation of rubber, *Journal of Dalian Institute of Technology*, 23, 1(1984).

ON PROBLEMS OF OPTIMAL DESIGN OF SHALLOW SHELL WITH DOUBLE CURVATURE ON ELASTIC FOUNDATION

Chongqing YINGYONG SHUXUE HE LIXUE [APPLIED MATHEMATICS AND MECHANICS] in Chinese Vol 7 No 3, Mar 86 pp 259-263

[English abstract of article by Cheng Xiangsheng [2052 4382 3932] of Tongji University, Shanghai]

[Text] The present paper discusses a method of optimal design of the shallow shell with double curvature on the elastic foundation. Substantially we take the initial flexural function as the control function or design variable which will be found and the potential energy of the external loads as the criterion of quality of the optimal design of the shallow shell with double curvature, therefore the functional of the potential energy will be aim function. The optimal conditions and the isoperimetric conditions belong to the constrained conditions, thus we obtain the necessary conditions of the optimal design for the given problems, at the same time the conjugate function is introduced, then the problems are reduced to the solutions of two boundary value problems for the differential equation of conjugate function and the initial flexural function. (Paper received 28 Apr 83.)

REFERENCES

[1] Haug, E. J. and J. S. Arora, *Applied Optimal Design*, New York, John Wiley (1979).

[2] Баничук Н. В., Оптимизация форм упругих тел, М, Наука (1980).

[3] Niordson, F. I. and P. Pedersen, A review of optimal structural design, *The Technical University of Denmark, DCAMM, Report*, 31 (1972).

[4] 钱令希等, *Selected Papers on Structural Optimization*, (1979).

[5] Sheu, C. Y. and W. Prager, Recent developments in optimal structural design, *Appl. Mech. Revs.*, 21, 10 (1968).

[6] 杨妖乾. 《薄壳理论》, 中国铁道出版社 (1981).

[7] Власов В. З., *Общая Теория Оболочек и её Приложения в Технике*, Гостехиздат (1949).

[8] Камке Э., Справочник по обыкновенным дифференциальным уравнениям, М., «Наука» (1976).

[9] Баничук Н. В. и А. Д. Ларичев, *МТТ*, 4 (1981), 134—139.

/7358
CSO: 4009/1105

Astronomy

DETERMINATION OF ERP WITH LLR DATA

Beijing TIANWEN XUEBAO [ACTA ASTRONOMICA SINICA] in Chinese Vol 27 No 2, Jun 86 pp 85-95

[English abstract of article by Jin Wenjing [6855 2429 2417] and Wang Qiangguo [3769 1730 0948] of the Shanghai Observatory, Chinese Academy of Sciences]

[Text] In this paper a comparison between the results (JD2443915.23-2443940.86) calculated by us and those of other analysis centers is listed in a table. Four questions are discussed as follows:

1. The influence of adopted initial values of UT1-UTC, x, y, is discussed. If the initial value of UT1-UTC sets to zero or equals that of Circular D of BIH, the same values of UT1-UTC can be obtained by iterating two times.

When the X, y values used deviate from those of BIH to 0.02", the influence of UT1-UTC may be 0.5 ms as listed in the table. Because the accuracy of x, y supplied by BIH is better than 0.01", it is reasonable to adopt x, y from Circular D of BIH for determination of UT1-UTC using the LLR data at a single station.

2. The influence of adopted spherical station coordinates (λ, ϕ, r) has been analyzed and the results are listed in a table.

3. The influence of the adopted constants of lunar physical liberation is analyzed. Two sets of the adopted value, MERIT Standards and the Eckhart-500 are used for UT1-UTC calculation. The results are listed in a table.

4. The choice of pre-residual or post-residual to determine UT1-UTC is also discussed. If the pre-residual is used for UT1-UTC calculation, then the initial reference system is adopted, while the post-residual corresponds to the corrected reference system (the initial parameters plus the corrected value obtained from adjusting a series of lunar observations). If the results between different analysis centers are to be compared, the pre-residual should be adopted.

The UT1-UTC values calculated from the LLR data in the main MERIT Campaign using our method and that of JPL are listed in a table.

CERGA (Grasse, France) and MLRS, used instead of McDonald's 2.7 m telescope, began regular observation of LLR in July 1982 and September 1983 respectively. There are two stations in the world which operate the LLR program in the main MERIT Campaign and whose longitudinal difference is about 111°. This means that the possibility of solving the three parameters of ERP now exists.

Due to the uncorrected station coordinates and the systematic error of observation, the systematic error should be reduced for ERP calculation.

In determining the ERP, each observational equation should be given a suitable weight based on the rms of the normal point (internal weight) and the square error (external error) obtained from adjusting the observations of LLR after about one year. This will ensure that the difference between p_{in} and p_{ex} is not obvious. The results are listed in a table.

Using the LLR data at two stations, Grasse and McDonald, in the main MERIT Campaign, the corrected station coordinates and the baseline length between the two stations are also obtained and listed in the tables. The precision is 10-50 cm and 20-40 cm respectively.

In determining the ERP, regular observations of LLR will be expected at these two stations or others which already have the observation conditions.

ON OPTIMAL CONDITIONS FOR DETERMINATION OF EARTH ROTATION PARAMETERS

Beijing TIANWEN XUEBAO [ACTA ASTRONOMICA SINICA] in Chinese Vol 27 No 2, Jun 86 pp 96-105

[English abstract of article by Zhao Ming [6392 6900] and Zhu Shengyuan [2612 5110 3298] of the Shanghai Observatory, Chinese Academy of Sciences]

[Text] There are various techniques used for determination of Earth Rotation Parameters (ERP). The basic observation principle for all these techniques is the same, i.e., the observation of generalized zenith distance. In this paper an observation equation suitable for all techniques is given, and the most favorable situation for determining generalized zenith distance is discussed. Under the assumption that all the equivalent observables have the same weight, the optimal conditions for determining ERP are reduced from the general observation principle. The results look very simple, yet they can be widely used for all techniques. It is also shown that, to obtain the optimal ERP, the distribution of the source vector is as important as that of the station vector.

INFLUENCE OF ATMOSPHERIC ZONAL TIDES ON EARTH'S ROTATION RATE

Beijing TIANWEN XUEBAO [ACTA ASTRONOMICA SINICA] in Chinese Vol 27 No 2, Jun 86 pp 106-112

[English abstract of article by Zhu Yaozhong [2612 5069 0112] of the Institute of Geodesy and Geophysics, Chinese Academy of Sciences]

[Text] Using the daily atmospheric pressure data obtained at Harbin, Beijing, Wuhan and Guangzhou meteorological stations during 1979-1983, the atmospheric zonal tidal effect is analyzed by means of the AR spectrum. In this paper, the response of the oceans to the variations in atmospheric pressure is discussed in four cases. The parameter K/c, which is proportional to the variation in the Earth's rotation rate, is solved. The main results are as follows:

1. If there were no oceanic responses to the variations in atmospheric pressure, then K/c = 1.005.
2. If all gravitational and deformational effects on the oceans due to the variations in atmospheric pressure are ignored, then K/c = 0.966.
3. If the gravitational and deformational effects are included, then K/c = 0.969.
4. In order to contribute to the effective Love number K, the inverted barometer and constant response should be about 36 percent of the solution in which the oceans are assumed to be freezing. The gravitational and deformational effects on sea level are about 14 percent of the pressure-induced effects. The atmospheric zonal tides are about 2 percent of the Earth tides.

CHORD AND RELATIVE HEIGHT ESTIMATION FROM SINGLE PASSES OF SATELLITE LASER RANGING DATA

Beijing TIANWEN XUEBAO [ACTA ASTRONOMICA SINICA] in Chinese Vol 27 No 2, Jun 86 pp 113-120

[English abstract of article by He Miaofu [0149 1181 4395] and Feng Chugang [7458 0443 0474], et al., of the Shanghai Observatory, Chinese Academy of Sciences]

[Text] The application of the multiple-very short arc technique to determining the chord and relative height between two laser tracking stations from single passes of satellite laser ranging data is described. It is shown through experiments that this technique for processing laser ranging data can be regarded as an important supplement to the conventional dynamic technique which requires more observations collected over several consecutive satellite revolutions. Consequently, while the scale and orientation of the interstation base line are provided by the dynamic technique using longer arcs of the satellite laser ranging data, the multiple-very short arc technique described here offers a useful method of checking the accuracy of the geodetic network consisting of the laser tracking stations.

9717
CSO: 4009/111

Electronics

SOME RESULTS OF THE RESEARCH ON THE FLUTE-TYPE HOLLOW CATHODE DISCHARGE USING A LOW-LIGHT LEVEL TV CAMERA

Beijing DIANZI KEXUE XUEKAN [JOURNAL OF ELECTRONICS] in Chinese Vol 7 No 5, Sep 85 pp 323-328

[English abstract of article by Wang Yuzhi [3769 2948 4249], and Wei Cong [7279 3829] of Chengdu Institute of Radio Engineering]

[Text] The breakdown processes of the flute-type hollow cathode discharge was observed by a low-light level TV camera of the SEM (Silicon Electron Multiplication) type, the most sensitive one of low-light level cameras of modern industry. An explanation for the mechanism of light development was presented. The light development was divided into two stages, i.e., the stage (1st stage) of self-sustained dark discharge developed in the space between the anode bar and the outer-side of the flute tube, and the stage (2nd stage) of entering of discharge through the hole into the flute tube. Corresponding to the two stages, there are two γ-processes, one existing at the metal surface around the hole and the other at the inner surface of the cathode. According to the above results, a discussion on the current principle of the design of geometrical parameters of the flute type was given. (Paper received 7 Feb 85.)

REFERENCES

[1] K. H. Wagner, *Z. Phys.* (Germany), **204** (1967), 177.
[2] K. H. Wagner, CRI VI Conf. Int. Phenomenes d'Ionisation dans les Gas, (Paris, S. E. R. M. A.), 2(1963), pp. 309—311.
[3] J. Kappitz, *Z. Naturforsch. A* (Germany). **26a** (1971), 700.
[4] Kan-Ichi Fujii, *Jpn. J. Appl. Phys.* **13** (1974), 571.
[5] Kan-Ichi Fujii, *IEEE J. of QE, Vol.* QE-15 (1979), 35.

IMPULSE RESPONSES OF APERTURE ANTENNAS WITH ARBITRARY APERTURE DISTRIBUTIONS

Beijing DIANZI KEXUE XUEKAN [JOURNAL OF ELECTRONICS] in Chinese Vol 7 No 5, Sep 85 pp 348-355

[English abstract of article by Hu Hannan [5170 3352 0589] of Shanghai Ship and Shipping Research Institute]

[Text] Based on the equation of Fresnel-Kirchhoff scalar diffraction field, impulse responses of parallel-fed aperture antennas of arbitrary configurations with arbitrary aperture amplitude distributions and those of end-fed rectangular aperture antennas with arbitrary aperture amplitude distributions can all be expressed in the aperture amplitude distributions, and that the impulse responses of rectangular aperture antennas with separable aperture distributions and those of circular aperture antennas with circularly symmetric distributions are special cases of the above general ones. (Paper received 23 Dec 83, finalized 20 Dec 84.)

REFERENCES

[1] R. E. Collin and F. J. Zucker, Antenna Theory, McGraw-Hill Book Co., New York, 1969, Vol. 1, Chap. 8.
[2] M. I. Skolnik, Radar Handbook, McGraw-Hill Book Co., New York, 1970, chap. 9 and 13.
[3] 胡汉南,电子科学学刊, 6(1984), 235.
[4] 胡汉南,电子科学学刊, 7(1985), 28.

DESIGN AND PERFORMANCE OF COMPACT LOW NOICE GaAs MESFET AMPLIFIERS FOR UHF OPERATION

Beijing DIANZI KEXUE XUEKAN [JOURNAL OF ELECTRONICS] in Chinese Vol 7, No 5, Sep 85 pp 374-380

[English abstract of article by Wang Wenqi [3769 2429 7496] of Shanghai University of Science and Technology, Branch, and Yang Xinmin [2799 2450 3046], et al., of Shanghai Institute of Metallurgy, Academia Sinica]

[Text] The design considerations and experimental results of compact low noice GaAs MESFET amplifiers for UHF operation were described. The miniaturized and optimized circuits were obtained by means of special matching network and CAD technique. Both two-stage unit at 700 MHz and three-stage unit of 1000 MHz were fabricated on 50x60 mm^2 alumina substrate, and the power gain of 29 and 30 dB, noice figure of 0.8 and 1.2 dB and bandwidth of 40(3 dB) and 100 MHz (1 dB) were obtained, respectively. The satellite direct broadcasting receiver constructed with the 700 MHz GaAs MESFET amplifier has clear pictures and good sound.

REFERENCES

[1] M. Miama and H. Katoh, *Electron. Lett.*, **14** (1978), 319.
[2] Takeshi Sato, et al., *National Tech. Report.* **26** (1980), 334.
[3] 王渭源等，半导体学报，**3**(1982)，493。
[4] Shotaro Nambu, et al., *IEEE J. of SC*, **SC-17** (1982), 648.
[5] 杨新民、王渭源、王文骐，应用科学学报，**3**(1985)，46.
[6] James Fawcette, *Microwave Systems News*, **10** (1980)2, 42.
[7] G. Barbari, *Microwaves and RF*, **23** (1984)2, 141.

A MICROWAVE SWITCH WITH OPTIONAL POWER DIVISION RATIO

Beijing DIANZI KEXUE XUEKAN [JOURNAL OF ELECTRONICS] in Chinese Vol 7 No 5, Sep 85 pp 385-390

[English abstract of article by Zheng Dunxiang [6774 2415 4382] of Beijing Aircraft Maintenance Engineering Development Corporation]

[Text] A microwave switch with optional power division ratio, which uses PIN diode for controlling, is introduced. Analytic formulas are given. They are straight-forward and feasible for engineering purposes. The theoretical analysis is in good agreement with the experimental result. (Paper received 21 Mar 84, finalized 14 Nov 84.)

REFERENCES

[1] W. L.Teeter and K. R. Bushore, *IRE Trans. On MTT*, **MTT-5** (1957), 227.

[2] 吴培亨，微波电路，科学出版社，(1980)，40.

[3] 上海无线电 17、26厂译，微波半导体器件及其应用，上海人民出版社，(1975)，293.

[4] R. V. Garver, *IRE Trans. on MTT*, **MTT-9** (1961), 224.

[5] R. E. Fisher, *IEEE Trans. on MTT*, **MTT-13** (1965), 706.

PIEZOELECTRIC CERAMICS WITH k_p=0.15

Beijing DIANZI KEXUE XUEKAN [JOURNAL OF ELECTRONICS] in Chinese Vol 7 No 5, Sep 85 pp 391-392

[English abstract of article by Zhang Hanjun [1728 3352 0689] of Guangzhou Communication Institute]

[Text] $PbNb_2O_6$-$PbCrO_4$-PZT piezoelectric ceramics with low radial coupling coefficient has been developed. Its chemical equation is given. This kind of ceramics is characterized by k_p=0.15, Q_m=5000, $\Delta f/f_r=6\times10^{-6}$. It has been used successfully to make low-frequency narrow-band ceramic filter. (Paper received 4 Jan 85.)

REFERENCES

[1] 电子工业部七所滤波器材料组,无线电陶瓷与器件,1970 年,第 1 期,第 8 页.

THE STUDY OF LATTICE MATCH IN GaInAsP/InP HETEROJUNCTION LPE LAYERS

Beijing DIANZI KEXUE XUEKAN [JOURNAL OF ELECTRONICS] in Chinese Vol 7, No 5, Sep 85 pp 395-400

[English abstract of article by Yang Yi [2799 2496], et al., of Shanghai Institute of Metallurgy, Academia Sinica]

[Text] The effects of the growth conditions of two-phase solution liquid phase epitaxy (LPE) (i.e. growth temperature, cooling rates and solution composition) on lattice mismatch and bandgap wavelength in GaInAs/InP heterojunction LPE layers have been investigated by X-ray double-crystal diffractometry and double-beam spectrophotometer. The interface stress in the grown interface free of misfit dislocations and the lattice mismatch at growth temperature have been calculated. (Paper received 25 Jul 83, finalized 20 Aug 84.)

REFERENCES

[1] M. A. Pollack, R. E. Nahory, J. C. Dewinter and A. A. Ballman, *Appl. Phys. Lett.*, 33(1978), 314.

[2] T. Yamamoto, K. Sakai and S. Akiba, *IEEE. J. of QE*, QE-15 (1979), 684.

[3] K. Nishida, K. Taguchi and Y. Matsumoto, *Appl. Phys. Lett.*, 35(1979), 251.

[4] W. A. Feibelman, *Appl. Opt.*, 16(1977), 800.

[5] M. Feng, L. W. Cook, M. M. Tashima and G. E. Stillman, *J. Elect. Mater.*, 9(1980), 241.

[6] V. G. Keramidas, S. Mahajan, H. Temkin and W. A. Bonner, Gallium Arsenide and Related Compounds, 1980 Inst. Phys. Conf. Ser. 56, 2, p. 95.

[7] 邬祥生,杨　易,李允平,唐皑妹,水海龙,半导体学报, 3(1982), 162.

[8] B. G. Cohen, *Solid-State Electronics*, 10(1967), 33.

[9] 杨　易,邬祥生,杨林宝、李允平,科技通讯, 1(1981),26.

[10] M. Feng, M. M. Tashima, T. H. Windharn and G. E. Stillman, *Appl. Phys. Lett.*, 33(1978), 533.

[11] K. Oe, Y. Shinado and K. Sugiyama, *Appl. Phys. Lett.*, 33(1978), 962.

[12] J. Matsui, K. Onabe, T. Kamejima and I. Hayashi, J. Electrochem. Soc., 126(1979), 664.

[13] Z. R. Zytkiewicz, *Physica Status Solidi* (A), 53(1979), K165.

/7358
CSO: 4009/1108

Engineering

A FEASIBILITY STUDY OF ON-LINE MONITORING FOR THE BURN OF GROUND SURFACE LAYER

Nanjing NANJING GONGXUEYUAN XUEBAO [JOURNAL OF NANJING INSTITUTE OF TECHNOLOGY] in Chinese Vol 16 No 3, Jul 86 pp 1-10

[English abstract of article by Shi Xiurong [2514 0208 2837] and Huang Ren [7806 0088] of Department of Mechanical Engineering]

[Text] This paper discusses the burn of ground surface layer in the view of surface integrity and demonstrates that the governing factor of influence is grinding temperature. A method to study for on-line controlling or monitoring the burn of ground surface layer via grinding spark temperature by the maximum entropy spectrum and infrared system and optical fibre/infrared system is proposed.

The results of investigations prove that the grinding process represented by the grinding sparks temperature is stationary and regularities of the clustered sparks ray temperature quite agree with the grinding temperature. When the ground surface layer has been burned, the characteristics of the spark ray temperature can be identified via maximum entropy spectral analysis. (Paper received 13 Jul 85.)

REFERENCES

[1] Malkin S., Anderson R. B.: Thermal aspect of grinding (Part 1 & 2) J. of Eng, for Industry, ASME, Nov. 1974.

[2] Snoeys R., Leuven K., et. al.: Thermally induced damage in grinding. CIRP Annals, 27(1), 1978.

[3] 黄仁、时修荣：精密磨削表面质量的研究，《南京工学院学报》，1978，№4。

[4] 黄仁、时修荣：用时间序列分析方法对磨削火花温度的研究，《机械工程》时间序列分析在机械工程中应用专刊．1984．9，

[5] Marple L.: A new autoregressive spectrum analysis algorithm, IEEE, Assp. 28(4), Aug., 1980.

KINEMATIC ANALYSIS OF 7R MULTI-JOINT MANIPULATORS

Nanjing NANJING GONGXUEYUAN XUEBAO [JOURNAL OF NANJING INSTITUTE OF TECHNOLOGY] in Chinese Vol 16 No 3, Jul 86 pp 11-20

[English abstract of article by Jin Wanmin [6855 8001 2404] of Department of Mechanical Engineering]

[Text] The rotational transformation matrix method and relevant equations derived by Hiroshi Makino are used to solve the indirect position problems of manipulators. This method is simple and generally accepted and convenient to computerize. (Paper received 4 Mar 85.)

REFERENCES

[1] [日]牧野洋著,胡茂松译:《自动机械机构学》,科学出版社1980，247—268。
[2] 张启先：《空间机构的分析与综合》，机械工业出版社，1984. 135～140。

DECOUPLED BRANCH DIFFERENCE LOAD FLOW FORMULATION

Part 1: Algorithms

Nanjing NANJING GONGXUEYUAN XUEBAO [JOURNAL OF NANJING INSTITUTE OF TECHNOLOGY] in Chinese Vol 16 No 3, Jul 86 pp 76-82

[English abstract of article by Shan Yuanda [0830 3220 6671], et al., of Dept. of Electrical Engineering]

[Text] This paper presents a new model or formulation for ac-load flow problem in terms of branch angle and voltage differences. This model is linear in these variables and quadratic to branch losses, thus yielding a formulation particularly suitable to linear and quadratic programming techniques.

In addition, this new formulation yields a symmetric A matrix even in the most general case where phase-shifters are present in the transmission system. Moreover, the decoupled coefficient matrix involves only branch susceptance. These features offer very important computational simplifications.

The 14, 11, 30, 57 and 118 bus systems are included as examples to illustrate the validity of the new model. (Paper received 11 Mar 85.)

REFERENCES

[1] Gilles M. L.: Operation and transmission expansion planning of integrated AC-DC power system, Ph. D. Thesis, ECE Dept., Wayne State University, 1981.

[2] Tinney W. F. and Hart C. E.: Power flow solution by newton's method, IEEE Trans, Pas-86, 1967: 1449-1460.

[3] Stott B. and Alsac O.: Fast decoupled load flow, IEEE Trans, Pas 93, 1974: 859-869.

[4] Tinney W. F.: Compensation methods for network solution by optimal ordered triangular factorzation, PICA, 1971: 377.

DECOUPLED BRANCH DIFFERENCE LOAD FLOW FORMULATION

Part 2: Alleviation of Ill-Conditioned Load-Flow Problems via the Decoupled Branch Difference Formulation

Nanjing NANJING GONGXUEYUAN XUEBAO [JOURNAL OF NANJING INSTITUTE OF TECHNOLOGY] in Chinese Vol 16 No 3, Jul 86 pp 83-92

[English abstract of article by Shan Yuanda [0830 3220 6671], et al., of Dept. of Electrical Eng.]

[Text] This paper presents a simplified index to recognize ill-conditioning for the basic linear equations and power system analysis problems. A new load-flow formulation is then presented. A key advantage of this new decoupled branch difference (DBD) load-flow algorithm is its ability to both recognize the physical parameters causing ill-conditioning, and thereby through a simple procedure to numerically eliminate the ill-conditioning. Test results on seven systems, four of which are taken from the literature of ill-conditioned power systems, are presented. (Paper received 11 Mar 85.)

REFERENCES

[1] 单渊达，Gilles M., L., Meisel. J.: 支路差值解耦潮流算法第一部分：计算方法，见本刊。

[2] Hildebrand F. D.: Introduction to Numerical Analysis, Second edition, 1974: 597.

[3] 何旭初、苏显城、包雪松编：《计算数学简明教程》人民教育出版社，224-226。

[4] Ostrowski, A. M.: Iterative Methods for the Solution of Equations and Systems of Equations, 1966.

[5] Sasson, A. M. Trevino, C. Aboytes: F. Improved Newton's load-elow through a minimization technique, IEEE Trans. Pas-90 Sept./Oct. 1971: 1974.

[6] Tripathy S. C., Prasad G. D., Malik O. P. and Hope G. S.: Load-flow solution for Ill-conditioned power systems by a Newton-like method, IEEE Trans. Pas-101 Oct. 1982: 3648.

[7] Deckmann S., Pizzolante A., Monticalli A., Stott B., Alsac O.: Studies on power system load flow equivalencing, IEEE PES Winter Meeting Feb. 1980.

/7358
CSO: 4009/1096

Microbiology

A STUDY ON AQUATIC ACTINOMYCETES IN THE PLATEAU LAKES IN YUNNAN

VIII. IDENTIFICATION OF THE GENUS ACTINOMADURA

Beijing WEISHENGWU XUEBAO [ACTA MICROBIOLOGICA SINICA] in Chinese Vol 26 No 2, Jun 86 pp 97-100

[English abstract of article by Jiang Chenglin [1203 2052 2651], and Xu Lihua [1776 7787 5478] of Yunnan Institute of Microbiology, Kunming]

[Text] Twelve strains belonging to the genus Actinomadura were isolated from the mud samples collected from Chenghai Lake in Yunnan. Two of them were described as two new species: Actinomadura chenghaiensis sp. nov. and Actinomadura viridoflava sp. nov. (Paper received 8 Apr 85.)

REFERENCES

[1] Преображенская, Т. П. и др., *Микробиология*, **44**: 524—527, 1975.
[2] Паврова, Н. В. и Т. П. Преображенская: *Антибиотики*, **20**: 483—488, 1975.
[3] Meyer, J.: *Zeit. Allgemeine Mikrobiologie* **19**: 37—44, 1979.
[4] Nonomura, H. & Y. Ohara: *J.Ferment. Technol.*, **49**: 904—912, 1971.
[5] Паврова, Н. В. и др.: *Антибиотики*, **17**: 965—970, 1972.

THE TWO NEW SUBSPECIES OF STREPTOMYCES

Beijing WEISHENGWU XUEBAO [ACTA MICROBIOLOGICA SINICA] in Chinese Vol 26, No 2, Jun 86 pp 101-104

[English abstract of article by Zhang Guowei [1728 0948 0251], et al., of Institute of Microbiology, Academia Sinica, Beijing, and Zhu Guiru [2612 2710 1172], et al., of Northwest Plateau Institute of Biology, Academia Sinica, Xining]

[Text] The A614, A3, and other strains was isolated from soils of Qing-Zang highland. The A614 was identified and named Streptomyces rubiginosohelvolus subsp. pallens n. subsp. The A3 was identified and named Streptomyces galilaeus subsp. xiningensis n. subsp. (Paper received 15 Jun 84.)

REFERENCES

[1] 高译, Г. Ф. (戴冠群、袁永生译) «拮抗性放线菌的分类问题», 科学出版社, 北京, 78—90 页 1959。

[2] 日本专利,昭和51, 15690, 1976。

[3] Shirling, E. B. & D. Gottlieb: *Intern. J.Syst. Bacteriol.*, **22**: 298, 1972

[4] 范 理等: 微生物学报, **19**(4):365－369,1979。

STUDIES ON THE STREPTOMYCES OF HYGROSCOPICUS GROUP

IV. IDENTIFICATION OF TWO NEW SPECIES

Beijing WEISHENGWU XUEBAO [ACTA MICROBIOLOGICA SINICA] in Chinese Vol 26,
No 2, Jun 86 pp 105-111

[English abstract of article by Zhou Qi [0719 0796] and Lin Kaichun [2651 7030 2504] of Agricultural Antibiotic Laboratory, Huazhong Agricultural University, Wuhan]

[Text] Two new species (type strain SH-121 and SH-4) of hygroscopieus group of Streptomyces, isolated from soil of Fangxian, province Hubei of China were found to produce antibiotics which are effective in preventing and controlling the citrus diseases during storage caused by Penicillium italicum, P. digitatum, Alternaria citri and Geotrichum candidum.

Strain SH-121: Spore-chain morphology belongs to section Retinaculum-Apertum (RA). Spore surface is smooth. In comparison with all the known species of Streptomyces, the strain SH-121 seems to resemble S. hygroscopicus f. glebosus Ohmori et al.. However, it has significant differences from the above organism in the following aspects: the color of substrate mycelium on the synthetic media and natural organic media, physiological properties, utilization of carbon sources and the production of antibiotics. As a result of the above mentioned characteristics, the designated as Streptomyces carneohygros copicus n. sp.

Strain SH-4: Spore-chain morphology belongs to section spirales with the tightly spiral tail, which likes sporangium. Spore surface is smooth. There are masses of spores enclosed by mucous substance in the middle or on the top of spore-chain. This strain has been found to belong to the hygroscopic group of Streptomyces, but differs from all known species of the group. It is considered as a new species and designated as Streptomyces glomeroplatensis n. sp.
(Paper received 15 Feb 85.)

REFERENCES

[1] 阮继生：«放线菌分类基础»，科学出版社，北京，1977。
[2] 欧阳谅：«微生物学实验法»，江西人民出版社，南昌，1980。
[3] 周 启等，华中农学院学报，2(4)：37—41，1983。
[4] 中国科学院微生物研究所放线菌分类组：«链霉菌鉴定手册»，科学出版社，北京，1975。
[5] Becker, B. et al.: *Appl. Microbiol.*, **12** (5): 421—423, 1964.
[6] Lechevalier, M. P. et al.: In Prauser,H. (ed), The Actinomycetales. Gustay Fischer Verlay. Jena, pp. 311—316, 1970.
[7] Marmur, J. J.: *Mol. Biol.*, **3**:203—218,1961.
[8] Ohmori, T. et al.: *J. Antibiotics*, **A15**: 21—27, 1962.
[9] Tresmer, H. D. et al.: *J. Bacteriol.*, **91**: 1998—2005, 1966.
[10] ——————: *Appl. Microbiol.*, **15**: 637—639 1967.
[11] Waksman, S. A. 著(阎逊初译)：«放线菌»(第二卷)，科学出版社，北京，1974。
[12] 李 群等：微生物学报，**23**(2)：105—107，1983。
[13] ——————：«全国第三次抗菌素学术会议论文集(第一册)»，科学出版社，北京，1965。
[14] 阎逊初：科学通报，**6**:171—172，1957。

ELECTRON MICROSCOPIC STUDY OF THE MORPHOLOGY OF VIRUS OF HAEMORRHAGIC FEVER WITH RENAL SYNDROME IN SUCKLING MICE

Beijing WEISHENGWU XUEBAO [ACTA MICROBIOLOGICA SINICA] in Chinese Vol 26 No 2, Jun 86 pp 112-115

[English abstract of article by Chen Dehui [7115 1795 5610], et al., of Institute of Basic Medical Sciences, Academy of Military Medical Sciences, Beijing, and Ni Dashi [0242 1129 4258], et al., of Institute of Medical Sciences of Anhui Province, Hefei]

[Text] Two-three-day old mice were inoculated with ALC96 strain HFRS virus. Routine ultrathin sections of infected mouse brain tissues were examined in electron microscope.

Four days after inoculation an increase in the amount and complexity of membranes and vacuoles of the Golgi apparatus in infected nerve cells occured predominately. Later (8 and 10 days after inoculation) a small number of matured virions were found within the distended Golgi sacculus and vesicalae of infected neurons. Most of viral particles observed in ultrathin sections were round or oval in shape and 70-110 nm in diameter. A lipid bilayered viral envelope with an external fringe of surface projections could be resolved at high magnification. The mode of maturation of the virus involved budding from cytoplasmic membrane into Golgi vesiclae.

The known morphological and morphogenetic findings of virus particles observed in mouse brain tissue gave the further evidence for taxonomic identification of HFRS virus as a member of the family Bunyaviridae. (Paper received 15 Feb 85.)

REFERENCES

[1] Lee, H. W. et al.: *J. Infect. Dis.*, **137**: 298–308, 1978.

[2] 宋 干等: 中国医学科学院学报, **4**: 73—77, 1982。

[3] 严玉辰等: 同上,**4**: 67—71, 1982。

[4] 倪大石等: 中华医学杂志, **63**: 65—68, 1983。

[5] 李钟铎等: 中华流行病学杂志, **4**: 198—201, 1983。

[6] McCormick, J. B. et al.: *Lancet*, **1** (8275): 765—768, 1982.

[7] White, J. D. et al.: *Lancet*, **1**(8275): 768—771, 1982.

[8] 洪 涛等: 中华微生物学和免疫学杂志, **3**: 69—72, 1983。

[9] 余澄之等: 电子显微学报, **3**: 42, 1984。

[10] 倪大石等: 安徽医学, **6**: 7—10, 1985。

[11] 河 浩等: 中华流行病学杂志, **4**: 148—152, 1983。

[12] Bishop, D. H. L. and R. E. Shope: Bunyaviridae. In "Comprehensive Virology" H. Fraenkel-Conrat and R. R. Wagner, eds., Vol. 14. Plenum, New York, pp. 1—156, 1979.

[13] 陈德惠等: 中华病理学杂志, **12**: 202—204, 1983。

[14] Murphy, F. A. et al.: *J. Virol.*, **2**: 1315—1325, 1968.

[15] Schmaljohn, C. S. et al.: *Virology*, **131**: 482—491, 1983.

CONSTRUCTION AND CHARACTERIZATION OF THE pCN HYBRID PLASMID FOR YEAST GENETIC ENGINEERING VECTOR

Beijing WEISHENGWU XUEBAO [ACTA MICROBIOLOGICA SINICA] in Chinese Vol 26 No 2, Jun 86 pp 127-133

[English abstract of article by Ni Jin [0242 3160], et al., of Institute of Microbiology, Academia Sinica, Beijing]

[Text] By means of the DNA recombinant technology, pCN plasmids were constructed from plasmids YRp7 and pAT153 for yeast genetic engineering vector. The pCN plasmids consist of 1.4 Kb DNA segment of yeast TRP1 gene and the intact plasmid pAT153 molecule. There are two different configuration of pCN plasmids, according to the orientation of inserted TRP1 DNA segment in pAT153 plasmid. The pCN vector obtains the properties of high transformation efficiency of YRp7 and high copy level of pAT153, furthermore, the stability of the pCN plasmid in yeast recipient is more than that of the YRp7. As a shuttle plasmid between yeast and E. coli, especially pCN60 from pCN plasmids can be used as yeast genetic engineering vector. (Paper received 8 May 85.)

REFERENCES

[1] Boliver, R. et al.: *Gene*, **2**: 95—113, 1977.
[2] Twigg, A. J. et al.: *Nature*, **283**: 216, 1980.
[3] Maniatis, T. et al.: Molecular Cloning, CSH, (a) p. 86—91, (b) p. 104—106, (c) p. 250—251, 1982.
[4] O'Farrell, P. H. et al.: *Mol. Gen. Genet.*, **179**: 421—435, 1980.
[5] Sherman, F. et al.: Methods in Yeast Genetics, CSH, p. 106—111c, 1983.
[6] Ito, H. et al.: *J. Bacterology*, **153**: 163—168, 1983.
[7] Projan, S. T. et al.: *Plasmid*, **9**: 182—190, 1983.

THE PLASMIDS CARRING CRYSTAL PROTEIN GENE OF BACILLUS THURINGIENSIS AND THEIR TRANSFER BETWEEN VARIOUS STRAINS

Beijing WEISHENGWU XUEBAO [ACTA MICROBIOLOGICA SINICA] in Chinese Vol 26 No 2, Jun 86 pp 143-150

[English abstract of article by Li Rongsen [2621 2837 2773] of Wuhan Institute of Virology, Academia Sinica, Wuhan]

[Text] The patterns of plasmids from 19 strains of Bacillus thuringiensis representing 7 subspecies were investigated by agarose gel electrophoresis. It was shown that the composition of plasmids of Bacillus thuringiensis was not only subspecies-specific but also strain-specific. The size of the plasmids associated with formation of the crystal protein was 42 and 50 Mdal in HD-191 (B. thuringiensis var kurstaki), 47 Mdal in HD-282 (B. thuringiensis var. aizawai), and 57 Mdal in IPS-82 (B. thuringiensis var. israelensis). The crystal protein gene of strain 140 (B. thuringiensis var. wuhanensis) was most possibly not located in plasmid, but in chromosomal DNA. The plasmid carring the crystal protein gene of the HD-191 was transfered into the mutant HD-1 (sp$^+$ cr$^-$) in high frequency and the gene encoding for crystal protein was expressed in the cells of HD-1. Transfer of the plasmid associated with crystal protein gene into cells of the IPS-82 from HD-1 (sp$^+$ cr$^-$) had failed, suggesting some incompatibility of the plasmid between them. (Paper received 5 Apr 85.)

REFERENCES

[1] Falcon, L. A.: Microbial Control of Insect and Mites, eds. Burges, H. D. and N. W. Hussey, Academic Press, p. 72—73, 1971.

[2] Gonzalez, J. M. et al.: *Plasmid*, **5**: 351—365, 1981.

[3] Ward, E. S. and D. J. Ellar: *FEBS Letters*, **158**(1): 45—49, 1983.

[4] Gonzalez, J. M. and B. C. Carlton: *Plsmid*, **11**: 28—38, 1984.

[5] Kamdar, H. and K. Jayaraman: *Biochem. Biophys. Research Commun.*, **110**(2): 477—482, 1983.

[6] Krostad, J. W. et al.: *J. Bacteriol.*, **154**(1): 419—428, 1983.

[7] Klier, A. et al.: *Mol. Gen. Genet.*, **191**(2): 257—262, 1983.

[8] Klier, A. et al.: *EMBO Journal*, **1**(7): 791—799, 1982.

[9] Martin, P. A. W. et al.: *J. Bacteriol.*, **145**(2): 980—983, 1981.

[10] Held, G. A. et al.: *Proc. Natl. Acad. Sci. USA*, **79**: 6065—6069, 1982.

[11] Kiier, A. et al.: *Nucleic Acids Research*, 3973—3987, 1984.

[12] Sharpe, E. S. et al.: *J. Invertebr. Path.*, **34**(3): 315—316, 1979.

[13] Goodman, N. S. et al.: *J. Bacteriol.*, 94(2): 485, 1967.

[14] Barbara, J. A. and K. W. Nickerson: *Appl. Environ. Microbiol.*, **36**(4): 625—626, 1978.

[15] Burges, H. D. et al.: *J. Invertebr. Path.*, **27**(1): 87—94, 1976.

[16] Eckhardt, T.: *Plasmid*, **1**: 584—588, 1978.

[17] Jarrett, P.: *FEMS Microbiology Letters*, **16**: 55—60, 1983.

[18] Laemmli, U. K.: *Nature* (London), **227**: 680—685, 1970.

[19] Gonzalez, J. M et al.: *Proc. Natl. Acad. Sci. USA*, **79**: 6951—6955, 1982.

THE CONDITIONS OF AMPICILLIN ACYLASE PRODUCTION BY AS 1.586

Beijing WEISHENGWU XUEBAO [ACTA MICROBIOLOGICA SINICA] in Chinese Vol 26 No 2, Jun 86 pp 154-159

[English abstract of article by Han Wenzhen [7281 2429 3791], et al., of Institute of Microbiology, Academia Sinica, Beijing]

[Text] An ampicillin acylase producing strain of Corynebacteria pekinense was selected, and conditions for the production of ampicillin acylase have been investigated. The suitable medium consisted of mono sodium glutamate 0.2 percent, yeast extract 0.2 percent. $K_2HPO_4 \cdot 3H_2O$ 0.3 percent, $MgCl_2$. $6H_2O$ 0.1 percent, $FeSO_4 . 7H_2O$ 0.01 percent, glucose 2 percent, $CdSO_4 . 3H_2O$ 0.1 percent, beef peptone 0.7 percent, pH 7.0. The optimal condition for enzyme production are as follows: 250 ml shake filled with 30 ml fermentation medium, 28°C, incubation period 24 h. Under such conditions, highest ampicillin acylase activities was about 5.4 u/ml. (Paper received 5 Feb 85.)

REFERENCES

[1] 张启先等: 微生物学报, **19** (3): 302—308, 1979。
[2] 王祯祥等: 微生物学报, **24** (4): 376—381, 1984。
[3] Kato, K. et al.: *Agric. Biol. Chem.*, **44**(5): 1069—1074, 1980.
[4] Smith, J. W. G. et al.: *Analyst*, **92**(1090 - 1101): 247—255, 1967.
[5] Marconi, W. et al.: *Agric. Biol. Chem.*, **39** (1—6): 277—279, 1975.
[6] Vandamme, E. J. et al.: Advances in applied microbiology, Academic press, New York, **17**: 311, 1974.

A STUDY ON ULTRA-LOW TEMPERATURE FREEZING OF BACTERIAL CULTURES

Beijing WEISHENGWU XUEBAO [ACTA MICROBIOLOGICA SINICA] in Chinese Vol 26
No 2, Jun 86 pp 164-169

[English abstract of article by Ma Yansheng [7456 1693 3932] of Institute of Microbiology, Academia Sinica, Beijing]

[Text] Response of the 19 bacterial strains belonging to 19 species in 10 genera subjected to liquid nitrogen freezing and thawing was reported. According to the cell survival rate, the protective efficiency of 10 percent glycerol and 10 percent DMSO was superior to distilled water after preservation at frozen state for 8 months. Only a few strains showed similar survival rate when they were protected with glycerol, DMSO or water. Rapid or slow freezing has no distinct effect on their viability. The high survival rate may be obtained with dense cell suspensions of Acetobacter rancens var. turbidans AS 1.41 and Brevibacterium ammoniagenes AS 1.844. Aerobacter aerogenes AS 1.489 was sensitive to freezing resulting to the lysis of cells as illustrated by electron microscopy.

After freezing and thawing, it was shown that the suspensions were transferred into test media, the lactic acid producing ability of Lactobacillus plantarum AS 1.557 and the sensitivity of Micrococcus lysodeikticus AS 1.634 to lysozyme were reduced. However, the ability of Corynebacterium crenatum AS 1.998 for L-isoleucine production, Escherichia coli AS 1.76 for penicillin acylase activity, Pseudomonas aeruginosa AS 1.647 for 2-keto-L-gulonic acid, and Lactobacillus plantarum AS 1.557 for lactic acid were not reduced when the frozen and thawed strains were activated. (Paper received 11 Oct 84.)

REFERENCES

[1] Smittle, R. E. et al.: *Appl. Microbiology*,**24**: 551−554, 1972.
[2] Bullen, J. J.: *Journal of General Microbiology*, **89**: 205−207,1975.
[3] 马德江等: 微生物学通报, **10**(3): 133−135, 1983。
[4] 潘家秀等: «蛋白质化学研究技术», 第 27−28 页,科学出版社, 北京, 1973。
[5] 张启先等: 微生物学报, **19**(3): 302−308, 1979。
[6] 北京大学生物系生物化学教研室: «生物化学实验指导»,第 163−166 页, 人民教育出版社, 北京, 1980。
[7] 蒋传葵等: «工具酶的活力测定», 上海科学技术出版社, 上海, 1982。

SUCCESS IN ESTABLISHING THE MSHA-POSITIVE PSEUDOMONAS AERUGINOSA FIMBRIAL STRAIN

Beijing WEISHENGWU XUEBAO [ACTA MICROBIOLOGICA SINICA] in Chinese Vol 26, No 2, Jun 86 pp 176-179

[English abstract of article by Mu Xiya [3664 1585 0068] of Department of Microbiology, Dalian Medical College, Dalian]

[Text] The author had successfully selected breeding a MSHA-positive Ps. aeruginosa fimbrial strain on April, 1984. This new MSHA-positive fimbrial strain was isolated and selected from clinical specimens.

It has strong MSHA and yeast agglutination characteristics. Up to more than one year, after propagating many generations, it still persists its main properties.

This fimbrial strain may be used as a standard positive control for fimbrial investigation in many area including microbiology, immunology, infection, epidemiology, etiology and genetics, etc. (Paper received 7 Dec 84.)

REFERENCES

[1] Sharon, N. et al.: Adhesion and Microorganism Pathogenicity. (Ciba Foundation Symposium 80) Pitman Medical, pp. 119--141, 1981.
[2] Ramphel, R. et al.: *Infect Immun*. 43: 34—40, 1984.
[3] Gaastron, M. and F. K. DeGraaf: *Microbiol. Rev*. 46: 129—161, 1982.
[4] Jann, K. et al.: *Infect Immun*. 34: 980—983, 1983.
[5] 余 㵑主编: «医用微生物学»，人民卫生出版社，北京，第 23 页；346 页，1983。
[6] Wolk, W. A. and M. F. Wheeler: Basic Microbiology, 3th ed., C. J. B. Lippincott Company, Philadelphic, Toronto, p. 46, 1973.
[7] Levine, M. et al.: *Infect Immun*. 39: 889—897, 1983.

TO INQUIRE INTO THE CLASSIFIABLE POSITION OF STREPTOMYCES ERYTHREUS 2577

Beijing WEISHENGWU XUEBAO [ACTA MICROBIOLOGICA SINICA] in Chinese Vol 26, No 2, Jun 86 pp 180-183

[English abstract of article by Wang Qianxing [3769 6197 5281], and Chen Xiaoqing [7115 5135 1987], of Sichuan Industrial Institute of Antibiotics, Chengdu, and Deng Yuxiu [6772 1342 4423] and Yan Xunchu [7051 6676 0443] of Institute of Microbiology, Academia Sinica, Beijing]

[Text] A erythromycin-producing strain previously named as Streptomyces erythreus 2577 was found having the chemical composition of cell wall of type IV and partly fragmented substrate mycelium and aerial spore chains of Streptomyces type. It has thick cell wall. The strain 2577 therefore is considered to belong to the genus Saccharopolyspora and renamed as Saccharopolyspora erythrea 2577 (Wakman & Curtis 1916; Waksman & Henrici 1948) Deng & Wang n. comb. 1984. (Paper received 21 Jan 85.)

REFERENCES

[1] 王谦兴等:«微生物学论文集»,科学出版社,北京,35—40页,1985。

[2] Waksman, S. A. and R. E. Curtis: *Soil Sci.*, 1: 99, 1916.

[3] Lechevalier, H. A. et al.: *J. Gen. Microbiol.*, 26: 11, 1961.

[4] Margaret, B. et al.: *Can. J. Microbiol.* 21 (10): 1500—1511, 1975.

[5] Cross, T. and M. Goodfellow: Actinomycetales charateristics and practical importance eds. Sykes, G. and Skinner, F. A. New York, 59—62, 1973.

[6] Henssen, A.: *Arch. Mikrobiol.* 26: 373—414, 1957.

/7358
CSO: 4009/1109

Neurology

Na, K$^+$-ATPASE ACTIVITY OF ERYTHROCYTE MEMBRANES IN PROGRESSIVE MUSCULAR DYSTROPHY

Beijing ZHONGHUA SHENJING-JINGSHENKE ZAZHI [CHINESE JOURNAL OF NEUROLOGY AND PSYCHIATRY] in Chinese Vol 19 No 3, 23 Jun 86 pp 129-131

[English abstract of article by Shen Dingguo [3088 1353 0948], et al., of the PLA General Hospital]

[Text] A study of the Na$^+$+K$^+$ ATPase activity of erythrocyte membranes in 34 patients with Duchenne's (pseudohypertrophic) muscular dystrophy and limb-girdle muscular dystrophy and also in 6 patients with infantile spinal muscular atrophy has been conducted. The control group consisted of 60 normal subjects of various ages. The results showed that in the control group the Na$^+$+K$^+$ ATPase activity was lower in normal children than in young adults and the same was true of the inhibitory reaction of ouabain on Na$^+$+K$^+$ ATPase activity. In the matched age groups of Duchenne's muscular dystrophy, the ATPase activity was found to be much lower while the inhibitory reaction of ouabain was increased. In cases of limb-girdle dystrophy, the ATPase activity was also lower, although the inhibitory reaction of ouabain did not reach the values of the normal subjects. However, neither the Na$^+$+K$^+$ ATPase activity nor the inhibitory reaction of ouabain showed any significant differences between the values found in infantile spinal muscular atrophy and those in the controls. This would seem to indicate that the presence of an enzyme defect might be shared by patients with Duchenne's muscular dystrophy and limb-girdle muscular dystrophy. (Paper received 28 March 1983, finalized 10 April 1985.)

REFERENCES

1. Brown HD, et al. Erythrocyte abnomarity in human myopathy. Sciences 1967;157:1577.
2. Peter JB, et al. Erythrocyte ghost adnosine triphosphatase in Duchenne muscular dystrophy. J Lab Clin Med 1969;74:103.
3. Araki S, Mawatari S. Ouabain and erythrocyte-ghost adenosine triphosphatase. Arch Neurol 1971; 24:187.
4. Niebroj-Dobosz I. Erythrocyte ghosts (Na$^+$+K$^+$) ATPase activity in duchenne dystrophy and myotonia. Zeit Für Neurol 1976;214:61.
5. Pearson TW. (Na$^+$+K$^+$)-ATPase of Duchenne muscular dystrophy erythrocyte ghosts. Life Science 1978;22:127.
6. Mawatari, et al. Biochemical abnormalities of erythrocyte membrances in Duchenne muscular dystrophy. Arch Neurol 1976;33:489.
7. Wacholtz MC, et al. Adenylate cyclase and ATPase activity in red cell membrances of patients and genitic carriers of duchenne muscular dystrophy. Clin Chim. Acta 1979;96:235.
8. Dunn MJ, et al. Erythrocyte ghost Na$^+$, K$^+$ ATPase in duchenne muscular dystrophy. J Neurol Science 1980;46:209.
9. Mawatari S, et al. Na$^+$+K$^+$-ATPase of erythrocyte membrances in Duchenne muscular dystrophy. Neurol 1981;31:293.

COMPUTERIZED SPECTRAL ANALYSES OF EEG IN PATIENTS WITH CEREBRAL THROMBOSIS

Beijing ZHONGHUA SHENJING-JINGSHENKE ZAZHI [CHINESE JOURNAL OF NEUROLOGY AND PSYCHIATRY] in Chinese Vol 19 No 3, 23 Jun 86 pp 136-137

[English abstract of article by Wu Xun [0702 6676] of Beijing Medical College; et al.]

[Text] The results of visual and computerized spectral analyses of the EEGs of 18 patients with cerebral thrombosis have been compared. Localized abnormalities were found in 7 of the 18 (38.9 percent) by visual analysis and in 12 of the 18 (66.7 percent) by computerized spectral analysis. Among 12 patients in the acute stage of the disease, localized abnormalities were observed in 6 of the 12 (50 percent) under visual analysis and in 10 of the 12 (83 percent) under computerized spectral analysis. Among six patients in the recuperative stage, localized abnormalities were seen in one of the six by visual analysis and in two of the six by computerized spectral analysis. The authors believe computerized spectral analysis can raise the positive rate of localized abnormalities in the EEGs of patients with cerebral thrombosis. (Paper received 3 November 1984, finalized 16 March 1985.)

REFERENCES

1. 冯应琨. 临床脑电图学. 北京：人民卫生出版社，1980:58.
2. Suess W, et al. EEG power spectrum during ballon occlusion test before carotid ligation. EEG Clin Neurophysial 1984;57:31.
3. 方丹群，等. 噪声对青少年脑功能的影响在诱发脑电脉冲响应指标上的表现. 环境与健康杂志 1984;1:17.
4. Sainio K, et al. Visual and spectral EEG analysis in the evaluation of the outcome in patients with ischemic brain infartion. EEG Clin Neurophysial 1983;56:117.
5. Tolonen U, et al. Comparison of quantitative EEG parameters from four different Analysis techniques in evaluation of relationships between EEG and CBF in brain infarction. EEG Clin Neurophysial 1981;51:177.

CYTOGENETIC CHANGES IN 48 CASES OF SCHIZOPHRENIA

Beijing ZHONGHUA SHENJING-JINGSHENKE ZAZHI [CHINESE JOURNAL OF NEUROLOGY AND PSYCHIATRY] in Chinese Vol 19 No 3, 23 Jun 86 pp 188-191

[English abstract of article by Hong Meiling [3163 5019 3781], et al., of the Military Medical School, Shenyang Unit, PLA; et al.]

[Text] A preliminary study in the field of cytogenetics was made in a group of 48 cases of schizophrenics, with 37 volunteers as the normal control group. Pericentric inversion of chromosome 9 was confirmed by c-band and G-band techniques in 10 cases of the patient group, whereas only 1 was found in the control group ($P > 0.05$). As documented in the previous literature, schizophrenic patients tend to have a higher occurrence rate of pericentric inversion of chromosome 9, indicating that there is a possible correlation between this sort of chromosonal abnormality and the pathogenesis of schizophrenia. In addition, 3 of the 10 cases studied were twins. All the twin brothers suffered from psychoses. Two of the three pairs of twins were nomozygotic with paranoic schizophrenia. Pericentric inversion of chromosome 9 may exert some pathogenetic significance. (Paper received 10 September 1984, finalized 23 May 1985.)

REFERENCES

1. Axelsson R and Wahlström J. Mental disorder and inversion on chromosome 9. Hereditas 1981;95:337.
2. 上海第二医学院生物教研组．医学遗传学基础．上海：上海第二医学院印刷厂，1982:140—141.
3. Chapelle AD, et al. Pericentric inversions of human chromosome 9 and 10. AMJ Hum Genet 1974;26:746.
4. Saxena R, et al. 精神治疗药甲硫达嗪对人体内染色体的断裂效应．国外医学遗传学分册 1983;5:271.
5. Grouchy JD, et al. Chromosome 9. Clinical Atlas of Human Chromosome. New York: John Wiley, 1977:71—93.

9717
CSO: 4009/1097

Oncology

REGIONAL DISTRIBUTION OF LIVER CANCER AND ITS RELATION TO SELENIUM LEVEL IN QIDONG COUNTY, CHINA

Beijing ZHONGHUA ZHONGLIU ZAZHI [CHINESE JOURNAL OF ONCOLOGY] in Chinese Vol 8 No 4, 23 Jul 86 pp 262-264

[English abstract of article by Li Wenguang [2621 2429 1639], et al., of Qidong Liver Cancer Institute, Jiangsu, and Yu Shuyu [0060 2885 3768], et al., of Cancer Institute, Chinese Academy of Medical Sciences, Beijing]

[Text] The selenium (Se) level in barley and maize from 43 communes of Qidong county, a high risk area of liver cancer in China, were assayed. An inverse correlation between the Se level and the liver cancer incidence was observed. An inverse correlation was also observed between the blood Se level and liver cancer incident of the local residents. When selenite solution was sprayed on the crops during their preflowering, the content of Se in barley and maize was increased by 6 fold over the control. It is suggested that the increase of blood Se level of the residents who live in the low-Se areas by this method be useful in the prevention of liver cancer. (Paper received 29 Jan 85, finalized 27 May 85.)

REFERENCES

1. 王光亚，等. 生物样品、水及土壤中痕量硒的荧光测定法. 营养学报 1985; 7(1):17
2. Griffin A C, et al. Effect of Selenium on azo dye hepatocarcinogenesis. Cancer Letters 1977, 3: 177
3. Passwaters RA. Selenium as Food and Medicine. New Canaan: Keats Rublishing Inc,1980:198.

DEVELOPMENT OF OCCULT THYROID CARCINOMA

Beijing ZHONGHUA ZHONGLIU ZAZHI [CHINESE JOURNAL OF ONCOLOGY] in Chinese Vol 8 No 4, 23 Jul 86 pp 280-282

[English abstract of article by Zhang Zhida [1728 1807 6671] of Nanjing Air Force Hospital, Nanjing]

[Text] Developmental features of 16 patients with occult thyroid carcinoma less than 1.0 cm in diameter as collected from our surgical specimens are described. They are classified into 3 types: non-capsular sclerosis, capsular non-sclerosis and non-capsular non-sclerosis types. Non-capsular non-sclerosis type is the developmental form at early stage. Tumors that grow rapidly and to which the host has a strong reactivity tend to change into the non-capsular sclerosis type. On the contrary, those which grow slowly to which the host is weak in reaction tend to change into the capsular non-sclerosis type. The relation between the histological classification and developmental form is discussed. (Paper received 12 Dec 85.)

REFERENCES

1. Sampson RL. et al. Smallest forms of papillary carcinoma of the thyroid: A study of 14 microcarcinoma less than 0.1cm in greatest dimension. Arch Path 1971, 91:334
2. 高嶋成光，他．潜在性甲状腺癌の臨床病理学の研究：乳頭癌の発育様式しいて．癌の臨床 1980，26:1,318
3. 坂本穆彦，他．剖検例にみられた甲状腺潜伏癌．癌の臨床 1982，28:106
4. Hazard TB. Small papillary carcinoma of thyroid: A study with special reference to socalled nonencapsulated sclerosing tumor. Lab Invest 1960,9:86
5. Klink GH, Winship T. Occult sclerosing carcinoma of the thyroid. Cancer 1955, 8:701
6. Woolner LB, et al. Occult papillary carcinoma of the thyroid gland: A Study of 140 cases observed in a 30 years peroid. J Clin Endocrinol 1960, 20:89
7. Mannel AS, et al. Latent thyroid carcinoma at autopsy. Cancer 1979, 43:1,702
8. Richard JS, et al. Occult thyroid carcinoma in Olmsted County Minnesota: Prevalence at autopsy compared with that in Hiroshima and Nagasaki Japan. Cancer 1974, 34:2,072

/7358
CSO: 4009/1112

Optics

16μm CW PbSnSe SEMICONDUCTOR TUNABLE LASERS AND THEIR USES IN HIGH RESOLUTION SPECTROSCOPY

Shanghai GUANGXUE XUEBAO [ACTA OPTICA SINICA] in Chinese Vol 6 No 7, Jul 86 pp 592-597

[English abstract of article by Wang Hailong [3769 3189 7893], et al., of Shanghai Institute of Optics and Fine Mechanics, Academia Sinica]

[Text] We report the tuning characteristics of 16μm CW PbSnSe diode lasers. We have measured CO_2 absorption spectra near $618cm^{-1}$, $623cm^{-1}$, $634cm^{-1}$ and $667\ cm^{-1}$ as well as N_2O absorption spectra near $618cm^{-1}$ and $588cm^{-1}$. These results show that the mode quality of these lasers is high and the single-mode tuning range is wide.

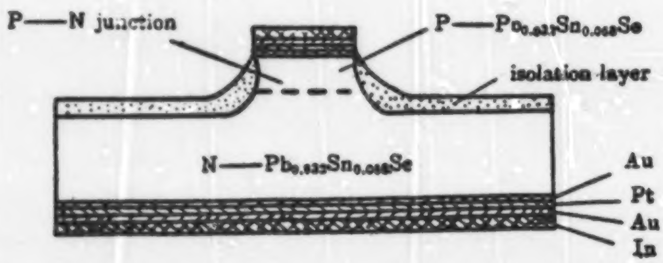
P—N junction
P—$Pb_{0.932}Sn_{0.068}Se$
isolation layer
N—$Pb_{0.932}Sn_{0.068}Se$
Au
Pt
Au
In

Fig. 1 Schematic diagram of a PbSnSe homojunction laser with stripe-geometry

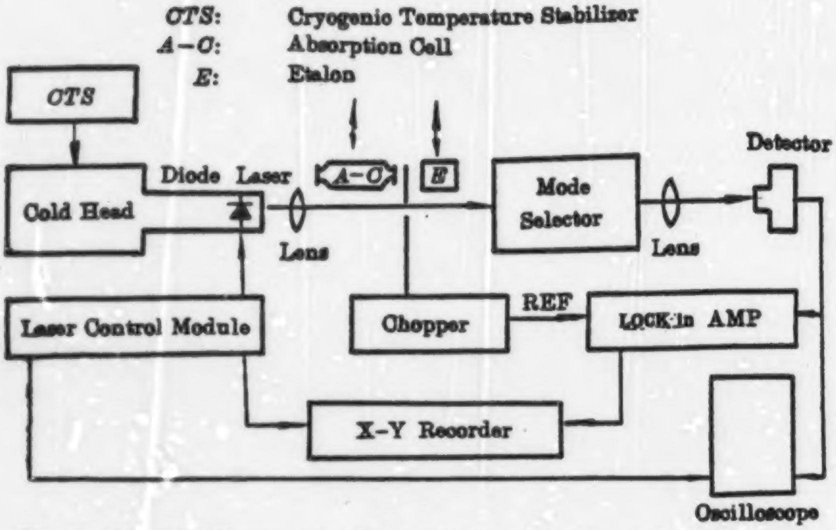
CTS: Cryogenic Temperature Stabilizer
A–C: Absorption Cell
E: Etalon
CTS
Cold Head
Diode Laser
Lens
A–C
E
Mode Selector
Lens
Detector
Laser Control Module
Chopper
REF
LOCK-in AMP
X-Y Recorder
Oscilloscope

Fig. 5 Schematic diagram of a high-resolution spectrometer using a diode laser

(Paper received 21 Nov 85.)

A NEW METHOD FOR SUPPRESSING RAYLEIGH NOISE IN AN OPTICAL FIBER GYROSCOPE

Shanghai GUANGXUE XUEBAO [ACTA OPTICA SINICA] in Chinese Vol 6 No 7, Jul 86
pp 630-636

[English abstract of article by Cao Xuelong [2580 7185 7893], et al , of Shanghai University of Science & Technology, Shanghai Institute of Optical Fibre Technology and Modern Communication]

[Text] After making analysis of Rayleigh noise characteristics in an optical fiber gyroscope, we developed a new method to suppress the noise. Theoretically, we found that with this method the Rayleigh noise can be suppressed by a factor of $|J_o(\phi m)|$, here $J_o(x)$ is the zeroth-order Bessel function and ϕ_m the modulation amplitude. Therefore, with a proper modulation the noise can be reduced to zero. This new method is simpler and more effective than that using band-pass noise phase modulation.

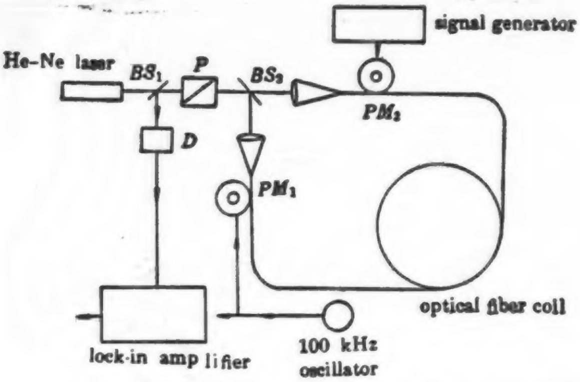

Fig. 1 Exprimental setup of an optical fiber gyroscope

(Paper received 9 Oct 85, finalized 9 Dec 85.)

ANALYSIS OF THE REFLECTION WAVE OF CONE BEAM FROM A MULTILAYER THIN FILM

Shanghai GUANGXUE XUEBAO [ACTA OPTICA SINICA] in Chinese Vol 6 No 7, Jul 86 pp 644-649

[English abstract of article by Qian Qiuming [6929 4428 2494], et al., of Shanghai Institute of Optics and Fine Mechanics, Academia Sinica]

[Text] The reflection wave of a cone beam, which is formed by a linearly polarized plane wave through a convergence system and then incident upon a stratified medium, is analyzed. The reflection phase shift in the whole aperture and the dispersion are figured out by using the expression of the electric field strength which is derived in the paper. Furthermore, aberrations can be discussed while the multilayer thin film is regarded as an element of an imagining system.

In addition, an expression of the intensity distribution of the interference field produced by two reflection waves with the initial waves of SM (the electric vector is perpendicular to the plane of main ray incidence) and PM (the electric vector is parallel to the plane of main ray incidence), is deduced. Specially applied to a multilayer composed of seventy-one layers, the numerical calculation conforms to experimental results quite well. (Paper received 22 Oct 85.)

/7358
CSO: 4009/110

Petrochemicals

MATHEMATICAL MODEL FOR HEAVY OIL CRACKING--PROCESS CALCULATION MODEL FOR RADIANT SECTION TUBES IN CRACKING FURNACE

Beijing SHIYOU HUAGONG [PETROCHEMICAL TECHNOLOGY] in Chinese Vol 15 No 1, Jan 86 pp 1-9

[English abstract of article by Huang Wen [7806 2429], et al., of China Huanqin Chemical Engineering Corporation; and Yang Yuanyi [2799 0337 0001], et al., of Beijing Research Institute of Chemical Industry]

[Text] This paper is the second part of an article on mathematical modeling of a cracking furnace tube. The process-calculation model is based on the correlation of product distribution with the cracking severity function $k\theta$ and hydrocarbon partial pressure, with due consideration taken of heat, mass and momentum balance within the furnace tube. According to different raw materials, the appropriate type of furnace can be selected, and the furnace tube size, operating parameters and product yields are calculated.

This model can also be used to select the proper process operating parameters and predicted yields when changing raw materials. (Paper received 13 February 1985.)

REFERENCES

〔1〕 化工部化工设计公司、北京化工研究院，"重质油品裂解辐射管工艺设计简介"，1982年（未发表）。
〔2〕 杨元一等，石油化工，13〔11〕，703(1984).
〔3〕 邹仁鋆，"石油化工裂解原理与技术"，化学工业出版社，1981.
〔4〕 Sundaram, K. M.; Froment G. F. *Ind. Eng. Chem. Fundam.*, 17〔2〕, 174(1978).
〔5〕 Kniel, L. et al. "Ethylene Keystone To the Petrochemical Industry". p. 121, Marcel Dekker, New York, 1980.
〔6〕 Shu, W. R. et al., *Oil Gas J.*, 77〔36〕, 72 (1979).
〔7〕 Van Damme, P. S.; Froment, G. F., *Ind. Eng. Chem. Process Des. Devolop.*, 20〔2〕, 366(1981).
〔8〕 Zdonik, S. B. et al., *Oil Gas J.*, 65〔26〕, 96 (1967).
〔9〕 兰化设计院："石油化工技术参考资料 石油化工工业炉设计"（未发表）.
〔10〕 "Technical Date Book—Petroleum Refining", 3rd ed., p. 179, American Petroleum Institute Refining Department, 1976.
〔11〕 Ernst Schmidt V. D. I著，西安热工研究所译，"水和水蒸汽热力学性质图表"，p. 165—166，水电电力出版社，1977.
〔12〕 北京石油化工总厂前进化工厂，"三十万吨乙烯装置工艺技术考核总结"，1976（未发表）.

INFLUENCE OF PRETREATMENT AND MODIFICATION WITH OXIDES ON ZSM-5 CATALYST FOR TOLUENE ETHYLATION

Beijing SHIYOU HUAGONG [PETROCHEMICAL TECHNOLOGY] in Chinese Vol 15 No 1, Jan 86 pp 10-14

[English abstract of article by Dong Jialu [5516 1367 74583-6922], et al., of the Department of Chemistry, Nanjing University]

[Text] The influence of pretreatment with steaming or coking and modification with oxides on ZSM-5 zeolite catalyst for ethylation of toluene has been studied. The increasing effect of pretreatment on the para-selectivity of ethylation was steaming < coking < steaming + coking. As for modification with oxides, the effect was $MgO < Sb_2O_5 < P_2O_5$, P_2O_5-MgO.

The conversion of toluene and *p*-selectivity over P_2O_5-MgO-ZSM-5 catalyst (20 cc) was about 12.5 percent and 97 percent respectively. (Paper received 2 April 1985.)

REFERENCES

〔1〕 Kaeding, W. W., et al., *J. Catal.*, 67, 159 (1981).
〔2〕 Kaeding, W. W., et al., *J. Catal.*, 69, 392 (1981).
〔3〕 Young, L. B., et al., *J. Catal.*, 76, 418(1982).
〔4〕 Anderson, J. R., et al., *J. Catal.*, 61, 477 (1980).
〔5〕 E. P., O, 014.545 A_1(1980).
〔6〕 U. S., 4,413,084(1979).
〔7〕 U. S., 4,365,104(1981).
〔8〕 E. P. O, 039,538 A_1(1981).
〔9〕 Kaeding, W. W., et al., *J. Catal.*, 89, 269 (1984).
〔10〕 须沁华、朱建华，"HZSM-5沸石催化剂上甲苯的烷基化反应"(待发表)。
〔11〕 Xu Qinhua, Zhu Jianhua, "Proceedings of the International Symposium on Zeolite Catalysis", p. 181, Sio'tok/Hungary, 1985.
〔12〕 Yashima, T., et al., "New Horizons in Catalysis", p. 739(A52). Vedrine, D. C., et al., *J. Catal.*, 59, 248(1979).

(本稿于1985年4月2日收到。)

PREVENTION OF QUENCH-BOILER CORROSION

Beijing SHIYOU HUAGONG [PETROCHEMICAL TECHNOLOGY] in Chinese Vol 15 No 1, Jan 86 pp 27-31

[English abstract of article by Wang Deying [3769 1795 5391], et al., of the Research Institute of Metal Corrosion and Protection, Chinese Academy of Sciences, Shenyang]

[Text] This paper investigates the prevention of corrosion in the quench boiler. By improving boiler feed water treatment, enhancing deoxygenation efficiency, implementing close automatic pH control and adopting better drainage processes so as to avoid accumulation of impurities and formation of precipitates, the international standards have been reached, with no deposition on the lower pipe plate. Therefore, boiler corrosion can be prevented without shutdown and the service life is extended, bringing about remarkable economic benefits. (Paper received 4 March 1985.)

REFERENCES

〔1〕 王德英等，石油化工，14〔12〕，(1985).
〔2〕 清水博著，许景文编译，"离子交换树脂" p. 198，上海科学技术出版社。
〔3〕 Evans. U. R., "The Corrosion and Oxidation of Metals". p. 427, Edward Arnold (Publishers) LTD., London 1960.
〔4〕 Betz Laboratories 编，秦裕珩等译，"工业水处理手册"，p.82，化学工业出版社，1982.
〔5〕 Mann, G. M. W., *Br. Corros. J.* 12〔1〕, 6 (1977).
〔6〕 Dennis, A. F., "Corrosion 80", Vol. 3, 77/1.
〔7〕 Cotton, I. J., "Corrosion 80", Vol. 3, 80/1.
〔8〕 Mann, G. M. W., *Mater. Perf.*, 19〔10〕, 32 (1980).
〔9〕 Gobrielli, F., et al., *Power*, 122〔7〕,46 (1978).
〔10〕 Ashford, J. H., et al., *Corrosion Sci.*, 14〔9〕, 515(1978).
〔11〕 Grabenski, H. A., *Trans. Am. Soc. Mech. Engrs.*, 77〔5〕,433(1955).
〔12〕 Mann, G. M. W., "Pro. Int. Conf. High Temp. High Press. Electrochem. in Aq. Solns." p. 34, Guildford, 1973.
〔13〕 Biernat, R. J., et al., *Electrochem. Acta*, 17〔7〕1261(1972).

(本稿于1985年3月4日收到。)

9717
CSO: 4009/1119

END

JPRS-CST-86-041

1 OCTOBER 1986

China Report

SCIENCE AND TECHNOLOGY

HUMAN, ANIMAL EXPERIMENTS DETERMINE LASER INJURY THRESHOLDS

FBIS FOREIGN BROADCAST INFORMATION SERVICE

NOTE

JPRS publications contain information primarily from foreign newspapers, periodicals and books, but also from news agency transmissions and broadcasts. Materials from foreign-language sources are translated; those from English-language sources are transcribed or reprinted, with the original phrasing and other characteristics retained.

Headlines, editorial reports, and material enclosed in brackets [] are supplied by JPRS. Processing indicators such as [Text] or [Excerpt] in the first line of each item, or following the last line of a brief, indicate how the original information was processed. Where no processing indicator is given, the information was summarized or extracted.

Unfamiliar names rendered phonetically or transliterated are enclosed in parentheses. Words or names preceded by a question mark and enclosed in parentheses were not clear in the original but have been supplied as appropriate in context. Other unattributed parenthetical notes within the body of an item originate with the source. Times within items are as given by source.

The contents of this publication in no way represent the policies, views or attitudes of the U.S. Government.

PROCUREMENT OF PUBLICATIONS

JPRS publications may be ordered from the National Technical Information Service, Springfield, Virginia 22161. In ordering, it is recommended that the JPRS number, title, date and author, if applicable, of publication be cited.

Current JPRS publications are announced in Government Reports Announcements issued semi-monthly by the National Technical Information Service, and are listed in the Monthly Catalog of U.S. Government Publications issued by the Superintendent of Documents, U.S. Government Printing Office, Washington, D.C. 20402.

Correspondence pertaining to matters other than procurement may be addressed to Joint Publications Research Service, 1000 North Glebe Road, Arlington, Virginia 22201.

JPRS-CST-86-041
1 OCTOBER 1986

CHINA REPORT
SCIENCE AND TECHNOLOGY
HUMAN, ANIMAL EXPERIMENTS DETERMINE LASER INJURY THRESHOLDS

Shanghai ZHONGGUO JIGUANG in Chinese Vol 12 No 10, 20 Oct 85 pp 577-640
Shanghai ZHONGGUO JIGUANG in Chinese Vol 12 No 12, 20 Dec 85 pp 735-738
Shanghai YINGYONG JIGUANG in Chinese Vol 6 No 3, Jun 86 pp 141-144

CONTENTS

ZHONGGUO JIGUANG No 10, 20 Oct 85

Editor's Note.......... 1

Measurement of Erythematous Reaction by Argon Laser Light for Skin of Yellow Race (pp 577-581)
(Li Jishi, et al.).......... 2

Study of Injury Threshold of CW Nd:YAG Laser Light for Human Skin (pp 582-585)
(Ma Baozhang, et al.).......... 11

Injury Threshold of Ruby Laser Irradiation on Human Skin (pp 586-588)
(Chen Ji, et al.).......... 17

Acute Injury Threshold Level of CO_2 Laser Light for Skin of Yellow Race (pp 589-591, 588)
(Shi Hongmin, et al.).......... 22

Study of Injury Threshold of Skin Irradiated With 265 nm Pulsed Laser Light (pp 592-596)
(Li Zhaozhang, et al.).......... 28

Investigation of Laser Injury Threshold of Skin (pp 597-599, 596)
(Wu Qingzhen, et al.).......... 35

Injury Threshold of Retina Irradiated by Argon Laser Light (pp 600-602)
(Wang Kangsun, et al.) 42

Experimental Study on Injury Threshold of Animal Retinas by 488 nm Laser Irradiation (pp 603-605)
(Zhao Tongzhen, et al.) 47

Research on Injury Threshold of Rabbit Cornea by CO_2 Laser (pp 606-608, 605)
(Wang Kangsun, et al.) 53

Research on Injury Threshold of Gray Rabbit's Retina by Q-Switched, Frequency Doubled Nd^{3+}:YAG Laser (pp 609-611)
(Wang Kangsun, et al.) 58

Retinal Injury Threshold by CW Nd^{3+}:YAG Laser Light (pp 612-614)
(Xu Jiemin, et al.) 63

Injury Threshold of Human Eye by Pulsed YAG Laser Beams, Pathological Observation (pp 615-617)
(Chen Rongjia, et al.) 68

Study of Retinal Injury Threshold for Nd:YAG Frequency-Doubled Laser Light (pp 618-620)
(Xu Jiemin, et al.) 72

Retinal Injury Threshold of Long Pulse Ruby Laser Light (pp 621-622)
(Xu Jiemin, et al.) 77

A Study of Single Mode He-Ne Laser Injury Threshold of Rabbit Eye (pp 623-625, 585)
(Ding Weiling, et al.) 81

Research on Injury Threshold of Chinese Yellow Skin by CW Nd:YAG Laser Beam Irradiation (pp 626-628)
(Wu Tingbi, et al.) 87

Research on Injury Threshold of Chinese Yellow Skin Irradiated With 300 μs Pulsed Neodymium Glass Laser Light (pp 628-630)
(Wu Tingbi, et al.) 92

Injury Threshold of Ruby Laser Irradiation on Pig Skin (pp 631-632)
(Wang Jun, et al.) 96

Morphological Analysis of Retinal Injury in Rabbits Arising From Argon Laser Irradiation (pp 633-634)
(Zhang Xiaoru, et al.) 101

Retinal Injury Threshold of Rabbits, Monkeys Irradiated by CW or Pulsed YAG Laser Beams (pp 634-635)
(Chu Renyuan, et al.) 104

Experimental Study on Retinal Injury Threshold of Animal by 694.3 nm Laser Irradiation (pp 636-637)
(Zhao Tongzhen, et al.) 108

Measurement of Laser Spot Diameter on Retina, Cornea (pp 637-638)
(Dang Zhiping, et al.) 112

Measurement of Transmissivity of Argon Laser Light Through Rabbit's Eyes (pp 638-639)
(Li Yujun, et al.) 114

ZHONGGUO JIGUANG No 12, 20 Dec 85

Injury Threshold of Skin Irradiated With 308 nm Excimer Laser Light Studied (pp 735-738)
(Li Zhaozhang, et al.) 117

YINGYONG JIGUANG No 3, Jun 86

Laser Safety, Protection Standards Reviewed (pp 141-144)
(Li Zhaozhang) 123

Editor's Note:

[Text] In the development of laser technology and application, laser safety and protection are becoming increasingly important. The State Science and Technology Commission of the People's Republic of China has given laser safety a high priority and ordered a study of "Laser Safety and Protection Standards--Measurement of the Laser Damage Threshold on Eyes and Skin." After 3 years of intensive research, the research units have accomplished their goals and a symposium was held in Guangzhou in March 1985 to summarize and exchange the results. This issue of ZHONGGUO JIGUANG is devoted to the reports of research results on the laser safety.

Limited by space, 23 papers are published in this issue and other articles will be published subsequently. Most of the papers report experimental results. Since a number of the experimental studies used basically the same method, the editors have abridged and revised some of the papers to avoid repetition and appreciate the understanding of the authors.

MEASUREMENT OF ERYTHEMATOUS REACTION BY ARGON LASER LIGHT FOR SKIN OF YELLOW RACE

Shanghai ZHONGGUO JIGUANG [CHINESE JOURNAL OF LASERS] in Chinese Vol 12, No 10, 20 Oct 85 pp 577-581

[Article by Li Jishi [2621 3444 2514], Shi Hongyu [0670 1347 3022], Tan Yankang [6223 1693 1660], Luo Panxiang [5012 3140 4382], and Chen Zhongben [7115 0112 2609] of the Department of Physics, Zhongshan Medical College, and Yuan Yuehuan [5913 1878 2970] of Zhongshan Medical College, Guangzhou]

[Text] Abstract: This paper describes an Ar^+ laser used for measuring the MRD_{50} value of the skin of the yellow race. The skin erythematous reaction threshold levels for two groups of volunteers are found to be at 488.0 nm and 514.5 nm. The skin of the volunteers is exposed to laser radiation at these two wavelengths and histological examination finds the capillaries expanded and filled with erythrocytes and light edema, but there is no significant change of the cuticle.

In addition to hazards to the human eye and the central nervous system, lasers can also cause various levels of skin damage.[1] As the radiation level increases, the skin may show erythema, erythema with white specks, whitening of the skin, blisters, burns, and vaporization.[2] The erythema is caused by capillary congestion and tissue reddening.[3] In research on laser safety, visual observation of the erythema is often used.[4] For a fixed exposure time, the minimum radiation level that causes 50 percent of erythema retention probability--the erythematous reaction threshold--is known as the MRD_{50} value.[5]

The MRD_{50} value depends on the wavelength, the radiation level, and the skin pigment. Measurement of the MRD_{50} of the skin of the white and black races using an Ar^+ laser with a wavelength in the 488-514 nm range has been reported.[5] In this work we measure the MRD_{50} of the skin of the yellow race using 488.0 nm and 514.5 nm Ar^+ lasers with a spot diameter of 0.5 cm for a duration of 1 second. The study is aimed at providing a data base for the establishment of a laser safety standard in China.

I. Experimental Setup and Conditions

Figure 1 shows the experimental setup. The CW Ar$^+$ laser operated in the fundamental transverse mode and produces a single spectral line. The output power is continuously tunable and the maximum output is 2.5 W.

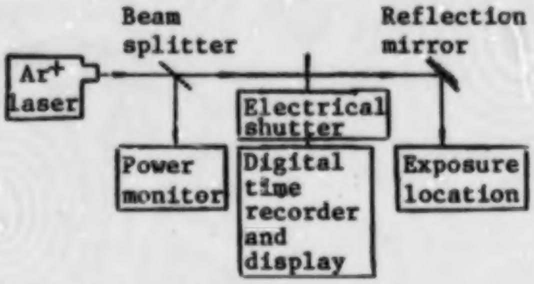

Figure 1. Experimental setup

The beam from the Ar$^+$ laser passes through a beam splitter, an electrically controlled shutter, and is reflected by a mirror. The beam then illuminates the skin at normal incidence. The Gaussian distribution amplitude of the laser power is measured by moving an orifice (less than 1/10 of the beam diameter) across the beam at the illumination location. The light spot diameter[2-4] is the distance between the two $1/e^2$ points. In our experiment the spot diameter is 0.5 cm.

A power monitor device is used in the experiment. The monitor consists of a silicon photocell (or a silicon photodiode) and a sensitive galvanometer. The stability of the photoelectric current is a measure of the light power stability. All experiments are made with the light power stabilized to within 5 percent.

For a fixed light power and spot size, the radiation of the skin depends on the illumination time. The time is controlled by an electrical shutter in the optical path. The irradiation time is 1 second with an error less than 5 percent. All measurements are made at room temperature (20 ± 5°C) and under a relative humidity less than 80 percent.

Each group of volunteers consists of half males and half females in the 20-22-year-old age range. The volunteers are all of the yellow race but with varying skin complexion. There is no damage on the skin of the side of the right forearm before the laser irradiation. After cleaning, the target location is marked with the lattice pattern in Figure 2. The center-to-center distance of the lattice is 2 cm, the numbers 1, 2, 3, 4, and 5 indicate the locations for five different radiation levels. No anaesthesia was applied. Observation and erythema counting were made 5 minutes after each irradiation.

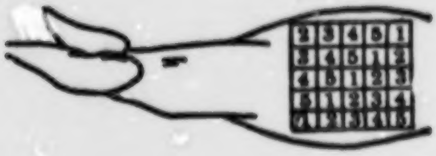

Figure 2. Arrangement of the irradiation spots on the side of the forearm

II. Experimental Method and Data

Using the setup described above, preliminary tests are made on several volunteers using Ar$^+$ lasers (488.0 nm and 514.5 nm). The minimum radiation level for producing erythema that vanishes within 5 minutes is estimated. The maximum radiation level for retaining erythema after 5 minutes but without causing whitening is also estimated. The formal measurements are based on the estimated maximum and minimum radiation level. The energy densities at 488.0 nm for the five spots numbered 1 through 5 are respectively 6.67, 6.07, 5.52, 5.03, and 4.58 J/cm^2. For the 514.5 nm Ar$^+$ laser, the energy densities are 8.85, 8.06, 7.33, 6.67, and 6.07 J/cm^2. The ratio of adjacent levels is 1:0.91.

In the formal tests, the six volunteers in the same group are subjected to 1-second exposures at the five different radiation levels of the same wavelength according to the pattern in Figure 2. Each volunteer is subjected to five radiation levels at five spots and n is equal to 30 for the whole group. Five minutes after the exposure, the erythema is examined by two observers under the same lighting conditions to determine the erythema retention number r and the probability r/n. The data are listed in Tables 1 and 2.

Table 1. Erythema Retention Number at 5 Minutes After a 1-Second Exposure of a 488.0 nm Ar$^+$ Laser

Number	Radiation level (J/cm^2)	Number of shots n	Erythema retention r	Probability P
1	6.67	30	28	0.93
2	6.07	30	21	0.70
3	5.52	30	14	0.47
4	5.03	30	6	0.21
5	4.58	30	0	0

Table 2. Erythema Retention Number at 5 Minutes After a 1-Second Exposure of a 514.5 nm Ar^+ Laser

Number	Radiation level (J/cm^2)	Number of shots n	Erythema retention r	Probability P
1	8.85	30	29	0.97
2	8.06	30	25	0.83
3	7.33	30	21	0.70
4	6.67	30	12	0.40
5	6.07	30	0	0

III. Data Processing and Results

Using the data in Tables 1 and 2, the linear regression equation of the unit retention probability y [out of 10] versus the logarithmic radiation level x, the MRD_{50} value and the confidence level are found by a statistical regression method.[6,7]

(1) MRD_{50} of 488.0 nm Ar^+ radiation

The linear regression equation for the 488.0 nm Ar^+ laser on the skin of the yellow race is found to be

$$y = 20.430\ x - 10.342$$

Figure 3 shows the regression straight line. As can be seen, four experimental points fall on the straight line and the first experimental point deviation slightly from the straight line.

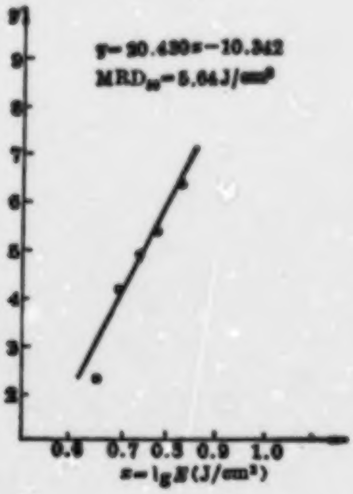

Figure 3. Regression straight line of the erythematous reaction due to 488.0 nm Ar^+ laser. The open circles are the experimental points.

Using the regression equation or Figure 3, the logarithmic radiation level $x = m$ corresponding to $y = 5$ (i.e., 50 percent probability for erythema retention) can be found and $MRD_{50} = lg^{-1}\ m$. Calculations show that

$$MRD_{50} = 5.64\ J/cm^2$$

and the 95 percent confidence range for MRD_{50} is

$$5.47\ J/cm^2 \sim 5.81\ J/cm^2.$$

(2) MRD_{50} of 514.5 nm Ar^+ radiation

Calculations show that the linear regression equation for the 514.5 nm Ar^+ laser is

$$y = 19.990\ x - 11.958$$

Figure 4 shows the regression straight line. Again, all except one point fall on the straight line. The calculated MRD_{50} is

$$MRD_{50} = 7.05\ J/cm^2$$

and the 95 percent confidence range for MRD_{50} is

$$6.76\ J/cm^2 \sim 7.28\ J/cm^2$$

The MRD_{50} results for the Ar^+ laser at the two wavelengths of 488.0 nm and 514.5 nm on the skin of the yellow race are summarized in Table 3.

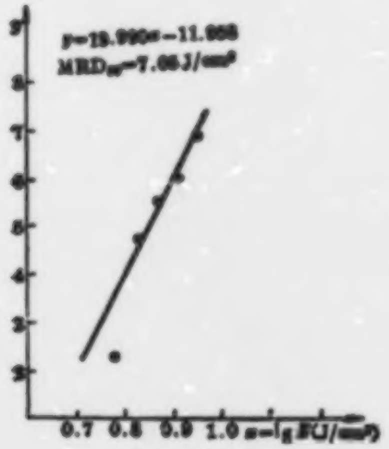

Figure 4. Regression straight line of the erythematous reaction due to 514.5 nm Ar^+ laser. The open circles are the experimental points.

Table 3. MRD_{50} of 488.0 nm and 514.5 nm Ar^+ Laser on the Skin of the Yellow Race

Ar^+ laser wavelength (nm)	MRD_{50} (J/cm^2)	MRD_{50} 95 percent confidence range (J/cm^2)
488.0	5.64	5.47 ~ 5.81
514.5	7.05	6.76 ~ 7.28

IV. Histological Examination

The normal skin on the side of the forearms of four volunteers of the yellow race in the 21-28 age range is irradiated with the MRD_{50} level of 5.6 J/cm^2 at 488.0 nm and with the MRD_{50} level of 7.1 J/cm^2 at 514.5 nm for 1 second. Histological and pathological examinations are then performed with an optical microscope for skin samples taken at the erythematous locations at 5 minutes and 30 minutes after the irradiation. On the samples taken 5 minutes after the irradiation, capillary expansion is found in the papillary layer and the shallow layer of the dermis. Most of the capillaries are filled with erythrocytes, the shallow layer of the dermis shows slight edema, the blood vessels in the deep layer of the dermis are also found to be expanded and congested, but the cuticle shows no obvious changes, as shown in Figures 5(a), 5(b), and 6(a). On the samples taken 30 minutes after the irradiation, capillary expansion is found, the congestion is slight, and no edema is observed, as shown in Figures 5(c), 5(d), and 6(b).

The histological examination results show that the effects of the MRD_{50} radiation on the skin are the congestion of the capillaries and slight edema of the shallow layer of the dermis. No serious histological damage is found. As the erythema recedes, so do the histological and pathological changes. The erythematous reaction is therefore a reversible reaction.

V. Discussion

Table 3 shows that the MRD_{50} of the 514.5 nm Ar^+ laser radiation is greater than that of the 488.0 nm radiation. For skin of the same color, the reflectivity of the skin for the Ar^+ laser light increases as the wavelength increases.[3-5] For the same radiation level, the absorption of the longer wavelength laser light is actually less. The radiation level leading to erythema is therefore greater for the longer wavelength.

In the multispectral output of a low power Ar^+ laser, the power of the 488.0 nm spectral line dominates. As the output power increases, the power of the 514.5 nm line becomes dominant. The MRD_{50} of a multispectral Ar^+ laser for the skin of the yellow race is therefore probably in the 5.6 to 7.1 range and further experimental confirmation is required.

(a) After 5 minutes, capillary expansion in the papillary layer and shallow layer of the dermis, slight edema of the shallow layer of the dermis

(b) After 5 minutes, capillary expansion in the deep layer of the dermis

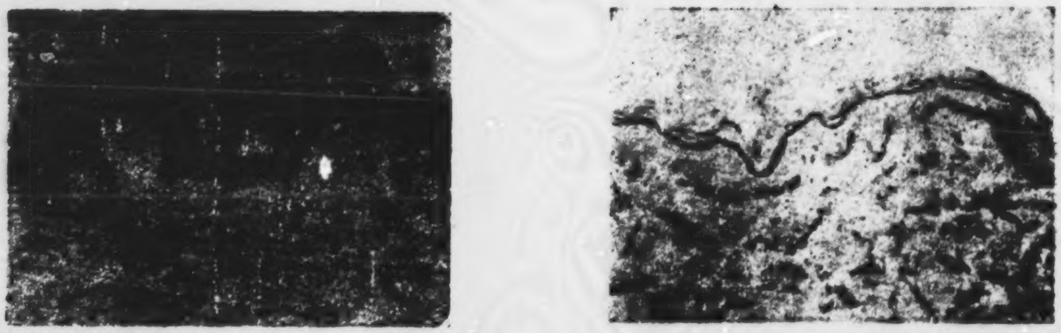

(c) After 30 minutes, capillary still expanded, congestion decreases, edema vanishes

(d) After 30 minutes, capillary still expanded, congestion decreases

Figure 5. Histological and pathological changes of the skin illuminated by 488.0 nm Ar^+ laser at 5.6 J/cm^2 for 1 second (magnified 120 times)

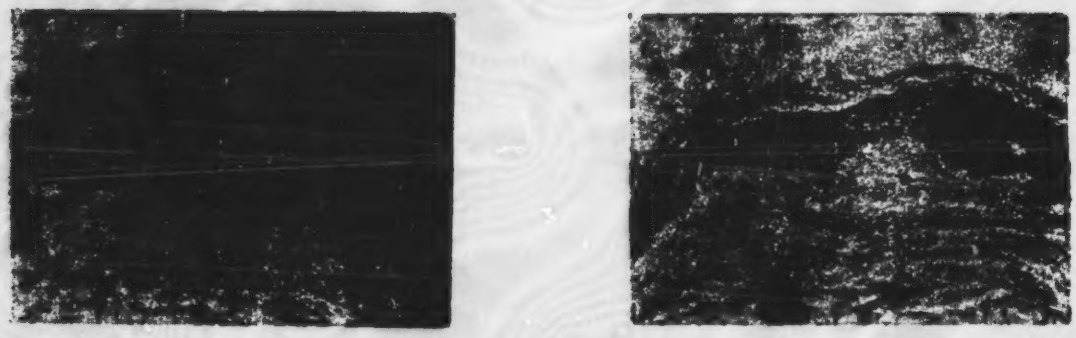

(a) Five minutes after irradiation, blood vessels in the papillary layer of the dermis are expanded and congested

(b) Thirty minutes after the irradiation, congestion of the capillaries decreases

Figure 6. Histological and pathological changes of the skin irradiated at a 514.5 nm Ar$^+$ laser at 7.1 J/cm^2 for 1 second (magnified 120 times)

In 1974 Rockwell and Goldman[5] in the United States measured the Ar$^+$ laser MRD$_{50}$ for the skin of the white race to be 4.0-8.2 J/cm^2. For the skin of the blacks the MRD$_{50}$ range is 4.5-6.0 J/cm^2. The MRD$_{50}$ in this work falls between the results for the white race and the black race. The reflectivity of the Ar$^+$ laser light by the white skin is greater than that by the black skin.[3] Generally speaking, the number of black pigments of the yellow skin is greater than that of the white skin but smaller than that of the black skin. The reflectivity of the yellow skin should therefore be less than that of the white skin and greater than that of the black skin. For the same erythematous reaction, the yellow skin requires a radiation level lower than that of the white skin but higher than that of the black skin. In this sense the results of this experiment are reasonable.

In the observation results of this experiment, zero percent erythema retention probability has been observed. This will lead to some error in the calculation and will not affect the results to any appreciable level.

REFERENCES

1. Liu Puhe [0491 2528 0735], "Guide to Laser Safety," Scientific Publishing Co., 1982.

2. A.N. Takata, "Development of Criteria for Skin Burns," AEROSP. MED., June 1974.

3. A. Mallow, L. Chabot, "Laser Safety Handbook," 1978.

4. D. Sliney, M. Wolbarsht, "Safety With Laser and Other Optical Sources," 1980, New York.

5. R.J. Rockwell, et al., "Research on Human Skin Laser Damage Threshold, Final Report," June 1974.

6. Zhou Haijun [0719 3189 6874], et al., "Statistical Method in Biological Evaluation," People's Hygiene Publishing Co., 1983.

7. Sun Ruiyuan [1327 3843 0337], "Quantitative Pharmacology," 1963.

9698/6091
CSO: 8111/1099

STUDY OF INJURY THRESHOLD OF CW Nd:YAG LASER LIGHT FOR HUMAN SKIN

Shanghai ZHONGGUO JIGUANG [CHINESE JOURNAL OF LASERS] in Chinese Vol 12, No 10, 20 Oct 85 pp 582-585

[Article by Ma Baozhang [7456 1405 4545] and Xia Weiya [1115 0251 0068] of the Ninth People's Hospital, Shanghai No 2 Medical University and Zhuo Ruipeng [0587 3843 7720], Jiang Lanying [3068 5695 5391], Hu Qingshen [5170 1987 3088], Li Zhaozhang [2621 0340 3864], and Wu Jianu [0702 1367 1166] of the Laser Laboratory, Shanghai No 2 Medical University]

[Text] Abstract: Based on the experimental results on animals and human subjects, the injury threshold MRD_{50} of CW Nd:YAG laser for Chinese is 65.519 J/cm^2 for light complexion skin, 60.989 J/cm^2 for yellow skin, and 52.321 J/cm^2 for dark complexion skin. The experiments also show a close correlation between the absorption of the Nd:YAG laser light and the pigment content of the skin.

China has been engaged in laser development for 20 years but still has not established systematic laser protection measures, partly due to the lack of damage threshold data on the Chinese people. In this work we study the skin damage threshold of CW Nd:YAG laser in order to provide some data for establishing China's laser protection standard.

This experiment consists of two parts: animal tests and tests on human skin. The Nd:YAG laser used (shown in Figure 1) was developed jointly by the Shanghai Navigation Equipment Plant and the Shanghai No 2 Medical University.

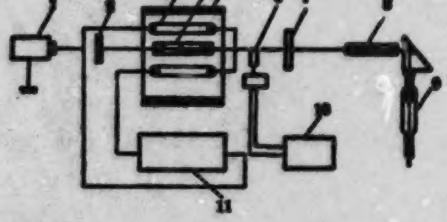

Figure 1. Schematic diagram of the Nd^{3+}:YAG laser
1--Energy monitor; 2--Total reflection film; 3--Krypton lamp; 4--YAG rod; 5--Focusing cavity (dual lamp); 6--Optical path control relay; 7--Transmission film; 8--Light guide system; 9--Power density control; 10--Timing control; 11--Power system

I. Animal Tests

1. Method

Three white-haired pigs weighing 6-7 kilograms were selected as test subjects, 2 cc/kg of 2.5 percent sodium isobarbiturate was injected into the subject's abdominal cavity. The test animals were anaesthetized and shaven, and 2 cm^2 grids were painted on the two sides of the abdomen. The tests were conducted at 15.5°C and 61 percent humidity.

Table 1. Experimental Parameters of the Laser Tests

Output wavelength (μm)	Output power (W)	Divergence angle (mrad)	Spot size (mm)	Mode of illumination	Exposure time (min)	Error in energy (%)
1.06 CW	50 stable to 5%	5	5	open shutter pulse mode	1 ± 0.7%	± 3

Five doses were used in the preliminary test, 30 shots were made at each dosage, 10 points on each animal, and the shots were made both on the abdomen and on the back. After each shot observations were made to determine the time for the erythema to appear, the size of the erythema, and the time for the erythema to disappear. For each dosage pathological observations were made on one of the animals during the erythema and after the erythema disappeared.

2. Results

The criterion for erythematous reaction is for the erythema to last at least 3 minutes. The results are shown in Table 2.

Table 2. Erythematous Results

Group	Power density (W/cm^2)	Number of shots	Erythematous rate (%)
1	43.82	30	3
2	49.43	30	17
3	57.58	29	38
4	65.73	29	69
5	73.89	30	93

The results were analyzed using a weighted linear regression method.

The regression equation was:

$$y = -9.644 + 18.788x$$

MRD_{50}: 59.385 J/cm^2

The 95 percent confidence level was:

$$56.950 \sim 61.923 \text{ J/cm}^2$$

The Chi square test showed $P < 0.05$ (see Figure 2). The histological biopsy showed normal reaction in most cases and a few cases of slight blood vessel dilation (see Figure 3).

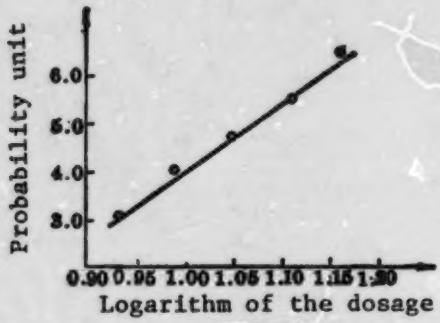

Figure 2. Regression line for animal test results

Figure 3. No obvious changes

II. Human Skin Tests

1. Method

Ten volunteers were chosen, five males and five females, from the 35-53 age group. All subjects had healthy skin, three had light complexions, two had dark complexions, and five had the usual yellow skin of the Chinese. The skin temperature before testing was measured to be 24-28.5°C. After washing the skin of the two forearms, 15 squares were drawn on the skin, with a total of 30 marked locations on each subject. Six shots each were made at 3-5 dosages, 3 on the left arm and 3 on the right arm.

Observations were made after each shot to determine the appearance time, size and retention time of the erythema. Histological observations were made on one skin sample at a dosage close to the MRD_{50} value. The tests were made at an ambient temperature of 11.5°C and a humidity of 77 percent.

2. Results

Because the skin complexions of the volunteers varied, the reactions to the laser illumination also varied. Statistical analysis was made according to skin complexion and the results are shown in Table 3.

Each group of data was subjected to a Chi square test and P is less than 0.05. The correlations are therefore significant.

Table 3. Erythema on Test Subjects of Three Skin Complexions

	Number of volunteers	Dosage	Power density (W/cm^2)	Number of shots	Erythema occurrence (%)	Weighted regression results
Light complexion	3	1	49.68	18	6	Regression formula $y=-14.487+17.570x$ MRD_{50}:65.519J/cm^2 Confidence level 95%: 61.295 ~ 70.173 J/cm^2 (Fig. 4)
		2	57.58	18	11	
		3	64.71	18	33	
		4	73.89	18	89	
Yellow skin	5	1	49.68	30	3	Regression formula $y=-14.664+18.249x$ MRD_{50}:60.989J/cm^2 Confidence level 95%: 58.867 ~ 63.188 J/cm^2 (Fig. 5)
		2	57.58	30	37	
		3	64.71	30	63	
		4	73.89	30	93	
Dark complexion	2	1	49.68	12	25	Regression formula $y=-23.137+27.744x$ MRD_{50}:52.821J/cm^2 Confidence level 95%: 46.112 ~ 59.367 J/cm^2 (Fig. 6)
		2	54.88	12	67	
		3	57.58	12	100	

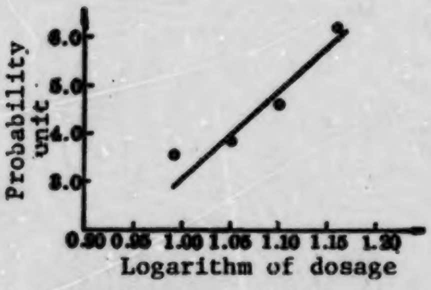

Figure 4. Regression straight line for data from light skin

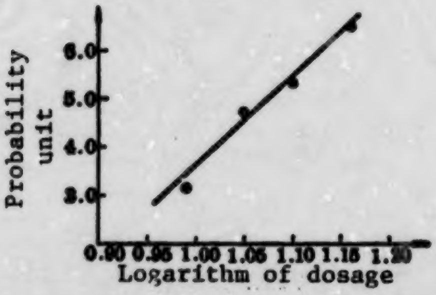

Figure 5. Regression straight line for data from yellow skin

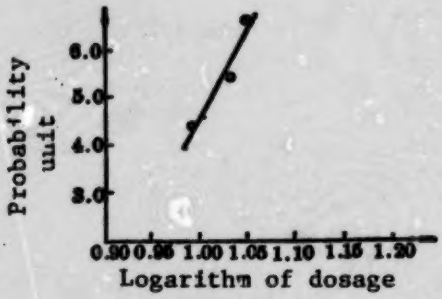

Figure 6. Regression straight line for data from dark skin

3. Histological biopsy

No obvious changes were noticed in histological examinations (see Figures 7 and 8).

Figure 7. No obvious changes

Figure 8. No obvious changes

III. Discussion

1. Comparison with foreign data

For the first time we have experimentally determined the laser damage threshold of the skin of the yellow race. The value falls between those of the white race and those of the black race. The results agreed with a priori expectation and served as useful data for establishing a Chinese standard for laser safety.

2. Both the animal tests and the human tests showed that the content of skin pigment had a definite effect on the damage threshold of laser at 1.06 μm wavelength. At a higher pigment level more laser energy was absorbed and the damage threshold occurred at a lower power density. Dark skin therefore had a lower damage threshold and light skin had a higher damage threshold. The results are shown in Figures 9, 10, and 11.

Figure 9. No obvious changes

Figure 10. The cytosol of the scaly epithelial cells became foamy, cell nuclei shrank, and capillaries showed slight dilation and edema

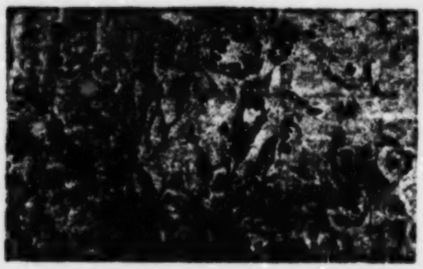

Figure 11. Blood vessels showed slight dilation and red blood cells roam outside the cavity

3. For the young white pigs, the value of MRD_{50} was 59.385 J/cm^2, the 95 percent confidence level was 59.950-61.923 J/cm^2. For the human subjects, the MRD_{50} was 52.321-65.519 J/cm^2 and the 95 percent confidence level was 46.112-70.173 J/cm^2. The animal results are quite close to that of the human and young white pigs are suitable experimental animals for this purpose.

4. Factors affecting the experimental results

(1) Level of anaesthesia

For the pigs the skin often displayed congestion before deep anaesthesia and while recovering from anaesthesia. During periods the absorption of the 1.06 μm laser light was greater and erythema were more likely to occur. In deep anaesthesia, the skin turned white and erythema were less likely to occur and easier to fade away quickly. Attention should therefore be given to the level of anaesthesia in order to obtain consistent results.

(2) Subjective assessment of erythema

The occurrence and growth of erythema by visual observation can generally be agreed upon but the recession of erythema depends on the observer. The retention time of the erythema is therefore less than objective.

(3) Ambient temperature

The observation of erythema may be affected by too high or too low ambient temperatures. The temperature of the laboratory should be controlled to ensure the reliability of the data.

Table 4. Comparison of Experimental Results from This Group and Foreign Materials

表4　本組实验结果与国外资料对比

Group	組　别	$MRD_{50}(J/cm^2)$	95% 可信限 (J/cm^2)	Confidence Range
Caucasian	高加索人	48～78		
Chinese(lt)	中国人(偏白)	65.519	61.295～70.173	
" (av)	中国人(黄白)	60.989	58.867～63.188	
" (dark)	中国人(偏黑)	52.321	46.112～59.867	
Black	黑　人	46～60		

9698/6091
CSO: 8111/1099

INJURY THRESHOLD OF RUBY LASER IRRADIATION ON HUMAN SKIN

Shanghai ZHONGGUO JIGUANG [CHINESE JOURNAL OF LASERS] in Chinese Vol 12, No 10, 20 Oct 85 pp 586-588

[Article by Chen Ji [7115 6619], Wang Jun [3769 6511], Lu Shanfen [4151 0810 5358], Xu Guidao [1776 6311 6670], Shi Liangshun [2457 5328 7311], Qian Huanwen [6929 3562 2429], and Wang Denglong [3769 6260 7893] of the Institute of Radiation Medicine, Academy of Military Medical Sciences]

[Text] Abstract: This paper reports experimental results of human skin exposed to ruby laser light. Statistical analysis of the erythema produced with 24 hours post-exposure showed that ED_{50} was about 4.7 J/cm^2.

Damage thresholds for human skin by ruby laser radiation has been reported in foreign journals.[1-4] However, all the studies were made on the skin of Caucasians or blacks, where the differences were great and not all the results were applicable to the case of the yellow race.

In this study we have extended the experimental investigation on pig skin with a ruby laser to the case of human skin. Observations of the occurrence of erythema and statistical analysis of the data produced a value for the 50 percent erythema reaction dosage.

I. Experiment

The ruby laser emits a multimode pulse with a pulse width of 0.32 ms, a divergence angle of 28-29 mrad, a maximum output of 18J, and a diaphragm diameter of 0.5 cm. The output energy was stable to within 5 percent and was monitored in real time with a model JNK-1 carbon laser energy meter and a gold-plated inverted cone energy meter. Both devices were calibrated.

The average ambient temperature was 30.1 ± 1.4°C and the average relative humidity was 74.7 ± 8.6 percent.

The 15 volunteers were male workers of the laboratory. They were all ethnic Han and their age range was 39.5 ± 8.9. Physical examinations and electrocardiograms were made before and after the tests and no abnormal changes were detected. The first illumination spot was 3 cm below the centerline of the fossa cubitale, and the spots were below the first spot and separated by 2 cm from each other. Five shots were made on each forearm and at different dosages (average 0.52-2.8 J). A total of 10 shots were made on the two forearms. Subjects with different skin complexion were distributed among the five dosage groups in order to obtain the collective 50 percent erythema dosage (ED_{50}). Observations were made immediately after the illumination for skin reaction and erythema. Subsequent observations were made at 2, 12, 24, and 48 hours respectively after the illumination.

II. Results

1. Occurrence of erythema

In this study 152 spots were illuminated at five different dosage levels. Each dosage group had 29-33 sample spots, as shown in Table 1. As can be seen, the erythema occurrence rate decreased with decreasing dosage. The occurrence time of the erythema depended on the dosage level, as shown in Table 2. At a high dosage level, the erythema occurs very quickly and at a low dosage level the occurrence rate was lower. The data show that as the radiation dosage decreased the time for erythema occurrence was delayed.

Table 1. Skin Erythema Occurrence Rate Under Ruby Laser Illumination

Group	Ave. dosage $\pm S_x$ (J/cm^2)	Ave. absorption $\pm S_x$ (J/cm^2)	No. of shots	Erythema occurrence rate (%)
1	14.01±0.72	8.63±0.61	29	100
2	7.01±0.56	4.32±0.30	30	90
3	5.45±0.35	3.37±0.24	33	57.6
4	3.92±0.31	2.43±0.24	30	36.7
5	2.63±0.08	1.62±0.11	30	6.7

Table 2. Forearm Skin Erythema Occurrence Rate and Subsiding Rate

Group	Occurrence rate (%)		Subsiding rate (%)		
	< 5 min	6 min~1 hr	2~12 hrs	13~48 hrs	> 3 days
1	96.6	3.4	10.3	20.7	69.0
2	66.7	33.3	18.5	48.1	33.4
3	36.8	63.2	47.4	52.6	—
4	27.3	72.7	63.6	18.2	18.2
5	50.0	50.0	100	—	—

2. Subsidence of the erythema

For a given length of the observation time after the illumination, the subsiding rate of the erythema depended on the dosage (see Table 2). At a high dosage the retention time was long; for a low dosage, the retention time was short.

3. Follow-up observation

The skin reaction was observed after different elapsed times following irradiation. (1) Severe erythematous reaction (20.7 percent of the cases): The skin was raised above the normal surface level and small papules formed. The skin became irritated or blistered. Scabs formed 1-2 days following the irradiation and sloughed off after 6-7 days. In some cases no blisters formed but the skin formed scabs. (2) Less severe erythema: The skin remained flat and no blisters or papules formed. The erythema was initially red in color and became dark red and then purple. The boundaries were clear and the retention time was long. The erythema generally subsided in 4-5 days. (3) Medium reaction: The skin became reddish, the outline was clear, the skin was not raised and no papules formed. The erythema was initially faintly visible and gradually became clear. In the No 2 dosage group only volunteer No 8 showed slight scabbing after 3 days and all the other erythematous reactions were light to very light. No papules or blisters were observed and the skin remained even. The color was initially pink and later turned red. The outline may or may not be clear. For the No 3 and No 4 dosage groups the reactions were light to very light. The erythema was pink in color, often circular in shape with a clear boundary. Two cases of erythema were found in the No 5 dosage group. One occurred within 5 minutes and the other occurred after 30 minutes. Both erythematous reactions were very mild and subsided on the second day, with slight traces of pigment precipitation. In the preliminary tests no erythema was found at a dosage level below 2.5 J/cm^2 (e.g., 2.4 J/cm^2). The lower limit in the experiment is therefore chosen to be 2.6 J/cm^2.

Calculation of the 50 percent erythema dosage (ED$_{50}$): The experimental data were processed statistically. The Bliss method of weighted regression was used in finding the equation, the ED$_{50}$ value and the 95 percent confidence level.

$$\hat{Y} = 0.95298 + 6.05599x$$

$$ED_{50} \simeq 4.7\ \mathrm{J/cm^2}$$

The 95 percent confidence level is 4.217-5.146 J/cm^2. The chi square test gives $x^2 = 1.8683$, $x^2_{0.05} = 7.8045$, and $P > 0.05$. The calculation model and the actually measured values were consistent and the results acceptable (see Figure 1).

III. Discussion

At the same dosage the absorption of the laser energy and the resulting erythematous reaction varied because the skin reflectivity varied from man to man. In our experiment the forearm skin of the volunteers had a maximum reflectivity of 43.8 ± 1.9 percent for the ruby laser light. The lowest reflectivity was 32.5 ± 1.8 percent and the average was 38.8 ± 3.6 percent. At the highest dosage used the skin with lower reflectivity absorbed more laser energy and showed a more severe reaction in the erythema whereas the skin with a high reflectivity does not. In addition, the darkness of the skin complexion and the reflectivity play an important role in the erythematous reaction.

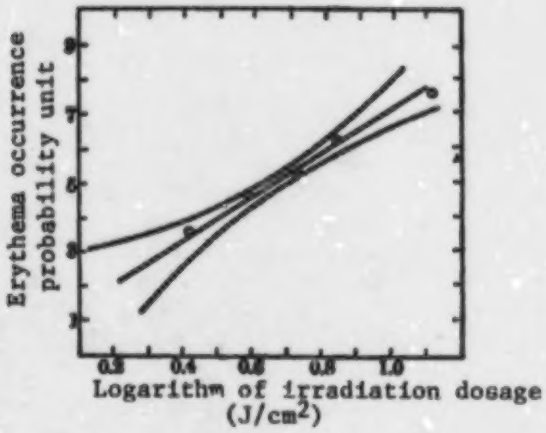

Figure 1. Rate of occurrence and dosage relationship for erythema of human skin irradiated by a ruby laser

Statistical analysis of the experimental data using the Bliss weighted regression method yielded a value of 4.7 J/cm^2 for ED$_{50}$. This differed from the Caucasian ED$_{50}$ by a factor of 2.3-4.3 and from the black ED$_{50}$ by a factor of 0.5-1.5, as shown in Table 3. This indicates that the skin color of the Chinese is closer to that of blacks and the effective dosage 1.4 J is the same as that of blacks.

Table 3. Comparison of Injury Thresholds of Human Skin Irradiated by Ruby Laser Light

	This work	Blacks	Caucasians
Number of volunteers	15	2	4
Number of shots	152	105	100
Dosage (J/cm^2)	2.6-14.0	0.5-8.0	5.0-30.0
Skin reflectivity (%)	32-44	30-41	52-62
Erythema occurrence rate (%)	57.9	32.4	72
ED$_{50}$ (J/cm^2)	4.7	2.2-6.9	11-20

The ANSI regulation states that the maximum permissible energy density (MPE) of the skin for visible light radiation is 150 mJ/cm^2. The ED$_{50}$ obtained in this experiment was 31 times the MPE value. The skin damage threshold of the Chinese is therefore close to the MPE value. This should be considered in establishing laser safety protection.

The authors acknowledge the contribution of Tang Zhongming [3282 0112 2494] in the statistical analysis of the data.

REFERENCES

1. J.G. Kuhn, et al., "Laser Injury in Skin," Lab. Invest., 1967, 17, No 1, 1-13.

2. L. Goldman, "The Skin," ARCH. ENVIRON. HELTH., 1968, 18, 434.

3. W.H. Parr, "Skin Lesion Threshold Values for Laser Radiation as Compared With Safety Standards," U.S. Army Medical Research Laboratory Report, 1964, Feb. 24, 813.

4. J.P.G. Williams, et al., "Final Report of Investigations of Laser Skin Hazards," AD-735794 (p 8161), 1971.

5. R.J. Rockwell, et al., "Research on Human Skin Laser Damage Thresholds," AD A-012703 (p 8947), 1974.

6. Wang Jun [3769 6511], et al., "Injury Threshold of Ruby Laser Irradiation on Pig Skin," this issue, p 631

9698/6091
CSO: 8111/1099

ACUTE INJURY THRESHOLD LEVEL OF CO_2 LASER LIGHT FOR SKIN OF YELLOW RACE

Shanghai ZHONGGUO JIGUANG [CHINESE JOURNAL OF LASERS] in Chinese Vol 12, No 10, 20 Oct 85 pp 589-591, 588

[Article by Shi Hongmin [0670 1347 2404], Li Jishi [2621 3444 2514], Tan Yankang [6223 1693 1660], Luo Panxiang [5012 3140 4382], Chen Zhongben [7115 0112 2609], Xie Xingbing [6200 2622 0393], and Yuan Yuehuan [5913 1878 2970] of Zhongshan Medical University, Guangzhou]

[Text] Abstract: Acute injury threshold level MRD_{50} of CO_2 laser light for the skin of eight white piglets was measured. On the basis of the animal experiments, the same measurement for the skin of six yellow people was made. MRD_{50} was found to be 2.3 J/cm^2. The skin of five volunteers was exposed to the above energy densities, and histological examination found that capillaries were expanded and filled with erythrocytes and light edema, but there was no significant change of cuticle. This indicates that the MRD_{50} erythematous reaction is minimal and reversible.

By studying the erythematous reaction of the skin of young pigs and human subjects irradiated by normally incident CO_2 laser light, we have determined the injury threshold level MRD_{50} (i.e., the radiation level for 50 percent reaction) and provided experimental data for establishing a laser safety standard.

I. Experimental Setup

A CW CO_2 laser (10.6 μm) with a fundamental mode output was used in the irradiation of the skin of 5 kg young pigs and the yellow race skin and the erythematous reactions were observed. The experimental setup is shown in Figure 1.

The output power of the CW CO_2 laser was 15-30 W and stable to within 4 percent. The beam was introduced into the optical path by the gold-plated reflection mirror #1 and the power monitored. The beam was reflected by the total reflection mirror #2, passed through the closed optical path consisting of the germanium lens (with antireflection coating) and the diaphragm and impinged on the animal or human skin. In order to control the radiation flux, the power at the exit of the diaphragm was calibrated for each laser output power and diaphragm to lens distance before the experiment. Before the irradiation of the animal or human skin, the power was again measured with a high-speed power meter in order to avoid the effects of other factors. Exposure time was controlled by an electric shutter and monitored by a photodiode and recorded by a digital time recorder to assure repeatability of the measurement.

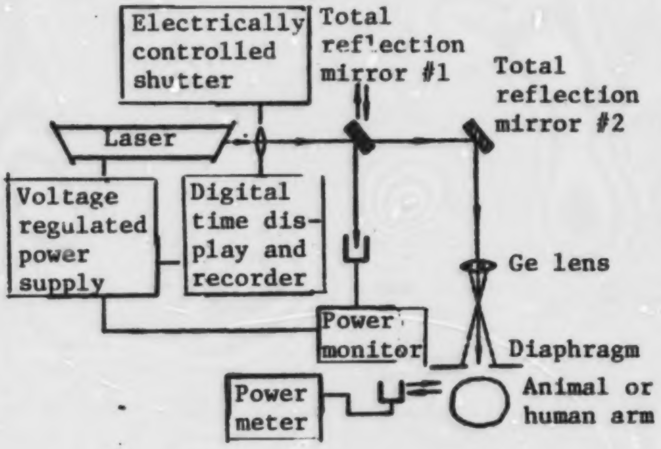
Electrically controlled shutter
Total reflection mirror #1
Total reflection mirror #2
Laser
Voltage regulated power supply
Digital time display and recorder
Ge lens
Power monitor
Diaphragm
Power meter
Animal or human arm

Figure 1. Experimental setup

II. Experimental Conditions and Data

The measurements were made at an ambient temperature of 20 ± 5°C and a relative humidity not higher than 80 percent.

Based on the results obtained from young pigs, the injury threshold of the yellow race skin for CO_2 laser was determined under the same experimental conditions. Using the modified Kou method, the MRD_{50} value of each volunteer was first determined. The exposure time was 1 second, the light spot diameter was 0.5 cm, and the erythema observation time was 5 minutes. Five exposure levels in geometric ratio were then selected. The minimum level D_n was chosen so that erythema appeared on all subjects but disappeared after 5 minutes. The maximum level D_m was chosen so that most of the erythema remain after 5 minutes and visual observation showed no edema and no skin abnormalities remain after the disappearance of the erythema.

In this study measurements were made on six volunteers--three females and three males--in the 20-21 age group. The irradiation location was the side of the forearm, as shown in Figure 2. The lattice spacing was 2 cm and the skin outside the marked lattice was used for preliminary tests. The numbers 1-5 inside the lattice represent five different exposure levels, and the layout of the dosage was based on symmetry and balance requirements. For each dosage 30 shots were made. After the exposure, careful observations were made to determine the appearance and disappearance time of the erythema. The number of remaining erythema was recorded after 5 minutes and the results are shown in Table 1.

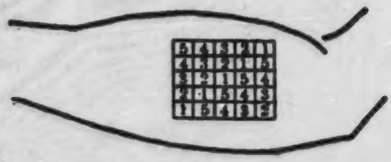

Figure 2. Exposure spots on the side of the forearm

Table 1. Erythema Reaction Number r at Different Dosages

Volunteer No.	Dosage level (J/cm^2)				
	2.48	2.33	2.19	2.06	1.94
2 (M)	5	4	2	0	0
3 (F)	5	4	2	1	0
4 (M)	5	3	2	1	0
5 (M)	5	3	3	2	0
6 (F)	4	3	1	0	0
7 (F)	5	4	2	1	0
Σ	29	21	12	5	0

Using a weighted regression method,[1] the relationship between the probability unit y and the logarithmic dosage x = log D was found:

$$y = \bar{y} + b(x - \bar{x}) = 40.738x - 9.318$$

This relationship is shown graphically in Figure 3. The significance index of the slope b is $g = 0.074 < 0.1$, and

$$MRD_{50} = 2.3 \text{ J/cm}^2$$

The 95 percent confidence level is 2.2-2.3 J/cm^2.

Under identical conditions, the skin on the side of the forearms of five volunteers (21-46 years old) was irradiated at a dosage level of $MRD_{50} = 2.3$ J/cm^2. Samples were taken 5 and 30 minutes after the CO_2 laser exposure for histological examinations. The results (see Figure 4) showed capillary dilation in the papillary layer of the corium, a few capillaries were filled with erythrocyte, and blood vessels close to the shallow layer of the corium and close to the sweat gland were also dilated. The cuticle showed no obvious changes. In individual biopsies, slight prickle cell edema and basal-cell liquidation (bubble formation) were observed. For the specimens taken 30 minutes after the laser exposure, most cases showed slight blood vessel dilation, lessening of congestion, and a few lingering prickle cell and basal-cell edema. Histological studies showed that the injuries at this dosage are reversible threshold damages.

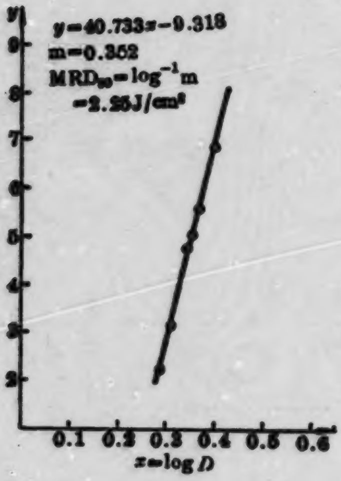

Figure 3. Relationship between the probability and the logarithmic dosage

III. Results and Discussion

The result of this study is that the acute injury threshold of CO_2 laser for the skin of the yellow race is determined to be $MRD_{50} = 2.3\ J/cm^2$. This is slightly lower than the MRD_{50} of $2.8\ J/cm^2$ obtained by Rockwell and Goldman for the white and black races. The main cause for this discrepancy is that in our experiment the standard time for erythema observation is 5 minutes whereas Goldman used 60 minutes. Our animal tests data showed that MRD_{50} increases somewhat when the observation time is prolonged. We have tested a 45-year-old male volunteer using 30 minutes as the standard time for erythema observation and obtained $MRD_{50} = 3.1\ J/cm^2$ with the modified Kuo method. This value is even larger than $2.8\ J/cm^2$. This is because our spot area is $0.196\ cm^2$ and that of Goldman is $0.865\ cm^2$. In general a small spot area is associated with more heat loss and therefore a higher MRD_{50} value.

We measured $MRD_{50} = 3.7\ J/cm^2$ ($\phi = 0.5$ cm, 1 sec) for the eight young pigs. This is greater than the MRD_{50} of human skin because the transmissivity for the CO_2 laser light of the young pig skin is greater than that of human skin[3] and the reflectivities fall within 5 percent of each other. The pig skin therefore absorbs less light energy than the human skin and has a greater threshold value. The difference is less than a factor of 2.

In terms of accuracy, Rockwell et al. obtained their MRD_{50} graphically using two data points on a normal log paper. In this work, three dosage levels were chosen between the maximum and the minimum dosage and the dosages were in the order of a geometric series. There were five points on the graph and the reliability was therefore better. The results obtained are sensible and can be used as reference data in establishing a laser safety standard.

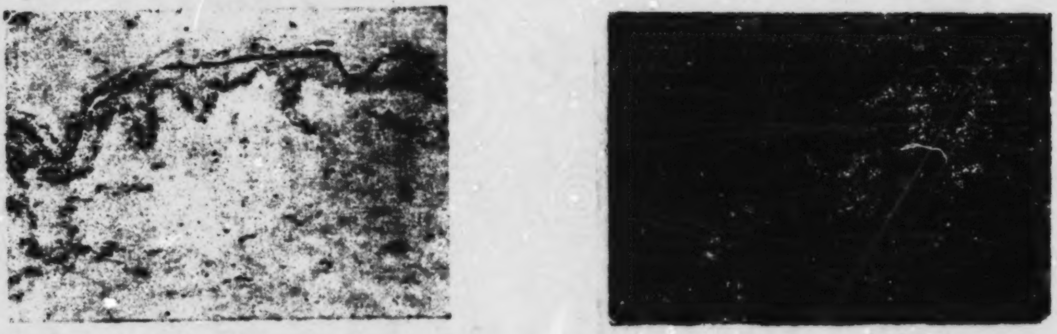

(a) Sample taken 5 minutes after exposure. Shallow layer capillaries and capillaries in papilla corium are dilated and congested.

(b) Sample taken 5 minutes after exposure. More obvious capillary dilation and congestion.

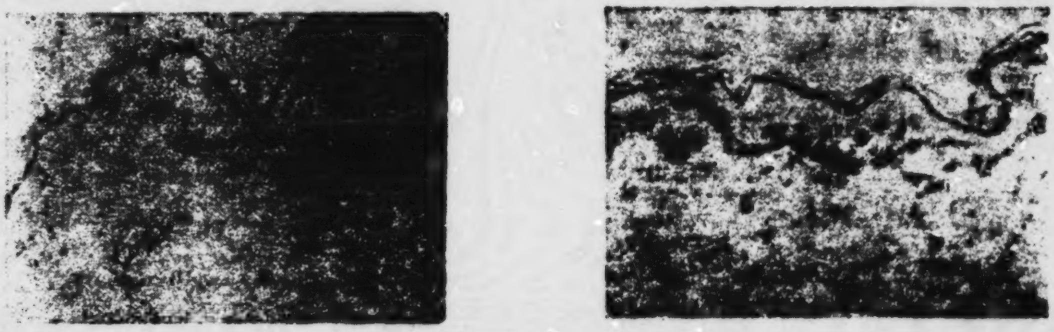

(c) Sample taken 5 minutes after exposure. Capillary dilation and congestion, prickle cell edema.

(d) Sample taken 30 minutes after exposure. Lessening of capillary dilation and congestion.

(e) Sample taken 30 minutes after exposure. Lessening of capillary dilation and congestion.

Figure 4. Physiodermatological changes after exposure to CO_2 laser irradiation (12x10 magnification)

REFERENCES

1. Zhou Haijun, et al., "Methods of Biological Testing Statistics," People's Sanitation Publishing Company, 1983.

2. Sun Ruiyuan, "Quantitative Pharmacology," 1963.

3. L. Goldman and J.R. Rockwell, Jr., "Laser in Medicine," New York, Gordan Press, 1971.

9698/6091
CSO: 8111/1099

STUDY OF INJURY THRESHOLD OF SKIN IRRADIATED WITH 265 nm PULSED LASER LIGHT

Shanghai ZHONGGUO JIGUANG [CHINESE JOURNAL OF LASERS] in Chinese Vol 12, No 10, 20 Oct 85 pp 592-596

[Article by Li Zhaozhang [2621 0340 3864], Wu Jianu [0702 1367 1166], and Gai Baokang [5556 1405 1660] of the Laser Research Laboratory, Shanghai No 2 Medical University, and Zhou Yan [0719 5888] of Jiaotong University]

[Text] Abstract: An investigation of erythema of the skin irradiated with 265 nm pulsed laser is presented. Two phases of reactions of ultraviolet erythema--immediate and delayed--were clearly observed in our experiment. The probability statistical analysis indicated that the minimal dose of 50 percent perceptible redness occurrence rate of the pig skin is 22.0 mJ/cm^2.

In general, ultraviolet radiation may be divided into three wavelength ranges: UVA (315-400 nm), UVB (280-315 nm), and UVC (200-280 nm). Since photons in these three ranges have different energy, they induce different biological reactions. Photons in UVC have a greater energy and can easily cause photochemical reactions. In the early part of this century researchers studied the effects of UVC on the skin. Later, Rottier (1953) and Magnus (1964) measured the minimum redness dosage (MRD) of ultraviolet of various parts of the human body. Their results (see Table 1) showed that UVC was more likely to cause redness than UVB. In order to investigate the effects of UV laser on the skin, we used a Nd:YAG quadruple frequency laser as the source and white pigs as a control animal to measure the injury threshold of 265 nm laser. Similar experiments have not been reported here or abroad. The test results may be used as a preliminary data base for establishing China's laser safety standard on the maximum permissible dosage (MPE) of UV laser on the skin.

Table 1. Ultraviolet Laser MRD of Human Skin

Investigator and date	Location	Area	Number of subjects	Observation time	UVC(nm) MRD	UVB(nm) MRD
Rottier (1953)	Arm	0.5x8 mm^2	7	6-14 hrs after exposure	257 nm 1130 mW/sterad	297 nm 1697 mW/sterad
Magnus (1964)	Back	3x10 mm^2	13	3-8 hrs after exposure	260 nm 25.12 mJ/cm^2	300 nm 50.12 mJ/cm^2

I. Experimental Setup and Method

A Q-switched Nd:YAG laser was used as the light source. The wavelength of the quadrupled frequency was 265 nm, the pulse width was 9 ns, the maximum single pulse energy was 20 mJ, the output stability was within ±5 percent, and the divergence angle of the beam was 0.36 mrad.

The optical path and the setup is shown in Figure 1. Two energy monitors were used: a model NJ-NI and a RJ7200 (made in USA). The dosages were computed based on a beam splitting ratio of K = 0.27 ± 0.019 and the energy measured in real time.

The laboratory conditions were 11.2 ± 0.8°C and 72.3 ± 8.1 percent relative humidity.

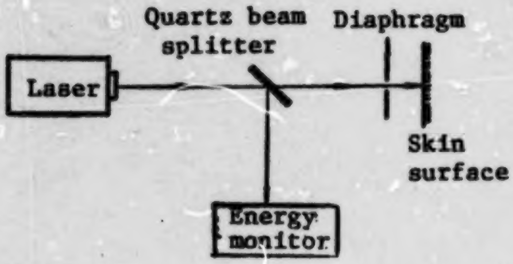

Figure 1. Schematic diagram of the experimental setup

The test animals were three 4.5 kg Shanghai white pigs. The animals were anaesthetized 2 hours before the test. Forty 2cm x 2cm squares were painted on shaven skin 2cm from the spine. Each square received one laser shot at normal incidence.

The observation of the erythema was made visually, according to the criteria in Table 2. Each irradiation group was followed by the conventional (H.E. Stain) histological test. Some electron-microscopy studies were also made for the MRD group.

Table 2. Criteria for Erythema

Grade	Visual observation	Histological examination
0	No reaction	Normal
±	Very light redness, no obvious boundary	Cuticle normal, hypodermal capillary dilation and congestion
+	Light redness, visible boundary	Normal cuticle, hypodermal capillary dilation and congestion, exudation of red blood cells
++	Medium redness, obvious boundary, edema	Hypodermal capillary dilation and congestion, edema of cuticular cells, some shrinkage of nuclei
+++	Redness, boundary may be accompanied by edema	Same as ++ grade; in addition, the collagen fibers in the corium thickens and the cuticle becomes puffy

II. Experimental Results and Analysis

A total of 224 shots were made, 21 points were examined histologically, and 203 points at 6 dosages were analyzed statistically. Tables 3 and 4 show the erythematous reaction to 265 nm laser pulses.

Table 3. Transient Erythematous Reaction of Pig Skin to 265 nm Laser Irradiation

			Transient erythema			
Group	Ave. dosage (mJ/cm^2) ± std. dev.	No of shots	Occurrence %	Time of occurrence (sec)	Duration (min,sec)	Grade
1	13.66 ± 0.13	31	-	-	-	-
2	16.61 ± 0.64	31	19.35	15" ~ 23"	30" ~ 5'	$\pm^{-}$
3	20.21 ± 0.33	33	39.39	12" ~ 18"	2' ~ 10'	±
4	24.23 ± 0.70	34	67.64	6" ~ 14"	2' ~ 12'	$\pm^{+}$
5	29.04 ± 1.22	34	88.23	4" ~ 12"	2' ~ 15'	$+^{-}$
6	39.44 ± 2.03	40	100	0 ~ 10"	5' ~ 20'	$+^{-}$

Table 4. Retaining Erythematous Reaction of Pig Skin to 265 nm Laser Irradiation

Group	Ave. dosage (mJ/cm^2) ± std. dev.	No of shots	No of erythema after 24 hrs	Delayed erythema occurrence rate after 24 hrs (%)	Highest grade reached in 24 hours
1	13.66 ± 0.13	31	4	12.90	±
2	16.61 ± 0.64	31	8	25.81	±
3	21.21 ± 0.33	33	14	42.42	+
4	24.23 ± 0.70	34	20	58.82	$+^{+}$
5	29.04 ± 1.22	34	25	73.53	++
6	39.44 ± 2.03	40	36	90.00	+++

The transient erythema produced by the 265 nm laser pulses had a maximum persistence time of 20 minutes and may expand to a diameter of 5-8 mm. Delayed erythema occurred at different time for different dosage groups and the redness grade also vary. Figure 2 shows the variation of the erythematous reaction with time. After 48 hours the erythema in groups 1-4 had all disappeared and pigment deposits were not pronounced. In groups 5 and 6 some shots had light brown pigment deposits lasting 1-2 days. Group 6 had blisters on about 25 percent of the shots.

Based on histological examinations under an optical microscope, the skin of the first group remained basically normal after irradiation. Skin in the second, third, and fourth dosage groups showed various degrees of dilation and congestion of the hypodermal capillaries. In group 4, a few cuticular cells showed light edema and the prickle cells showed ambiguous boundaries. In group 5 after 24 hours, there were also signs of cuticle deterioration, edema within cuticle cells, and nuclei shrinkage. The reaction in group 6 was the most severe. Cavities formed in cuticle cells, basal cell arrangement became locally randomized, and collagen fibers of deep layer corium cells thickened. The histological examinations made 2 hours after irradiation revealed basically the same results except the indications of cell nuclei shrinkage, edema within the cells, and collagen fiber thickening were less obvious. Electron microscope examinations of the groups 3 and 4 skin 24 hours after irradiation showed that some of the chondriosome ridges of the basal cell had become blurred or disappeared, some of the chondriosome had enlarged, and the spacing between the cells had increased. Electron microscope examinations made 2 hours after the shots revealed no abnormality (see Figure 3).

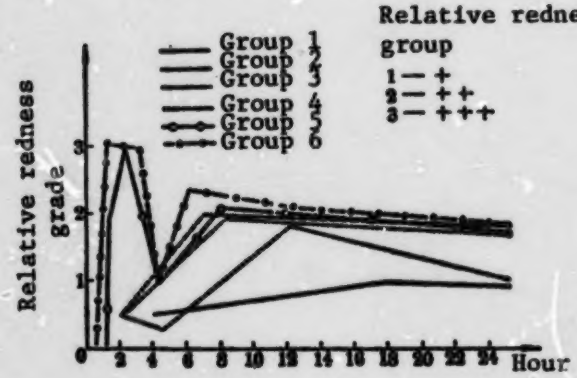

Figure 2. Erythematous reaction as a function of time at various radiation dosages

(a) Histological study of group 4 at 2 hours after irradiation. Dermal capillaries dilated and congested.

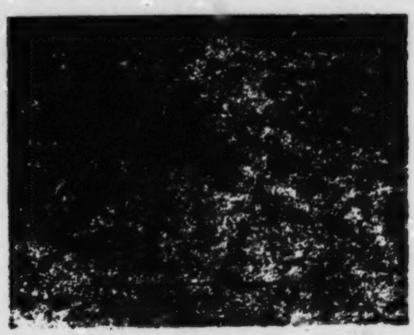

(b) Histological study of group 5 at 2 hours after irradiation. Dermal capillaries dilated and congested.

[Figure 3 continued on following page]

(c) Histological study of group 3 at 24 hours after irradiation. Dermal capillaries dilated and congested.

(d) Histological examination of group 4 at 24 hours after irradiation. Blood vessels dilated and congested. Some basal cells showed slight edema.

(e) Histological examination of group 5 at 24 hours after irradiation. Dermal capillaries dilated and congested, edema within cuticle cells and some cell nuclei showed shrinkage. Cuticle became puffy.

(f) Histological examination of group 6 at 24 hours after irradiation. Bubbles in cuticle cells, collagen fibers in deep dermal layer thickened.

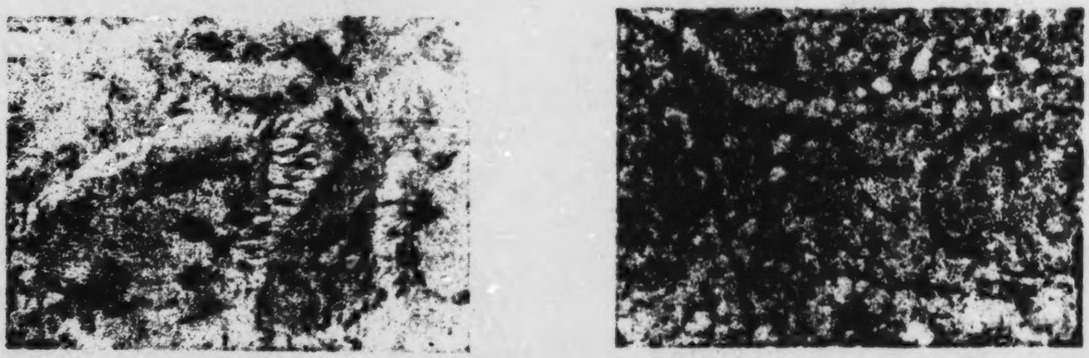

(g) Electron microscopic examination of group 4 after 2 hours. Cuticle cells remained normal.

(h) Electron microscope examination of group 4 after 24 hours. Prickle cell spacing increased, bridge point blurred, chondriosome ridge blurred or disappeared.

Figure 3

Table 5 and Figure 4 show the MRD_{50} and the 95 percent confidence limit of the pig skin irradiated by 265 nm laser pulse as obtained by the visual method and by the weighted regression method. The equation obtained by the weighted regression method was tested for x^2 and the x^2 value of 0.0836 was much less than the value of $x^2(3)0.05$. The equation is therefore acceptable.

Table 5. Injury Threshold Statistics of White Pig Skin Irradiated by 265 nm Laser Pulses

	Visual method	Weighted regression method
Regression equation		$y = 5.2066x - 1.9892$
MRD_{50} (mJ/cm^2)	22.13	22.00
95% confidence limit (mJ/cm^2)	19.79 ~ 24.75	20.20 ~ 23.94

Note: x is the logarithm of the dosage, y is the erythema occurrence probability

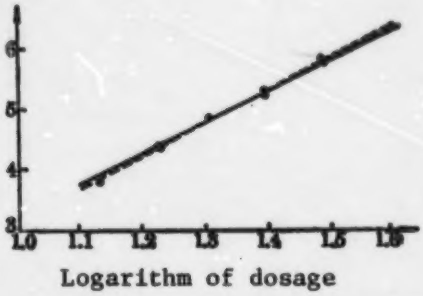

Figure 4. Relationship between erythema occurrence probability and logarithm of the dosage
Solid line by visual method; dashed line by weighted regression; open circles are experimental points; solid dots are computed values

III. Discussion

1. Comparison of UVC and UVB

Both UVC (200-280 nm) and UVB (280-315 nm) cause transient and delayed erythematous reactions in pig skin. When we used 265 nm pulsed laser and 308 nm excimer laser in irradiating the pig skin, the erythematous reactions were very obvious and the behaviors were not the same. The transient erythema caused by the 265 nm laser pulse lasted a longer time than that produced by 308 nm laser pulse. Both required a certain period of time to induce delayed erythema, characteristic of photochemical reactions. The delayed erythema generated by the 265 nm laser occurred 0.5-4.5 hours after the irradiation, while that produced by the 308 nm laser occurred 5-18 hours after the irradiation. Possibly this had something to do with the higher photon energy of the 265 nm laser, a greater photon energy causes a faster photochemical reaction. Moreover, the observed behavior of the delayed erythema as a function of time seemed to imply that several photochemical materials were coming into play at different stages of the reaction. This agrees with the viewpoint reported in foreign journals.

Ultraviolet erythema is the result of photochemical reactions. The heat generated in the skin is less than that produced by a thermal effect but heat is nonetheless generated. We considered the heat effect and measured the skin temperature with a model 7151 semiconductor thermometer made by the Shanghai Medical Equipment Plant. We found that, as the radiation dosage increased, the temperature of the erythematous skin was higher than the unaffected skin 1 hour after the shot was 29.1°C whereas the temperature of the unaffected skin was 27.8°C. This also shows that the laboratory temperature should be kept constant during such experiments.

2. Safety standard of UV laser

According to the UV radiation health standard issued by the World Health Organization in 1979 and the laser safety standards issued recently by ANSI and IEC, the maximum permissible exposure of the skin for 260-270 nm ultraviolet radiation is 3 mJ/cm^2. The MPE for 308 nm UV with a pulse width of 15 ns is 6.2 mJ/cm^2. Based on our experimental results, the injury thresholds (MRD_{50}) are 22.0 mJ/cm^2 for 265 nm, and 53.84 mJ/cm^2 for 308 nm. The computed MRD_{50}/MPE ratios are 7 and 9 for 265 nm and 308 nm respectively. These data show that the MPE safety factor based on animal experiment should be at least 10. Since the UV section of the spectrum has significant biological effects, more animal tests should be made using short UV laser pulses in order to assume the reliability of the laser safety standard.

9698/6091
CSO: 8111/1099

INVESTIGATION OF LASER INJURY THRESHOLD OF SKIN

Shanghai ZHONGGUO JIGUANG [CHINESE JOURNAL OF LASERS] in Chinese Vol 12, No 10, 20 Oct 85 pp 597-599, 596

[Article by Wu Qingzhen [0702 1987 6297] and Dong Peiying [6772 0160 5391] of the Department of Dermatology, Ruijin Hospital, Shanghai No 2 Medical University and Zhuo Ruipong [0587 3843 7720], Hu Qingshen [5170 1987 3088], Li Zhaozhang [2621 0340 3864], Gai Baokang [5556 1405 1660], Jiang Lanying [3068 5695 5391], and Wu Jianu [0702 1367 1166] of the Laser Research Laboratory, Shanghai No 2 Medical University]

[Text] Abstract: This paper reports the research results on laser injury threshold of skin irradiated by 200 µs pulsed Nd glass laser, CO_2 laser and 488 nm Ar ion laser light.

The study of laser injury threshold of the skin has been reported since 1969, when Rockwell and Goldman of Cincinnati University first reported the minimum reaction dosage of five kinds of laser radiation for skin of Caucasians. In 1974 they reported more detailed injury threshold results of the skin of Caucasians and blacks by six different lasers. The injury thresholds were given in terms of the dosage corresponding to a 50 percent probability for producing a minimum injury (erythema) reaction, or, MRD_{50}. In this paper we report the research results on laser injury thresholds of the skin of young pigs and of humans by Nd:glass laser, CO_2 laser and argon ion laser.

I. 200 µs Pulsed Nd:glass Lasers

Figure 1 shows the experimental light path for the pulsed Nd:glass laser. The maximum energy output of the laser is 7 J, the stability is better than ±5 percent, the pulse width is 200 µs, and the repetition rate is one shot in every 5 minutes.

1. Animal Experiment

The test animals were young Shanghai pigs and hybrid colored pigs. A grid of 2 cm^2 lattice was painted on the skin of the chest and abdomen 2 cm from the spine, as shown in Figure 2.

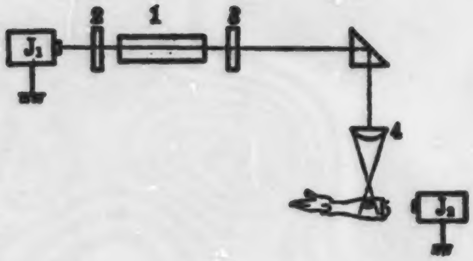

Figure 1
1--Nd glass; 2,3--Reflection mirrors; 4--Focusing lens (f/45); 5--Skin to be irradiated; J_1--Real time energy monitor; J_2--Energy meter for output beam

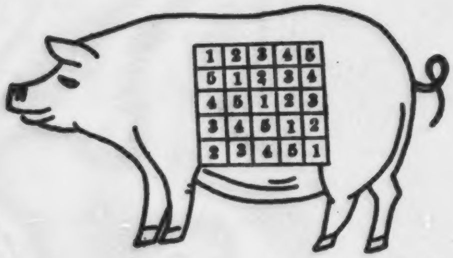

Figure 2. Fifty squares are marked on the skin of each pig

The energy density was determined in some preliminary test shots. For the hybrid pigs the energy density used was 2.753-11.562 J/cm^2. Tests were made at five energy density levels and the results are shown in Table 1. The MRD_{50} value was based on local erythema without edema or blister and persistent for more than 5 minutes.

Table 1. Results of Hybrid Pigs Irradiated by Nd:glass Laser

Group	Energy density	No of shots	No of erythema	Pathological examination
1	2.45 J/cm^2	30	4	(-)
2	4.267 J/cm^2	30	13	(-)
3	5.891 J/cm^2	30	20	(-)
4	9.415 J/cm^2	30	26	20%(+)
5	11.755 J/cm^2	30	30	70%(+)

In Table 1, a "-" sign in the pathological examination column means no pathological changes, a "+" sign means the pathological changes are confined to the cuticular layer. The data were processed using a weighted linear regression method:

Regression equation: $y = 2.121 + 4.326\ x$
MRD_{50}: 4.628 J/cm^2
95 percent confidence level: 4.071 - 5.261 J/cm^2
x^2 test: $P < 0.05$

2. Injury threshold of human skin

The irradiation scheme is shown in Figure 3. The inner surface skin of the two forearms 5 cm above the wrist to the elbow was used, 30 2x2.5 cm^2 grids were marked on the skin surface. Each volunteer was irradiated at a dosage level close to the MRD_{50} value. Skin specimens were taken for erythema that persisted more than 5 minutes after the laser shots and pathological examinations were made using H.E. staining. The results are shown in Table 2.

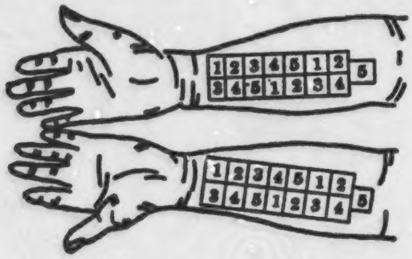

Figure 3

Table 2. Statistics of Erythema Occurrence With 5 Minutes or Longer Persistence

Group	Energy density	No of shots	No of erythema	Pathological examination
1	3.422 J/cm^2	60	1	
2	5.891 J/cm^2	60	7	3 cases of (-)
3	9.751 J/cm^2	60	24	6 cases of (-)
4	12.284 J/cm^2	60	41	3 cases of (-)
5	15.263 J/cm^2	60	51	
6	17.435 J/cm^2	60	59	

The data were analyzed using a weighted linear regression method:

Regression equation: $y = -0.686 + 5.705\ x$
MRD_{50}: 9.921 J/cm^2
95 percent confidence level: 9.269 - 10.618 J/cm^2
x^2 test: $P < 0.05$, acceptable

II. Injury Threshold of CO_2 Laser*

Figure 4 shows the experimental setup. The maximum output power of the laser was 20 W, the divergence angle was less than 3 mrad, the power stability was ±2 percent, and the laser was operated in its fundamental mode.

---

*Xiao Yurui of the burn ward, Ruijin Hospital, Shanghai No 2 Medical University participated in this experiment.

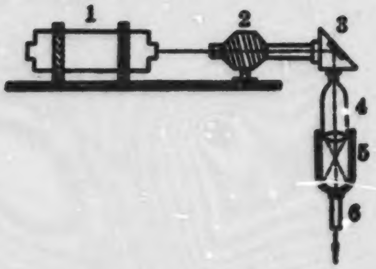

Figure 4
1--CO_2 laser tube; 2--Fixture; 3--Light guide articulation arm; 4--Germanium lens f/35; 5--Telescope tubing; 6--Irradiation aperture 5 mm diameter

1. Animal experiment

Table 3 shows the CO_2 laser test results on animals. The value of MRD_{50} was obtained from the occurrence rate of the erythema that persisted 5 minutes.

Table 3. CO_2 Laser Test Results of Young White Pigs

Group	Power density	No of shots	No of erythema	Pathological changes
1	1.281 W/cm^2	100	2	(-)
2	1.734 W/cm^2	100	17	(-)
3	2.218 W/cm^2	100	42	(-)
4	2.877 W/cm^2	100	66	20%(+)
5	3.593 W/cm^2	100	95	60%(+)

Note: "-" indicates no abnormalities or light edema of shallow hypodermal layer.
"+" indicates changes limited to the cuticle.

The data were analyzed using a weighted linear regression method:

Regression equation: $y = 2.173 + 7.464 x$
MRD_{50}: 2.391 W/cm^2
95 percent confidence level: 2.290 - 2.496 W/cm^2
x^2 test: $P < 0.05$, acceptable

2. Human skin injury threshold for CO_2 laser

Ten volunteers were tested at dosages close to their MRD_{50} level. Using the data shown in Table 4, a linear regression analysis yielded a MRD_{50} of 2.4-2.9 W/cm^2. Skin samples were taken from five volunteers exposed at 2.467 W/cm^2 and interavital microscopy were performed on five volunteers exposed at 2.757 W/cm^2. Seven-tenths of the slides showed shallow hypodermal capillary dilation and congestion and no other abnormalities were observed.

Table 4. CO_2 Laser Injury Results

Group	Power density	No of shots	No of erythema	Pathological changes
1	2.176 W/cm^2	60	3	
2	2.467 W/cm^2	60	17	5 cases of (-)
3	2.757 W/cm^2	60	35	5 cases of (-)
4	3.047 W/cm^2	60	49	
5	3.337 W/cm^2	60	59	

Weighted linear regression of the data yielded:

Regression equation: $y = -2.861 + 18.446 x$
MRD_{50}: 2.668 W/cm^2
95 percent confidence level: 2.607 - 2.730 W/cm^2
x^2 test: $P < 0.05$, acceptable

III. Skin Injury Threshold of Ar Ion Laser

Figure 5 shows the experimental setup. The output power (at 488 nm and 514.5 nm) was 5-6 W, the power at 488 nm was 1.5 W [sic], the stability was better than 3.5 percent and the beam divergence angle was 2.5 mrad.

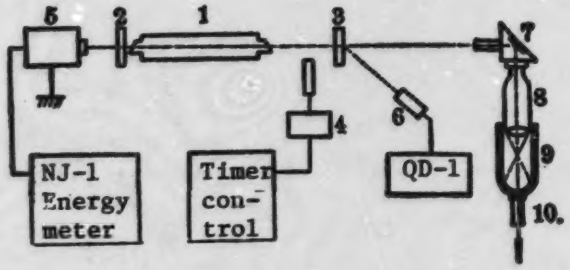

Figure 5
1--Argon laser tube; 2,3--Reflecting mirrors; 4--Time control relay; 5--Model NJ-1 energy meter; 6--Photosensitive element; 7--Light guiding articulation arm; 8--f/45 lens; 9--Lens tube (with movable outer sleeve); 10--5 mm diameter irradiation diaphragm

1. Animal experiment

In the dosage range of 3.918-9.86 W/cm^2, only pink spots were observed on the skin and the redness lasted less than 2 minutes. The hybrid pigs were exposed to 3.337-8.27 W/cm^2 and uniform erythematous reactions were observed after the shots. The redness lasted 5 minutes and the results are listed in Table 6.

Table 6. Argon Laser Test Results on Hybrid Pigs

Group	Power density	No of shots	No of erythema	Pathological examination
1	3.337 W/cm^2	30	0	
2	3.918 W/cm^2	30	3	(-)
3	4.788 W/cm^2	30	12	(-)
4	5.659 W/cm^2	30	20	Cuticle (+)
5	6.82 W/cm^2	30	26	Cuticle (+)
6	8.27 W/cm^2	30	30	

Note: "-" indicates no abnormalities or slight edema of shallow hypodermis. Cuticle "+" indicates changes of some cuticular cells (network changes of prickle cells) and liquification of basal cells.

The data in Table 6 were analyzed by a weighted linear regression method and the results are:

Regression equation: $y = -2.380 + 10.352 x$
MRD_{50}: 5.179 W/cm^2
95 percent confidence level: 4.917 - 5.455 W/cm^2
x^2 test: $P < 0.05$, acceptable

2. Human skin injury threshold

Each volunteer was exposed to a dosage level close to his MRD_{50} to generate erythema that lasted 5 minutes skin samples were then taken for examination. Three volunteers with dark complexions were exposed to 4.933 W/cm^2. Two showed no obvious pathological changes and one showed cuticular cell edema, some basal cell liquification, and hypodermal capillary dilation and congestion. Seven volunteers with an average complexion were exposed to 5.804 W/cm^2. Six showed no changes, one showed slight pathological changes within the cuticular layer. Two volunteers with lighter complexions were exposed to 6.674 W/cm^2 and showed no pathological changes. The results are shown in Table 7.

Weighted linear regression of the data yielded:

Regression equation: $y = -7.388 + 16.550 x$
MRD_{50}: 5.603 W/cm^2
95 percent confidence level: 5.490 - 5.719 W/cm^2
x^2 test: $P < 0.05$, acceptable

Table 7. Human Skin Injury Caused by 488 nm Argon Ion Laser

Group	Power density	No of shots	No of erythema	Pathological changes
1	3.337 W/cm^2	60	0	
2	3.918 W/cm^2	60	2	
3	4.933 W/cm^2	60	10	Three with darker complexion two (-), one (+)
4	5.369 W/cm^2	60	18	
5	5.804 W/cm^2	60	36	Seven with ave. complexion six (-), one (+)
6	6.239 W/cm^2	60	48	
7	6.674 W/cm^2	60	53	Two with lighter complexion both (-)
8	6.96 W/cm^2	60	57	
9	7.25 W/cm^2	60	60	

9698/6091
CSO: 8111/1099

INJURY THRESHOLD OF RETINA IRRADIATED BY ARGON LASER LIGHT

Shanghai ZHONGGUO JIGUANG [CHINESE JOURNAL OF LASERS] in Chinese Vol 12, No 10, 20 Oct 85 pp 600-602

[Article by Wang Kangsun [3769 1660 1327], Wang Ling [3769 3781], Zhang Mingheng [1728 2494 3801], Shi Xianghe [2457 7449 5440], and Chen Gangqiang [7115 0474 1730] of the Department of Ophthalmology, Ruijin Hospital, Shanghai No 2 Medical University, and Hu Qingsheng [5170 1987 3088], Zhuo Ruipeng [0587 3843 7720], Jiang Lanying [3068 5695 5391], and Wu Jianu [0702 1367 1166] of the Laser Research Laboratory, Shanghai No 2 Medical University]

[Text] Abstract: The material, method, results and discussion of the research on the injury threshold of the retina of rabbits, monkeys, and human beings irradiated by argon laser light are introduced. When exposure time is 0.1 s, the retinal injury threshold (ED_{50}) is 0.506 W/cm^2 for rabbits, 0.834 W/cm^2 for monkeys, and 1.757 W/cm^2 for human beings. When exposure time is 1 s, the retinal injury threshold is 0.428 W/cm^2 for rabbits.

Argon lasers are frequently used for medical purposes because their wavelengths--4880 Å and 5145 Å--correspond to a high absorption coefficient by the pigment in the retina and the choroid and by the hemoglobin. Since the argon laser has a unique focusing ability, it is particularly harmful to the eyes. In order to reduce and avoid eye injuries, a safety standard for the argon laser light is much needed. Here we report the retinal injury threshold of rabbits, rhesus monkeys, and humans.

I. Experimental Setup

The light source used in the experiment was a 4880 Å argon ion laser. The setup consisted of the laser, the optical system, and the work bench, as shown in Figure 1. The output power of the laser was 1.2 W, the mode was close to a single mode, the divergence angle was 1.4 mrad, the power was stable to within 2 percent and the energy output was stable to within 3 percent. Irradiation times were 0.1 sec and 1 sec with an error of 0.004 sec. The spot size at the cornea was 2.76 mm. The optical system consisted of a time monitor, an energy monitor, an aiming system and an observation system.

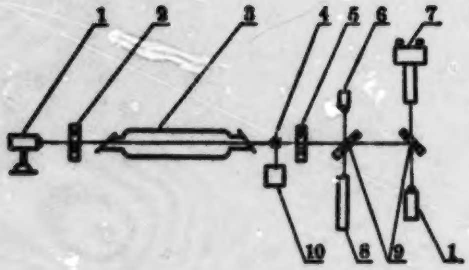

Figure 1. Optical system used in the experiment

1--Laser energy meter; 2--Total reflection mirror of cavity; 3--Argon ion laser tube; 4--Electronic shutter; 5--Half reflecting mirror of cavity; 6--Time monitor probe; 7--Intraocular camera; 8--He-Ne laser; 9--Beam splitter; 10--Timer control

Time monitor: To facilitate the experiment and the monitoring, two 45° coated beam splitters were placed in the optical path to steer the laser beam. The irradiation time was controlled by a high-precision electronic shutter installed in the cavity. The time was controlled to 0.01 sec.

Energy monitor: A model NJ-1 laser energy meter was used to measure and monitor the energy. Extensive tests were made before the animal experiments and the calibrated energy differed very little from the actual value. The energy stability was better than 3 percent.

Aiming and observation: The irradiation was controlled by the shutter. A He-Ne laser was used at the aiming beam. By using a beam splitter, the red He-Ne beam was made to coincide with the blue 4880 Å argon laser beam for accurate aiming. The laser light was directed to the bottom of the eye. On the other side of the beam splitter, a Nikon intraocular camera was installed for real time observation and for photography.

II. Experimental Results

The damage assessments were based on pigment spots on the retina or small light gray coagulation points that appeared within 1 hour after irradiation.

1. Intraocular camera indications

Damages near the threshold consisted of minute pigment isolation or light gray small coagulation spots, sometimes the size of a pinhead. No hemorrhage or bubbles were observed and damage indications often appear a few minutes after the laser shot. As the laser energy was increased, the coagulation spots became bigger, the color became lighter, and the boundary became clearer. No retina hemorrhage observed even for laser energies near the ED_{100} level.

2. Optical microscope indications

(1) The retina of rabbits was irradiated with 5.6-6.0 mJ for 0.1 seconds and samples taken 30 minutes after irradiation. Optical microscopy showed that the fibrous layer of the retina had expanded, the number of dendrites decreased, and the core layer became cystic. The retina blood cells showed noticeable dilation but no hemorrhage.

(2) The retina was irradiated with 4.1-4.5 mJ for 0.1 second and the specimens were taken 24 hours after the irradiation. Optical microscopic observation revealed one surface bulge on the retina with local cell inflammation and exudation of spherical hemachromatin. The fibrous layer showed no noticeable injury but the chorioidea vessels were congested.

(3) Samples taken 48 hours after 0.1 sec irradiation at 4.4-4.9 mJ were examined. No abnormalities were observed except some congestion of the chorioidea blood vessels.

3. Electron microscope indications

Rabbit retinal specimens taken 30 minutes after irradiation at 5.6-6.0 mJ for 0.1 second were examined under an electron microscope. Some blister-like structures filled with medium electron density material were observed on the pigment epithelium, as shown in Figure 2. Cells showed myelin sheath-like structure and the chordriosome was damaged. The plate-like structure of the outer sector of visual cells had local cavities. The membrane had dissolved and high electron density material appeared between membrane structures, as shown in Figure 3. The inner section showed extensive chordriosome swelling, crest breakage, and local cavities (see Figure 4). The cytoplasm was not dissolved but the nuclear membrane showed shrinkage (see Figure 5).

Figure 2

Figure 3

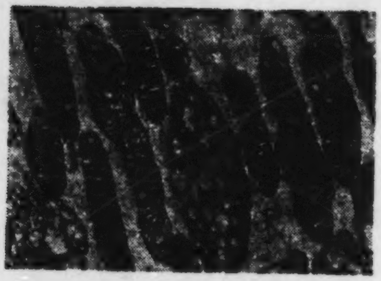

Figure 4

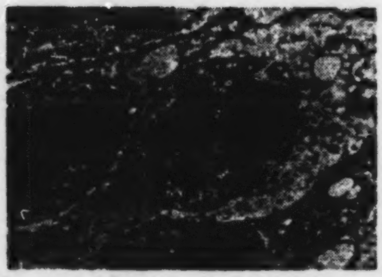

Figure 5

4. Statistics of experimental results (see Tables 1-4)

Table 1. Injury Threshold of Rabbit Retina by 0.1 Sec Exposure to Argon Laser

Group	Average energy (mJ)	Average power density (W/cm^2)	No of shots	No of positive reactions	Percent of positive reaction
1	1.40	0.234	20	0	0
2	1.80	0.301	86	15	17.44
3	2.39	0.399	68	28	41.18
4	3.06	0.512	21	9	42.86
5	4.00	0.669	36	22	61.11
6	4.50	0.752	42	30	71.43
7	5.53	0.925	23	21	91.30

ED_{50} energy = 3.03 mJ (front of cornea), 95 percent confidence limit = 2.74-3.34 mJ; ED_{50} power density = 0.506 W/cm^2 (front of cornea), 95 percent confidence limit = 0.458-0.558 W/cm^2.

Table 2. Injury Threshold of Monkey Retina by 0.1 Sec Exposure to Argon Laser

Group	Average energy (mJ)	Average power density (W/cm^2)	No of shots	No of positive reactions	Percent of positive reaction
1	3.55	0.593	20	3	15.00
2	3.85	0.643	40	8	20.00
3	4.25	0.710	20	5	25.00
4	4.55	0.760	39	13	33.33
5	5.05	0.844	24	11	45.83
6	5.55	0.928	10	8	80.00
7	6.90	1.153	10	9	90.00

ED_{50} energy = 4.985 mJ (front of cornea), 95 percent confidence limit = 4.533-5.482 mJ; ED_{50} power density = 0.834 W/cm^2 (front of cornea), 95 percent confidence limit = 0.757-0.916 W/cm^2.

Table 3. Injury Threshold of Human Retina by 0.1 Sec Exposure to Argon Laser

Group	Average energy (mJ)	Average power density (W/cm^2)	No of shots	No of positive reactions	Percent of positive reaction
1	6.4	1.07	6	0	0
2	8.27	1.382	16	3	18.75
3	10.13	1.694	13	5	38.46
4	12.15	2.031	15	10	66.67
5	13.73	2.295	12	10	83.33

ED_{50} energy = 10.51 mJ (front of cornea), 95 percent confidence limit = 9.43-11.71 mJ; ED_{50} density = 1.757 W/cm^2 (front of cornea), 95 percent confidence limit = 1.576-1.958 W/cm^2.

Table 4. Injury Threshold of Rabbit Retina by 1 Sec Exposure to Argon Laser

Group	Average energy (mJ)	Average power density (W/cm^2)	No of shots	No of positive reactions	Percent of positive reaction
1	18.72	0.313	16	2	12.50
2	21.36	0.357	28	5	17.86
3	23.28	0.389	42	18	42.85
4	26.40	0.441	17	9	52.94
5	28.56	0.477	53	31	58.49
6	30.72	0.513	20	14	70.00
7	32.88	0.549	20	18	90.00

ED_{50} energy = 25.64 mJ, 95 percent confidence limit = 24.14-27.23 mJ; ED_{50} power density = 0.428 W/cm^2, 95 percent confidence limit = 0.403-0.455 W/cm^2.

From the 0.1 sec exposure experiments, the ED_{50} power density is 0.506 W/cm^2 for the rabbit retina, 0.834 W/cm^2 for the monkey retina, and 1.757 W/cm^2 for the human retina. The ratios are rabbit:monkey:human = 1:1.65:3.47. Bringruber[1] has measured the injury threshold of monkey and rabbit retinae by 1 sec exposure of ruby laser and found that the threshold of the monkey retina was 50 percent higher than that of the rabbit retina.

REFERENCES

1. B. Bringruber, Health Physics, 44, 519 (1983).

9698/6091
CSO: 8111/1099

EXPERIMENTAL STUDY ON INJURY THRESHOLD OF ANIMAL RETINAS BY 488 nm LASER IRRADIATION

Shanghai ZHONGGUO JIGUANG [CHINESE JOURNAL OF LASERS] in Chinese Vol 12, No 10, 20 Oct 85 pp 603-605

[Article by Zhao Tongzhen [6392 2717 4176], Dang Zhiping [7825 3112 1627], An Xiaoyue [1344 2556 1471], Zhang Xiaoru [1728 1321 0320], and Guo Wenqi [6753 2429 3823] of the First Affiliated Hospital, Xi'an Medical University]

[Text] Abstract: The experimental results on retinal injury of animals arising from the 488 nm laser irradiation are reported. The ED_{50} of the retinal injury in rabbits and monkeys were obtained for a parallel laser beam and for a beam passing through a convergent lens. The spot diameter at the cornea and the retina was also measured for the two illumination conditions.

I. Experimental Conditions

Light source: Model 360 argon ion laser, continuous wave output, TEM_{00}-TEM_{01} mode, maximum power output of 6 W, 0.5 mrad divergence, stability better than 4 percent.

Optical path: The laser light was expanded into a 6 mm diameter parallel beam by an inverted telescopic system. An electromagnetic shutter controlled the exposure time. The beam then passed through a 3 mm diameter diaphragm and a compensating concave lens. The light spot was positioned on the rabbit eye with the rabbit held on a platform with five degrees of freedom.

Monitor system:

1. The output power stability and the drift of the light spot entering the 3 mm diaphragm were monitored with a model GG-3 high-speed power meter and a model Rj 7200 energy meter respectively.

2. The exposure time was controlled by a model SDK-4 timer control. The actual time when the shutter was open was recorded by a model QD-1 digital timer. The error in time control was less than 0.001 percent.

Measurement equipment:

The measurement errors of the model LW-1 power meter and the model SD2490 high-speed digital power meter were less than ±2 percent.

A microscope eyepiece reticule was used to obtain the light spot diameters on the cornea and on the retina. They were respectively 833 μm and 62 μm. The spot diameter on the retina when the 3 mm diameter parallel beam was incident on the cornea was 900 μm. The ambient temperature was 17-22°C and the relative humidity was 75-80 percent.

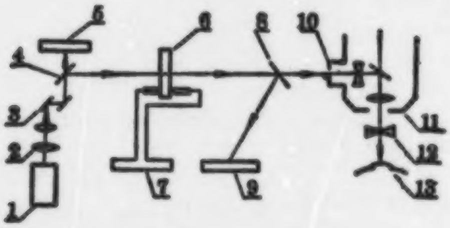

Figure 1. Optical path for retina irradiation by 488 nm argon ion laser

1--Argon ion laser; 2--Inverted telescope as beam expander; 3--Light guide arm; 4--Beam splitter; 5--Power monitor; 6--Electromagnetic shutter; 7--Time monitor; 8--Beam splitter; 9--Energy meter; 10--3 mm beam defining diaphragm; 11--Slit lamp; 12--Compensating concave lens; 13--Eyeball

II. Experiment

1. Grouping of the dosage level: Based on test-run results (Table 1), the dosage was divided into seven groups in the ratio of a geometric series (Table 2).

Table 1. Test-Run Results

	Exposure time (s)	
Dosage (W/cm^2)	1	0.145
Max. dosage	6.54	11.28
Min. dosage	3.77	4.16
Measurement device	LW-1 power meter and SD2490 power meter	

Table 2

Dosage (W/cm^2)	Exposure time (s) 1	 0.145
1	6.54	11.28
2	5.967	9.56
3	5.444	8.09
4	4.967	6.85
5	4.532	5.90
6	4.143	4.92
7	3.77	4.16

2. Selection and grouping of animals: Gray rabbits weighing 2 kg or so were selected. Animals with large pigment discrepancies were rejected. A total of 56 rabbits were used and 718 laser shots were made, 231 injury spots were examined and 3590 data points were collected.

In addition 11 rhesus monkeys weighing 4-5 kg were also used. Due to the small number of monkeys, they were not grouped. The monkey retinas were irradiated using the rabbit eye ED_{50} dosage and the reactions were examined visually and with microscope. The results are shown in Table 3.

Table 3

Rabbit group	1(s)	0.145(s)
No. of group	7	7
No. of rabbits/group	7	4
Sampling points/eye	6	7-8
Total sampling points	248	470

3. Experimental method: After pupil dilation and anaesthesia, the animal was held on a five-degree-of-freedom platform. The slit lamp was held fixed and the platform adjusted so that the laser beam was perpendicular to the cornea. Two horizontal rows of shots were made at 1/4 to 1 visual disk diameters below the visual disk (in the case of the monkeys; between the papilla and the yellow spot). There were three shots in each row with a spacing equal to two spot diameters. For the convenience of observation and locating the injury spots in the low dosage groups, one shot was made at a higher dosage to produce a level II reaction spot as a marker.

4. Observation and recording: Immediate reactions were assessed right after the exposure. The criterion for a positive reaction was a barely discernible injury spot observed in an ophthalmoscope 1 hour after the exposure. The size of the injury spot was far smaller than the smallest level I reaction spot in clinical laser coagulation. The diameter was less than 1 radian and the spot appeared as a light gray circle.

III. Experimental Results

The experimental results on the rabbits and the monkeys are shown in Tables 4-7.

Table 4. Reaction of Rabbit Retina 1 Hour After a 1 Sec Exposure of 488 nm Argon Ion Laser (with compensating lens)

Group	Dosage (W/cm^2)	No of shots	Reaction spots	Reaction rate (%)
1	6.54	48	48	100
2	5.967	48	41	85
3	5.444	48	33	69
4	4.967	48	26	54
5	4.532	48	17	35
6	4.134	48	9	19
7	3.77	48	0	0

Table 5. Reaction of Rabbit Retina 1 Hour After a 0.145 Sec Exposure of 488 nm Argon Ion Laser (with compensating lens)

Group	Dosage (W/cm^2)	No of shots	Reaction spots	Reaction rate (%)
1	11.28	64	64	100
2	9.56	64	53	82.81
3	8.09	64	44	68.75
4	6.85	56	31	55.35
5	5.80	64	23	35.94
6	4.92	64	16	25.00
7	4.16	64	0	0

Table 6. Reaction of Monkey Retina 1 Hour After a 0.145 Sec Exposure to 488 nm Argon Ion Laser (with compensating lens)

Group	Dosage (W/cm^2)	No of shots	Reaction spots
1	6.54x0.5	12	0
2	6.54x1	12	2
3	6.54x1.5	18	3
4	6.54x2	10	5

Table 7. Reaction of Monkey Retina 1 Hour After a 0.145 Sec Exposure to a Parallel Beam of 488 nm Argon Ion Laser

Group	Dosage (W/cm^2)	No of shots	Reaction spots	Reaction rate (%)
1	6.54x2	20	4	20
2	6.54x3.5	20	9	45
3	6.54x4	20	11	55
4	6.54x5	13	9	69
5	6.54x5.5	12	10	83
6	6.54x5.8	11	11	100

Note: 6.54 W/cm^2 is the ED_{50} value for rabbits.

Using the same procedure, 50 shots were also made on human retinas at multiples of the rabbit ED_{50} dosage. The dosage for a 50 percent reaction rate was about 2.7 times the rabbit ED_{50} dosage. The overall results showed a positive correlation between the injury rate and the irradiation dosage. For a fixed laser wavelength, a high dosage was required to produce the same injury when the exposure time was shortened.

IV. Data Processing

The data were processed using a weighted regression method. The ED_{50} results of corneas are shown in Table 8 and the ED_{50} results are shown in Table 9.

Table 8

Expt. subject	Exposure time (sec)	Mode of exposure	Spot diameter (mm)	ED_{50} (W/cm^2)
Rabbit	1	With compensating lens	0.833	4.827
		Parallel light	3	0.396
	0.145	With compensating lens	0.833	6.54
		Parallel light	3	0.504
Monkey	0.145	With compensating lens	0.833	13.08
		Parallel light	3	1.8
Human	0.145	With compensating lens	0.833	17.65

Table 9

Expt. subject	Exposure time (sec)	Mode of exposure	Spot diameter (mm)	ED_{50} (W/cm^2)
Rabbit	1	With compensating lens	0.062	510.09
	0.145	With compensating lens	0.062	629.27
	0.145	Parallel light	0.9	3.08

Note: Corrections were made for compensating lens and eye medium losses.

V. Histological Examination

Two rabbit eyes were irradiated in the same manner using the computed ED_{50} dosage. For the 0.145 sec exposure time, two dosage increments were used above and below the threshold, one eyeball was exposed to each dosage with a total of six eyeballs. Samples were taken 1 hour after the exposure. HE staining observations were made on 30-90 sections of paraffin imbedded samples, the results are published elsewhere.

Participants of the experiments were: Zhang Dexiu [1728 1795 4423], Geng Lide [5105 4539 1795], Ai Hong [5337 4767], Li Yujun [2621 3768 0193], Jiang Beisheng [1203 0554 3932], Wu Tingbi [0702 1694 1084], Yan Wenhui [1693 2429 1920], Zhang Hong [1728 4767], and Ma Shuxian [7456 3219 1288].

9698/6091
CSO: 8111/1099

RESEARCH ON INJURY THRESHOLD OF RABBIT CORNEA BY CO_2 LASER

Shanghai ZHONGGUO JIGUANG [CHINESE JOURNAL OF LASERS] in Chinese Vol 12, No 10, 20 Oct 85 pp 606-608, 605

[Article by Wang Kangsun [3769 1660 1327], Wang Ling [3769 3781], Zhang Mingheng [1728 2494 3801], Shi Xianghe [2457 7449 5440], Chen Gangqiang [7115 0474 1730], and Shi Haiyun [4258 3189 0061] of the Department of Ophthalmology, Ruijin Hospital, Shanghai No 2 Medical University, and Zhuo Ruipeng [0587 3843 7720], Hu Qingsheng [5170 1987 3088], Jiang Lanying [3068 5695 5391], Wang Yuejin [3769 6460 6651], and Gai Baokang [5556 1405 1660] of the Laser Research Laboratory, Shanghai No 2 Medical University]

[Text] Abstract: The material, methods, and results of research on the injury threshold of rabbit cornea caused by CW CO_2 laser light are introduced. The dose for causing ED_{50} varies with the time of exposure: they are 3.62 W/cm^2 and 4.01 W/cm^2 for 1 sec and 125 ms irradiation respectively.

CO_2 lasers are finding broad clinical applications as well as laboratory and industrial uses. Since its wavelength 10.6 μm falls in the invisible far infrared regime, it may cause injuries if not used carefully. The eye injury by the CO_2 laser light occurs primarily in the cornea and not in the interior of the eyeball. In this paper we report an injury threshold study of the rabbit cornea by CO_2 laser. It is intended to provide some basis for establishing China's laser safety standard.

I. Experimental Setup

The CO_2 laser used in the experiment had an output power of 20 W, a divergence angle of less than 3 mrad, and the beam mode was close to the fundamental. The fluctuation of the output power was controlled to within 3 percent. In order to maintain a stable power output, the thermal equilibrium of the cavity was carefully guarded. The beam was first focused with a germanium lens (f/35 mm), and was then diverged. The power density at the target tissue was varied by adjusting the outer sleeve of the lens tube and by attaching extensions of different length. The spot diameter on the cornea was 1 mm and the exposure was made through a thin stainless tube, as shown in Figure 1.

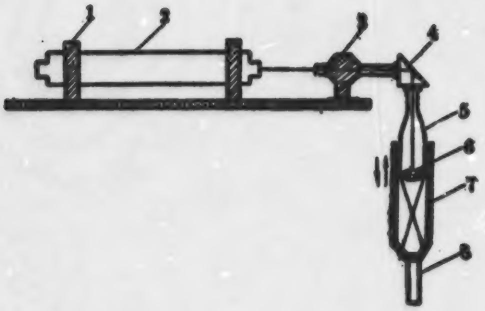

Figure 1. Optical transmission system

1--Hold-down ring for laser tube; 2--CO_2 laser tube; 3--Holder for light transmission system; 4--Light guide arm (one section); 5--Germanium lens tube (inner tube); 6--f/35 germanium lens; 7--Movable outer sleeve; 8--Variable length extension (set of five)

II. Experimental Method

The experimental animals were 2-3 kg gray rabbits with similar eye color. Animals with cornea disease such as cloudiness, white spots, and cornea epithelium detachment were rejected. The rabbits were anesthetized with 2.5 percent isobarbituric sodium 25 mg/kg intravenous solution without dilating the pupils. The 10.6 μm CW CO_2 laser light was directed onto the cornea perpendicularly through the 1 mm diameter extension with the cornea 5 mm from the exit of the extension tube. The laser beam irradiated the cornea in the pupil region at five points: the center of the pupil and four peripheral points in the 1:30, 4:30, 7:30, and 10:30 directions. The spacing between two shots was at least two spot diameters (see Figure 2). One group was exposed for 1 second and the other group exposed for 125 ms. Each group of rabbits was further divided into 6-7 dosage levels. A minimum of 30 eyeballs were exposed at each dosage level and a total of 402 eyeballs of 202 rabbits [sic] were irradiated. A 10-minute observation period followed the laser shots and small white spots on the cornea found in this period were considered a positive reaction. The observations were conducted by two experimental ophthalmologists.

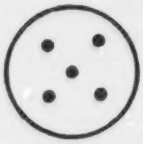

Figure 2. Irradiation positions on the cornea by CO_2 laser

III. Experimental Results

1. Cornea examination

For the 1 second exposure group the cornea showed larger spots, 0.1-0.3 mm in diameter, light gray in color, usually circular in shape, and very few strip-like or crescent in shape. This may depend on whether the laser beam is perpendicular to the cornea. All spots disappeared within 24-48 hours.

The 125 ms exposure group showed much smaller spots on the cornea, all of them the size of a pinhead, white in color and disappeared within 24 hours.

2. SEM examination

(1) The corneas of gray rabbits were irradiated at an energy level close to the ED_{50} dosage (32 mW) for a second and specimens were taken 30 minutes after the shots. SEM examination showed rupture of the epithelium cells and a reduction of the number of microfibril on the nucleus (as shown in Figure 3). The epithelium cells recovered after 48 hours, as shown in Figure 4.

Figure 3. 2100 X magnification

Figure 4. 5620 X magnification

(2) The gray rabbit corneas were also irradiated at a dosage level exceeding the ED_{100} dose (60 mW) for 1 second and specimens were taken 30 minutes after the shots. SEM examination showed a decrease of microfibril of some epithelium cells and necrosis of nucleus (see Figure 5). Some cell membrane detachments were observed, showing the underlying microfibril (Figure 6). After 48 hours, some epithelium cells still showed sparse microfibril and the cells showed lattice-like changes (Figure 7).

3. Statistical analysis of data

The results of the six groups exposed for 1 sec and the seven groups exposed for 125 ms are listed in Tables 1 and 2. Both sets of data were analyzed with a weighted linear regression method to find ED_{50}. The results are:

1 second exposure groups:

$ED_{50} = 3.62 \text{ W/cm}^2$
95 percent confidence limit = $3.56\text{-}3.68 \text{ W/cm}^2$

125 ms exposure groups:

$ED_{50} = 4.01 \text{ W/cm}^2$
95 percent confidence limit = $3.97\text{-}4.03 \text{ W/cm}^2$

Figure 5. 1060 X magnification

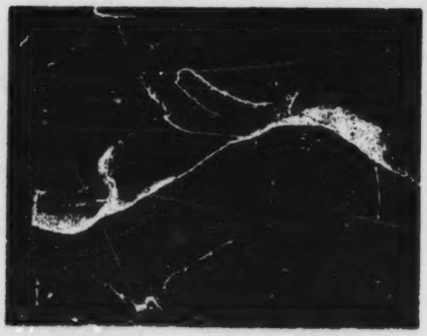

Figure 6. 2100 X magnification

Figure 7. 1060 X magnification

Table 1. 1 Sec Exposure Results

Group	Ave. energy (mJ)	Ave. power density (W/cm^2)	No of shots	No of reactions	Positive reaction rate (%)
1	21.61	2.75	150	4	2.67
2	23.16	2.95	155	14	9.03
3	27.24	3.47	150	68	45.33
4	30.35	3.86	150	90	60.00
5	34.60	4.40	155	136	87.74
6	37.01	4.71	150	148	98.67

Table 2. 125 ms Exposure Results

Group	Ave. energy (mJ)	Ave. power density (W/cm^2)	No of shots	No of reactions	Positive reaction rate (%)
1	3.13	3.19	160	1	0.62
2	3.40	3.47	340	11	3.24
3	3.67	3.74	155	50	32.26
4	3.98	4.05	155	92	59.35
5	4.26	4.34	155	112	72.26
6	4.55	4.63	150	139	92.67
7	4.83	4.92	150	148	98.67

IV. Discussion

Judging from our experimental results, cornea injuries occurred in 1 sec exposures at 3.62 W/cm^2 and 125 ms exposures at 4.01 W/cm^2. Of course the injuries near the threshold were light and reversible, and limited to the epithelium of the cornea. Slit lamp cornea microscope and SEM observations showed that the injuries were repaired within 24-48 hours without remnants. The absorption of the visible light depended on the amount of pigment whereas the absorption of the far infrared laser light depended on the water content; most of the far infrared energy was absorbed by the water. The water content of the cornea is greater than 75 percent. The absorption curve of the cornea is greater than 75 percent. The absorption curve of the cornea is similar to that of water,[1] the majority of the energy of the CO_2 laser is therefore absorbed by the water-rich cornea tissue and the generated heat produces the damage. An increased power or exposure time leads to an increase of the cornea temperature and results in thermal injury and protein coagulation.[1] The injuries at doses above the threshold are much more complex. Campbell found that an exposure to a CO_2 laser at 100 mW for 3 seconds caused shrinkage of the shallow layer of the cornea. At 500 mW the injury extended to the deep layer of the cornea, accompanied by the formation of new blood vessels. Such injuries may heal but the scarred tissue affected the transparency of the cornea. At a dose above 1000 mW, cornea puncture and crystal injury may occur.[2]

As CO_2 lasers find increasingly wide uses in laboratories, hospitals, and in industries, and the power levels are generally higher (at least several tens of watts), cornea injuries may be caused by CO_2 laser beams reflected from tools, surgical instruments and mirrors. The results are of course disastrous if one inadvertently looks directly into the beam. Since infrared lights are invisible, the danger is higher.

REFERENCES

1. H.M. Leibowitz, et al., ARCH. OPHTHALMOL., 1969, 81, 713.

2. C.J. Campbell, et al., AM. J. OPHTHALMOL., 1968, 66, 604.

9698/6091
CSO: 8111/1099

RESEARCH ON INJURY THRESHOLD OF GRAY RABBIT'S RETINA BY Q-SWITCHED, FREQUENCY DOUBLED Nd^{3+}:YAG LASER

Shanghai ZHONGGUO JIGUANG [CHINESE JOURNAL OF LASERS] in Chinese Vol 12, No 10, 20 Oct 85 pp 609-611

[Article by Wang Kangsun [3769 1660 1327], Wang Ling [3769 3781], Zhang Minheng [1728 2494 3801], Shi Xianghe [2457 7449 5440], Chen Gangqiang [7115 0474 1730], and Shi Haiyun [4258 3189 0061] of the Department of Ophthalmology, Ruijin Hospital, Shanghai No 2 Medical University, and Jiang Lanying [3068 5695 5391], Zhuo Ruipeng [0587 3843 7720], Hu Qingsheng [5170 1987 3088], and Wu Jianu [0702 1367 1166] of the Laser Research Laboratory, Shanghai No 2 Medical University]

[Text] Abstract: The material, methods, and results of the research on the injury threshold of gray rabbit's retina caused by Q-switched and frequency doubled Nd^{3+}:YAG laser light are introduced. When exposure time is 8 ns, ED_{50} is 232.05 $\mu J/cm^2$ (precornea).

Frequency doubled Nd^{3+}:YAG laser emits a green light of a wavelength 5300 Å. The wavelength corresponds to a high transmissivity in the vitreous humor and a high absorptivity by the retina and choroid. It is also near an absorption peak of the hemoglobin and can cause more injury to the eye than other wavelengths. This is especially true for large pulses. In this work we studied the retinal injury threshold of gray rabbits by the Nd^{3+}:YAG laser and collected data for establishing a laser safety standard.

I. Experimental Setup

The laser used in our experiment was a Q-switched YAG pulse laser built by the Shanghai Jiaotong University. The maximum energy output was 20 mJ, the divergence angle was 4.5 mrad, the pulse width was 8 ns, the laser may be operated to produce a single pulse or be pulsed once every second, and the output was multimode.

The optical system consisted of a He-Ne laser, a beam splitter, a filter, an attenuation and an ophthalmoscopic camera, shown in Figure 1.

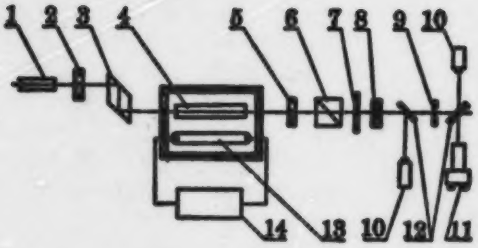

Figure 1. Q-switched frequency doubled YAG laser setup

1--He-Ne laser; 2--Total reflection mirror; 3--LN Q-switch crystal; 4--YAG rod; 5--Half-reflecting mirror; 6--KDP frequency doubling crystal; 7--Filter; 8--Attenuator; 9--Diaphragm; 10--Energy meter; 11--Ophthalmoscopic camera; 12--Beam splitter; 13--Pulsed xenon lamp; 14--Power supply

The He-Ne laser followed the same optical path as the 5300 Å green laser light and served as an alignment and aiming beam. The beam splitter with a ratio of 1:1 was used to measure the laser energy.

The filter eliminated the infrared component and the attenuator controlled the intensity of the 5300 Å output. Since the laser had a multimode output, the homogeneity of the spot was poor. A 2.5 mm diameter diaphragm was therefore placed in front of the eyeball to limit the spot size and shape and to improve the homogeneity. The beam diameter at the cornea was 4.0 mm. A Nikon ophthalmoscopic camera was used to observe and photograph the bottom of the eyeball. The laser passed through the cornea directly without any compensating lens or contact lens.

The pulse width of the Q-switched laser was very narrow. A Tektronics 466 storage oscilloscope with a sweep time of 20 ns/div was used to capture the optical signal. Real time monitoring was used to assure accuracy. The model RJP-700 laser light energy meter was equipped with two probes and the measured energies and their ratio were stored in the unit. The two probes were placed behind the two beam splitters for real time monitoring. Extensive tests showed that the error was less than 5 percent.

II. Experimental Method

Gray rabbits weighing 2-3 kg without eye diseases were selected for the experiment. The animal was anesthetized and placed in the cage with multiple degrees of freedom. The He-Ne laser was aimed at the region below the papilla of the rabbit. The eye was first examined with the Nikon ophthalmoscopic camera and the Q-switched YAG laser was then used for the irradiation. Ten to 20 shots were made in each eyeball with a spacing equal to at least two spot diameters. A total of 691 shots were made on 64 eyeballs on 32 rabbits. Ophthalmoscopic photos were taken after the shots. Some eyeballs were removed for optical and electron microscope specimen preparation. The ambient temperature was 25-28°C and the humidity was 62-82 percent.

III. Experimental Results

Two experimental ophthalmologists made the observations after the irradiation. A positive reaction was recorded if pigment spots, coagulation spots or hemorrhage were observed on the retina within 1 hour.

1. Ophthalmoscopic camera indications: Depending on the laser energy, the reaction of the rabbit retina to the Q-switched YAG laser irradiation may be divided into six cases: 1) Pigment spreading like soap bubbles; 2) small coagulation spots with small pigment spots at the center; 3) coagulation spot surrounded by pigment rings; 4) cauliflower-like hemorrhage pattern with central coagulation spot; 5) circular hemorrhage in the deep layer with central coagulation spot. The hemorrhage may occur with or without delay; and 6) extensive hemorrhage of the retina and flowing into the vitreous humor. For a dosage level up to ED_{100}, the retina reactions were generally pigment spreading, small coagulation spots, and sometimes hemorrhage spots. The injuries were very minor and difficult to detect under an ophthalmoscope.

2. Optical microscope indications: The retina was irradiated with 330.41 $\mu J/cm^2$ (ED_{100} dose) and the specimens were taken 30 minutes after the laser shot. Optical microscopic examinations failed to show any obvious injuries of the retina pigment epithalium or the visual cell layer. Slight congestion of the choroid blood vessels and hemorrhage were observed.

3. SEM indications: After an exposure at a dosage level of 330.41 $\mu J/cm^2$ (ED_{100} dose), blisters were observed at local sites on the pigment epithalium and they were filled with a material of medium electron density. Medullary sinus-like structures appeared in the cells, the chondriosome swelled and the crest was broken (shown in Figure 2). The disk structures on the outer section of the optic cells showed local voids, the membrane structure dissolved and high electron density particulates showed up between the membrane structures, as shown in Figure 3. Extensive inner section chondriosome swelling, crest breaking, and cavitation (Figure 4) were observed. The cytoplasm of the outer particulate layer had dissolved and the nucleus showed no obvious changes (Figure 5).

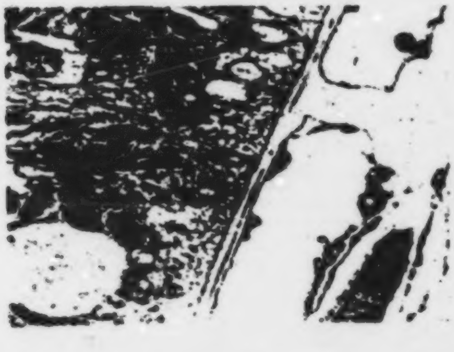

Figure 2. 9250 X magnification

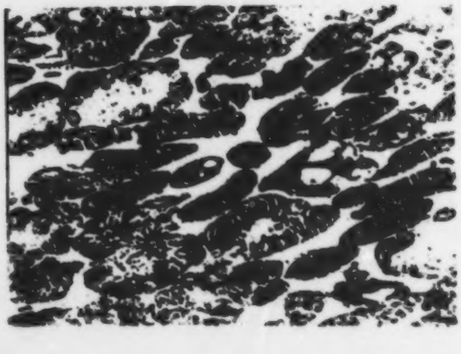

Figure 3. 5550 X magnification

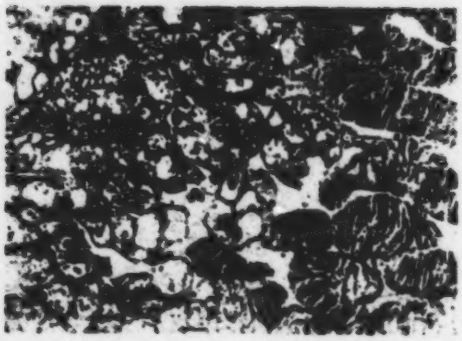

Figure 4. 7600 X magnification

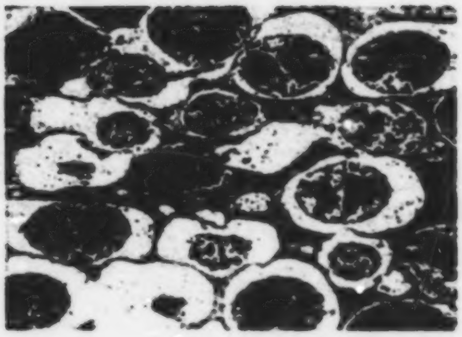

Figure 5. 5700 X magnification

4. Statistical analysis of data

A weighted linear regression method was used in analyzing the positive reaction of 691 laser shots on 64 pairs of rabbit eyeballs. The results are listed in Table 1.

Table 1. Retinal Reaction of Rabbits Irradiated by Q-Switched Frequency Doubled YAG Laser

Group	Average energy (μJ)	Energy density (μJ/cm^2)	No of shots	No of reactions	Positive reaction rate (%)
1	21.5	171.18	79	7	8.86
2	25.5	203.03	97	32	32.99
3	29.5	234.87	98	55	56.12
4	33.5	266.72	100	72	72.00
5	37.5	298.57	90	71	78.89
6	41.5	330.41	84	77	91.67

Note: ED_{50} = 232.05 μJ/cm^2 (before cornea)
95 percent confidence limit = 224.87–239.45 μJ/cm^2

IV. Discussion

Since the Q-switched frequency doubled YAG laser has a wavelength of 5300 Å, the absorption by the retina, choroid, and hemoglobin is high. Since the laser pulse is short (of the order of nanoseconds), retinal hemorrhage is likely. The energy causing hemorrhage is close to the threshold dosage. The ED_{50} energy is 29.14 μJ. At 40 μJ, about one-third of the reaction points showed hemorrhage. The study of the injury threshold of Q-switched YAG laser is therefore very important for laser safety standards.

In terms of the reaction at the back of the eye, optical and electron microscopic observations show that short duration large energy pulses at 5300 Å have both a thermal effect and a shock wave effect on the retina and the choroid. The thermal effect led to coagulation spots. SEM showed local blisters of the pigment epithalium filled with medium electron density material. The inner and outer sections of the optic cell had suffered various degrees of damage such as the dissolving of the disk structure, the swelling of the chondriosome, and the dissolving of the cytoplasm. The shock wave effect led to hemorrhage of the back of the eye. Optical microscope showed hemorrhage of the choroid but only slight congestion.

9698/6091
CSO: 8111/1099

RETINAL INJURY THRESHOLD BY CW Nd^{3+}:YAG LASER LIGHT

Shanghai ZHONGGUO JIGUANG [CHINESE JOURNAL OF LASERS] in Chinese Vol 12, No 10, 20 Oct 85 pp 612-614

[Article by Xu Jiemin [1776 4309 2404], Hu Fugen [5170 1381 2704], Zhou Shuying [0719 3219 5391], Cao Weiqun [2580 4850 5028], Xu Guidao [1776 6311 6670], Qian Huanwen [6929 3562 2429], Shi Liangshun [2457 5328 7311], and Wang Denglong [3769 6260 7893] of the Institute of Radiation Medicine, Academy of Military Medical Sciences]

[Text] Abstract: One hundred rabbit eyes were exposed to CW Nd^{3+}:YAG laser light. Using ophthalmoscopic criteria for retinal injury, the intraocular injury points (ED_{50}) were 2.52 W/cm^2 and 5.42 W/cm^2 for exposure time of 1.02 s and 0.12 s, respectively.

The purpose of this investigation is to study the injury threshold of the eye by CW Nd^{3+}:YAG laser and to provide biological data for the establishment of a laser safety standard.

I. Experimental Setup and Method

The experimental setup consisted of a model JQY-1 CW Nd^{3+}:YAG laser, a time monitor, an electronic shutter, an He-Ne laser, and a beam defining jaw. The maximum output power of the laser was about 9.5 W. The beam divergence angle after a 3x collimating telescope and a 510 mm focal length lens were respectively 16 mrad and 3 mrad. The stability of the output power was better than ±5 percent. The diameter of the beam defining jaw was 5 mm. The setup and the optical path are shown in Figures 1 and 2.

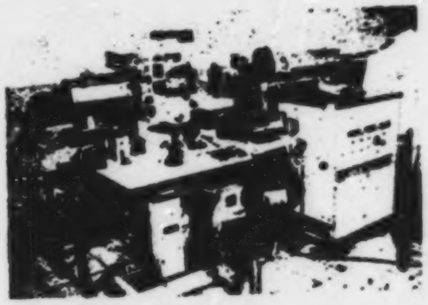

Figure 1. Irradiation setup using CW Nd^{3+}:YAG laser

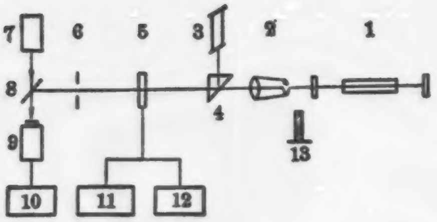

Figure 2. Optical path for CW Nd^{3+}:YAG laser output power measurement

1--CW Nd^{3+}:YAG laser; 2--Telescope; 3--He-Ne laser; 4--Right-angle prism; 5--Shutter; 6--Diaphragm; 7--TOPCON ophthalmoscopic camera; 8--Reflecting mirror; 9--RKP-545 probe; 10--RK-5200 laser power rate meter; 11--Timer control; 12--Time monitor; 13--Shielding plate

The experimental animals were 2-3 kg gray rabbits. Examinations were made of the back of the eye before laser irradiation. The hyperopia was less than 2.25 D, the myopia was less than 1.00 D, and no corrections were made.

The irradiation was confined to the central visual zone of the back of the eye and 10 shots were made for each eye. Ophthalmoscopic observations were made 1 hour and 24 hours after irradiation and the observations were made by two people. Some of the rabbits were killed and the eyeballs removed for pathological and histological examinations.

II. Experimental Results

The dosage range was 2.02-9.09 W/cm^2 for cornea incidence. The average irradiation times were 1.02 sec and 0.12 sec, with five dosage levels for each irradiation time. A total of 1000 shots was made on 100 rabbit eyes.

1. Retinal injuries

For the dosage used in this study, the retinal injuries were light. Ophthalmoscopic examinations made 1 hour after the shots showed small circular or elliptical light gray spots with sparse dark pigment particles at the center and the perimeter. Some spots were surrounded by a light gray edema ring. The more severe injuries showed a small black burn spot at the center. Some spots showed small hemorrhage at the center.

Observations made after 24 hours showed a spreading of the damage and a noticeable increase of black pigments at the perimeter. The edema receded after 3-5 days and the damage shrank toward their center after 5-10 days and became light gray pigment deposits.

The retinal injuries caused by the CW Nd^{3+}:YAG laser are shown in Figure 3.

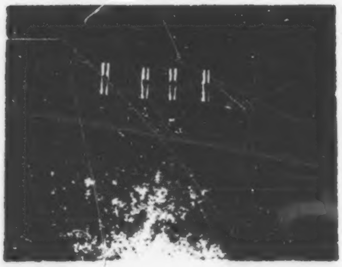

Figure 3. Light gray injury spots of the rabbit retina caused by 0.1 sec irradiation of CW Nd^{3+}:YAG laser light at 5.09 W/cm^2

2. Retinal injury rate as a function of dosage and time

Irradiation was conducted at 10 dosage levels. For the first five groups the average exposure time was 1.02 sec. For the second five groups the average exposure time was 0.12 sec. Table 1 lists the dosage, exposure time, and injury rate. As can be seen, the rate of retinal injury increased with the incident power density and the incident power density for a given injury decreased with an increase in exposure time. The injury occurrence rate was 11-92 percent for an exposure time of 1.02 sec and an average incident power density of 2.02-3.21 W/cm^2 at the cornea. The injury occurrence rate was 13-91 percent for an exposure time of 0.12 sec and an average incident power density of 3.56-9.09 W/cm^2 at the cornea.

Table 1. Irradiation Dosage, Exposure Time, and Retinal Injury Rate of Rabbit Eyes Irradiated by a CW Nd^{3+}:YAG Laser

Group	Ave. exposure time (s)	Ave. incident dose (W)	Ave. incident dose (W/cm^2)	Injury rate Injury/ No of shots	Injury rate %
1	1.019	6.30×10^{-1}	3.21	92/100	92
2	1.022	5.62×10^{-1}	2.87	73/100	73
3	1.023	4.99×10^{-1}	2.55	53/100	53
4	1.019	4.50×10^{-1}	2.30	33/100	33
5	1.020	3.96×10^{-1}	2.02	11/100	11
6	0.116	1.78	9.09	91/100	91
7	0.117	1.27	6.47	67/100	67
8	0.118	9.98×10^{-1}	5.09	44/100	44
9	0.119	8.37×10^{-1}	4.27	28/100	28
10	0.118	6.97×10^{-1}	3.56	13/100	13

3. Calculation of the injury threshold of a CW Nd^{3+}:YAG laser

The experimental data were analyzed using a Bliss probability unit, weight regression method to find the regression equation for the CW Nd^{3+}:YAG laser. For the 1.02 sec exposure time, the regression equation was

$$\hat{Y} - 12.45X + 0.0065$$

where X is the logarithm of the dosage and $\hat{Y}$ is the probability unit for rabbit retinal injury. Also computed was

$$ED_{50} \simeq 2.52\ \mathrm{W/cm^2}$$

(95 percent confidence limit = 2.46-2.58 W/cm^2)

For the average exposure time of 0.12 sec, the regression equation was found to be

$$\hat{Y} = 5.950X + 0.6835$$

$$ED_{50} \simeq 5.42\ \mathrm{W/cm^2}$$

(95 percent confidence limit = 5.16-5.69 W/cm^2)

The regression line was checked for X^2. The X^2 values for the 1.02 sec and 0.12 sec exposure time groups were respectively 1.0401 and 0.1695, much less than the $X^2_{0.05}$ value of 7.8045 in both cases ($P > 0.05$). This showed that for both exposure conditions the linear relationship held. Figures 4(a) and (b) show the regression curves.

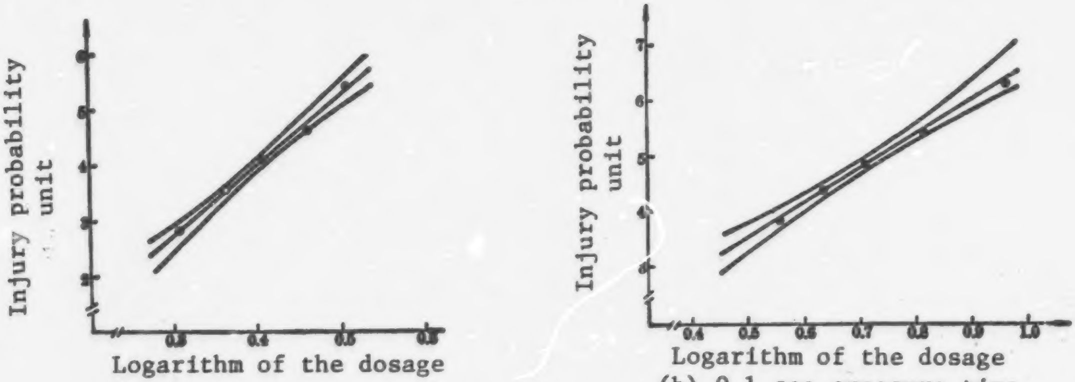

(a) 1 sec exposure time

(b) 0.1 sec exposure time

Figure 4. Regression lines of rabbit retinal injury by a CW YAG laser

4. Pathological indications of retinal injury by CW YAG laser

Using dosage close to the injury threshold, irradiations were made at an average incidence power density of 2.55-3.21 W/cm^2 for 1.02 sec and at 5.09 W/cm^2 for 0.12 sec. The retinal injuries showed the following pathological changes:

Particle-like exudates and vaporized regions were present under the retina, causing a slight bulge in the retina. The vaporized regions were located between the liquid exudate and the particles and spread outward in a circular pattern. Detachment of dead cells was visible in the vaporized region.

Some pigment epithalium cells showed severe swelling and even rupture. Black pigment was dispersed or piled into pigment bands. Damaged optic cells showed broken outer sections. Typical damages were 200-300 μm long (see Figure 5).

(a) Exudation and vaporization under the retina (exposed for 1 sec at 2.55 W/cm^2)

(b) Exudation under the retina, pigment segregation, and vaporized region ruptured the inner and outer granular layer (exposed for 1 sec at 5.09 W/cm^2)

Figure 5. Retinal injury caused by CW Nd:YAG laser (x63 magnification)

For dosage greater than the injury threshold shrinkage of the cell nucleus in the inner and outer granular layer, swelling or detachment of the ganglia nucleus were observed in the vaporized region.

III. Conclusions

We made 1000 shots on 100 gray chinchilla rabbit eyes with a model JQY-1 CW Nd:YAG laser. The data were analyzed with a Bliss weighted regression method to find the retinal injury threshold for 1.02 sec and 0.12 sec exposure. The values of ED_{50} were respectively 2.52 W/cm^2 and 5.42 W/cm^2. The injury indications and pathological changes were described.

The authors thank Tang Zhongming [3282 0112 2494] for computer analysis of the data.

9698/6091
CSO: 8111/1099

INJURY THRESHOLD OF HUMAN EYE BY PULSED YAG LASER BEAMS, PATHOLOGICAL OBSERVATION

Shanghai ZHONGGUO JIGUANG [CHINESE JOURNAL OF LASERS] in Chinese Vol 12, No 10, 20 Oct 85 pp 615-617

[Article by Chen Rongjia [7115 2837 1367], Chu Renyuan [5969 0088 6678], Li Mengchang [2621 5492 2490], Li Ling [2621 1515], Lu Jiahua [0712 0857 5478], and Fu Tiansheng [0265 1131 3932] of the Ophthalmic Research Institute of Shanghai Medical University and Cui Jixiu [1508 1323 4423], Zhu Baoqian [2612 1405 6870], and Lu Zhenzhen [0712 3791 3791] of the Shanghai Institute of Optics and Fine Mechanics, Chinese Academy of Sciences]

[Text] Abstract: The injury threshold of human retina by 150 μs pulsed YAG laser beam irradiation is reported. Pathological phenomena of injured retina were observed directly using optical microscope and electron microscope.

Based on the animal test results, we have obtained some retinal injury data of the human eye by 150 μs wide YAG laser pulses at a wavelength of 1.06 μm. We also gained preliminary understanding of the retinal damage of human eyes by laser by comparing the pathology of retinal injuries in animals and in humans.

I. Measurement of the Injury Threshold of Human Eyes

150 μs YAG laser pulse irradiations were performed on five human eyeballs in five patients with malignant eye socket tumor and scheduled for eye removal. The cornea, lens, vitreous humor and the back of the eye of these eyeballs were all normal. Several tens of shots were made in each eyeball and observations were made immediately after the shots and after 1 hour and 24 hours.

In order to obtain accurate data, the pupil was enlarged and detailed examinations were made to check vision, the cornea, the vitreous humor and the back of the eye. Eyes with cornea diseases and with cloudy vitreous humor were rejected. A total of 426 shots were made on five eyeballs. Figures 1 and 2 show the back of one eye before irradiation and 1 hour after irradiation. The retinal injury threshold ED_{50} was obtained by analyzing the data with a weighted linear regression method. The results are

$$ED_{50} = 1.55\ \mathrm{mJ}$$

and the 95 percent confidence limit of ED_{50} was

$$\Delta ED_{50} = (1.80\,\mathrm{mJ}, 1.86\,\mathrm{mJ})$$

The spot area of the laser entering the eye was $\Delta S = 2.41\ \mathrm{mm}^2$. When the energy level reached the injury threshold, the incident laser power density was

$$P = 429\ \mathrm{W/cm}^2$$

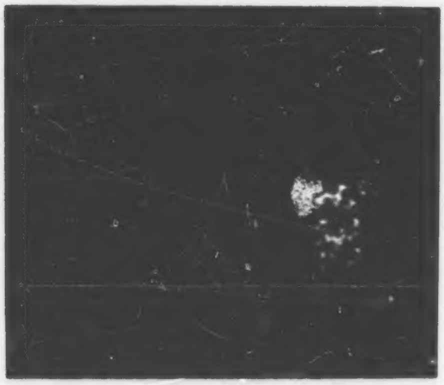

Figure 1. The right eye of a patient before laser irradiation

Figure 2. The back of the right eye 1 hour after the laser irradiation (the white spot is the laser damage)

By comparing the injury threshold of the human eye with that of rabbits and monkeys, we have

$$E_{rabbit}:E_{monkey}:E_{human} = 1.0:3.4:6.0$$

II. Pathological Observation of Laser Retinal Damages in Rabbits, Monkeys, and Humans

Optical and electron microscope examinations were made on irradiated rabbit, monkey, and human eyes. The specimen preparation methods are as follows:

TEM specimen preparation: Specimens were taken within 4 minutes after the eyeball was removed from the body. It was first fixed in a 2.5 percent pentaldehyde and then fixed again in 1 percent osmic acid, followed by TEM observation.

Optical microscope specimen preparation: The removed eyeball was placed in an eyeball fixing solution for 24 hours. After being removed from the solution the eyeball was imbedded in collodion and then sectioned, HE stained, and examined under an optical microscope.

Observation results:

Figures 3 and 4 show the histological changes of the retina of a gray rabbit exposed to a CW YAG laser at 207 mJ for 137 ms as observed by a TEM. The magnification for Figure 3 is 1700 times. The figure shows local disarrangement of the retina pigment epithalium, swelling of the chondriosome, and cavities. The magnification of Figure 4 is 1500 times and the figure shows swelling of the endoplasmic reticulum and wrinkling of the membrane structure to become lace-like.

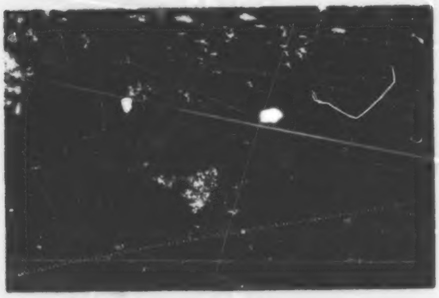

Figure 3

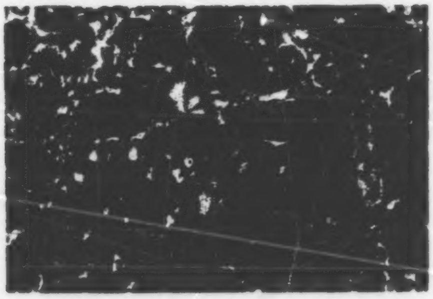

Figure 4

Figure 5 shows the retinal injury of a monkey eye observed under an optical microscope at a magnification of 200 times. The irradiation energy was 0.66 mJ. As can be seen, the structure of the retinal nerve fiber layer was disarranged. The endoplasmic reticular layer at the irradiated spot showed slight swelling and exudation. The inner membrane was intact and the inner granular layer showed noticeable changes. The number of nuclei decreased and the inner reticular layer collapsed toward the other reticular layer.

Figure 6 shows the retinal damages of a monkey eye exposed to 1.21 mJ of laser light. The inner membrane and the nerve fiber layer had suffered traumatic damages and extensive exudation. The inner granular layer showed a decrease in the number of nuclei and an indentation.

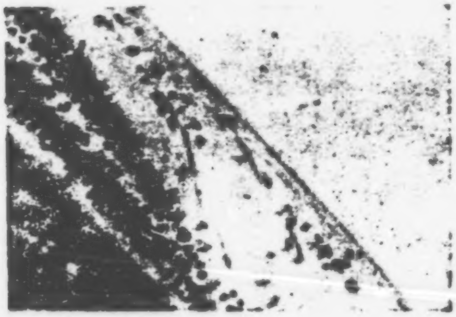

Figure 5

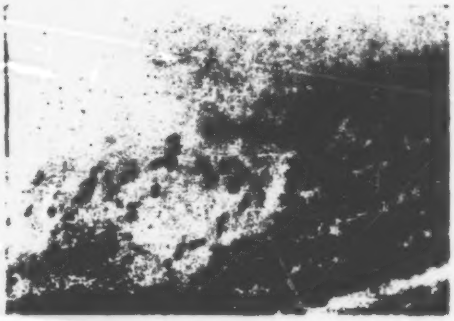

Figure 6

Figure 7 shows the retinal damages by 0.91 mJ of laser irradiation. The inner membrane was fused to the nerve fiber layer and concaved downward. The inner granular layer showed a decrease of number of cells and indentation. The outer granular layer and membrane remained normal.

Figure 8 shows the retinal injury caused by 2.17 mJ of laser irradiation. The inner membrane ruptured and the nerve fiber layer suffered severe damage. The lymph cells were infiltrated and the ganglia cells showed noticeable swelling and fragmentation. The inner granular layer was also affected somewhat.

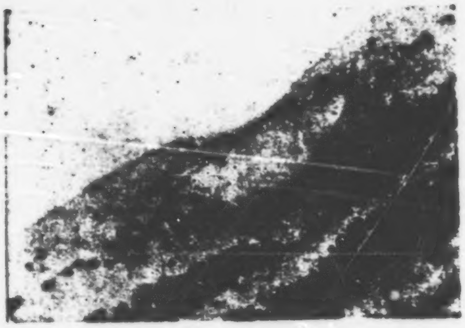

Figure 7

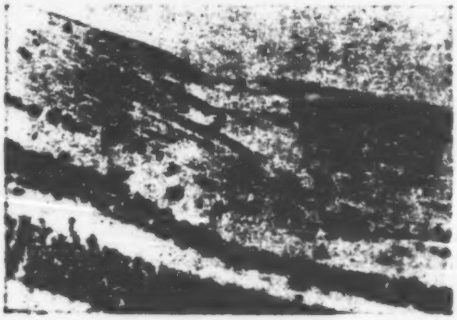

Figure 8

III. Discussion of Results

Any disruption of the metabolism of the retina may lead to irreversible results. Optical microscope observations showed that lower energy laser irradiation led to local injury of the retinal nerve fiber layer. We have made consecutive sectioning and examination of the retinal damage and found that the surrounding tissues were nearly normal and unaffected. At lower energy the laser may damage the nerve fiber layer while leaving the inner membrane intact. This is because that the fiber layer tends to absorb more light energy at 1.06 μm. As the energy increased the degree of damage increased and the number of the layers and the area damaged also increased. This showed that the physical inhibition reaction of the thermal burning caused damage in the surrounding tissue. This physical damage was directly proportional to the energy of the laser light.

The damage observed under the electron microscope was mostly pathological changes due to burn injury. The cell morphology of the retinal pigment epithelium suffered changes, the chondriosome showed irregular swelling and voids were formed. According to Kuwabara (1979), the swelling of the chondriosome and the voids may be compensated by the surrounding tissue within a few days. For severe cases this may last for several months. The endoplasmic reticulum showed swelling and the membrane structure showed wrinkles and lace-like structural changes. Even though the surrounding histocytes may play a compensating role, considerable histological disarrangement may lead to functional changes of the cells and necrosis at large energy levels. The damaged cells accumulating at the injury site can interfere with the metabolism of the light sensitive cells and disrupt the vision of the damaged region.

9698/6091
CSO: 8111/1099

STUDY OF RETINAL INJURY THRESHOLD FOR Nd:YAG FREQUENCY-DOUBLED LASER LIGHT

Shanghai ZHONGGUO JIGUANG [CHINESE JOURNAL OF LASERS] in Chinese Vol 12, No 10, 20 Oct 85 pp 618-620

[Article by Xu Jiemin [1776 4309 2404], Zhou Shuying [0719 3219 5391], Hu Fugen [5170 1381 2704], Cao Weiqun [2580 4850 5028], Chen Zongli [7115 1350 4409], Zhang Guisu [1728 2710 4790], Wang Denglong [3769 6260 7893], Qian Huanwen [6929 3562 2429], and Xu Guidao [1776 6695 6670] of the Institute of Radiation Medicine, Academy of Military Medical Sciences]

[Text] Abstract: When the eyes of rabbits and rhesus monkeys were exposed to a laser pulse with a wavelength of 0.53 µm, the ED_{50} values were found to be 39.2 $\mu J/cm^2$ and 187 $\mu J/cm^2$ for rabbits and monkeys respectively. The experimental results showed that the monkey fundus is considerably less sensitive than the rabbit fundus.

This is an investigation of the retinal injury threshold in rabbits and monkeys by a Nd^{3+}:YAG frequency doubled laser and the goal is to provide reference data for establishing a laser safety standard.

I. Irradiation Setup and Experimental Method

A Nd^{3+}:YAG laser with KD*P Q-switching and first order oscillation at 1.06 µm wavelength was used. The output was frequency-doubled with a KDP crystal to produce 0.53 µm green light. The pulse width was 5 ns, the beam divergence was less than 0.5 mrad, and the output was a transverse mode.

Figures 1 and 2 show the irradiation setup and the optical path. 1.06 µm and 0.53 µm attenuator plates were installed respectively before and after the frequency doubler and the beam splitter. The desired irradiation dosage was obtained by adjusting the charging voltage and the attenuators.

The laser dosage is given in terms of the incidence energy at the cornea. The dosage was monitored by beam splitting in real time. The dosage levels of 1,382 shots in 13 groups were measured. 496 data points in 45 groups were analyzed and the measurement errors were in the 1.7-4.8 percent range. The accuracy was adequate for the biological experiments.

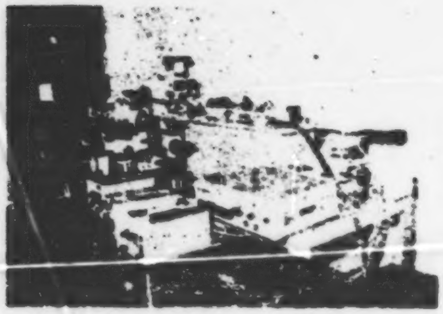

Figure 1. Irradiation setup for measuring retinal injury by Nd^{3+}:YAG frequency doubled laser

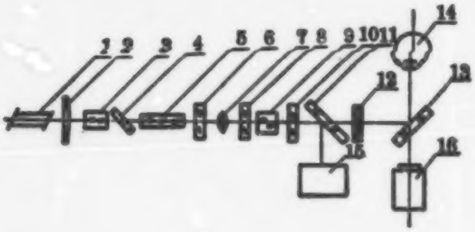

Figure 2. Optical path of the experimental setup

1--He-Ne laser; 2-7--Plano-convex unstable laser cavity; 8,12--Attenuators; 9--Frequency doubling crystal; 10--1.06 μm filter; 11--Beam splitter; 13--Reflecting mirror; 14--Animal eyeball; 15--Energy monitor; 16--TOPCON ophthalmoscopic camera

The animals were gray rabbits weighing 2-3 kg and rhesus monkeys weighing 2-7 kg with normal eyes. Ophthalmoscopic examinations were performed 1 hour and 24 hours after the irradiation by at least two persons. A total of 530 shots was made on 70 rabbit eyes and 220 shots on 10 monkey eyes.

II. Experimental Results

1. Rabbit retinal injury threshold

The average incident energy density for rabbit eyes ranged from 14.4 to 70.1 $\mu J/cm^2$ and the average incident energy ranged from 2.83 to 13.7 μJ. The lightest retinal injury indicators were small pigment rings or aggregates that disappeared mostly after 24 hours. Light injuries showed round light gray coagulating edema with some pigment precipitation at the center and an ill-defined boundary, as shown in Figure 3 [sic]. Some of the injuries disappeared after 24 hours and most formed pigment spots in 72 hours. As the dosage was increased, a small number of circular or chrysanthemum-shaped hemorrhage spots were observed.

The injury rate increased with increasing incident energy density at the cornea. Table 1 shows the dosage dependence of the retinal injury rate for 1 hour after the shots. Using a Bliss probabilistic weighted regression method, the regression equation in terms of dosage (X) and injury rate ($\hat{Y}$) and the injury threshold ED_{50} were obtained:

$$\hat{Y} = 3.888X - 1.116$$

$$ED_{50} \simeq 89.2 \mu J/cm^2$$

(95 percent confidence limit 36.5 ~ 42.1 $\mu J/cm^2$)

The regression curves were shown in Figure 3.

Table 1. Rabbit Retinal Injury Rate and Dosage of Nd^{3+}:YAG Frequency Doubled Laser

	Ave. incident dosage at the cornea		Injury rate	
Group	(J)	(J/cm^2)	No of injuries/ No of shots	%
1	2.83×10^{-6}	1.44×10^{-5}	0/22	0
2	3.61×10^{-6}	1.84×10^{-5}	7/44	15.9
3	4.44×10^{-6}	2.27×10^{-5}	7/48	14.6
4	5.54×10^{-6}	2.83×10^{-5}	20/58	34.5
5	7.04×10^{-6}	3.59×10^{-5}	37/91	40.7
6	8.64×10^{-6}	4.41×10^{-5}	47/80	58.8
7	1.09×10^{-5}	5.55×10^{-5}	74/107	69.2
8	1.37×10^{-5}	7.01×10^{-5}	69/80	86.2

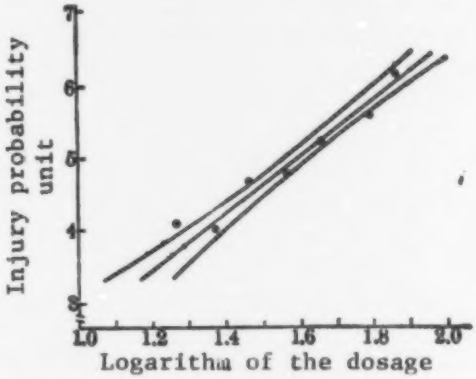

Figure 3. Rabbit retinal injury rate as a function of the irradiation dosage of a frequency doubled Nd^{3+}:YAG laser

2. Monkey retinal injury threshold

The average incident energy density at the cornea of the monkey eye was 210-327 μJ/cm^2 and the energy ranged from 412 to 642 μJ. Under such dosage levels, the injuries were slight and showed up as small circular light gray coagulation spots with well defined boundaries. A total of 220 shots were made and 52 coagulation injuries appeared within 1 hour. After 24 hours some of the injuries had disappeared but 13 new injury spots showed up.

Table 2 lists monkey retinal injuries occurring within 1 hour after irradiation by 0.53 μm laser light. Using the Bliss weighted regression method, we obtained the regression equation relating the retinal coagulational injury probability ($\hat{Y}$) and the logarithm of the dosage (x). The regression curve is shown in Figure 4.

$$\hat{Y} = 2.804x - 1.873$$

$$ED_{50} \simeq 187\ \mu J/cm^2$$

(95 percent confidence limit = 156 ~ 238 μJ/cm^2)

Table 2. Monkey Retinal Injury Rate and Frequency Doubled Nd^{3+}:YAG Laser Dosage

Group	Ave. incident dosage at the cornea (J)	Ave. incident dosage at the cornea (J/cm^2)	Injury rate: No of injuries/ No of shots	Injury rate: %
1	4.12×10^{-6}	2.10×10^{-5}	1/59	1.69
2	9.13×10^{-6}	4.66×10^{-5}	2/54	3.70
3	1.78×10^{-5}	9.08×10^{-5}	4/31	12.9
4	3.42×10^{-5}	17.5×10^{-5}	27/54	50.0
5	6.42×10^{-5}	32.7×10^{-5}	18/22	81.8

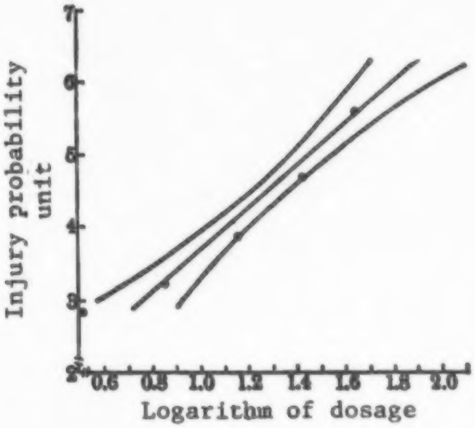

Figure 4. Monkey retinal injury rate versus logarithm of the dosage of frequency doubled Nd^{3+}:YAG laser

3. Pathological examination of retinal injuries

Typical indications of [rabbit] retinal injury caused by threshold dosage irradiation are exudation under the retina, swelling of the pigment epithelial cells, segregation of black pigment particles, breakage of outer section, break up of outer granular layer by edema exudation and gasification, pyenotic nucleus in inner and outer granular layers, and light bulging of the injured area. Blood vessel dilation was observed in the choroid, as shown in Figure 5. Typical injuries of the monkey retina are coagulation, edema exudation, liquid exudation under the retina, bulging of the outer granular layer, pyenotic nucleus in the outer granular layer, and a volcano mouth-shaped injury with an indented and coagulated center (see Figure 6). No obvious changes were found in the choroid.

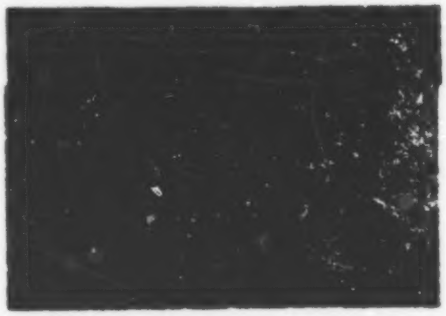

Figure 5. Injury of the rabbit retina caused by a frequency doubled Nd^{3+}:YAG laser (x126) (Exudation under the retina, pigment segregation, gasified region, 7.28 μJ incident energy at the cornea)

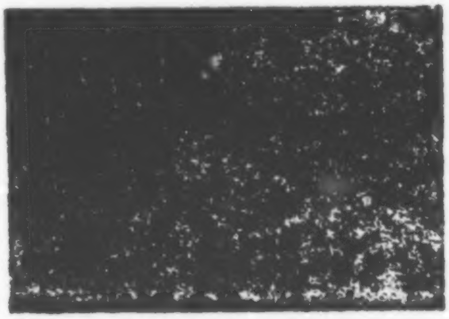

Figure 6. Injury of the monkey retina caused by a frequency doubled Nd^{3+}:YAG laser x63) (Exudation under the retina, inner layer coagulation and indentation)

9698/6091
CSO: 8111/1099

RETINAL INJURY THRESHOLD OF LONG PULSE RUBY LASER LIGHT

Shanghai ZHONGGUO JIGUANG [CHINESE JOURNAL OF LASERS] in Chinese Vol 12, No 10, 20 Oct 85 pp 621-622

[Article by Xu Jiemin [1776 4309 2404], Hu Fugen [5170 1381 2704], Zhou Shuying [0719 3219 5391], Cao Weiqun [2480 4850 5028], Qian Huanwen [6929 3562 2429], Zhang Guisu [1728 2710 4790], and Wang Denglong [3769 6260 7893] of the Institute of Radiation Medicine, Academy of Military Medical Sciences]

[Text] Abstract: Threshold of observable retinal injury was determined for rabbits exposed to long pulse ruby laser light irradiation. The threshold, ED_{50} was 14.9 mJ/cm^2 and its 95 percent confidence limit was 13.6 ~ 16.5 mJ/cm^2 for intraocular energy density.

The wavelength of a ruby laser is 6943 Å and the damage to the eye by a ruby laser is mainly on the retina. In this work we study the rabbit retinal injury threshold by a long ruby laser pulse for the establishment of a safety standard.

I. Experimental Setup and Method

The setup consisted of a ruby laser, a laser irradiation locating device, a copper sulfate attenuation solution, a quartz comparator, an output energy monitor system, a beam spread suppression lens, and a diaphragm (see Figures 1 and 2).

Figure 1. Ruby laser irradiation setup

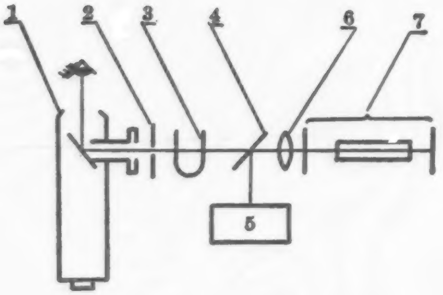

Figure 2. Schematic diagram of the optical path

1--Laser irradiation locating device; 2--Diaphragm; 3--Attenuator cup; 4--Beam splitter; 5--Monitor system; 6--Compression lens; 7--Ruby laser

The output energy of the laser was 0.1-1.8 J per pulse, the pulse width was 0.6 ms, the output was stable to within ±6.6 percent, the divergence angle was 4.5 mrad and the beam diameter was 5 mm.

The laser irradiation locating device was used to observe the back of the eye and to select the location for the irradiation. The device consisted of an observation system, an image inversion system, and an illumination system. The magnification was 1.44 times, the field of the view angle was 64° and the resolution was 0.5 mm.

The laser energy was measured with a model NJ-J_1 thermal energy meter with a 10 mm diameter receptor, a wavelength response range from ultraviolet to infrared and a repeatability better than 0.5 percent. Within the dosage range used, the response was linear. The system was monitored with an integration sphere energy meter. The dosage of 240 shots in 5 groups were measured. Statistical analysis of 115 data points in 23 groups showed that the error in the beam splitting ratio was less than 3 percent and the measurements were reliable.

The animals were gray rabbits weighing 2-2.9 kg with normal eye examination results. No corrections were made for hyperopia (less than 2.25 D) or myopia (less than 1.0 D). Ophthalmoscopic examinations were made after 1 hour and 24 hours by at least two persons. Some of the eyeballs were removed for pathological and histological examinations. A total of 240 shots were made on 77 rabbit eyes.

II. Experimental Results

The irradiation dosage was 11.7-25.0 mJ/cm^2 for the average cornea incidence and was divided into five groups.

1. Retinal injury indications: Under the ophthalmoscope, light gray or grayish white circular injury spots were visible. The boundaries had scattered black pigment particles and sometimes edema rings. A few injury

spots had a small black dot of burn spot at the center. The injury spots slightly increased their size after 24 hours, followed by recession of the edema. After 3-5 days most of the injury spots had only residual pigment deposits or formed a small white circular scar.

2. Relationship between irradiation dosage and retinal injury rate: Table 1 shows the retinal coagulation injury rate after 1 hour and the corresponding dosages. As can be seen, the retinal injury rate increased with the average incident energy density at the retina. Ophthalmoscopic examinations made 1 hour after the shots showed an injury rate of 138/240 (57.5 percent). After 24 hours the injury rate was 80.6 percent.

Table 1. Rabbit Retinal Injury Rate and Corresponding Ruby Laser Irradiation Dosages

Group	Ave. incident dosage at the cornea (J)	(J/cm^2)	Injury rate No of injuries/ No of shots	%
1	4.91×10^{-3}	2.50×10^{-2}	42/48	87.5
2	3.65×10^{-3}	1.86×10^{-2}	35/54	64.8
3	3.25×10^{-3}	1.66×10^{-2}	26/52	50.0
4	2.74×10^{-3}	1.40×10^{-2}	18/42	42.9
5	2.30×10^{-3}	1.17×10^{-2}	17/44	38.6

3. Calculation of the retinal injury threshold: The injury threshold (also known as ED_{50}) often refers to the irradiation dosage corresponding to 50 percent probability for the smallest observable injury in ophthalmoscopic examinations made 1 hour after the shot. A Bliss probability weighted regression method was used to analyze the data and the regression equation for the logarithm of the long pulse ruby laser irradiation dosage (X) and the coagulation injury probability of the rabbit retina was found:

$$\hat{Y} = 4.332X - 0.0937$$

$$ED_{50} \simeq 14.9 \text{ mJ/cm}^2$$

(95 percent confidence limit was 13.6~16.5 mJ/cm^2)

4. Pathological changes of the injuries: The pathological changes of the injuries caused by threshold dosage irradiations were mostly on the outer layer of the retina. Edema and exudation under the retina caused slight bulging. There were swelling or rupture of the pigment epithelium cells, segregation of black pigment particles, and some local "vaporized zone." Some pyenotic nuclei occurred in the outer granular layer and in the vaporized zones. Some swelling or necrosis of the nuclei of ganglia cells and void formation in the cytoplasm were observed. Most of the outer membranes were intact and the choroid and the sclera showed no noticeable changes. Figure 3 shows a typical case.

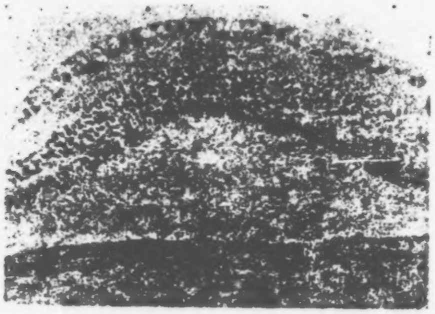

Figure 3. Retinal injury of the rabbit eye by a ruby laser (x126) (Exudation behind the retina, pigment cell swelling and separation) (Average incidence energy density at the cornea = 16.6 mJ/cm^2)

A modified JLX ruby laser slit light microscope was used to irradiate 240 spots in 76 eyes of gray rabbits. The coagulation injury threshold for a long ruby laser pulse was found to be ED_{50} = 14.9 mJ/cm^2 with a 95 percent confidence limit of 13.6~16.5 mJ/cm^2. Injury indications and pathological changes were described.

Tang Zhongming helped with the computer statistical analysis of the data.

9698/6091
CSO: 8111/1099

A STUDY OF SINGLE MODE He-Ne LASER INJURY THRESHOLD OF RABBIT EYE

Shanghai ZHONGGUO JIGUANG [CHINESE JOURNAL OF LASERS] in Chinese Vol 12, No 10, 20 Oct 85 pp 623-625, 585

[Article by Ding Weiling [0002 4850 3781], Zhao Tianji [6392 1131 0679], and Qiang Ruling [1730 5423 3781] of the Tianjin Institute of Laser Technology, Wu Guifang [2976 2710 5364] of the Tianjin Ophthalmic Hospital, and Liu Changting [0491 2512 1656] and Mu Ruidong [4476 3843 2639] of the Tianjin Institute of Industrial Hygiene and Occupational Diseases]

[Text] Abstract: In this study, gray rabbits were exposed to He-Ne laser light at six and five different dosages respectively. The exposure time was 1 second and 1/8 second. Thirty points were exposed for every dosage. The probability of injury to the retina at a rate of 50 percent (ED_{50}) was obtained.

Helium-Neon lasers are most widely used today. Since the output power is generally less than 100 mW, people often overlook the danger of physical injury and eye damage by such low-power lasers. Due to the focusing effect of the eye, the power density at the retina[1] is increased by a factor of 10_5 [sic] and can cause eye injuries. After studying multimode lasers,[2] we now study the injury threshold of rabbit eyes by single mode He-Ne lasers as a function of exposure time.

I. Experimental Setup and Animals

1. Experimental setup

Figure 1 is a schematic diagram of the experimental setup. It consists of an illumination system, an aiming system, and an observation system.

The illumination system consists of a HN-T_4 He-Ne laser with a single transverse mode output power greater than 50 mW and a divergence angle less than 1 mrad, a shutter and an attenuator. The exposure time is controlled automatically by a model PKM-4 electronic shutter. The exposure time used in this experiment was 1 sec and 1/8 sec. Our fixed point illumination device consists of an alignment illumination system, an observation system, and reflection mirror #1. The aiming system makes use of a low power He-Ne laser. The aiming laser light is reflected from the semi-reflecting mirror and follows the path of the irradiation laser and enters the pupil after bouncing off reflection mirrors #1 and #2. The experimenter may select an ideal target spot through the observation system and observe the ocular condition and injury spots. The power of the irradiation is controlled by the attenuator.

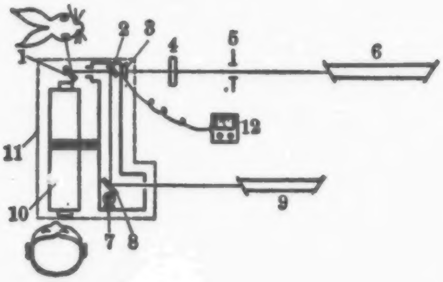

Figure 1. Schematic diagram of the experimental setup

1--Reflection mirror #1; 2--Reflection mirror #2; 3--Power meter probe; 4--Attenuation; 5--Electronic shutter; 6--HN-T_4 He-Ne laser; 7--Lamp; 8--Semi-reflecting mirror; 9--Alignment He-Ne laser; 10--Observation system; 11--Fixed point illumination setup; 12--Power meter

The measurement of the laser power is made with our own miniature photoelectric power meter with an error of ±5 percent. The probe of the power meter is mounted on the fixed point irradiation setup and real time monitoring is realized. The laser power entering the cornea may be obtained from the measured power and a correction factor.

The light beam for irradiation is the original beam of the laser, as shown in Figure 2. The light intensity has a Gaussian distribution in the radial direction. The diameter of the light spot is taken as the distance between the two $1/e^2$ points of the maximum power. The diameter of the light spot at the cornea is computed to be 4.30 mm and the area of the spot is 0.145 cm^2.

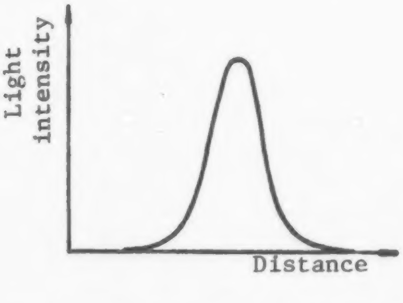

Figure 2. Light intensity distribution of the cross-section of the beam

2. Experimental animals

Small gray chinchilla rabbits bred at the Shanghai Breeding Facility were carefully selected to meet the following requirements: 1) weight is in the 2-2.5 kg range; 2) ocular pigments are similar, free from cornea, lens, and vitreous abnormalities or ocular diseases; 3) diopter in the +15 to +30 range and axis length in the 15-17 cm range.

II. Experimental Method and Procedures

Before exposure the irradiation laser and the aiming laser are aligned. The animal is first put under total anesthesia, the pupil sufficiently enlarged and then held on the platform with five degrees of freedom. The experimenter then chooses the ocular spot for exposure by adjusting the platform position. The exposure is controlled by an electronic shutter, as shown in Figure 3. Three observations are made of the rabbit eye immediately after the exposure and 30 and 60 minutes after the exposure. A positive reaction is recorded when two ophthalmologists observe the presence of a small light gray injury spot.

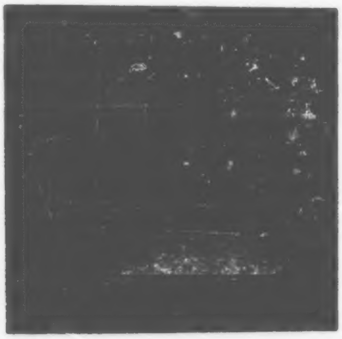

Figure 3. Retinal injury of the rabbit eye

The pathological specimens are taken using a modified retinal opening location method. The experiment first aims the ophthalmoscopic beam at the center of the injury spot and then observes the light spots going through the sclera. The spot is marked with gentian violet and sutures are made with a cornea needle at this location. After the localization, the animal is put to death by an intravenous injection of air and the eyeball removed after the blood has coagulated. The eyeball is fixed with a 10 percent formalin solution, embedded in paraffin and the injured location is sectioned and stained with H-E.

III. Experimental Results

1. 1 second exposures

A total of 30 eyeballs from 15 rabbits are exposed to the laser radiation at six dosage levels. The rabbits are divided randomly into three groups of five.

Each eye is exposed to two different dosages at three spots. The distance between the spots are greater than the diameter of the injury spots by at least a factor of 2. A total of 30 shots are made at each dosage level. The results are listed in Table 1.

Table 1. Acute Retinal Injury of Rabbit Eyes by He-Ne Laser

Laser power (mW)	Power density (mW/cm^2)	No of shots	No of injuries	Positive reaction (%)
38.0	262	30	28	93.3
30.0	207	30	21	70.0
27.0	186	30	18	60.0
24.0	166	30	14	46.7
20.0	138	30	3	10.0
15.0	103	30	0	0

The results in Table 1 show that the injury rate versus the irradiation dosage is an S-shaped curve. No cornea, lens, or vitreous damages were observed after the irradiation. The 6328 Å radiation only causes retinal injury.[3] A weighted linear regression analysis of the data on the microcomputer yielded a regression equation of $\hat{y} = -8.19 + 9.32\,x$, an ED_{50} value of 26.0 mW (or 179 mW/cm^2) and a confidence limit of 24.5~27.5 mW (or 169~190 mW/cm^2). The correlation coefficient of the regression straight line is $r = 0.988$, indicating that the results are reliable.

2. 1/8 sec shots

Thirty eyes of 15 gray chinchilla rabbits are exposed to five different dosage levels for 1/8 sec in the same manner as the 1 sec exposures. The results are listed in Table 2.

Table 2. Acute Retinal Injury of Rabbit Eyes Exposed to He-Ne Laser for 1/8 Sec

Laser power (mW)	Power density (mW/cm^2)	No of shots	No of injuries	Positive reaction (%)
43.0	297	30	30	100
38.0	262	30	24	80.0
33.0	228	30	20	66.7
28.0	193	30	10	33.3
23.0	159	30	0	0

The results of Table 2 show that, like the 1 sec exposure results, the injury versus the irradiation dosage is again an S-shaped curve. The linear regression equation is $\hat{y} = -15.8 + 14.0\,x$, the ED_{50} value is 31.2 mW (or 215 mW/cm^2), and the confidence limit is 29.8~32.6 mW (or 206~225 mW/cm^2).

3. Pathological changes observed ophthalmoscopically

Based on the ED_{50} confidence limit of the 1 second exposures, three dosages of 27, 25, and 23 mW are chosen. The retinal injuries at these dosages are:

27 mW--Retinal injuries are observable under a low power microscope. The choroid and the sclera are fused together and the epithelium is ruptured. Under a high power microscope, edema of the nerve fiber layer and disarrangement of the outer granular layer are also observed.

25 mW--Injuries observed at the irradiated location include retinal bulging, edema, hemorrhage under the retina, local retinal detachment, separation of the outer granular layer, growth of the collagen cells, local pleiomorphic nuclear infiltration of the choroid, and changes of the ganglia cells.

23 mW--Light edema of the retina, epithelium rupture, and local pleiomorphic nuclear infiltration of the choroid.

The results show that pathological changes are observed under the light microscope at retinal injuries found under the ophthalmoscope. In addition, retinal edema, hemorrhage and pleiomorphic nuclear infiltration of the choroid are observed. Due to the limited number of pathological specimens, no correlation between pathological changes and laser power is observed.

IV. Discussion

1. In our study of the retinal injury threshold of rabbit eyes due to He-Ne laser irradiation, we found that the injury not only depends on the laser power, the divergence angle, the ocular pigment, but also depends on the laser mode, the irradiation location, and the exposure time.

2. In the pathological observation we found that specimen preparation was crucial. Our procedures were laser irradiation, exposing the sclera surface, localization, killing the animal, and removing the eyeball. The advantages of this method are: 1) accurate localization, 2) short time duration, and 3) making use of the favorable conditions of the rabbit eye.

3. Based on extensive data from animal experiments and based on the fact that the eye is one of the most important organs of the human body, we believe that the safety level should be 100 times lower than the lower limit of the 95 percent confidence range of the minimum injury threshold (ED_1). We therefore recommend that the maximum allowable irradiation dosage of He-Ne laser in China should be 8.76×10^{-4} W/cm^2 for 1 second exposure and 13.0×10^{-4} W/cm^2 for 1/8 second exposure. This standard is slightly more stringent than the U.S. standard.

REFERENCES

1. M.L. Wolbarsht, "Laser Applications in Medicine and Biology," 1971.

2. Liu Changting, et al., "Occupational Hygiene and Environmental Medicine," No 1, 1 (1983).

3. A. Kohtiao, et al., Amer. J. Ophthal., 1966, 62, 524-527.

4. W.P. Hansen, et al., Appl. Opt., 1976, 6, 1973-1975.

9698/6091
CSO: 8111/1099

RESEARCH ON INJURY THRESHOLD OF CHINESE YELLOW SKIN BY CW Nd:YAG LASER BEAM IRRADIATION

Shanghai ZHONGGUO JIGUANG [CHINESE JOURNAL OF LASERS] in Chinese Vol 12, No 10, 20 Oct 85 pp 626-628

[Article by Wu Tingbi [0702 1694 1084], Li Yujun [2621 3768 0193], Dang Zhiping [7825 3112 1627], An Xiaoyue [1344 2556 1471], Guo Wenqi [6753 2429 3823] of the Xi'an Medical University Hospital No 1, Medical Laser Research Laboratory, and Wang Kejin [3769 0344 3866] of the Dermatology Group, Liang Luanxian [2733 7762 0103], Wang Peng [3769 7720], and Chen Mingxia [7115 2492 7209] of the Electron Microscope Laboratory, Xi'an Medical University, Xu Linmiao [1776 2651 5379] of the Xi'an Fifth Ministry of Machine Building, and Lu Zhiguo [7120 3112 0948] of the Laser Laboratory, Physics Department, Northwest University]

[Text] Abstract: This paper deals with laser injury threshold for Chinese yellow skin by exposure to 1 sec CW Nd:YAG laser beam. The results of the experiment are: MRD equals to 71.37 W/cm^2, and its 95 percent confidence limit is 67.47 ~ 75.49 W/cm^2.

I. Experiment

1. CW YAG laser

Single lamp cavity, 100 mm long by 6 mm diameter, output power ~30 W, lower order modes, stability better than ±1 percent with feedback control.

2. Optical path

(1) CW YAG laser, (2) electromagnetic shutter for exposure time control, digital millisecond counter for exposure time monitor, (3) 5 mm diameter diaphragm, (4) two beam splitters in the optical path to direct lights into the power monitor and the feedback system (see Figure 1).

3. There were 10 volunteers, five males and five females, 19-57 years old, half the volunteers had a light complexion and the other half had a dark complexion. The inner surface of the right arm was divided into three rows with eight zones in each row. Each volunteer was exposed for 24 shots. Each power dosage group had 30 shots and a total of 240 shots were made.

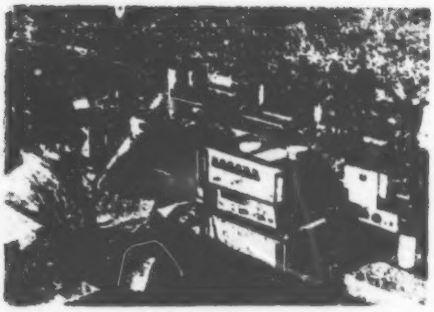

Figure 1

4. **Observation time:** Each irradiation location was observed 22 times--immediately after the exposure (1 observation), 6 observations within the first minute, 9 observations within the first hour, and 6 observations within the first day.

5. **Injury classification:** Ambiguous (±1), erythema (+), blister (++), and ulcer (+++).

6. **Ambient conditions:** Ventilation, dust guard, 20°C ± 1.0°C, 60-64 percent relative humidity.

II. Experimental Observation Results

Table 1 lists the experimental observation results. (See next page).

III. Statistical Analysis of Data

A weighted regression method yielded MRD_{50} of 71.37 W/cm^2 and a 95 percent confidence limit of 67.47 ~ 75.49 W/cm^2.

IV. Measurement of the Skin Reflectivity

Listed in Table 2 are the skin reflectivity measured on the forearms of volunteers using a CW YAG laser.

Table 2

Location	Outer row	Middle row	Inner row
Average value	41.1%	41.7%	40.8%

Note: The laser power absorbed by the skin = measured power - (measured power x reflectivity)

Table 1. Human Skin Injury Threshold by 1 Sec Exposure of a CW YAG Laser

Power	Power density	No. of shots	Temporal distribution for erythema occurrence																							Max. No. of reactions	Reaction rate
			Minute								Hour									Day							
W/ ϕ5mm	W/ cm²		inst	5	10	15	20	25	30	~59	1	2	3	4	5	6	12	18	~24	1	2	3	4	5	6		
19.00	96.77	30	23	26	24	20	18	18	18	18	18	18	17	16	16	13	12	12	13	12	12	12	12	11	11	26	86.7
17.21	87.65	30	19	23	23	21	22	20	17	16	16	15	17	17	17	14	14	14	13	13	14	13	14	12	13	25	83.3
15.58	79.35	30	19	19	19	19	18	18	19	16	13	11	10	9	11	10	10	9	9	8	9	9	8	8	9	19	63.3
14.11	71.86	30	11	12	13	13	11	9	9	9	8	6	6	6	6	6	5	4	4	3	4	4	4	4	4	15	50.0
12.78	65.09	30	10	11	11	12	12	11	10	9	6	5	5	5	5	5	5	5	4	4	4	4	4	4	4	13	43.3
11.57	58.93	30	2	3	3	3	4	3	2	2	2	1	0	0	0	0	0	0	0	0	0	0	0	0	0	5	16.1
10.48	53.37	30	1	2	2	2	1	1	1	1	0	0	0	0	0	0	0	0	1	1	1	1	1	1	0	4	13.3
9.49	48.33	30	2	2	2	3	3	3	3	2	2	2	2	2	2	2	2	2	2	2	2	2	2	1	1	3	10.0
Total No. of reactions			87	97	97	93	89	83	79	73	65	58	57	55	57	50	48	46	45	43	46	45	45	41	42		
Reaction rate			36.2	40.4	40.4	39	37	34.1	33	30	27.1	24.2	23.8	22.9	23.8	20.8	20.0	19.1	18.8	17.9	19.1	18.8	18.8	17.1	17.5		

V. Pathological Changes of Erythema Near Threshold

(1) Optical microscope observations

Halos around the nuclei of basal cells and prickle cells. Slight edema between the cells, dilation and congestion of papillary vessels, and occasionally blood vessel congestion under the papillary corii.

(2) Electron microscope observation

Small bubbles were observed in the cytoplasm of the prickle cells. The link node of some prickle cells showed noticeable damage (Figures 2-266, 2-270) and most basal cells showed bubbles in the cytoplasm. The gap between some basal cells had widened and rarefied. Portions or most of the link node structures were damaged (Figures 2-620, 2-624).

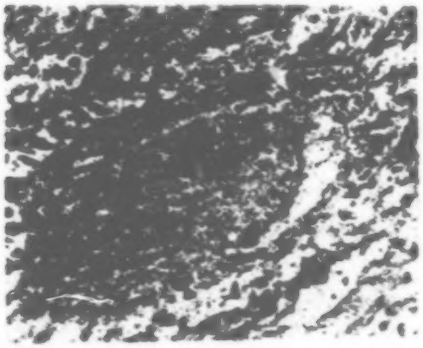

Figure 2-266. Three bubbles observed in the prickle cell. No obvious changes between the cells were observed. (5000x)

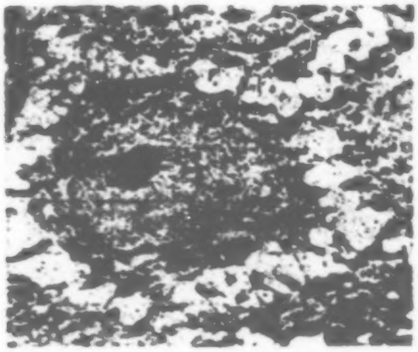

Figure 2-270. Most of the connecting structures between prickle cells were damaged

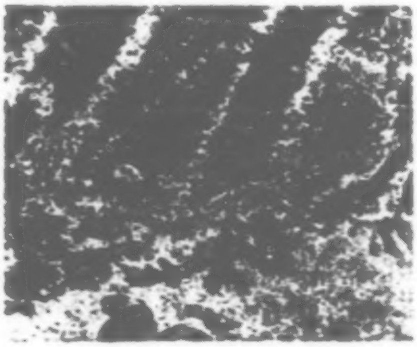

Figure 2-620. Slight shrinkage of the basal cells and bubbles in the cytoplasm were observed. Connecting structures between basal cells were rarefied. (3000x)

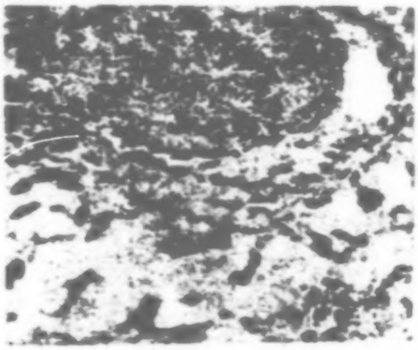

Figure 2-624. Three bubbles were seen in the basal cell cytoplasm. Connecting structures between cells were destroyed. (10000x)

In 1974 Rockwell and Goldman reported a study of the skin injury threshold by 1 sec exposure of CW YAG lasers. They showed that the threshold was 48-78 W/cm^2 for Caucasians and 46-60 W/cm^2 for blacks. We obtained a MRD threshold of 67.47-75.49 W/cm^2 for the Chinese and the value falls between those of the blacks and the Caucasians and close to the Caucasians. The result seemed reasonable.

The authors acknowledge the collaboration of the Northwest University, Institute No 205 of the Ministry of Ordnance Industry, the Northwest Military Communication Engineering College, the Shaanxi Teacher's University, and the Xi'an Dongfeng Meter Plant.

9698/6091
CSO: 8111/1099

RESEARCH ON INJURY THRESHOLD OF CHINESE YELLOW SKIN IRRADIATED WITH 300 μs PULSED NEODYMIUM GLASS LASER LIGHT

Shanghai ZHONGGUO JIGUANG [CHINESE JOURNAL OF LASERS] in Chinese Vol 12, No 10, 20 Oct 85 pp 628-630

[Article by Wu Tingbi [0702 1694 1084], Li Yujun [2621 3768 0193], Dang Zhiping [7825 3112 1627], and Guo Wenqi [6753 2429 3823] of the Medical Laser Research Laboratory, Xi'an Medical University Hospital No 1, Liang Luanxian [2733 7762 0103], Wang Xinhui [3769 2450 2585], and Wang Peng [3769 7720] of the Electron Microscope Laboratory, Xi'an Medical University, Wang Kejin [3769 0344 3866] of the Dermatology Laboratory, Xi'an Medical University Hospital No 1, Liu Shikai [0491 1102 2818] of Institute 213, Xi'an Ministry of Ordnance Industry, and Lian Rulin [1670 3067 2651] of Institute 205, Xi'an Ministry of Ordnance Industry]

[Text] Abstract: This paper studies laser injury threshold of 300 μs pulsed neodymium glass laser. The experimental results are: MRD equals to 20.27 J/cm^2, and its 95 percent confidence limit is 19.49~ 21.08 J/cm^2.

Pulsed Nd:glass lasers have a large output energy and a strong penetrating power and can cause severe damage. They are therefore important lasers to consider from a safety point of view. The skin injury threshold depends on the exposure time and the dosage. The injury threshold is often taken as the dosage causing 50 percent erythema reactions. The maximum allowable dosage is obtained by first finding the ED_{50} or MRD_{50} and then multiplying this dosage by a safety factor.

I. Experimental Conditions

1. Pulsed Nd:glass laser: Pulse width 300 μs, output energy ~35 J, stability better than 2.5 percent, and repetition rate one shot in every 5 minutes.

2. Optical path: (1) The irradiation light source was a Nd:glass laser and the indicating light source was a He-Ne laser. (2) Beam splitters were used to tap off the monitor beam. (3) A focusing lens was added. (4) A 5 mm diameter limiting aperture was used. (5) A three-degrees-of-freedom platform was used for accurate positioning.

3. Eight volunteers, five males and three females, 19-57 years old participated in the experiments. Half of the volunteers had a dark complexion and the other half a light complexion. The inner surface of the left forearm was chosen for the irradiation. The area was divided into three rows with eight zones per row. Each volunteer was exposed to 24 shots. Together with the six shots for determining the upper limit, a total of 198 shots was made. Four standby volunteers were subjected to 12 shots each. The observations were made by dermatologists and supplemented by the experimenters.

4. Observation time: Each shot was observed 22 times immediately after the shot, six observations within the first minute, nine observations within the first hour, and six observations in the first day.

5. Injury classifications: Questionable (±1), erythema (+), blister (++), and ulcer (+++).

6. Experimental conditions: The room temperature was kept between 12°C and 22°C, and the relative humidity was 67-72 percent.

II. Experimental Observation and Results

Table 1 lists the experimental results of delayed erythema injuries.

III. Histological and Pathological Changes

1. Light microscope observations: In the erythema specimens caused by threshold level dosages, extremely small bubbles were observed in the cytoplasm of the prickle cells in the lower portion of the cuticle. Noticeable deformation of cells in the granular layer was observed. Spare fissures and capillary congestion were seen at the top of the papilla corii.

2. Electron microscope observations: A number of bubbles (recessional changes) were observed in the cytoplasm of the generating cells. At locations the links between the generating cells and the basal cells had rarefied. The connecting structure suffered light damage and voids appeared in the cytoplasm of fibrous cells in the dermis.

IV. Results and Discussion

1. Statistical analysis of the data yielded the results in Table 2.

The ED_{50} of $19.032 \sim 21.48$ J/cm^2 obtained in this work is quite close to the international standard.

2. The Nd:glass laser produces a near infrared light of 1.06 μm wavelength. Some researchers believe that, like a YAG laser, the biological effect of the Nd:glass laser is in causing persistent delayed erythema. The erythema usually appear 10 minutes after the irradiation and last about 1 day. The erythema that appear 1-2 minutes after the laser shot are extremely weak, about half of them disappear within 10 minutes and all of them vanish

Table 1. Experimental Results of Human Skin Injury Threshold for a 300 μs Pulsed Nd:Glass Laser (based on observations of delayed erythema injury)

Dosage group	Energy (J)	Energy density (J/cm^2)	No. of shots	Temporal distribution of erythema occurrences																								Total No. of reactions	Reaction rate (%)
				Minute								Hour									Day								
				inst.	5	10	15	20	25	30	~59	1	2	3	4	5	6	12	18	~24	1	2	3	4	5	6		
1	5.07	25.82	6	2	6	6	6	6	6	6	6	6	6	6	6	6	6	6	6	6	6	6	6	6	6	6	6	100
2	4.77	24.30	24	0	6	14	17	19	19	19	19	20	20	19	19	20	20	19	17	17	17	16	14	14	16	16	20	83
3	4.49	22.89	24	0	4	8	11	11	12	14	14	16	17	18	17	17	17	16	15	15	11	10	10	10	11	11	18	75
4	4.22	21.50	24	0	0	1	5	6	8	13	13	13	13	13	13	13	13	13	13	13	7	7	7	8	8	8	13	67
5	3.98	20.27	24	1	3	4	5	5	6	5	5	8	8	10	10	10	10	8	6	6	5	3	3	3	3	3	10	46
6	3.75	19.08	24	0	0	0	1	3	4	7	7	7	8	8	7	7	5	4	3	3	3	2	1	1	0	0	8	33
7	3.50	17.85	24	1	1	1	3	3	6	6	6	7	7	6	6	6	6	4	2	2	2	2	1	1	1	1	7	29
8	3.32	16.93	24	0	0	1	2	3	3	3	3	4	4	4	4	3	4	4	4	4	3	2	2	2	2	2	4	17
9	3.12	15.89	24	0	0	0	0	0	0	0	0	0	0	0	0	0	0	0	0	0	1	1	1	1	1	1	1	4
No. of reactions				4	19	15	49	55	64	73	73	81	83	84	83	83	81	74	66	66	55	49	45	46	48	48		
Reaction rate (%)				2.02	9.6	17.7	24.7	27.8	32.3	36.9	36.9	40.9	41.9	42.4	41.4	41.4	40.9	37.9	33.3	33.3	27.8	24.7	22.7	23.2	24.2	24.2		

after 25 minutes. Such temporary reversible weak erythema may be due to a heating effect of the blood vessels. Since no pathological changes can be seen, it is debatable whether they can be considered an erythema associated with the injury threshold.

Table 2

Laser type	Exposure method and skin type	Wavelength (μm)	Exposure time (sec)	ED_{50} or MRD_{50} (J/cm^2)
Nd:glass	Ordinary pulse, yellow skin	1.06	3×10^{-4}	ED_{50} 20.27 19.49 ~ 21.08 MRD_{50} 13.28 11.86 ~ 14.86

9698/6091
CSO: 8111/1099

INJURY THRESHOLD OF RUBY LASER IRRADIATION ON PIG SKIN

Shanghai ZHONGGUO JIGUANG [CHINESE JOURNAL OF LASERS] in Chinese Vol 12, No 10, 20 Oct 85 pp 631-632

[Article by Wang Jun [3769 6511], Chen Ji [7115 6619], Lu Shanfen [4151 0810 5358], Xu Yidao [1776 6695 6670], Shi Liangshun [2457 5328 7311], Qian Huanwen [6929 3562 2429], and Wang Denglong [3769 6260 7893] of the Institute of Radiation Medicine, Military Medical Science University]

[Text] Abstract: This paper reports the experimental results of pig skin exposed to ruby laser light. By statistical analysis of the erythema produced within 24 hours post-exposures, ED_{50} about 53.3 J/cm^2 was obtained. The microscopic and scanning electron microscopic examinations showed nothing but the blood vessels dilation of derma after a near threshold-dose irradiation on skin.

The wavelength of the ruby laser is 694.3 nm. Upon incidence on the skin surface, 99 percent of the energy are absorbed in a shallow layer 3.6 mm thick. The main characteristics of the skin effect include darkening of the pigment, precipitation of the pigment, photo-alergic reactions and burns.[1] In this experiment we observed the skin reaction of the white pig irradiated by a ruby laser and obtained the 50 percent erythema dose (ED_{50}).

I. Experiment

1. Laser: Ruby laser, working medium dimension = 530 mm x 21.5 mm diameter, Xenon pump, multi-mode output. Pulse width = 0.32 ms, spot diameter = 0.5 cm, output stability better than ±5 percent.

2. Animals: Eight young white pigs of the Changbai species, both males and females, weighing 4.6 ± 0.8 kg. Three more pigs for histological specimens only. The animals were put under total anesthesia by injecting 3 percent penta-sodium barbiturate solution (45 mg/kg). The skin was shaven, cleaned and painted with a square lattice of 2.5 cm spacing. A total of 64 grids were painted on the two sides of the body. A total of 210 shots in five dosage groups were made along the diagonal direction.

II. Results

Macroscopic observations made immediately after the irradiation produced the results in Table 1.

Table 1. Erythema Occurrence Rate of the Pig Skin Irradiated With a Ruby Laser

Group	Ave. dosage $\pm S_x$ (J/cm^2)	Ave. absorption $\pm S_x$ (J/cm^2)	No of shots	Occurrence rate (%)
1	66.2 ± 1.4	35.3 ± 0.8	41	87.8
2	59.6 ± 2.0	31.8 ± 1.1	40	60.0
3	51.4 ± 1.3	27.4 ± 0.7	43	48.8
4	45.7 ± 1.3	24.4 ± 0.7	42	31.0
5	41.0 ± 2.0	21.9 ± 1.1	44	4.54

The erythema occurrence rate at the minimum dosage (41.0 J/cm^2) was 4.54 percent. The erythema were uniform and pink in color with a diameter of 5 mm. Individual dark red spots had a diameter of about 2 mm. This group of erythema lasted for a relatively short time, generally 8-31 hours.

Irradiations at the maximum dosage (66.2 J/cm^2) produced red patches about 7x8 mm with irregular shapes. As time went on the redness became smaller and darker in color. It shrank to a size of 2x2 mm after 10 minutes. The boundary became clear and the color darkened, sometimes to cherry red. Some of the irradiated spots bulged up and the skin at the center of the bulge appeared almost transparent. The erythema rate at the highest dosage was 87.8 percent. The redness persisted longer, generally 24-72 hours and sometimes 4-5 days.

Erythema produced by the intermediate dosage (51.4 J/cm^2) were red or light red in color, 5 mm in diameter, up to 8 mm, the occurrence rate was 48.8 percent, and the redness persisted for 9 hours up to 4 days.

Histological observations were made on specimens taken immediately after the irradiation and 1-2 hours and 24 hours after the irradiation.

(1) Optical microscopic examination

Group 1 (66.2 J/cm^2): Basal cells became more rounded and flattened. The number of bubbles in the basal cells increased and pyenotic nuclei were observed. Hypodermic blood vessels showed noticeable dilation and extravasation. Infected cells surrounded the vessel cavity. Some connective structure cells became stained. The region of blood vessel dilation had a clear boundary and no edema of the papilla corii were observed.

Group 2 (59.6 J/cm^2): The surface skin became somewhat thinner. The number of bubbles (voids) in the cell increased. The hypodermic blood vessels showed dilation, extravasation, and aggregation of infectious cells.

Group 3 (51.4 J/cm^2): Very few bubbles in the basal cells. Blood vessel dilation remained visible in the dermis but infectious reactions became less obvious (see Figure 1).

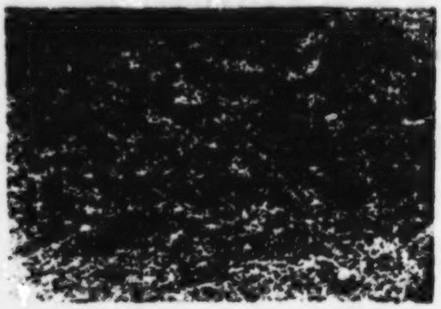

Figure 1. Ten minutes after irradiation at 50.8 J/cm^2. Hypodermic blood vessel dilation and extravasated blood were clearly visible. Infectious cell reaction not obvious.

Groups 4 and 5 (45.7 and 41.0 J/cm^2): No obvious changes on the surface. Hypodermic blood vessel dilation and extravasation were obvious. Very few infectious cells were observed.

(2) SEM examinations: The erythema of group 1 and group 3 were examined using an SEM.

Group 1 (66.2 J/cm^2): The irradiated skin swelled up and the surface became rough or honeycomb-like. The skin hair became sparse and the remaining hair became curly, and the sheaths became detached.

Group 3 (51.4 J/cm^2): Skin surface swelled slightly. The center of the irradiated region showed slight indentation. The hair sheaths remained intact and hair loss was insignificant (see Figure 2).

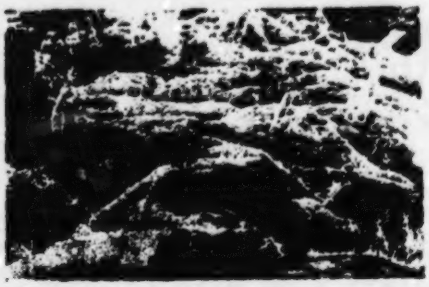

Figure 2. SEM photo of a specimen taken immediately after 52.4 J/cm^2 irradiation. The skin surface swelled, the texture became ill-defined, the center of the irradiated region showed a slight indentation, the hair loss was insignificant, and the sheaths remained intact.

III. Discussion

Over the years very little had been reported on the injury threshold of the pig skin by ruby laser light. The reports are either pure destructive damage at high power levels[2] of 64-318 J/cm^2 or multiple pulse irradiation.[3] Such data cannot be used in the evaluation of the minimum erythema dosage. By visual observation, Kuhn[4] found that the dosage for light injury was 42-190 J/cm^2. Kuhn also found that the dosage was 50-100 J/cm^2 by microscopic observation. Our dosage is essentially the lower limit of Kuhn's dosage for light injury.

The factors affecting the occurrence rate of erythema are:

(1) Erythema retention time: We used the recommendation made by the 1983 national conference on laser safety that the erythema retention time must be at least 1 hour. In fact we found some erythema that disappeared within 1 hour or even 10 minutes. If such short retention erythema are also counted, the value of ED_{50} will be reduced to 41.0 J/cm^2. The mechanism of the short retention erythema calls for further study.

(2) Irradiation location: At the same dosage level, the occurrence rate varied greatly with irradiation location. Erythema occurred more in bony regions with an occurrence rate as high as 60-100 percent. In regions of soft tissue, the erythema occurrence rate is only 0 to 25 percent. An even distribution of the irradiation locations should therefore be used in the experiment.

As far as the dosage calculation, we used the experimental data on pigs as a transition to that of humans. Although the thickness, optical and thermal properties of the pig skin are similar to those of the human skin, there are significant differences in the hair, the density of the collagen fibers under the skin, and the blood vessel distribution.[5] One must therefore exercise caution in extrapolating the data of a pig model to the human. We have measured the reflectivity for all the animals used in our tests. The average reflectivity of the pig skin is 46.7 percent whereas that of the human is 38.8 percent. Since the pig skin and the human skin have histological differences and the reflectivity of the former is higher than the latter, we used the minimum dosage of the pig as the upper limit dosage for the humans. Our data show that when the minimum absorption dosage of the pig (21.3 J/cm^2, Table 1) is multiplied by the absorptivity of the human skin, the result 13.3 J/cm^2 is quite close to the upper limit dosage 14.0 J/cm^2 of the human skin.[7]

In addition, an analysis of the existing threshold data shows that when the human skin is subjected to a radiation dosage of 2.6-14.0 J/cm^2, it is 4-5 times lower than the dosage for a white pig skin and the thresholds differ by a factor of 11.3. The threshold of the white pig differs from that of the Caucasian skin by a factor[8] of 2.7-4.8, and from that of the black skin by a factor[8] of 7.6-24.2. The ED_{50} of a white pig is therefore very close to the ED_{50} of a Caucasian but differs somewhat more from the ED_{50} of yellow and black skin. More experimental data are needed to aid the proper selection of animals and the conversion of animal data to that for the human.

REFERENCES

1. J.S. Michael, "Nonionizing Radiation Protection," 1982, 39.

2. E.B. Helwig, et al., "Anatomic and Histochemical Changes in Skin After Laser-Irradiation," Fed. Proc. (Suppl. 14), 1965, 24, s-83.

3. A.N. Takata, et al., "Laser-Induced Thermal Damage of Skin," AD A054 612, 1977.

4. J.G. Kuhn, et al., "Laser Injury in Skin," Lab. Invest., 1967, 17 (1), 1.

5. W. Iliam Montagna, "The Skin of the Domestic Pig," J. Invest. Dermatology, 1964, 43, 11.

6. W. Blum, "Histology," translated by Wang Qiyuan, Scientific Publishing Company, 1984.

7. Chen Ji, et al., Ibid., p 596.

8. R.J. Rochwell, et al., "Research on Human Skin Laser Damage Thresholds," ADA-012703 (p 8947), 1974.

9698/6091
CSO: 8111/1099

MORPHOLOGICAL ANALYSIS OF RETINAL INJURY IN RABBITS ARISING FROM ARGON LASER IRRADIATION

Shanghai ZHONGGUO JIGUANG [CHINESE JOURNAL OF LASERS] in Chinese Vol 12, No 10, 20 Oct 85 pp 633-634

[Article by Zhang Xiaoru [1728 1321 0320], Zhao Tongzhen [6392 2717 4176], and Guo Wenqi [6753 2429 3823] of Xi'an Medical University Hospital No 1]

[Text] Abstract: The pathological changes of retinal injury arising from argon laser irradiation with various laser densities and exposure time, and the characteristics of retinal biological effect arising from the irradiation are reported.

Lasers can cause retinal damages in humans, as proven by some of the eye injuries suffered by laser workers.[1,2] It is therefore important to explore the pathological changes of injury spots visible (and visible) under an ophthalmoscope. The study of the retinal changes caused by low level laser radiation are also important for laser safety and retinal injury treatment.

I. Experimental Results

According to the medium through which the laser passes, the experiments are divided into two groups.

Group A: with pre-lens

Eight rabbit eyes were irradiated with different exposure time and dosage. The cornea injury thresholds were 6.54 W/cm^2 for 0.145 sec and 4.827 W/cm^2 for 1 sec. Table 1 shows that the length of the retinal injury is proportional to the laser dosage. The degree of injury depends on the threshold value. The injuries are more severe when the dosage is greater than the threshold, and vice versa. Injuries caused by adjacent dosages above and below the threshold (cases 1 and 2, and 5 and 6) are similar. At the same dosage, the injury becomes more severe (cases 7 and 8) when the exposure time is increased. In addition to the retinal injury, the choroid blood vessels also show significant dilation and extravasation.

Table 1. Retinal Injuries in Rabbits 1 Hour After an Argon Laser Irradiation Through a Slit Lamp and a Pre-Lens

Case	Dosage (W/cm^2)	Exposure time (sec)	Length of damage (μm)	Damage level	Exudation
1	8.09	0.145	300	II	-
2	6.85	0.145	230	II	-
3	6.54	0.145	130	I	-
4	6.54	0.145	50	I	-
5	5.8	0.145	120	I	-
6	4.92	0.145	100	I	-
7	4.827	1	170	III	-
8	4.827	1	300	III	-

Group B: with contact lens

Four rabbit eyes were irradiated for 1 second with the laser passing through a contact lens. Ophthalmoscopic observations showed that the retinal injury threshold is 28.3 W/cm^2. The results are summarized in Table 2. Even though the dosages are different, there are certain common features of the injuries caused by the laser passing through a pre-lens and a contact lens. Within a certain dosage range, adjacent dosage levels cause similar injuries.

Table 2. Retinal Injuries in Rabbits 24 Hours After an Argon Laser Irradiation Through a Slit Lamp and a Contact Lens

Case	Dosage (W/cm^2)	Exposure time (sec)	Length of injury (μm)	Damage level	Exudation
1	26	1	250	I	-
2	26	1	200	I-II	-
3	28.3	1	250	III	-
4	30.4	1	120	III	-

Notes: Based on the classification of laser coagulation spots of Lu and Noyori,[2] we made some slight modification and divided the injuries into four classes:

Class I: Epithelial cell changes, pigment diffusion, swelling of the rod and cone layer, loss of fibrous structure.

Class II: In addition to symptoms of class I, formation of gas bubbles in the rod and cone layer, pyenotic changes or fragmentation of outer nuclei.

Class III: In addition to symptoms of class II, partial rupture of the retina, significant nuclear pyenotosis.

Class IV: Rupture of the entire retina, hemorrhage.

II. Discussion

1. There is generally a positive correlation[4] between the laser dosage and the degree of retinal injury. Based on retinal injuries observed ophthalmoscopically, the threshold dosage is a dividing line for the degree of injuries. For dosages within a certain range above or below the threshold, the injuries are similar, as shown in Tables 1 and 2. Therefore, from a pathological point of view, the threshold should not be a point but a range. Irradiations made within this range are similar. In addition, the degree of injury depends on the exposure time. In this work irradiations in Group A were made below the threshold but the exposure time was increased from 0.145 sec to 1 sec. For 0.145 sec, the injury was class I, but the injury for 1 sec was class III. Even at dosage levels well below the threshold, serious injuries can still be induced with a sufficiently long exposure time.

2. Morphological studies showed that retinal injuries at 1 hour after the irradiation had the following characteristics:

(1) Retinal injuries undergo a qualitative change from slight changes to obvious necrosis. Table 1 shows that the changes are mainly qualitative below the threshold and necrosis above the threshold. The threshold that we established on the basis of the ophthalmoscopic observations is therefore pathologically significant. Below the threshold the changes are reversible whereas retinal changes caused by above threshold radiation are irreversible.

(2) In general, after histological injuries caused by physical or chemical forces, white cell infiltration occurs as soon as 5 to 10 minutes afterwards. However, even 1 hour after the retina was irradiated by a laser, almost no material exudation was observable except occasional liquid exudation and choroid blood vessel dilation. This is true even for class III injuries. This suggests that the injuries to the retina and the blood vessel wall by the laser dosages used in our experiments are lighter than the usual physical, chemical or biological injuries. This makes the laser special in terms of retinal disease treatment. The same phenomenon has also been observed in hepatectomy and splenectomy operations using lasers.

Due to the limited number of observation cases in our study, some of the conclusions must be verified with more extensive experimental work in the future.

REFERENCES

1. J. Jacobson, Arch. Ophthal., 1965, 74, 882.

2. J. Curtin, Amer. J. Ophthal., 1968, 65, 188.

3. Lu Xinyin, "Laser Ophthalmology," First edition, People's Hygiene Publishing Co., 1981, p 88.

4. G. Bresnich, Inryest. Ophthal., 1970, 9, 901.

9698/6091
CSO: 8111/1099

RETINAL INJURY THRESHOLD OF RABBITS, MONKEYS IRRADIATED BY CW OR PULSED YAG LASER BEAMS

Shanghai ZHONGGUO JIGUANG [CHINESE JOURNAL OF LASERS] in Chinese Vol 12, No 10, 20 Oct 85 pp 634-635

[Article by Chu Renyuan [5969 0088 6678], Li Mengchang [2621 5492 2490], Li Leng [2621 1515], Lu Jiajua [0712 0857 5478], Fu Tiansheng [0265 1131 3932], Chen Rongjia [2621 2837 1367], and Jiang Yongming [3068 3057 2494] of the Ophthalmology Institute, Shanghai Medical University, Zhu Baoqian [2612 1405 6870], Cui Jixiu [1508 1323 4423], and Lu Zhenzhen [0712 3791 3791] of the Shanghai Institute of Optics and Fine Mechanics]

[Text] Abstract: The injury thresholds of rabbit retina by CW and pulsed YAG laser (1.06 μm) have been determined. The injury thresholds of monkey retina have also been studied using 150 μs pulsed YAG laser beams. The experimental method and the results are described in this paper.

In order to obtain the retinal injury threshold of the human eye by YAG lasers with a wavelength of 1.06 μm, we made the study reported here. The injury threshold is taken as the laser energy that causes 50 percent retinal injury. To determine the maximum allowable dosage of the YAG laser on the human eye, we first irradiated the eyes of gray rabbits and rhesus monkeys with CW and pulsed YAG laser. Using a weighted linear regression method we analyzed the data and calculated the YAG laser injury thresholds of rabbit eyes and monkey eyes and the laser energy for a 50 percent injury rate.

I. Experimental Setup and Method

Both the CW and the pulsed YAG lasers had a single mode output. The output energy was controlled to within 5 percent. The optical path is shown in Figure 1. The laser beam passed through a beam spreader, a slit lamp, a pre-lens, and reached the eye. In designing the optical path, the established diopters of the rabbit eye and the monkey eye were used. The beam spreader and the pre-lens were chosen to focus the laser beam accurately on the retina.

The laser energy was monitored in real time. To assure a stable beam splitting ratio, we used a polarization compensation method. The accuracy of the measurement was improved by reducing the energy level variation due to polarization changes upon reflection and transmission.

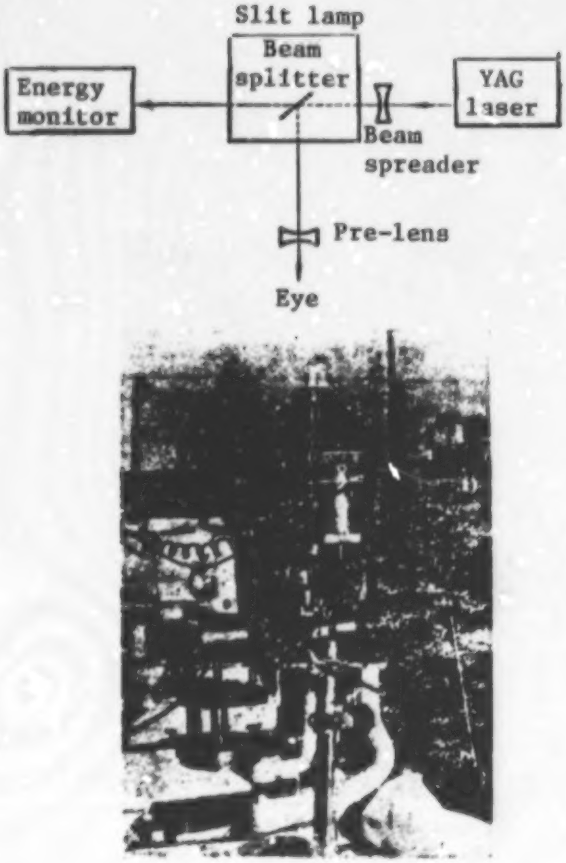

Figure 1

The light spot area was measured with a video camera and the light spot displayed on a television screen was photographed. The actual spot area was then computed from the magnification. The exposure time Δt was controlled by a step motor.

The transmissivity of the YAG laser light through the rabbit eye was first measured in order to calculate the actual energy level reaching the retina. To measure the transmissivity, the eyeball was removed from the rabbit and a 5 mm diameter opening was immediately cut at the rear apex of the eye. A piece of cellophane with a known transmissivity was used to cover the opening and prevent the vitreous liquid from flowing out. The incident laser energy E and the transmitted laser energy E' were then measured and the transmissivity is then equal to $T = E/E'$. The average measured transmissivity of the rabbit eye was 36 percent.

In measuring the retinal injury threshold for gray rabbits, three exposure times were used: 1 sec, 137 ms, and 150 μs. Before the irradiation the pupil of the rabbit eye was dilated for 3 days with an atropine ointment.

The muscles of the rabbit were anesthetized with sodium phenobarbital. Six shots were made on each eye. The retina injuries occurred in the region below the papillary. Three observations were made after the shots: immediately after the irradiation, and 1 hour and 24 hours afterwards. The injury statistics were based on the observation made 1 hour after the irradiation and injuries appeared afterwards were not counted. Figure 2 shows the retina damage of the rabbit eye.

Figure 2. Ocular photograph of a laser-damaged rabbit eye

To measure the retinal injury threshold in rhesus monkeys, we used 150 μs YAG laser pulses. The pupil was dilated with atropine and the muscles were anesthetized with copper chloramine. The irradiation spots were distributed in different quadrants. Each eye was used for several tens of days. Like the rabbit eyes, the monkey eyes were also examined three times after the irradiation.

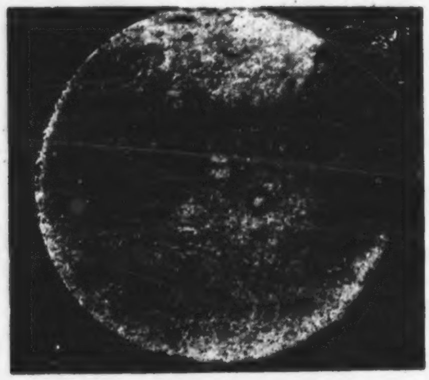

Figure 3. Ocular photograph of a laser-damaged monkey eye

II. Experimental Results

The laser injury thresholds of the rabbit eye and the monkey eye were obtained from the statistical analysis of irradiation data in a number of animal groups at various laser energies. Different injury rates were obtained at different laser dosages. When the retina showed a 50 percent injury rate, the laser energy was taken to be the injury threshold or ED_{50}.

A weighted linear regression calculation yielded the results listed in the following table:

Animal	Exposure time Δt	Spot area Δs (mm^2)	No of eyes	Total No of shots	Injury threshold ED_{50} (mJ)	Energy reaching retina $E_R = E \cdot T$ (mJ)	95 percent confidence limit (mJ)	Power density $P = \frac{ED_{50}}{\Delta t \Delta s}$ (W/cm^2)
Rabbit	1s	2.27	64	384	396.3	142.7	379.3~416.9	17.5
Rabbit	137 ms	2.27	86	516	208.9	75.2	174.4~250.2	67.2
Rabbit	150 μs	1.77	40	240	0.259	0.093	0.197~0.329	97.6
Monkey	150 μs	1.77	4	254	0.885		0.883~0.887	333.3

The trend shown by the above results is that, as the exposure time decreases, the higher the laser power, the lower the injury threshold. Under the same irradiation conditions (exposure time, laser output), the threshold of the monkey eye is greater than that of the rabbit eye and the ratio is $E_{rabbit}:E_{monkey} = 1:3.4$.

9698/6091
CSO: 8111/1099

EXPERIMENTAL STUDY ON RETINAL INJURY THRESHOLD OF ANIMAL BY 694.3 nm LASER IRRADIATION

Shanghai ZHONGGUO JIGUANG [CHINESE JOURNAL OF LASERS] in Chinese Vol 12, No 10, 20 Oct 85 pp 636-637

[Article by Zhao Tongzhen [6392 2717 4176], An Xiaoyue [1344 2556 1471], Dang Zhiping [7825 3112 1627], Zhang Xiaoru [1728 1321 0320], and Guo Wenqi [6753 2429 3823] of the Xi'an Medical University Hospital No 1]

[Text] Abstract: This paper reports experimental results on retinal injury of animals by 694.3 nm irradiation. The ED_{50} of retinal injury was obtained. The pathological characteristics of retina was observed and experimental techniques are presented.

I. Experimental Conditions

Irradiation source: A model HJY-3 ruby laser ophthalmology unit. The pulse width was 0.7 ms, the divergence was 3 mrad, the multimode output energy was 2.5 J, and the stability was better than 3 percent.

Optical path: The optical path is shown in Figure 1. The ruby laser beam passed through a 5 mm diameter beam defining diaphragm and entered a modified slit lamp system. The beam divergence angle was 4.09 mrad. The beam was then attenuated in passing through a cup of copper sulfate solution and entered the rabbit eye. Similation runs were made with a low power argon laser to adjust the optical path and the irradiation spot.

Real time monitoring: The stability of the beam energy was monitored by a model R_j 7200 energy meter via a beam splitter. The energy entering the rabbit eye was monitored by another R_j 7200 unit. The measurement errors were less than ±2 percent. The ambient temperature was 17-22°C and the relative humidity was 75-80 percent.

II. Experiments

1. Irradiation dosage and grouping

In the preliminary tests the dosage received by 100 percent and zero percent of the cornea surface are respectively 67.53 mJ/cm^2 and 5.23 mJ/cm^2. Using the ratios of a geometric series the dosages are divided into 7 groups: 67.53, 43.31, 27.96, 17.42, 12.10, 7.64, and 5.23 mJ/cm^2.

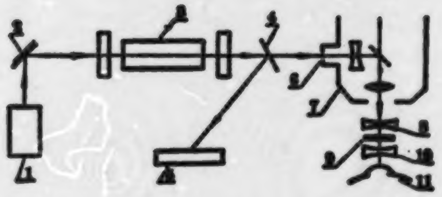

Figure 1. Optical path of the 694.3 ruby laser

1--Argon ion laser; 2--Total reflection mirror; 3--Ruby laser; 4--Beam splitter; 5--R_j 7200 energy meter; 6--5 mm diameter beam defining diaphragm; 7--Slit lamp; 8--Compensating concave lens; 9--Copper sulfate solution cup; 10--Contact lens (for observation); 11--Eyeball

2. Animal selection and grouping

Gray chinchilla rabbits weighing 2 kg or so were examined visually and, if necessary, ophthalmoscopically. Animals with significantly different pigments were excluded. A total of 35 rabbits were used, 420 shots were made, 217 injury spots were examined, producing 1680 data points. Five rhesus monkeys were used. Due to the limited number, no grouping was made. Instead, the irradiation of the monkey retina was made using the rabbit ED_{50} or its multiples. The reactions were examined visually and ophthalmoscopically.

3. Results

Immediate reactions were assessed right after the shots. Observations under an ophthalmoscope after 1 hour ranked barely visible injury spots as a positive reaction. The morphological indications of such injuries were considerably weaker than a class I coagulation spot in the treatment of laser injury. The diameter was smaller than 1 radian, the color was light gray, and the injuries were caused by pigment accumulation and uneven distribution.

III. Experimental Results (see Tables 1 and 2)

The results on rabbits showed that the positive reaction rate increased with increasing dosage. The results on the monkeys were essentially similar.

Data analysis:

Using a weighted regression method, we obtained the following ED_{50} values:

For rabbit retina: $ED_{50} = 16.61$ mJ/cm^2, 95 percent confidence limit = 19.97-13.81 mJ/cm^2.

For monkey retina: $ED_{50} = 42.53$ mJ/cm^2, 95 percent confidence limit = 61.17-29.56 mJ/cm^2.

Table 1. Reaction of Rabbit Retina 1 Hour After 694.3 nm Ruby Laser Irradiation (parallel light)

Group	Dose (mJ/cm^2)	No of shots	No of reactions	Reaction rate (%)
1	67.5	60	60	100
2	43.31	60	48	80
3	27.69	60	38	63.3
4	17.42	60	31	51.6
5	12.10	60	24	40
6	7.64	60	16	26.6
7	5.23	60	0	0

Table 2. Reaction of Monkey Retina 1 Hour After 694.3 nm Ruby Laser Irradiation (parallel light)

Dosage (mJ/cm^2)	No of shots	No of reactions
16.61	6	0
16.61x1.5	6	2
16.61x2	12	5
16.61x2.5	12	6
16.61x3	12	5
16.61x3.5	6	5
16.61x4	6	6

Note: 16.61 mJ/cm^2 is the ED_{50} for rabbits

IV. Histological and Pathological Data

After the completion of all the measurements, two rabbit eyes were irradiated with the ED_{50} dosage for rabbits and two monkey eyes were irradiated with respectively 2 times and 2.5 times the ED_{50} dosage for rabbits. Each eye was irradiated at six points and the usual paraffin slicing procedures were followed. Under an optical microscope the following pathological changes were found:

1. The long axis of the rabbit retina injury caused by the ED_{50} dosage of 16.61 mJ/cm^2 ranged from 120 µm to 1100 µm, mostly around 500 µm. The injured retina showed bulges and edema and thickening of the rod and cone layers. Some pigment diffusion had occurred and sometimes voids had formed between the pigment layer and the rod and cone layer. The voids were filled with exudants and some detached nuclei. The pigment layer showed a reduction or diffusion of the pigments. The choroid showed neutral white cell infiltration and sometimes congestion and pigment increase.

2. For the monkey retina irradiated at 16.61 mJ/cm^2, the injury length was in the 200-500 µm range and located at 1200 µm from the disk. The inner membrane bulged out, with light pink exudation at the lower part.

3. The monkey retina irradiated at a dose of twice the rabbit ED_{50} showed considerable pyenotic nucleus, edema and thickening of the rod and cone layer, and pigment diffusion into the rod layer.

4. The monkey retina irradiated at a dosage of 2.5 times the rabbit ED_{50} showed local pointed protrusions. The laser beam penetrated the retina and caused retinal rupture, hemorrhage, and loss of cells.

9698/6091
CSO: 8111/1099

MEASUREMENT OF LASER SPOT DIAMETER ON RETINA, CORNEA

Shanghai ZHONGGUO JIGUANG [CHINESE JOURNAL OF LASERS] in Chinese Vol 12, No 10, 20 Oct 85 pp 637-638

[Article by Dang Zhiping [7825 3112 1627], An Xiaoyue [1344 2556 1471], and Li Yujun [2621 3768 0193] of the Laser Medicine Laboratory, Xi'an Medical University Hospital No 1, Chen Kuanlin [7115 1401 2651], Huang Xianqin [7806 6272 2953], and Zhang Hong [1728 4767] of the Xi'an No 1001 Plant]

[Text] Abstract: A method for measuring the laser spot diameter on the retina and cornea is described. The method is simple, fast, accurate, and harmless to the eye. It is an important development for basic research and clinical treatment.

After studying techniques reported in foreign journals, we have developed a "microscope eyepiece reticule method" using ordinary slit lamp.

1. Measurement of light spot diameter on the retina

(1) Application: When the ocular crosshair is sharply focused through the slit lamp and the contact lens, the laser beam is introduced into the eye through the slit lamp and the contact lens to measure the light spot diameter (or injury dimension) on the retina.

(2) Procedure

a. A glass reticule plate with known graduation is placed in the eyepiece housing at the image plane of the compound objective.

b. Introduce the laser beam through the slit lamp and the contact lens into the eye.

c. Through the slit lamp objective, read the number of divisions occupied by the light spot on the reticule. Multiply by the value of one division to obtain the diameter of the magnified spot.

d. Divide the size of the magnified spot by the magnification of the objective to obtain the diameter of the light spot on the retina.

(3) Example

A 3 mm diameter 488 nm argon ion laser beam was introduced into a rabbit eye through a slit lamp and a contact lens. Looking through the eyepiece, the magnified image of the light spot occupied A divisions (A = 2) on the reticule. The length of one division B was known to be 50 µm and the magnification of the objective was 1.6. Hence, the light spot diameter is

$$d=\frac{A\times B}{K_{obj}}=\frac{2\times 50}{1.6}\approx 62(\mu m)$$

2. Measurement of the light spot diameter on the cornea

(1) A glass reticule with a graduation size B of 41 µm was placed at the image plane of the compound objective.

(2) A vernier scale was placed at the original cornea location (13.58 mm from the pre-lens). The magnified image of a 1 mm object occupied A divisions on the reticule (A = 30). The magnified image of 1 mm was therefore 30x41 = 1230 µm.

(3) The objective has a magnification of

$$K_{obj} = \frac{1230}{1000} = 1.23$$

(4) The 3 mm diameter 488 nm argon ion laser beam was introduced onto the vernier scale through the slit lamp and the pre-lens. Through the eyepiece, the magnified image of the light spot occupied 25 divisions. The magnified image was therefore 25x41 = 1025 µm.

(5) The light spot diameter on the cornea is therefore

$$d = \frac{AxB}{K_{obj}} = \frac{25x41}{1.23} = 833\ \mu m$$

9698/6091
CSO: 8111/1099

MEASUREMENT OF TRANSMISSIVITY OF ARGON LASER LIGHT THROUGH RABBIT'S EYES

Shanghai ZHONGGUO JIGUANG [CHINESE JOURNAL OF LASERS] in Chinese Vol 12, No 10, 20 Oct 85 pp 638-639

[Article by Li Yujun [2621 3768], Dang Zhiping [7825 3112 1627], and Zhao Tongzhen [6392 2717 4176] of the Laser Laboratory, Xi'an Medical University Hospital No 1]

[Text] Abstract: The measurement of transmissivity of 488 nm argon laser light through refractive system of the rabbit's eyes in vitro is reported.

In order to measure the retinal injury threshold (ED_{50}) of an argon laser, we measured the transmissivity of a rabbit eye to 488 nm argon laser light by introducing an opening on the sclera of a rabbit eye in vitro. The ED_{50} value was then computed from the transmissivity and the light spot diameter on the retina.

The transmissivity of the human eye is similar to that of other mammals (rabbits, cats, monkeys, and cows). The measured transmissivity of the rabbit eye is therefore useful in research and in clinical treatment of eye diseases.

I. Measurement Method

The 488 nm laser beam from an argon laser passes through a slit lamp and the measurements are made after the slit lamp, see Figure 1.

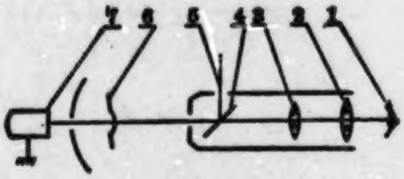

Figure 1. Optical path used in measuring the transmissivity of the rabbit eye

1--Observer's eye; 2--Eyepiece; 3--Objective; 4--45° reflection mirror; 5--Laser beam; 6--Rabbit eye; 7--Laser power meter (2, 3 and 4 constitute the slit lamp system)

The laser output was stable to within 2 percent. Using an alternation method, we repeatedly measured the laser power before the eyeball and after the eyeball. At least three measurements were made on a given eyeball at different energy levels and the average was then taken. A total of four eyeballs were used.

In order for the entire laser beam to enter the eyeball, pass through the medium and detected by the power meter, the pupil was sufficiently dilated. After the eyeball was removed from the body, a 3 mm diameter small hole was opened immediately on the sclera so that the laser may exit freely.

II. Results and Analysis

For a hole opened below the disk the transmissivity is 90.1 percent. For a hole opened at the disk the transmissivity is 94.1 percent. The table below lists the measurement data.

Table 1. Measurement Data

Eyeball No.	Sclera location	Laser power (mW)	Laser power after passing through the eyeball (mW)	Transmissivity (%)	Ave. transmissivity (%)	
1	On the retina, below the disk	16.4	14.8	90.4	90.2	90.1
		21.6	19.5	90.5		
		33.0	29.1	88.3		
		38.2	34.9	91.4		
2	"	18.5	16.3	88.3	88.6	
		28.2	25.2	89.5		
		38.1	33.3	87.3		
3	"	16.5	15.1	91.8	91.5	
		24.0	22.0	91.8		
		40.0	36.4	91.0		
4	At the disk	17.0	15.9	93.6	94.1	
		25.5	21.4	94.5		
		40.5	38.1	94.1		

The results in the table show that:

1. For a given eyeball, the transmissivity obtained with different laser energy varied slightly. These are measurement errors.

2. For the same laser energy, the transmissivity of different eyeballs varied slightly. These are due to differences in the eyeballs and due to misalignment of the axis.

3. The transmissivity is more sensitive to the location where the laser passes through the eye. The transmissivity is higher when the laser passes

through the visual disk. This can be attributed to two reasons: First, variations of the sclera opening and the axis lead to different optical paths in the eye and hence a different transmissivity. Second, the opening of the hole caused some loss of the vitreous liquid and hence affected the transmissivity.

It has been reported that the medium of a rabbit eye absorbs 10 percent of the argon laser energy, that is, the transmissivity of the rabbit eye to the argon laser is 90 percent. Our results are in agreement with this and can be trusted.

9698/6091
CSO: 8111/1099

INJURY THRESHOLD OF SKIN IRRADIATED WITH 308 nm EXCIMER LASER LIGHT STUDIED

Shanghai ZHONGGUO JIGUANG [CHINESE JOURNAL OF LASERS] in Chinese Vol 12, No 12, 20 Dec 85 pp 735-738

[Article by Li Zhaozhang [2621 0340 3864], Wu Jianu [0702 1367 1166], and Gai Baokang [5556 1405 1660] of the Laser Medicine Laboratory, Shanghai No. 2 Medical University, and Zhou Zhengzhuo [0719 2398 0587] of the Shanghai Institute of Laser Technology]

[Text] Abstract: The paper reports the preliminary results of ultraviolet erythema on the skin irradiated with 308 nm excimer laser light. Using white pigs as an animal model, we obtained injury threshold data of the skin. The 95 percent confidence limit of MRD_{50}, an energy density that results in 50 percent perceptible redness occurrence rate for all points irradiated ranges from 45.97 to 63.05 mJ/cm^2.

The biological study of irradiating the skin with ultraviolet light began at the turn of the century. The Danish physicist Niels Finsen first treated lupus with an artificial UV source. Hausser and Vahle of West Germany investigated the effect UV of various wavelengths on the human skin using a low pressure mercury lamp and a double quartz prism monochromatic light source and found that irradiation at 300 nm tended to cause erhthema. In the 1930's Coblentz et al measured the UV induced erythema and found that wavelengths from 200-280 nm could cause noticeable transient erythema and wavelengths of 254 nm and 197 nm were most likely to produce retaining erythema. In 1965 Everett and coworkers measured the erythema curve of the human skin with a Xenon arc monochromatic source equipped with a grating. They found that, as the UV wavelengths increased, the energy required to produce minimum erythema also increased. For wavelengths longer than 300 nm, the erythema effect was considerably reduced. In the 1970's Parrish irradiated the Cavcasian skin with a nitrogen laser and found that the minimum dosage of a multipulse N_2 laser for producing lasting erythema was 2.6±4.8 J/cm^2. Aufmuth reported in 1979 the effects of a dye laser (tunable from 260 to 345 nm) on the human skin and found that the MRD (minimum redness dosage) of a 300 nm UV laser was 5 mJ/cm^2. In recent years Anderson and Parrish studied the effects of short pulse UV lasers on the human skin and found that the photochemical reaction played an important role.

The skin injury threshold by a 308 nm excimer laser has not been reported in China or abroad. Work in this area is really needed in order to establish a laser protection standard in China.

I. Experimental Material and Method

An XeCl excimer laser was used as the irradiation source. The wavelength was 308 nm, the pulse width was 15 ns, the maximum output energy per pulse was 100 mJ, the divergence angle was 12.8 mrad along the major axis direction and 7.1 mrad along the minor axis.

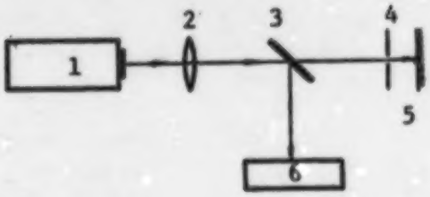

1. 308 nm excimer laser
2. Focusing lens
3. Quartz beam splitter
4. Diaphragm
5. Skin surface
6. Energy monitor

Fig. 1. Schematic diagram of the experimental setup

Figure 1 shows the experimental setup. The dosage was determined by monitoring the energy and the beam splitting ratio ($K = 2.1 \pm 0.087$). The calibration of the energy meter used can be traced to the State Institute of Measurement. The ambient conditions were 25°C ± 1.1°C and 79.3 ± 8.4 percent humidity.

The experimental animals were three 5.5 kg Shanghai White pig. Two hours before the irradiation, the animals were put under anaesthesia by injecting 1 ml per kilogram of body weight of 2.5 percent sodium isobarbiturate. The pig was then washed with warm water and soap. The back and abdomen of the animal were shaved clean. From the two sides of the spine to the abdomen, 40 2cm x 2cm grids were painted on the skin. The laser beam was then trained to the center of the squares after passing through a 5 mm diameter diaphragm.

The observation of the erythema was done mainly with the unaided eyes. The criteria for judging the erythema will not be discussed here. The injury threshold in this experiment was based on the "+" grade erythema. The dosage for 50 percent "+" erythema occurence within 24 hours after the irradiation was measured. Optical microscopic examinations were made at different time intervals after the irradiation of the 7 groups. Electron microscopic inspections were also made for the near threshold runs.

A total of 230 shots were made in the course of the experiment, 18 of them were examined histologically. The 212 data points in the 7 irradiation dosage groups were subjected to statistical analysis. Using a weighted regression method (performed on a PDP11-23 computer), the MRD_{50} value and the 95 percent confidence level for the white pig skin irradiated by a 308 nm excimer laser were obtained.

Table 1. Transient erythema reaction of the pig skin irradiated by a 308 nm excimer laser

Group	Ave. dose ± std. dev. (mJ/cm²)	No. of shots	Transient erythema			Redness indication
			Rate %	Occurence time (sec. after the shot)	Lasting time (min, sec)	
1	22.28±2.26	32	—	—	—	—
2	29.44±1.80	32	—	—	—	—
3	39.76±3.85	30	33.33	9"~18"	49"~2'17"	±
4	53.56±5.19	31	41.94	7"~12"	1'28"~2'26"	±
5	69.14±4.51	27	70.37	4"~13"	1'54"~5'	+
6	91.27±1.96	30	83.33	5"~15"	45"~8'42"	+
7	106.17±3.18	30	100.00	Instantly to 15"	39"~10'	++

Table 2. Delayed erythema reaction of the pig skin irradiated by a 308 nm excimer laser

Group	Ave. dose ± std. dev. (mJ/cm²)	No. of shots	No. of red spots after 24 hours	Delayed erythema occurrence rate(%)	Redness indication
1	22.38±2.26	32	5	15.63	±
2	29.44±1.80	32	9	28.13	±
3	39.76±3.85	30	11	36.67	±
4	53.56±5.19	31	14	45.16	+
5	69.14±4.51	27	15	55.56	++
6	91.27±1.96	30	22	73.33	++
7	106.17±3.18	30	25	83.33	+++

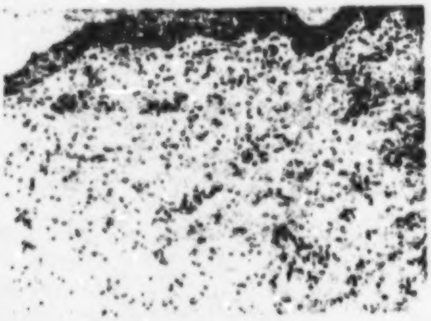

(a) Histological examination of Group 4 with H.E. stain made 24 hours after the laser shot showing dilation and congestion of the blood capillaries in the dermis.

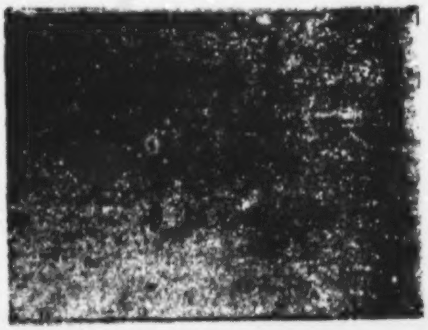

(b) Histological examination of Group 5 with H.E. stain made 24 hours after the laser shot showing dilation and congestion of the blood capillaries in the dermis.

(c) Histological examination of Group 6 with H.E. stain made 24 hours after the laser shot showing dilation and congestion of the blood capillaries in the dermis and edema of the cuticular cells

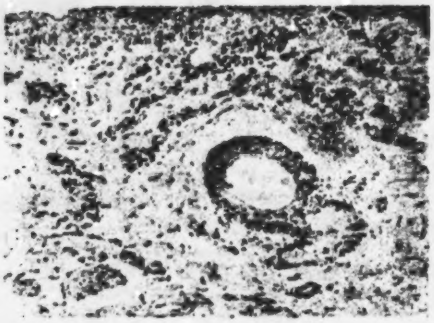

(d) Histological examination of Group 7 with H.E. stain made 24 hours after the laser shot showing dilation and congestion of the blood capillaries in the dermis, accumulation of infectious cells, and edema of the cuticular cells

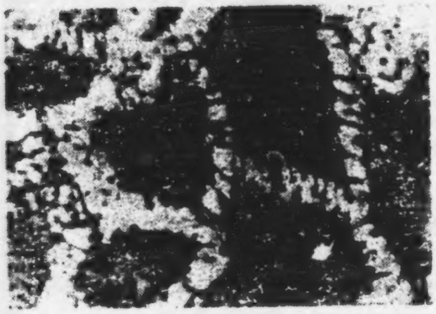

(e) Specimen taken 5 minutes after the laser shot at a dosage of 53.56 ± 5.19 mJ/cm^2 showing an increased prickle cell spacing. (x11,200 by electron microscope)

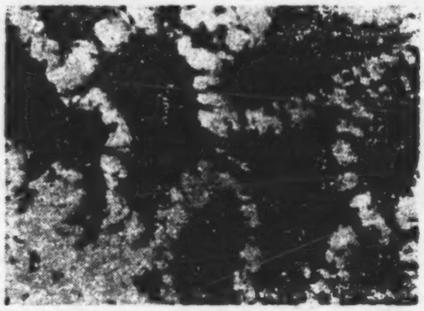

(f) Specimen taken 5 minutes after the laser shot at a dosage of 69.14 ± 4.51 mJ/cm^2 showing an increased prickle cell spacing. (x11,200 by electron microscope)

II. Experimental Results and Analysis

Table 1 and Table 2 show the transient and delayed erythema reaction of the pig skin irradiated with 308 nm laser light. Delayed erythema usually appeared 8-9 hours after the shots, although in Groups 6 and 7 the erythema appeared after only 5 hours. The number of erythema in all groups reached a maximum at 24 hours and the color also became the darkest. The redness usually lasted for 2-3 days. The delayed erythema in Group 6 had all become pigment precipitates after 48 hours delayed erythema in Group 7 formed scabs.

Histological examinations made after 24 hours of the skin irradiated at different dosage were: Group 1 showed no observable reactions, Groups 2 through 4 showed various degrees of capillary dilation and congestion in the dermis together with some red blood cell exudation, Group 5 showed the same reactions as Groups 2-4 and also the appearance of lymphocytes around the blood vessels, Group 6 showed groups of infectious cells in the dermis, and Group 7 showed basal cell edema accompanied by some cavieties and rarification of the cells. Photomicrographs a-d show the detailed changed. Optical and electron micrographs (e,f) showed basically normal structure of the transient erythema skin in Groups 3-5.

The MRD_{50} value and the 95 percent confidence limit of the irradiated pig skin by the 308 nm laser light were obtained from visual observation and weighted regression. The results are shown in Table 3 and Fig. 2. Here x is the logarithm of the laser dosage, y is the delayed erythema occurrence probability, and a x^2 test of the regression formula showed satisfactory results.

Table 3. Probability analysis of the pig skin injury threshold by 308 nm laser radiation

	Visual observation	Weighted regression
Regression equation		$y=0.4759 + 2.6134x$
MRD_{50}(mJ/cm^2)	53.09	53.84
95% confidence limit (mJ/cm^2)	43.36-65.00	45.97-63.05

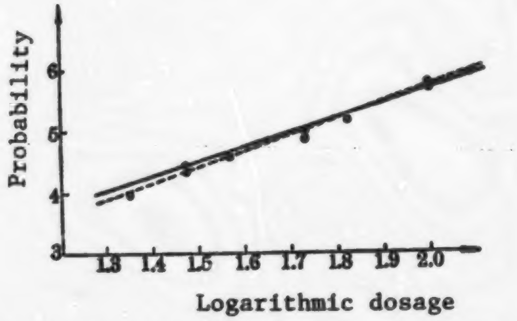

Fig. 2. Erythema occurrence probability as a function of the logarithmic dosage. Solid line -- visual observation, dashed line -- weighted regression. o -- experimental value, • -- computed by weighted regression.

III. Discussion

1. Two-phase erythema reaction caused by short ultraviolet laser pulse

The two phases of the skin erythema reaction caused by ultraviolet reaction--transient and delayed--were clearly observed in our experiments. The transient erythema caused by the 308 nm laser radiation occurred quickly and disappeared quickly--lasting no more than 15 minutes. This phenomenon may be due to the pressure effect of the short ultraviolet laser. When the pressure reached a certain critical value, the transport of the blood cell was changed and resulted in transient erythema. Delayed erythema occurred after a delay period, characteristic of photochemical reactions. It was reported in foreign journals that photochemical reactions may produce histamine, 5-hydroxylamin, activated peptide, and prostaglandin E, F, and G, which in turn caused the delayed reaction. Biochemical studies are needed to further understand the generation mechanism of skin erythema by ultraviolet radiation.

2. Minimum redness dosage (MRD) and laser protection standard

In our experiments we used pigs as an animal model and obtained 53.84 mJ/cm^2 as the injury threshold MRD_{50} for the short ultraviolet laser pulses. At this dosage, 50 percent of the irradiated points showed barely visible redness. Similarly, the 10 percent dosage (MRD_{10}) was obtained from the regression equation to be 6.91 mJ/cm^2. Compared to current international laser safety standards (IEC, ANSI, WHO environmental health standard 23, etc), the ratio of the maximum permissible dosage 6.19 mJ/cm^2 for a 308 nm short laser pulse on the skin and the MPE value is only 1.1. This means that the boundary between safety and possible injury is not clearout. One must therefore take proper precaution in consulting the existing maximum permissible dosage when ultrashort ultraviolet laser pulses are used.

9698/7358
CSO: 8111/1421

APPLIED SCIENCES

LASER SAFETY, PROTECTION STANDARDS REVIEWED

Shanghai YINGYONG JIGUANG [APPLIED LASER] in Chinese, Vol 6, No 3, Jun 86
pp 141-144

[Article by Li Zhaozhang [2621 0340 3864] of the Shanghai Second Medical University, Division of Laser Medicine: "Review of the Studies on Laser Safety and Production Standards"]

[Text] Abstract: The recent development of laser safety studies in China is reviewed. Based on the analysis and comparison of the biological data in China and abroad, and in terms of international advanced laser safety standards, some essential factors are briefly discussed for setting the Chinese Safety Standard of Laser Radiation.

Laser technology has found increasingly wide uses in China's industry, agriculture, medicine, technology and defense and the number of people involved in the use of lasers is increasing rapidly. The laser safety and protection issue has been placed on the agenda to carry out the preventive policy of protecting the environment and the welfare of the people.

Based on technical information from abroad, all developed nations have organized special efforts to research and formulate laser safety and protection standards. Such standards have also been revised repeatedly as laser technology development and research progress. Today, the U.S., the U.K., West Germany, the U.S.S.R., Canada, Sweden, France, Denmark, and Austria have established the respective national standards and regulations. In addition, we have learned that Japan is also working hard on laser safety research. China is one of the first countries engaged in laser applications and, as a major nation, cannot do without its own laser safety standards that are applicable to the physiological characteristics of the yellow race.

From 1982 to 1985 the Chinese State Science and Technology Commission organized a national laser protection standard research group and conducted experiments for 3 years. Based on the experience of laser safety research conducted abroad and surveys of laser usage in China, the group conducted eye and skin damage threshold experiments using eight commonly used laser at eleven wavelengths.

Probability statistical analysis methods are used internally in the evaluation of laser damages. The damage threshold is usually defined as the laser radiation dosage corresponding to a 50 percent probability for detecting the minimum damage visually. The damage threshold for the eye and the skin are respectively denoted as ED_{50} and MRD_{50}. Since the measurement of the laser damage thresholds is a delicate quantitative endeavor, the various units in the research group have set stringent critera on experimental apparatus including lasers and optical systems and on the measurement of dosages, data processing, and biological observations to insure reliability of the results. The criteria are:

(1) Laser source--Continuous outputs are desired from single mode lasers, pulsed outputs must have a stability better than ±5 percent.

(2) The equipments used for dosage measurements must be periodically calibrated by the State Measurement Institute.

(3) All biological reactions must be examined histologically with optical or electron microscopes.

(4) Weighted regression analysis should be used in data processing so that the results may be compared with those from abroad.

(5) Experiments for each wavelength should be conducted by at least two units to ensure accuracy.

For the damage threshold of the eye, the research group used rabbits and monkeys, whose eyes closely resemble those of humans, as animal models and irradiation was conducted at eight different laser wavelengths. The E_{50} data obtained are listed in Table 1.

For the study of the skin damage threshold, small white pigs were used as the animal model. Eight laser wavelengths were used for irradiation of various time durations. Table 2 shows the MRD_{50} value obtained for the skin.

The research results listed above served as the biological data base for establishing China's laser safety and protection standards. One hundred twenty volunteers of the yellow race participated in the skin damage threshold tests conducted at five laser wavelengths. The number of human subjects exceeded that of similar research in foreign countries. The damage threshold of the eye by 222 nm and 308 nm ultraviolet lasers and the skin damage threshold by 265 nm (quadruple frequency YAG laser) and 308 nm ultraviolet laser are original results not previously reported in China or abroad. Such data have helped the formulation of safety standards for ultraviolet lasers.

Table 1. ED_{50} of laser damage of the eye

Wavelength (nm)	Subject*	Irradiation time(s)	Spot dia. cornea (mm)	Incident energy or power density (J/cm^2 or w/cm^2)	Remarks
222	1	8×10^{-9}	1	54.4×10^{-3} J/cm^2	Cornea damage
308	1	$8-10 \times 10^{-9}$	1	0.83 J/cm^2	
488	1	1×10^{-1}	2.76	0.51 w/cm^2	Retina damage threshold
488	1	1.45×10^{-1}	3	0.50 w/cm^2	
488	1	1	2.76	0.43 w/cm^2	
488	1	1	3	0.40 w/cm^2	
488	2	1×10^{-1}	2.76	0.834 w/cm^2	
488	2	1.45×10^{-1}	3	1.8 w/cm^2	
488	3	1×10^{-1}	2.76	1.76 w/cm^2	
488	3	1.45×10^{-1}	0.833	17.65 w/cm^2	
530	1	5×10^{-9}	5	39.2×10^{-6} J/cm^2	
530	1	8×10^{-9}	4	232.1×10^{-6} J/cm^2	
530	2	5×10^{-9}	5	187×10^{-6} J/cm^2	
632.8	1	1	4.3	178×10^{-3} w/cm^2	
632.8	1	1.25×10^{-1}	4.3	215×10^{-3} w/cm^2	
694.3	1	6×10^{-4}	5	14.9×10^{-3} J/cm^2	
694.3	1	7×10^{-4}	5	16.6×10^{-3} J/cm^2	
694.3	2	7×10^{-4}	5	42.5×10^{-3} J/cm^2	
1060	1	5×10^{-9}	5	1.2×10^{-3} J/cm^2	
1060	1	1.5×10^{-4}	1.5	97.6 w/cm^2	
1060	1	1.2×10^{-1}	5	5.4 w/cm^2	
1060	1	1.37×10^{-1}	1.7	67.2 w/cm^2	
1060	1	1	1.7	17.5 w/cm^2	
1060	1	1.02	5	2.5 w/cm^2	
1060	2	1.5×10^{-4}	1.5	333.3 w/cm^2	
1060	2	5×10^{-9}	5	4.3×10^{-3} J/cm^2	
1060	3	1.5×10^{-4}	1.75	429 w/cm^2	
10600	1	1.2×10^{-1}	1	10.7 w/cm^2	Cornea damage
10600	1	1.25×10^{-1}	1	4.0 w/cm^2	
10600	1	1	1	3.6 w/cm^2	
10600	1	1.03	1	5.7 w/cm^2	

* 1. Rabbit 2. Monkey 3. Eye of yellow race

Table 2. MRD_{50} for laser damage of the skin

Laser wavelength λ (nm)	Subject	Exposure time(s)	MRD_{50} (J/cm^2)	λ (nm)	Subject	Exposure time(s)	MRD_{50} (J/cm^2)
10600	white pig	1	3.7	694.3	white pig	3.2×10^{-4}	53.3
10600	white pig	1	2.4	694.3	human, yellow race	3.2×10^{-4}	4.7
10600	human, yellow race	1	2.7	514.5	human, yellow race	1	7.1
10600	human, yellow race	1	2.3	488	grey pig	1	5.2
1060	white pig	1	59.4	488	human, yellow race	1	5.6
1060	white pig	2×10^{-4}	4.6	488	human, yellow race	1	5.6
1060	human, yellow race	1	60.6	37.1	white pig	4.5×10^{-9}	8.3
1060	human, yellow race	1	71.4	308	white pig	15×10^{-9}	53.8×10^{-3}
1060	human, yellow race	2×10^{-4}	9.9	308	white pig	$50-70\times10^{-9}$	73.0×10^{-3}
1060	human, yellow race	3×10^{-4}	20.3	265	white pig	9×10^{-9}	22.0×10^{-3}

The eye and skin damage thresholds are criteria for evaluating safe laser dosages. The national laser safety standard research group has carefully studied the entire results. Based on health statistics procedures and using probability equations, the values of ED_{10} and MRD_{10} (10 percent probability for minimum damages) have been computed and compared to ED_{50} and MRD_{50}.

$$ED_{50} : ED_{10} = 1.2\text{-}2.2 : 1$$

$$MRD_{50} : MRD_{10} = 1.23\text{-}3.1 : 1$$

Both ratios are greater than unity. Therefore, a safety factor of 5-20 may be used in computing the maximum permissible exposure (MPE) or exposure limit (EL) from ED_{50} or MRD_{50}. Since most of experimental data are obtained from animal tests, the safety factor should be on the high side when MPE is computed from ED_{50}.

In comparison with similar studies made abroad, the MRD_{50} for the Chinese falls between that for Caucasians and blacks, see Table 3. The ED_{50} for rabbit and monkey eyes in the Chinese studies is somewhat higher, but their dependence on the exposure time is consistent with the foreign data. We can therefore use the laser safety standards of advanced nations as references in formulate China's own standards.

Table 3. Comparing the MRD_{50} for Chinese with foreign study results

Laser	λ (nm)	Exposure time (s)	Subject	MRD_{50} (J/cm²)	EL (J/cm²)	MRD_{50}(min)/EL
Ruby laser	694.3	2.5×10^{-3}	White	11—20	0.25	44
			Black	2.2—6.9		9
		0.32×10^{-3}	Chinese	4.2—5.1	0.147	28
Nd:glass laser	1060	75×10^{-9}	White	4.2—5.7	0.1	42
			Black	2.5—3.0		25
		2×10^{-4}	Chinese	9.3—10.6	0.65	14
		3×10^{-4}	Chinese	19.0—21.9	0.72	26
CO_2	10600	1.0	White	2.8	0.56	5
			Black	2.8		5
			Chinese	2.3—2.7		4
Nd:YAG	1060	1.0	White	48—78	5.5	9
			Black	46—60		8
			Chinese	60—71		11
Ar^+	488.0	1.0	White	4.0—8.2	1.1	4
			Black	4.5—6.0		4
			Chinese	5.6—5.64		5

In order to establish China's laser safety and protection standards, the national research group has not only completed the biological tests described above, but have also collected extensive data in China and from abroad and translated and compiled important international laser safety standards including the IEC stnadard on laser product specification, the World Health Organization environmental health standard 23, and the ANSI standard Z136-1 1980 on the safe use of lasers. The group has also interviewed laser workers in Beijing, Shanghai, Tianjin, Xi'an, Henan, and in northeastern China to assess the causes for laser accidents and the physical examination of laser workers. By combining the experimental research results, the international data, and the survey results, the national laser safety and protection research group consulted dozens of laser production and research units and formulated the proposal on laser standards after several modifications.

Today there are more than 300 laser research and production units in China and many laser medical units. The number of workers involved with the usage of lasers exceeds 10,000. The establishment of the laser safety and protection standards is therefore very important to the safety of the workers.

REFERENCES

1. D.H. Sliney et al; Safety with Lasers and Other Sources, a Comprehensive Handbook, 1980 Plenum Press.

2. A. Mallow et al; Laser Safety Handbook, 1978.

3. American National Standard for the Safe Use of Lasers. ANSI Z 136.1, 1980.

4. Lasers and Optical Radiation from WHO 1982, Environmental Health Criteria 23

5. R.J. Rockwell et al; AD A 012/703, 1974

6. Radiation Safety of Laser Products Equipment Classification, Requirements, and User's Guide. International Electrotechnique Commission, April 1980

7. ZHONGGUO JIGUANG [CHINESE JOURNAL OF LASERS], Vol 12, No 10, 1985; Vol 12, No 12, pp 732-741, 1985.

9698/7358
CSO: 4008/88

END

[redacted]

JPRS-CST-86-042

2 OCTOBER 1986

China Report

SCIENCE AND TECHNOLOGY

FBIS FOREIGN BROADCAST INFORMATION SERVICE

JPRS-CST-86-042

2 OCTOBER 1986

CHINA REPORT

SCIENCE AND TECHNOLOGY

CONTENTS

PEOPLE'S REPUBLIC OF CHINA

NATIONAL DEVELOPMENTS

Systematized Microcomputer Nomenclature Introduced
(Qian Dongjun; WUXIANDIAN, No 4, 11 Apr 86) 1

PHYSICAL SCIENCES

Sea-Air Heat Exchange Over North Pacific
(Zhao Yongping; HAIYANG YU HUZAO, No 1, Jan 86) 3

APPLIED SCIENCES

Optimum Output Power of Self-Sustained Discharge Transverse Flow CO_2 Laser
(Chu Zexiang, et al.; ZHONGGUO JIGUANG, No 6, 20 Jun 86) 15

UV Nitrogen Laser Using Hydrogen Thyratron as Switch
(Ou Zhenya, et al.; ZHONGGUO JIGUANG, No 6, 20 Jun 86) 25

Experimental Study of Stimulated Raman Scattering of High-Pressure H_2 Frequency Shifter
(Gao Guochang, et al.; ZHONGGUO JIGUANG, No 6, 20 Jun 86) 31

ABSTRACTS

APPLIED MATHEMATICS

NANJING DAXUE XUEBAO (ZIRAN KEXUE) [JOURNAL OF NANJING UNIVERSITY (NATURAL SCIENCES)], No 1, Mar 85 37

NANJING GONGXUEYUAN XUEBAO [JOURNAL OF NANJING INSTITUTE OF TECHNOLOGY], No 4, 20 Oct 85 38

CHEMISTRY

HUAXUE XUEBAO [ACTA CHIMICA SINICA], No 8, Aug 85 40

CHROMATOGRAPHY

SEPU [CHINESE JOURNAL OF CHROMATOGRAPHY], No 4, Jul 86 43

COMPUTER SCIENCE

NANJING DAXUE XUEBAO (ZIRAN KEXUE) [JOURNAL OF NANJING UNIVERSITY (NATURAL SCIENCES)], No 1, Mar 85 44

TONGXIN XUEBAO [JOURNAL OF CHINA INSTITUTE OF COMMUNICATIONS], No 3, Jul 85 45

NANJING GONGXUEYUAN XUEBAO [JOURNAL OF NANJING INSTITUTE OF TECHNOLOGY], No 4, 20 Oct 85 48

ELECTRONICS

TONGXIN XUEBAO [JOURNAL OF CHINA INSTITUTE OF COMMUNICATIONS], No 3, Jul 85 51

FOUNDRY PRODUCTION

ZHUZAO [FOUNDRY], No 6, Nov 85 54

LASERS

YINGYONG JIGUANG [APPLIED LASER], No 3, Jun 86 56

MEDICINE

ZHONGHUA YUFANG YIXUE ZAZHI [CHINESE JOURNAL OF PREVENTIVE MEDICINE], No 3, 25 May 86 59

SHANGHAI YIKE DAXUE XUEBAO [ACTA ACADEMIAE MEDICINAE SHANGHAI], No 4, Jul 86 60

NUCLEAR POWER ENGINEERING

HE DONGLI GONGCHENG [NUCLEAR POWER ENGINEERING], No 3, Jun 86 ... 61

PHYSICS

WULI [PHYSICS], No 3, Mar 86 64

WULI [PHYSICS], No 4, Apr 86 66

WULI [PHYSICS], No 5, May 86 69

SEMICONDUCTORS

NANJING DAXUE XUEBAO (ZIRAN KEXUE) [JOURNAL OF NANJING UNIVERSITY (NATURAL SCIENCES)], No 1, Mar 85 71

TEMPERATURE CONTROL

NANJING DAXUE XUEBAO (ZIRAN KEXUE) [JOURNAL OF NANJING UNIVERSITY (NATURAL SCIENCES)], No 2, Jun 85 72

/7310

NATIONAL DEVELOPMENTS

SYSTEMATIZED MICROCOMPUTER NOMENCLATURE INTRODUCED

Beijing WUXIANDIAN [RADIO] in Chinese No 4, 11 Apr 86 p 8

[Article by Qian Dongjun [6929 2639 6511]: "Nomenclature for Chinese-Made Microcomputers"]

[Text] In the wake of the development of China's computer industry, product series and types of Chinese-made computers have been increasing rapidly. To enable readers to understand these computer series and models, here is a brief introduction on how the Computer Industrial Administration Bureau names these computers.

The nomenclature pattern consists of three parts, i.e., code name or trade name of the enterprise; a 4-digit number; and a suffix as shown in the figure.

Enterprise code or Trademark	0	x	x	x	Suffix
(1)	(2)	(3)	(4)	(5)	(6)

(1) Enterprise code name or trade name:

There is no uniformity in manufacturers' code names or trade names. For example, "Changchen" [Great Wall], "Zijin" ["Purple Gold", "TQ"; "DJS", etc.

(2) Computer series number:

It is expressed from 0~9, in which "0" indicates the microcomputer series. The other numbers represent minicomputers series or large-, and medium-size computer series.

(3) System classification number:

This numeral here pertains to the type of central processing unit (CPU) and is expressed as follows:

1 -------------- bit machine;
2 -------------- 4-bit machine;
3 -------------- 6502 CPU;
4 -------------- Z80/Z8000 CPU;
5 -------------- 8080/8086 CPU (including 8085; 8088);
and 6 -------------- 6800/68000 CPU (including 6809).

(4) Microcomputer series type expressed in numerals:

0 -------------- singleboard machine;
1 -------------- 8-bit personal machine;
2 -------------- quasi 16-bit personal machine;
3 -------------- 16-bit personal machine;
4 -------------- 32-bit personal machine;
5 -------------- 8-bit bus structured microcomputer;
6 -------------- quasi 16-bit bus structured microcomputer;
7 -------------- 16-bit bus structured microcomputer;
8 -------------- 32-bit bus structured microcomputer;
and 9 -------------- other types of microcomputer.

(5) Microcomputer bus types expressed in numerals:

0 -------------- not bus organized structure, such as the personal computer, singleboard machine, etc.;
1 -------------- S-100 bus;
2 -------------- multiple bus (MULTIBUS);
and 4 -------------- other bus types.

(6) Suffix:

This part is used selectively and is not yet standardized. It is denoted by a letter or numeral to differentiate the product-number of performance capability.

The aforementioned standardization is suited for the state priority microcomputer series. As for the non-state priority series, console type computers and pocket type computers, are all named by individual enterprise units.

The following example of a Chinese-made computer using this nomenclature method illustrates a quick assessment of the domestic product.

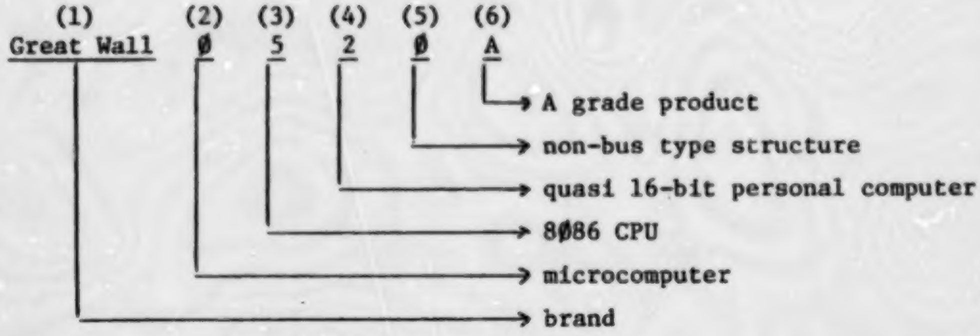

/6091
CSO: 4008/1117

PHYSICAL SCIENCES

SEA-AIR HEAT EXCHANGE OVER NORTH PACIFIC

Beijing HAIYANG YU HUZAO [OCEANOLOGIA ET LIMNOLOGIA SINICA] in Chinese Vol 17 No 1, Jan 86 pp 57-65

[Article by Zhao Yongping [6392 3057 1627], Institute of Oceanology, Chinese Academy of Sciences, Qingdao: "A Preliminary Study on the Influence of Sea-air Heat Exchange in the Mid-latitude of the North Pacific on the Atmospheric Circulation There," Contribution No 1264 from the Institute of Oceanology, Chinese Academy of Sciences, paper received on: 25 November 1983]

[Text] English Abstract: Characteristics of the sea-air heat exchange in the mid-latitude of the North Pacific showed that there was a good relationship between the sea-air heat exchange on the Kuroshio and the long wave over the North Pacific and that the strength of the cold air made a great contribution to the sea-air heat exchange, which might be a more effective factor for prediction than the air or sea temperature alone. Based upon the analysis, a simple irreversible model was proposed: the stronger (weaker) the cold air, the bigger (smaller) the sea-air heat exchange, the more improvement in the longitudinal (latitudinal) circulation, the stronger (weaker) the cold air, ... This process generally began in the late autumn and continued till the adjustment of the circulation in the summer half year.

In recent years there have been great advances in research on sea-air interaction, with specially clear results in research on interaction between low latitude equatorial seas and atmospheric circulation. The expanse of mid-latitude sea surface, especially the warm northward currents at the western border of the ocean, carry the heat radiated by the sun and absorbed by the ocean at low latitudes to mid-high latitude seas, and through the sea-air interface, the seas transfer heat to the atmosphere all year. Research shows that the abnormalities of the sea-air heat exchange in these sea areas has a definite influence on the atmosphere. But how great is the influence of the mid-latitude seas on the atmosphere? By what kind of process does this influence take place? These questions have not yet been researched in detail, and the results of work that has already been done are not uniform[1,4]. This paper is an attempt to explore the facts of the interrelationship between mid-latitude sea-air heat exchange and the atmospheric circulation in the air above it and to discuss the process of the possible influences between them.

I. Characteristics of Sea-Air Heat Exchange in the Mid-Latitudes of the North Pacific

Using average hydrometeorological data for many years Wyrtki[5] calculated the average heat-air exchange distribution for the entire Pacific Ocean and pointed out that the greatest sea to atmosphere heat transfer area was along the axis of the Kuroshio. We have calculated the values of sea-air latent heat and sensible heat exchange at 35°N, 130°E-130°W and graphed them in Figure 1 to explain the latitude distribution of sea-air heat exchange. From the graph it can be seen that the average annual heat transfer to the atmosphere is the greatest in the western part of the Pacific, especially in the area of the Kuroshio, with a total heat transfer (a combination of latent heat and sensible heat) which reached 400 cal/cm^2.d, with the maximum at 140°E rapidly diminishing towards the east, and becoming very small in latitudes east of 180°. The average total transfer is approximately 150 cal/cm^2.d. The average heat transfer of the western seas is approximately three-times that of the eastern part.

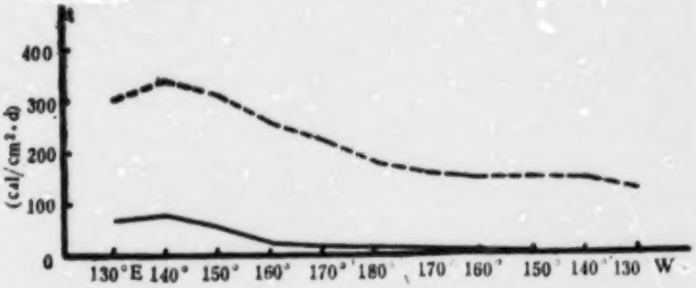

Figure 1 Latitudinal Distribution of Sea-Air Heat Exchange in the Mid-latitudes of the North Pacific (cal/cm^2.d)

--------- Latent Heat; _________ Sensible Heat

The annual changes in the sea-air heat exchange (sensible heat) of the western and eastern parts of the mid-latitudes of the North Pacific are illustrated in Figure 2. In the figure, 33°N, 140°E and the buoy station N (30°N, 140°W) represent the changes in sea-air heat exchange in the western and eastern parts of the ocean, respectively. From the figure it can be seen that there is a trend in annual changes between the two, with the winter the maximum and the summer the minimum, but the extremes of the annual changes in the two are not the same. In the western part of the North Pacific, the sea gives the most heat to the atmosphere in winter, with a value of about 320 cal/cm^2·. In the summer, the sea obtains heat from the atmosphere, with a value of 10 cal/cm^2.d, for an annual range of 330 cal/cm^2.d. The sea in the eastern part of the North Pacific transfers heat to the atmosphere all year, with a maximum summer value of 324 cal/cm^2.d, and a summer minimum of 127 cal/cm^2.d, for an annual range of 200 cal/cm^2.d, the former being 2.5 times the latter.

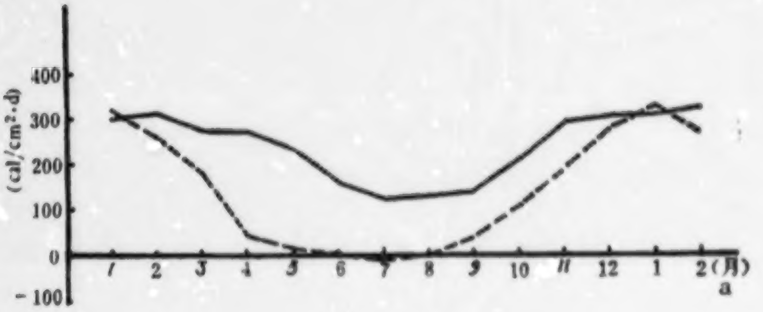

Figure 2 Annual Changes in Sea-Air Heat Exchange in Western and Eastern Parts of the North Pacific (cal/cm².d)

--------- Latent Heat; _________ Sensible Heat

Key: a. Month

Summarizing the above, we can tell that the western sea region (primarily the Kuroshio warm current region) occupies a very important place in the mid-latitude seas sea-air heat exchange in the North Pacific since the volume of sea-air heat exchange in this region and the annual changes are much greater than in the eastern seas. It can be predicted that the abnormality in the sea-air heat exchange in this region can have an important influence on mid-latitude atmospheric circulation.

II. Influence of Sea-Air Heat exchange in the Mid-latitudes of the North Pacific on Air Circulation Above It

After calculating the sea-air heat exchange values for the western part of the North Pacific by month for the 114 months between July 1963 and December 1972, we calculated the average values for the 10 stations at 21°N, 125°E; 25°N, 125°E; 29°N, 130°E; 30°N, 135°E, 33°N, 140°E; 33°N, 145°E; 35°N, 150°E; 37°N, 155°N, 160°E; 37°N, 165°E. These stations are in the vicinity of the axis of the Kuroshio current, and the changes in their average values can represent the characteristics of sea-air heat exchange in the western seas. Because the sensible heat values are rather small, especially in the summer, the latent heat transfer values (Q_E) were adopted to represent the total sea-air heat exchange of this sea region. To eliminate annual changes, we subtracted the multi-year average values of the months from the month by month latent heat values calculated and arrived at anomalous values month by month. To eliminate small perturbations, we also carried out running averages for 5 months on the data.

For the characteristics of atmospheric circulation above the North Pacific we indicated it by using the air latitudinal circulation coefficient of this area, taking 25°N, 50°N, 140°E-140°W, and the 500mb altitude (h) at each 10° longitude calculated according to the following equation

$$I_z = \sum_{i=1}^{9} h_{\varphi_{35}} - \sum_{i=1}^{9} h_{\varphi_{50}}$$

Since Pacific air observation data is sparse, we discovered in some of the calculation results that the time sequences of latitudinal circulation coefficient for some months was very irregular, clearly these are caused by data errors. To eliminate the errors, we first of all plotted the circulation coefficients we had calculated, and on the basis of the continuity of the circulation after carrying out regularized corrections of the data, then carried out anomalous sliding. Thus we obtained filtered annnual changes and anomalies of small perturbations of less than 5 successive months.

The above results are plotted in Figure 3. From the figure it can be seen that the two exhibit a clear negative correlation; the correlation coefficient is -0.45. The number of sequential samples in this data was N=114, and the confidence of this correlation is far beyond 0.001. That is, in the mid-latitudes of the western part of the North Pacific, when a greater than normal amount of heat is transferred from the sea to the atmosphere, the latitudinal circulation index above the Pacific Ocean becomes weaker. This means that the longitudinal direction of the atmospheric long waves increases, and a ridge develops; conversely, when a less than normal amount of heat is transferred from the sea to the atmosphere, the latitudinal circulation index above the Pacific Ocean becomes stronger, and at this time the west wind intensifies and the atmospheric long waves are shallow.

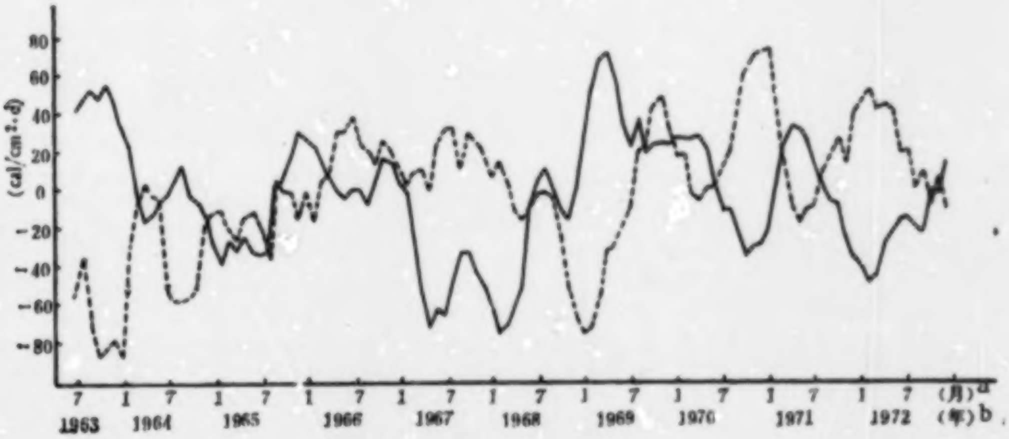

Figure 3 Development Curve of the Sea-Air Heat Exchange Anomalous Value (cal/cm^2.d) and Anomalous Value of the Latitudinal Circulation Indicator (Geopotential Shi Meters) of Mid-Latitudes of the Western Part of the North Pacific

--------- Sea-Air Heat Exchange; ________ Latitude Circulation Indicator

Key: a. Month b. Year

To understand the interaction process of the sea and the atmosphere, we also calculated the time lag correlation of the two (Figure 4). Zero on the horizontal axis is the synchronous correlation of the two, greater than zero is the correlation of latent heat on atmospheric circulation in a later period, smaller than zero is the correlation of earlier period circulation on latent heat. The vertical axis is the absolute value of the correlation coefficient, the broken line parallel to the horizontal axis is the critical degree of confidence value 0.001 ($r=0.32$). From the figure it can be seen that the synchronous correlation of the two is best ($r=-.045$). The correlation of the atmospheric flow of the preceding 1-2 months with regard to the latest heat for that month and that month's latent heat with regard to the atmospheric flow of following 1-2 months exceeded a degree of confidence of 0.001. This result indicates how much the atmospheric circulation of the preceding 1-2 months and the current month influences the sea-air heat transfer of that month and how much of the sea-air exchange of that month influences the atmospheric circulation of that month and the following 1-2 months, the two are in a negative correlation.

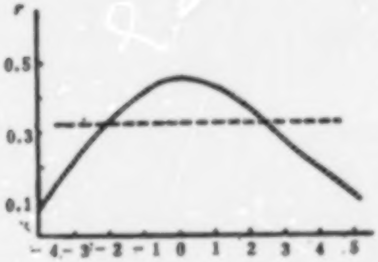

Figure 4 Time Lag Correlation of Sea-Air Heat Exchange and Latitudinal Circulation Indicator (Dashed Line in the Figure is the 0.001 Degree of Confidence Line)

To explain further the circulation characteristics of the abnormal heat time, we selected two typical months, in which the latitudinal circulation indicator of November 1963 was a large zhengjunian [2973 6415 1628] and the sea-air heat transfer was a large funjunian [6298 6415 1628]; but November 1970 was the reverse, the latitudinal circulation indicator was a large funjunian and the sea-air transfer was a large zhengjunian. For the warming above the seas in these 2 months see Figure 5. From the figure it can be seen that in November 1963 along the Kuroshio there is a belt of high values, with the maximum above 600 cal/cm^2. In November, 1970, along the Kuroshio there is also a belt of high values, but the maximum is above 1,000 cal/cm^2, far greater than the value for November, 1963. Figure 6 is a 500mb vorticity field of the same period. For November, 1963, the vorticity field exhibits a latitudinal distribution. Above 45°N is a positive vorticity area and south of 45°N is a negative vorticity area. This indicates that in this month, the circulation regular, and the west wind is strong. In November 1970, the primary characteristic of the vorticity field is the longitudinal distribution of the vorticity. Negative vorticity in the central Pacific clearly extends towards the north, and the two sides are positive vorticity, this indicates that at this time, the longitudinal direction of the atmospheric circulation is great, and the high ridge in the central Pacific rises towards the north.

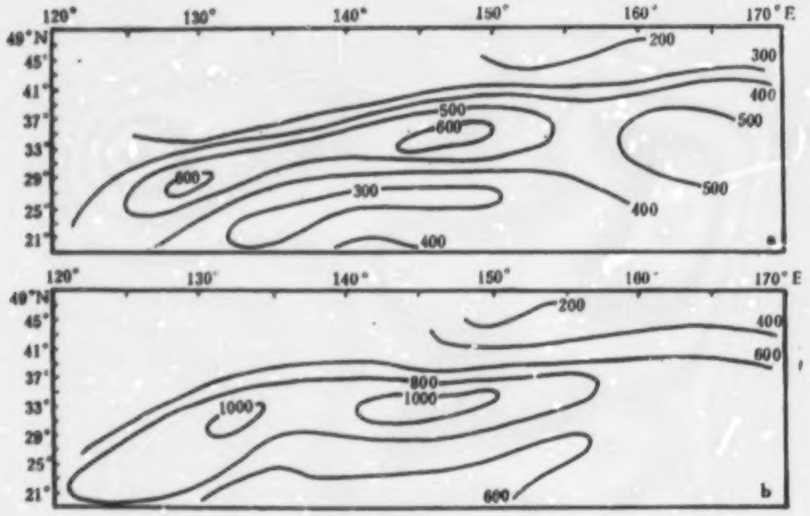
120°
130°
140°
150°
160°
170° E
49°N
45°
41°
37°
33°
29°
25°
21°
200
300
400
500
600
800
300
400
500
400
a
120°
130°
140°
150°
160°
170° E
49°N
45°
41°
37°
33°
29°
25°
21°
200
400
600
800
1000
1000
600
b

Figure 5 Warming Field Above the Western Part of the North Pacific in November, 1963 (a) and November, 1970 (b) (cal/cm^2.d)

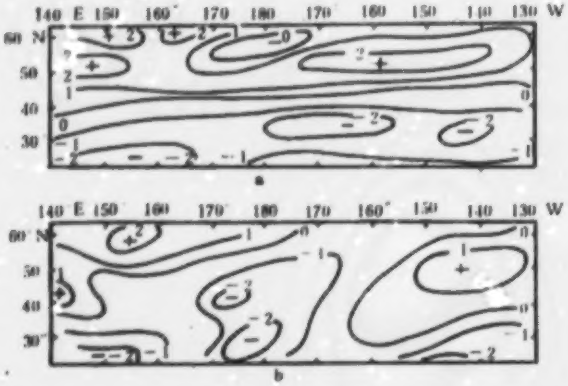
140 E 150 160 170 180 170 160 150 140 130 W
60 N
50
40
30
a
140 E 150 160 170 180 170 160 150 140 130 W
60 N
50
40
30
b

Figure 6 500mb Vorticity above the North Pacific in November, 1963 (a) and November, 1970 (b)

The above facts show that the mid-latitudinal seas in the central part of the North Pacific have a clear influence on the atmospheric circulation in the air above it. When the heat received by the sea is greater than in normal years, the latitudinal circulation indicator of the air above the North Pacific diminishes, and the longitudinal nature of the circulation increases. When the sea receives less heat than in a normal year, the latitudinal circulation indicator of the air above the North Pacific increases and circulation is smooth.

III. Discussion

Below is a preliminary discussion of the characteristics and process of sea-air interaction in the mid-latitude seas.

1. Characteristics of Mid-latitude Sea Sea-air Interaction

Sea-air interaction is primarily carried out through sea-air heat exchange. Existing researches show that in equatorial seas, changes in water temperature make a large contribution to sea-air heat exchange in that region. El Nino is a characteristic in which the rise in water temperature is primary. This water temperature abnormality leads to changes in woke [3087 0344 Walker?] circulation. Kraus[4] pointed out that the contribution of water temperature to sea-air heat exchange increases as the latitude decreases. The author[1] has also pointed out that the sea-air heat exchange in the eastern sea in the winter is primarily determined by the strength or weakness of the cold air, and the contribution of water temperature is secondary. This article further calculated the relationship of the month to month heat exchange and water temperature, air temperature and wind speed for stations at 33°N,135°E, 33°N,150°E, and 33°N,165°E, and using the average correlation of these three stations as representative further discussed the characteristics of mid-latitude seas sea-air heat exchange.

Table 1 Average Correlation of Sea-Air Sensible Heat and Meteorological Factors at Stations at 33°N,135°E, 33°N,150°E, and 30°N,165°E (N=14)

item 项 / month 月 / r	1	2	3	4	5	6	7	8	9	10	11	12
Q_c-T_a	−0.70	−0.82	−0.75	−0.33	−0.62	−0.64	−0.23	−0.40	−0.75	−0.50	−0.72	−0.90
Q_c-T_w	0.29	0.07	0.10	−0.32	0.06	−0.28	0.24	0.45	0.20	0.22	0.18	−0.02
Q_c-v	0.37	0.32	0.55	0.16	0.39	−0.13	−0.20	−0.05	0.34	0.33	0.55	0.39

Taking 0.01 as the standard of confidence, it can be seen from Table 1 that the correlation of sea-air heat exchange and air temperature is closest during November to March, and in the other months it deviates, although for individual months the correlation is good, the time is not continuous; there is no correlation between the months' sensible heat exchange and the water temperature and wind speed. There is also a type of relationship between latent heat transfer and meteorological factors. This result indicates that in mid-latitude seas, in the winter months (mainly November through march) the strength of northern cold air makes a decisive contribution to sea-air heat exchange. Actually, the sea-air heat exchange in mid-latitude seas is an important cause of changes in surface layer water temperature. Jacobs[3] made sea surface sea-air heat exchange an important upper boundary conditions of changes in water temperature for forecasting water temperature. In the summer months (April through October) meteorological factors do not make a big contribution to sea-air heat exchange, and it can be accepted that in this time period, sea-air heat exchange is the

result of the combined action of meteorological factors. Clearly, this is not the same as the characteristics of sea-air heat exchange is low latitude seas.

Summing up the above, in changes in sea-air heat exchange in mid-latitude seas, the strength of the cold air has an unusually important contribution, especially in the winter. When discussing the influence of mid-latitude seas on the atmosphere, sea-air heat exchange should be considered as a basic factor.

2. The Influence Of Sea-Air Heat Exchange On Atmospheric Circulation Above the North Pacific

The area of the Kuroshio is in the vicinity of the long wave ridge in the Pacific. According to long wave theory, when there is abnormally high warming in front of the ridge, it is favorable for developing low layer cyclones and high air high pressure ridge in front of the ridge. Conversely, when there is abnormally low warming in front of the ridge, it is not favorable for the development of high air high pressure ridge in front of the ridge. Since the large circulation changes in the west wind zone is a process of destroying and establishing latitudinal circulation, the strength of the latitudinal circulation indicator reflects this change. When a ridge develops in the west wind zone the latitudinal circulation indicator diminishes; when the circulation in the west wind zone is regular, the latitudinal circulation indicator increases. Thus, we can explain from a theoretical perspective, the negative correlation of sea-air heat exchange in the mid-latitude seas of the western part of the Northern Pacific and circulation over the Northern Pacific, i.e., when the sea-air heat exchange is great (little), then the latitudinal circulation indicator is small (large).

This paper further explains this process using the 500 mb altitude field and corresponding sea-surface air pressure field of November 1963 and November 1970. Figure 7 is the 500 mb altitude anomalous field situation and comparing the distribution in November 1963 and November 1970, one can see clearly that when the sea-air heat exchange is less than in a normal year (November, 1963) the western and central part of the North Pacific is positive anomalous with its maximum value at 9 geopotential shi [0087] meters, the eastern part is negative anomalous, with its maximum at -12 geopotential shi meters; when the sea-air heat transfer is greater than in a normal year (November, 1970), the central and eastern parts of the North Pacific is greatly positive anomalous with a maximum value of +19 geopotential shi meters, and the western part is negative anomalous with a maximum value of -18 geopotential shi meters. The distribution of these two anomalous fields indicates that the circulation of the former (west positive and east negative) is smooth and the longitudinal degree of circulation of the latter (west negative and east positive) becomes greater, becoming stronger in the high pressure ridge in the central and eastern parts of the Pacific. Figure 8 is the corresponding sea surface air pressure field. Com ing the two, we note the following differences: in November, 1963, low pressure was continuous from central Pacific to the North American continent, indicating that cyclone exhibited primarily latitudinal activity; in November, 1970, the longitudinal activity of the cyclone increased, and at this time the continental cold high pressure was also stronger than the cold high pressure of November, 1963; in November, 1963 the secondary high ridge line tended south; in November, 1970, the secondary high ridge position was inclined north. Clearly these distributions correspond one-for-one with the 500 mb altitude field situation.

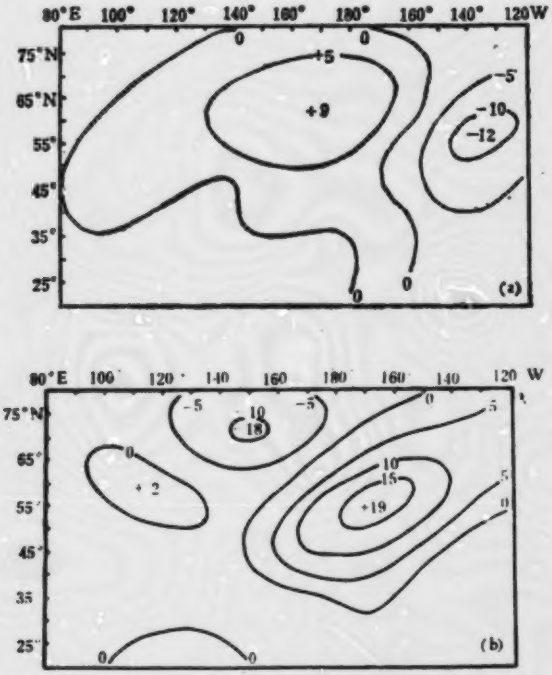
80°E 100° 120° 140° 160° 180° 160° 140° 120W
75°N
65°N
55°
45°
35°
25°
0
+5
+9
-5
-10
-12
(a)
80°E 100 120 140 160 180 160 140 120 W
75°N
65°
55
45
35
25
-5
-10
-18
+2
10
15
+19
5
0
(b)

Figure 7 Anomalous Field at 500mb Altitude in November, 1963 (a) and November, 1970 (b) (Geopotential Shi Meters)

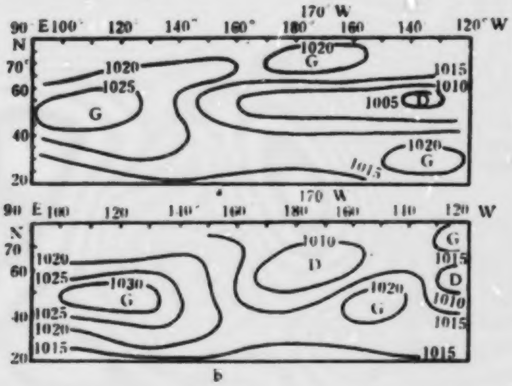
90 E 100 120 140 160 180 160 140 120 W
170 W
N
70
60
40
20
1020
1025
G
1015
1010
1005
D
1020
G
1015
90 E 100 120 140 160 180 160 140 120 W
170 W
N
70
60
40
20
1020
1025
1030
G
1025
1020
1015
1010
D
1020
G
G
1015
D
1010
1015
1015
b

Figure 8 Sea Surface Atmospheric Pressure Field in November, 1963 (a) and November, 1970 (b)

From this we can draw the conclusion that abnormalities in heat fields received by the seas clearly have an impact on atmospheric circulation. When the sea-air heat exchange in the Kuroshio seas is greater (lesser) than in normal years, the non-adiabatic heat obtained by the atmosphere is greater (lesser) than a normal year, it heats up, promoting the development (weakening) of a North Pacific high pressure ridge, and corresponding changes occur in the sea-surface air pressure field also changes due to this.

There has been much research on the question of the time lag of sea-air interaction, but the results are still not uniform. Namias holds that there is a clear seasonal time lag between North Pacific atmosphere and the sea; Kraus holds that if the time lag is too long, it cannot produce resonance between the sea and the air and weakens the interaction. Bjerknes also points out that the time lag between large-scale atmospheric circulation and initial abnormalities of equatorial marine heat transfer are very small and can be calculated daily. The calculation results of this paper show (Figure 4) that correlation between the sea-air heat exchange and latitudinal circulation of a particular month are the closest and that there is a clear influence of the sea-air heat exchange of a particular month on the circulation of the succeeding 1-2 months and of the circulation of the preceding 1-2 months on the sea-air heat exchange of that month. This phenomenon where the correlation of the same period is best may also be another feature of mid-latitude sea-air interaction. As far as the causality of its interaction, one can imagine that a specific west wind circulation field first of all determined the sea-air heat exchange field, and once the atmosphere had obtained an abnormal sea heat transfer, the original circulation circumstances would be strengthened and maintained, and then the two would constantly interact.

From Figure 3 it can be seen that once the heat exchange field or latitudinal circulation field have been established, they can frequently be maintained for a long time. Between 1963 and 1972 a total of 12 exchange processes took place, of which 8 were as long as 6 months and 4 were as long as 10 months, with the longest being 25 months. Adding up the exchange periods, most occurred in the summer (10/12), while only 2 occurred during the early winter (December). Under ordinary circumstances, the longitudinality of the west wind-borne long wave in the North Pacific is favorable to strengthening the southward trend of the cold air; conversely, if the cold air position tends northward, the strength weakens. From this we can tell that in the winter half-year, when cold air is colder (warmer) than in a normal year, it creates an abnormal strength (weakness) in the heat exchange in that part of the sea increasing (decreasing) and maintaining the low (high) indicator of the corresponding latitudinal circulation] the longitudinality of the long wave in the air above the Northern Pacific. This situation also further benefits the increasing (decreasing) southward movement of cold air and thus forms an irreversible process. Once this process is established, it can be maintained for a long time. In the summer half-year, due to exchanges which occur in the circulation field, sea-air heat exchange also changes with them. Once a new circulation field is established, a new round of irreversible processes begins immediately between the sea-air heat exchange in the Northern Pacific and the atmospheric circulation in the air above it. Since this is an irreversible regenerative action, there must be a good correlation between a month's sea-air heat exchange with regard to the circulation field of the following month and the circulation field of the preceding month with regard to the sea-air heat exchange field of that month. Thus explaining fact that the correlation of the preceding and succeeding months in Figure 4 has a high degree of confidence.

Summarizing the Above, we get a simple irreversible model of the interaction of the mid-latitude seas of the North Pacific and the atmospheric circulation above it, i.e., cold air strength (weakness)-->the sea transmits much (little) heat to the atmosphere-->the Pacific Ocean's long wave high pressure ridge intensifies (weakens) and longitudinal (latitudinal) circulation intensifies and is maintained-->cold air intensifies (weakens)-->the sea transmits much (little) heat to the atmosphere-->... Generally speaking, the length of the period of maintenance is determined by the adjustment of the summer half year circulation field.

IV. Brief Conclusion

1. Year-round heat transfer to the atmosphere in the mid-latitudes of the Northern Pacific is clearly greater in the western part than in the eastern part; annual changes in heat exchange is clearer in the western part than in the eastern part; strength of winter cold air determines the extent of sea-air heat exchange.

2. Sea-air heat exchange in the mid-latitudes of the western part of the North Pacific clearly influences the atmospheric circulation above the North Pacific. When a greater amount of heat is transferred to the atmosphere than in a normal year in these seas, the Pacific Ocean high pressure ridge weakens, and latitudinal circulation intensifies. The maintenance of this process is closely related to abnormal sea surface non-adiatic heating.

3. Mid-latitude sea sea-air interaction is an irreversible process which is determined by the strength of the cold air of the winter months. When the cold air strengthens (weakens) the sea-air heat exchange strengths (weakens), and the development of the long-wave ridge above the Pacific Ocean is strengthened (weakened). These results also on the other hand promote the continued strength (weakness) of the cold air. It continues this way uninterruptedly until the summer months (April-October) circulation is adjusted.

The changes in circulation caused by the west wind are created by a variety of factors and the sea-air heat exchange of the low latitude seas also has an important impact on the mid-latitude circulation. Thus, low-latitude seas should be considered as a research topic in itself. In addition, the irreversible process of mid-latitude seas sea-air interaction and under what conditions the exchange occurs and can be maintained are also key questions in long range forecasting. We should carry out further research and exploration on these topics.

REFERENCES

1. Zhao Yongping [6392 3057 1627], Zhang Bicheng [1728 1801 2052], Jing Licai [0064 4539 2088], 1983. DONGHAI HECHAI HAI-QI RELIANG JIAOHUAN DUI CHANG-JIANG ZHONG-XIA YOU XUNGQI JIANGSHUIDE YINGXIANG [INFLUENCE ON EASTERN SEA KUROSHIO SEA-AIR HEAT EXCHANGE ON THE FLOOD STAGE PRECIPITATION ON THE MID- AND LOWER REACHES OF THE CHANGJIANG], Haiyang Yu Chaozhao [Oceanlogica et Limnologica Sinica], 14(3): 256-262.

2. Pan Yihang [3382 0110 5300], 1975. DONG-CHUN HAIYANG JIARECHANG YU LIANGHU PENDI XUNQI JIANGSHUIDE CHUBU FENXI [ANALYSIS OF WINTER-SPRING OCEAN WARMING FIELDS AND PRECIPITATION DURING THE FLOOD PERIOD IN THE TWO LAKE BASINS], Zhongguo Kexueyuan Daqi Wuliso Jikan [Publication of the Atmospheric Physics Institute of the Chinese Academy of Sciences], 6:102-115.

3. Jacobs, J., 1967. NUMERICAL SEMIPREDICTION OF MONTHLY MEAN SEA SURFACE TEMPERATURE, J.G.R. 172 (6): 1681-1689.

4. Kraus, B., 1972. THREE-DIMENSION INTERACTIONS. ATMOSPHERE-OCEAN INTERACTION, PART 7, Oxford University Press, pp 200-254.

5. Wyrtki, K., 1965. THE AVERAGE ANNUAL HEAT BALANCE OF THE PACIFIC OCEAN AND ITS RELATION TO OCEAN CIRCULATION. J.G.R. 170(18):4547-4559.

8226/7358
CSO: 4008/1092

APPLIED SCIENCES

OPTIMUM OUTPUT POWER OF SELF-SUSTAINED DISCHARGE TRANSVERSE FLOW CO_2 LASER

Shanghai ZHONGGUO JIGUANG [CHINESE JOURNAL OF LASERS] in Chinese Vol 13 No 6, 20 Jun 86 pp 328-333

[Article by Chu Zexiang [2806 3419 3276], Chen Liyin [7115 7737 0692], and Wu Zhongxiang [0702 0022 4382] of the Institute of Mechanics, Chinese Academy of Sciences]

[Text] Abstract: The output power of a transverse flow CO_2 laser is studied as a function of the shape of the discharge zone, the position of the cavity, the size and coupling of the mirrors and the velocity of the gas flow. The trends obtained are useful for experimental research and laser design.

I. Introduction

Kopferman[1] used the simple discharge model of Condon and Shortley[2] to calculate the saturation gain and output power of a transverse flow CO_2 laser. He obtained a simple scheme for computing the output power of a quasi-two-dimensional transverse flow electrically excited CO_2 laser. Using this scheme we studied the effects of the shape of the discharge zone, the position of the cavity, the size and coupling of the mirrors and the velocity of the gas flow on the output power.

Figure 1 shows the setup schematically. The metal plate ABCD is the anode, plate EFGK is the cathode (the cathode can have a tubular, plate, or needle geometry), and the electrode separation is AE = H.

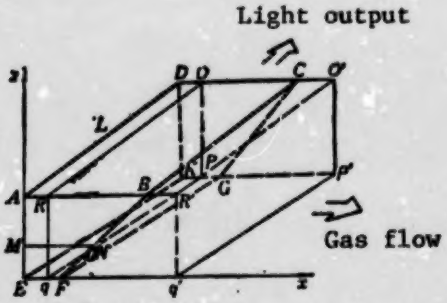

Figure 1. Transverse flow self-sustained discharge CO_2 laser
Anode--ABCD, AB = a; Cathode--EFGK, EF = b

If the electron density n_e in the excitation zone is uniform along the x direction but may vary in the z direction, then,

$$n_e = \frac{J}{L \cdot f(z) \cdot e \cdot v_D} \tag{1}$$

where J is the total current, L is the cavity length, v_D is the drift velocity, e is the electron charge, and

$$f(z) = \left[b + \frac{(a-b)}{H} z\right] \tag{2}$$

in which z is the width of the excitation zone, and a = AB, b = EF are respectively the X direction dimension of the anode and the cathode. The CO_2, N_2 and H_e gas mixture flows in through the AEKD plane. Cavity mirrors OO'P'P and qq'R'R are placed perpendicular to both the gas flow and the electric field. The reflection coefficients are respectively R_1 and R_2.

Following the approach of Ref. 1, we solve simultaneously the conservation equation and the relaxation equation of an ideal one-dimensional gas for a fixed height z to obtain the one-dimensional distribution of the field strength, the saturation gain, and the gas parameter for the layer z. From the calculation results for different z, we obtain the quasi-two-dimensional distribution in the xz plane caused by the electron density differences in the layers. For the relaxation model we still use the three vibration mode system. As can be seen from Eq. (1), for a triangular or trapezoidal excitation region, the electron density n_e in the cavity will change with the height z and so will the light intensity I. In order to evaluate the effects of the shape of the excitation region on the light intensity, we estimate the output power of a layer at height z and take the intensity I to be a constant in the x direction. This is equivalent to slicing the cavity in the z direction. For each layer the stable oscillation condition of the cavity[1] is:

$$\int_0^w G\,dx = \frac{w}{2L} \ln(R_1 R_2) \tag{3}$$

where w is the width of the mirror. This equation describes the gain and loss relationship for a radiation field moving in the gas flow direction in the cavity.

II. Calculation Results and Analysis

Typical conditions used in the calculation are: initial temperature T_o = 293 K, initial velocity u_o = 70 m/s, initial pressure P_o = 20 Torr, $\psi_{CO_2}:\psi_{N_2}:\psi_{He}$ = 5:27:68, and E/N = 2.2×10^{-10} V·cm^2.

1. Effects of the shape of the discharge zone

Figure 2 shows the z dependence of the light intensity for a triangular (AB = 10 cm) and a trapezoidal (AB = 8 cm, EF = 3 cm) discharge zone with the front edge of a 5 cm long 3 cm high mirror at 1 cm from the gas inlet.

As can be seen, the light intensity of triangular discharge zone has a stronger z dependence. This may be explained by the dependence of the electron density on the height z and on the shape of the discharge zone. Equation (2) shows that n_e and f(z) are inversely proportional; the narrower the greater the n_e. However, since f(z) is directly proportional to z, the z dependence of the electron density and the light intensity is stronger. For a trapezoidal discharge zone, $b \neq 0$ and the z dependence of f(z) is relatively flat. If the discharge zone is rectangular (AB = EF), then n_e is a constant in the z direction and the light intensity will not vary with height. But since E/N increases slightly in the x direction (E is the field intensity and N is the total number of particles per unit volume), the power will increase. From the calculated results, this was found to be a 10 percent effect.

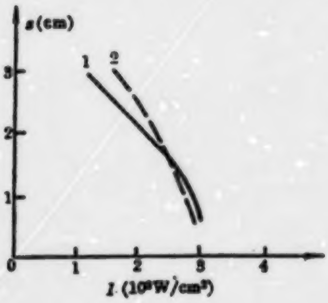

Figure 2. Effects of the shape of the discharge zone on the light intensity
Curve 1--Triangular zone; Curve 2--Trapezoidal zone

For the conditions investigated in this work, a higher n_e leads to a higher light intensity and output power. Therefore, increasing n_e by suitably increasing the input current or decreasing the discharge zone dimension along the flow direction will improve the light intensity in the cavity and the output power.

2. Effects of mirror length and position

In order to test the effects of the mirror length, we computed the light intensity at the center of the mirror and the output power for a 3 cm high mirror with its leading edge at x = 1 cm and a length of 3, 5, 7, 8, 9, 10, 12, 14, and 17 cm. The output power is

$$W = \bar{I} \cdot A \cdot C$$

where $\bar{I}$ is the average light intensity along z, A is the area of the mirror and C is the output coupling coefficient (taken to be 0.28). Figure 3 shows the variation of the output with the mirror length. The output first changes very fast and then becomes flater. The output power is a maximum at a mirror length of 10 cm. The power actually decreases when the mirror length is increased further. The decrease in power is caused by collicion relaxation.

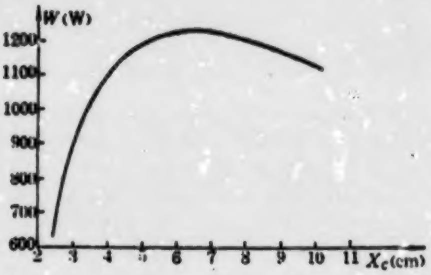

Figure 3. Output power as a function of the mirror length (mirror center position X_c). The leading edge of the mirror is at X = 1 cm.

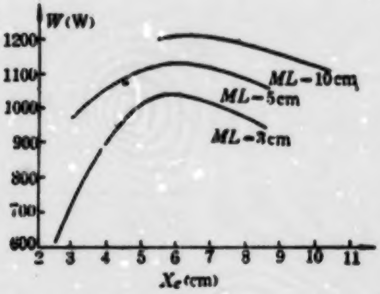

Figure 4. Output power as a function of the center position of the mirror for different mirror length (ML). For f(z) = 5 cm, G_{omax} at 5.5 cm.

Figure 4 shows the relationship between the output power and the center position of the mirror for fixed mirror lengths (10, 5 and 3 cm). It shows that:

(1) Regardless of the mirror length, the output power is a maximum when the center of the mirror is placed at the peak of the small signal gain (see Figure 7).

(2) The output power changes when the center of the mirror is moved along the flow direction. For greater mirror lengths, the mirror covers the entire region of the small signal gain curve (curve 2, Figure 7) and the output variation is not large. For a shorter mirror, it covers a shorter amplification zone and the X_c dependence of output power is greater. When the center of the mirror is moved forward from its optimum position, the power drops quickly. This is because the gain is small at the input of the mirror, the discharge is insufficient and the output gain is compromised. When the mirror is moved backward by a few millimeters, the power decreases slowly. In this case the small signal gain at the input of the mirror is greater, the change becomes more gradual after the peak and the vibrational energy of the discharge can be derived.

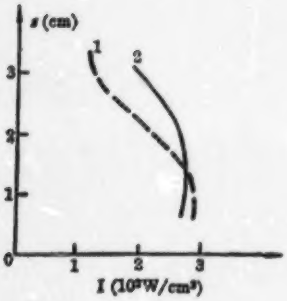

(a) Distribution of light intensity in the z direction for a triangular electric field.
Curve 1—$X_c = 3.5$ cm, $\bar{I} = 215$ W/cm²;
Curve 2- $X_c = 5.5$ cm, $\bar{I} = 251$ W/cm²

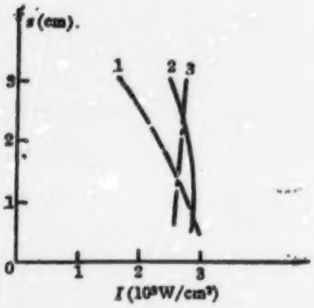

(b) Distribution of light intensity in the z direction for a trapezoidal electric field.
Curve 1—$X_c = 3.5$ cm, $\bar{I} = 225$ W/cm²;
Curve 2—$X_c = 5.5$ cm, $\bar{I} = 267$ W/cm²;
Curve 3—$X_c = 7.5$ cm, $\bar{I} = 268$ W/cm²

Figure 5. Distribution of light intensity in the z direction

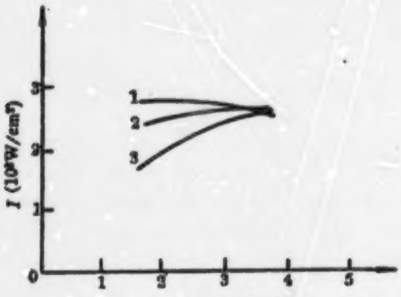

Figure 6. Light intensity as a function of the center position of the mirror for different electrode width
Curve 1--f(z) = 3.8 cm;
Curve 2--f(z) = 5.5 cm;
Curve 3--f(z) = 8 cm

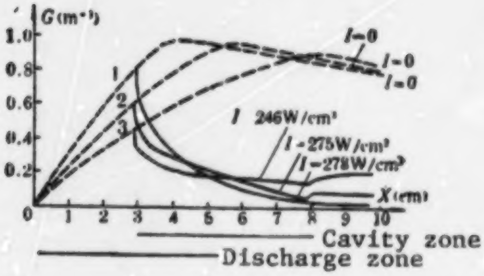

Figure 7. Small signal gain and saturation gain at different height
Curve 1--f(z) = 3.8 cm;
Curve 2--f(z) = 5.5 cm;
Curve 3--f(z) = 8 cm

(3) The output powers of a 5 cm mirror and a 3 cm mirror placed at the optimum position are lower than that of the 10 cm mirror by 9 percent and 14 percent respectively. This shows that the cavity loss using a small mirror is greater but not too great.

We now investigate the effects on the z direction distribution of the intensity and the output power by the position of a given (3x5 cm^2) mirror. For a fixed cavity position, Equation (2) indicates that the discharge zone is narrow for small values of z. For the same total current J, the electron density should be greater and the small signal gain can reach its maximum more quickly (curve 1, Figure 7). If we then place the leading edge of the mirror at the peak of the small signal gain, then the light intensity and the output power will be greater for a smaller value of z. When z is large, the discharge zone becomes longer, the electron density decreases correspondingly and the peak of the small signal gain moves backward (curves 2 and 3 in Figure 7). If the position of the mirror is fixed, the gain is smaller at a greater z in the cavity and less light intensity can be derived. This causes the light intensity I (or output power) to drop as z increases and explains the z dependence of the curves in Figure 5. Such distribution depends strongly on the shape of the electrode and the position of the cavity.

Actual measurements showed, however, that the peak position of the small signal gain was not very sensitive to changes in z. This is because that electron densities at various heights were treated as homogeneous distributions in the discharge model in this work. Moreover, the discharge zone changes substantially with height in this model and hence exaggerating the z dependence. Corrections will be made in future modifications of the model. The calculation did explain the effects of n_e on G_0 and I and the criterion for the optimum cavity position based on the peak position of the small signal gain is essentially consistent with the experiments.

For given initial conditions, the z distribution of the light intensity on the mirror surface and the output power depend on the position of the mirror. Figure 5(b) shows the z dependence of the light intensity with the center of the mirror X_c at 3.5, 5.5, and 7.5 cm. As X_c moves backward, the z distribution of the intensity becomes more uniform because all the usable gains at different heights in the entire cavity are near their peak values. Figure 6 shows the relationship between the light intensity (output power) and mirror position for different electrode widths. Each curve has its own optimum mirror position and the maximum light intensities (output power) of the curves do not vary greatly. The optimum position moves back as f(z) is increased. This can also be explained by the distribution of the small signal gain and the different efficiency in the cavity. These dependences show that the output power not only depends on the electron density and width of the discharge zone but also on the relative position of the mirror and the electrode. For electrodes of the needle-plate or tube-plate structure, the effective usage of the gain is different at different z levels since the width of the discharge depends on z. The initial position of the mirror should be such that gains at various z levels in the cavity are effectively utilized.

3. Relationship between flow speed and mirror position

Because the gain curve is affected by the flow speed,[1] so is the optimum mirror position. For a flow speed of u = 70 m/s, the light intensity is more uniform and the output power is higher when the mirror center is at X_c = 7.5 cm. However, the optimum position is between X_c = 3.5 and 5.5 cm for u = 30 m/s (see Figure 8 and Table 1). The results depend sensitively on the gain distribution. For the operating conditions considered here, X_c = 4 cm for u = 30 m/s and X_c = 7.5 cm for u = 70 m/s.

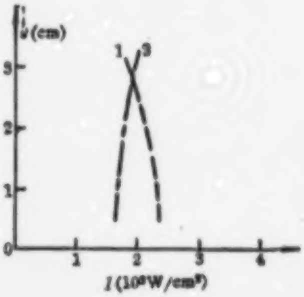

Figure 8. Relationship between mirror position and light intensity for a flow speed of 30 m/s
Curve 1--X_c = 3.5 cm, $\overline{I}$ = 198 W/cm^2 (trapezoidal field)
Curve 2--X_c = 7.5 cm, $\overline{I}$ = 169 W/cm^2

Table 1. Relationship Between Light Intensity, Output Power, and Mirror Position. (X_c is the mirror center position and the mirror length is 5 cm)

u	30 m/s			70 m/s		
X_c(cm)	3.5	5.5	7.5	3.5	5.5	7.5
$\overline{I}$(W/cm^2)	198	197.7	169	225	267	268
W(W)	832	830	710	945	1121	1126

4. Effects of output coupling coefficient

For given discharge zone profile, mirror position and operating conditions, the output power depends on the output coupling coefficient. The coupling corresponding to the maximum power is called the optimum coupling. The optimum coupling depends on the mirror position.

Figure 9 shows the output power as a function of the coupling coefficient for a trapezoidal discharge zone (anode width = 8 cm, cathode width = 3 cm) and a mirror 5 cm long and 3 cm tall. The average light intensity is based on the intensity at the half height of the cavity. Curves 1 and 2 correspond respectively to X_c = 5.5 cm and 3.5 cm. As can be seen, the cutoff coupling is greater for curve 1 and both curves have an optimum coupling between 15 and 21 percent. It can also be seen that the output power drops rapidly when the coupling is less than the optimum but drops slower when the coupling is greater than the optimum. The discharge model[2] used in this work is still rather crude and the computed optimum coupling does not agree accurately with the measured value. The optimum coupling is best determined experimentally in the vicinity slightly greater than the computed optimum coupling. Experimental results on JL6A showed that the intensity is greatest and changed the least when the coupling was 20-30 percent, in agreement with the above conclusion.

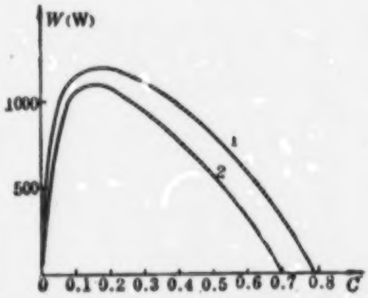

Figure 9. Relationship between output power and coupling in a trapezoidal electric field
Curve 1--X_c = 5.5 cm; Curve 2--X_c = 3.5 cm

Figure 10 shows the results for plate electrodes (triangular discharge zone). The results are similar to that in Figure 9 except that the decrease in power is even more rapid when the coupling is less than the optimum value and the change in output power is even more gradual when the coupling is greater than the optimum value.

Figure 11 shows the relationship between the output power and the coupling for different electrode widths (corresponding to different z). The figure shows that, for different electrode widths, the optimum and cutoff coupling are different. Under the given conditions, the cutoff coupling has a maximum variation of about 10 percent and the optimum coupling has a maximum variation of about 5 percent. Such variation can also be explained in terms of the differences in electron density.

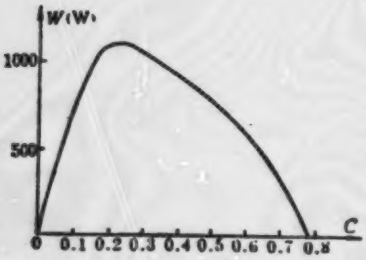

Figure 10. Relationship between output power and coupling in a triangular electric field
$X_c = 5.5$ cm

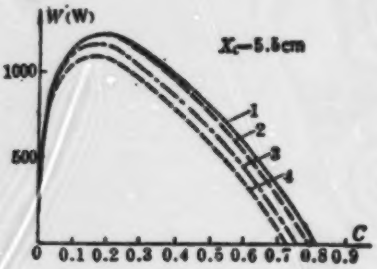

Figure 11. Output power as a function of the coupling for different electrode widths
Curve 1--f(z) = 3.8 cm; Curve 2--f(z) = 5.5 cm;
Curve 3--f(z) = 7.2 cm; Curve 4--f(z) = 8 cm

When the electrode distance changes, E/N changes correspondingly. Figure 12 shows the effect of E/N on the coupling. When E/N is in the 2.8-2.0x10^{-16} V·cm range, the output power and the cutoff coupling increase with E/N, but the optimum coupling does not change very much, only about 6 percent. The effect of E/N on the optimum coupling is therefore not large.

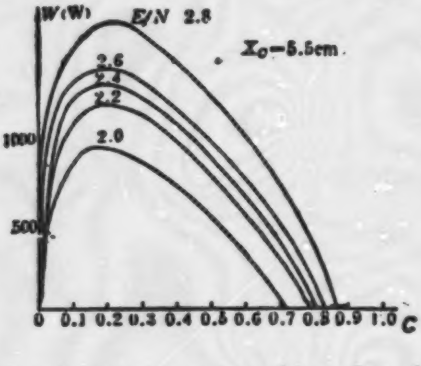

Figure 12. Output power versus coupling for different E/N
$E/N=(2.0\sim2.8)\times10^{-16}$V·cm^2;
$f(z)=5.5$cm

REFERENCES

1. Chen Liyin, et al., GUANGXUE XUEBAO [ACTA OPTICA SINICA] Vol 5, No 2, pp 135-142, 1985.

2. Chen Liyin, et al., ZHONGGUO JIGUANG [CHINESE JOURNAL OF LASERS] Vol 11, No 5, pp 257-262, 1984.

9698/6091
CSO: 4008/79

APPLIED SCIENCES

UV NITROGEN LASER USING HYDROGEN THYRATRON AS SWITCH

Shanghai ZHONGGUO JIGUANG [CHINESE JOURNAL OF LASERS] in Chinese Vol 13 No 6, 20 Jun 86 pp 338-340, 372

[Article by Ou Zhenya [2962 7201 0088] and Yang Liming [2799 4539 2494] of Qinghua University and Song Zhanxia [1345 0594 0204] of the National Standard Bureau]

[Text] Abstract: A UV nitrogen laser, which uses a domestic hydrogen thyratron as a switch and an isotope as a preionizer, is reported. The maximum pulse energy is 5 mJ, the time delay jitter is ±1 ns, and the energy stability for a single laser pulse is 5 percent.

All the nitrogen lasers made in China today have spark triggers. Spark triggers have a simple structure and are easy and inexpensive to produce, but they also have some problems. Problems such as unstable triggering and, sometimes, extra or missed triggers cause large drifts in the pulsed laser energy, especially at low repetition rates. Jitters in the pulse delay make the synchronization very difficult, and the spark trigger is more susceptive to electromagnetic interference. The above difficulties can be overcome when a hydrogen thyratron is used as a trigger.

Reports[1] on triggering nitrogen lasers with a hydrogen thyratron began to appear abroad since 1973. Some quality products began to appear in 1977. We have made an experimental study of the hydrogen thyratron as a trigger, with energy storage and transfer by ceramic capacitors, preionization by an isotope, and shielding by the metallic outer case. An equivalent circuit was proposed for calculating the circuit parameters.

I. Circuit Principle

We used a capacitive transfer circuit, shown in Figure 1. The electrooptic characteristics of the laser cavity can be found in Ref. 2 and are omitted from here. We shall only analyze the energy transfer efficiency in charging C_2 by C_1 and the effects of the peak current and capacitance ratio of the thyratron. In the process, there was no breakdown emission in the laser cavity. Calculation[2] showed a low electrical conductivity. It can therefore be viewed as an open circuit without affecting the results below.

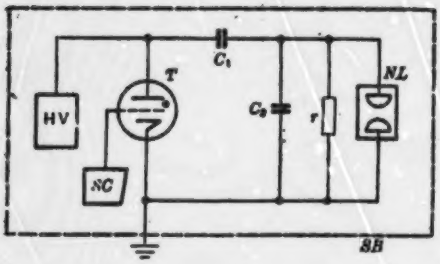

Figure 1. Circuit diagram of the nitrogen laser

HV--DC high voltage source 0.25kV
r--1 kΩ resistance
T--Ceramic hydrogen thyratron
NL--Laser cavity, electrode length = 800 mm, discharge area = 10x25 mm
C_1--Storage capacitor (ceramic), 30 nF
C_2--Transfer capacitor (ceramic), 22 nF
SB--Shielding box

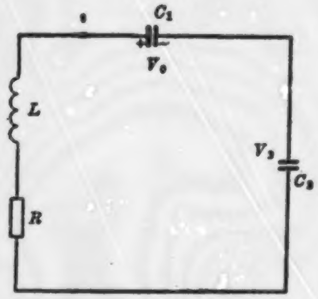

Figure 2. Equivalent circuit for energy transfer between the capacitors

The circuit equation is

$$L\frac{di}{dt}+Ri+\frac{1}{C_2}\int_0^t i\,dt=V_0-\frac{1}{C_1}\int_0^t i\,dt \tag{1}$$

and the solution is

$$i=\frac{C\omega_0^2}{\omega}V_0e^{-\frac{t}{\tau}}\sin\omega t \tag{2}$$

$$V_2=\frac{C\omega_0}{C_2\omega}V_0\left[\frac{\omega}{\omega_0}-e^{-\frac{t}{\tau}}\cos(\omega t-\theta)\right] \tag{3}$$

where

$$C=\frac{C_1C_2}{C_1+C_2},\quad \omega_0^2=\frac{1}{LC},\quad \tau=\frac{2L}{R},$$
$$\theta=\sin^{-1}\frac{1}{\omega_0\tau},\quad \omega^2=\omega_0^2-\frac{1}{\tau^2}.$$

Since the value of R used is very small and $0<t<\frac{\pi}{\omega}$, the following conditions are satisfied:

$$\omega_0\gg\frac{1}{\tau},\quad \omega\approx\omega_0,\quad t/\tau\approx 0 \quad\text{and}\quad \theta\approx 0.$$

The two equations above can therefore be simplified to

$$i=C\,\omega_0V_0\sin\omega_0t \tag{4}$$

$$V_2=\frac{C}{C_2}V_0(1-\cos\omega_0t) \tag{5}$$

(1) Energy transfer efficiency η for C_1 to C_2 charging

The energy of the laser pulse depends mainly on the energy stored in C_2. Based on (5), the energy in C_2 is a maximum when $t=\pi/\omega_0$. The maximum laser intensity will be obtained by adjusting the nitrogen pressure and inducing a discharge at this time.

$$\eta=\frac{1}{2}C_2V_{2\max}^2\Big/\left(\frac{1}{2}C_1V_0^2\right)=\frac{4n}{(1+n)^2}$$

where $n = C_2/C_1$. When $n = 1$, η is 100 percent. At $n = 0.7$, η is 97 percent.

(2) Peak current i_{max} of the thyratron

From (4), the maximum current occurs at $t=\pi/2\omega_0$ and is equal to

$$i_{\max}=\left[\frac{nC_1}{(1+n)L}\right]^{\frac{1}{2}}V_0$$

When n changes from 1 toward zero, i_{max} decreases. A small value of n is good for the thyratron but not for the energy transfer. After weighing the advantages and disadvantages, we chose $n = 0.7$. The value of L is known to be 0.5 μH. We also selected $C_1 = 0.03$ μF, $V_0 = 20$ kV, and obtained $i_{max} = 3$ kA.

Hydrogen thyratrons made in China meet the above requirement and can handle an anode peak current of 20-30 kA and a cathode voltage higher than 20 kV.

It should be noted that, from economic and other considerations, it is permissible to operate above the peak value. However, cautions should be used in exceeding the peak current as it shortens the service life of the thyratron and is also not economical.

II. Experimental Results

All the components are installed in a metal shield to prevent external electromagnetic interferences. In the gas system, an isotope preionizer is installed to improve the stability of the laser pulses. Measurements are made using a RK-3230 (336 probe) thermoelectric energy meter. Using single-shot manual triggering, we measured the laser pulse energy for 50 consecutive pulses and the results are shown in Figure 3, where the solid line is the average energy of 5.56 mJ. Points between the two dashed curves have an energy fluctuation value less than or equal to ±5 percent of the average value. Only three data points had a greater fluctuation. We can therefore claim that the stability (90 percent pulse number) is ±5 percent, it is the best stability[3] achieved for the nitrogen laser here and abroad.

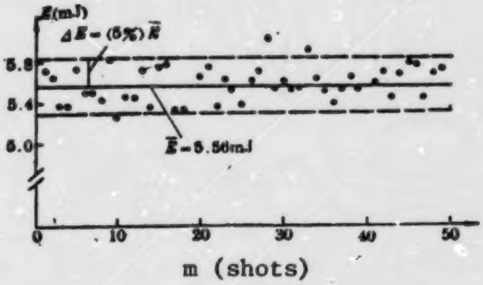

Figure 3. Distribution of the laser pulse energy

Using a photodiode as a receiver, the integrated pulse was displayed on an oscilloscope. The peak value is proportional to the laser pulse energy (see Figure 4). For repetition rates below 10 Hz, the energy is unaffected. At higher repetition rates, the energy decreases. The decrease is 10 percent at 20 Hz.

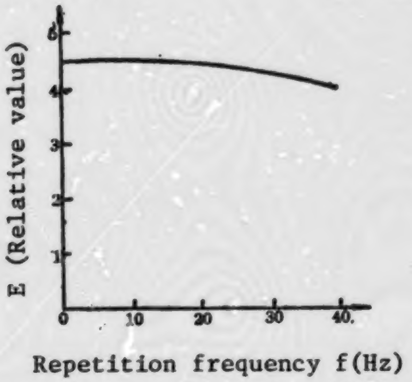

Figure 4. Laser energy E as a function of repetition frequency f

The pulse widths of the nitrogen laser and the pumping dye laser are only a few nanoseconds. When several lasers are used, synchronization is needed so that the delay jitters are no more than 1 or 2 ns.

We measured the delay jitters of a small nitrogen laser with low C_1, C_2, and rated peak current of the hydrogen thyratron.

Using a TF1850 tube as the receiver, the steep edge may reach 1 ns. The response frequency of a SS-5321 S oscilloscope used in the laser waveform observation can reach 250 MHz. Figure 5(a) shows a laser waveform obtained using the internal trigger of the oscilloscope, the waveform line is thin. Figure 5(b) shows the same waveform obtained with the synchronous external trigger and the trace line becomes thick due to the delay jitters of the hydrogen thyratron (including the laser cavity). Taking the half-width of the trace as the delay jitter $\Delta\tau$ of the laser, we have

$$\Delta\tau = \pm 1 \text{ ns}$$

This shows that the Chinese made nitrogen laser triggered by a hydrogen thyratron has a small delay jitter and can be synchronized.

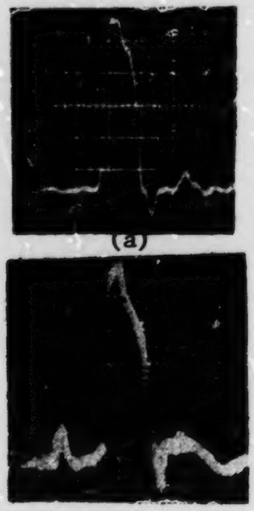

(a)

(b)

Figure 5. Laser waveform

Horizontal axis: time (10 ns/div), Vertical axis: intensity (relative)
(a) Triggered by internal trigger of oscilloscope
(b) Triggered externally

It should be pointed out that a number of factors contribute to the delay jitter. Examples are the steepness and height of the thyratron trigger voltage, filament voltage stability, quality of the thyratron, and internal pressure of the laser cavity. Careful adjustments and selections must be made in the experiments.

When the nitrogen laser discharges, it produces strong electromagnetic interference in the vicinity, affecting the normal function of electronic instruments and leading to large measurement discrepancies. The interference is greatly reduced when all the components are enclosed in a small case. Using a thyratron in place of the spark trigger, the interference is a minimum.

We have described some of the advantages of the hydrogen thyratron, but the price of a thyratron is high and the economic payoff depends directly on the life of the thyratron. We have developed a total of five such lasers and all the thyratrons have functioned normally. One of the units has been in use for 3 years and another unit, with microprocessor controlled data acquisition and processing, has been used in uranium acyl ion laser induced fluorescence spectral measurements with good economic payoff.

Some of the measurements in this work were directed by Zhang Heyi [1728 0678 5030] of Beijing University, Zhang Peilin [1728 1014 2651] assisted portions of the experiments, and Zhao Shuoyan [6392 2592 1280] provided the isotope preionization design. The authors acknowledge their contribution.

REFERENCES

1. Woodward, B.W., et al., Rev. Sci. Instrum., 1973, 44, 882.

2. Fitzimmons, W.A., et al., IEEE J. Quant. Elect., 1976, QE-12, No 10, 624.

3. Molectron UV Series II Nitrogen Lasers, Molectron Corporation, California, 1980, 1-4.

9698/6091
CSO: 4008/79

APPLIED SCIENCES

EXPERIMENTAL STUDY OF STIMULATED RAMAN SCATTERING OF HIGH-PRESSURE H_2 FREQUENCY SHIFTER

Shanghai ZHONGGUO JIGUANG [CHINESE JOURNAL OF LASERS] in Chinese Vol 13, No 6, 20 Jun 86 pp 359-361, 358

[Article by Gao Guochang [7559 0948 2490], Li Rongping [2621 2837 1627], Guo Ningning [6753 1380 1380], Gao Wenbin [7559 2429 2430], Chen Junde [7115 0193 1795], and Lu Shiping [7627 1102 1627] of the Anhui Institute of Optics and Fine Mechanics, Chinese Academy of Sciences]

[Text] Abstract: Experimental setup and results of RS-1 model high efficiency high pressure H_2 Raman shifter are presented. Main factors affecting the energy conversion efficiency are discussed. When the Raman shifter was pumped by Nd:YAG SHG, 1st to 4th order Stokes lines and 1st to 8th anti-Stokes lines have been observed. An overall energy conversion efficiency of 56 percent and an energy conversion efficiency of 34 percent in the 1st Stokes component have been achieved.

I. Introduction

We have designed and developed a RS-series high pressure H_2 stimulated Raman frequency shifters. Using sealed lens window and precision mechaning, the energy utilization rate of the pumping beam and the frequency shift beam was greatly improved to reach or excel the level in foreign frequency shifters such as the Lambda Physik RS-75 Raman cell. Under 8 atm of H_2 pressure and at an input pumping energy of 26 mJ, we have observed the first through the eighth anti-Stokes lines. At 18 atm H_2 pressure and under the same pumping conditions, the first through the fourth Stokes lines were observed. As compared to a recent study in China,[1] the number of Stokes lines and anti-Stokes lines and the energy conversion efficiency have shown considerable increases.

In addition, the new technology of sealed window has allowed the RS-I frequency shifter to operate continuously under 20 atm of H_2 pressure for 18 months without any sign of leaking. The requirement of long-term safe operation is therefore met.

II. Experimental Setup and Results

Figure 1 shows the experimental setup. The pumping laser is a Nd:YAG frequency doubled laser with $LiNbO_3$ crystal Q-switching. The output wavelength is 532 nm and the pulse width is 15 ns. The 1.06 μm total reflection plate eliminates the residual 1.06 μm light after frequency doubling. The RS-I Raman frequency shifter is made of a stainless steel body and the lens window is sealed. The stainless steel body houses the inner H_2 cell, the outer liquid N_2 jacket, the high pressure control valve and the H_2 pressure monitor. A pair of confocal lenses serves the function of pressure seals and focusing. Pinhole caps are installed outside the lens window for alignment and serve as dust covers.

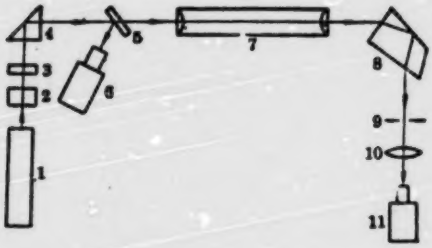

Figure 1. Experimental setup

1--Nd:YAG laser; 2--KDP frequency doubling crystal; 3--1.06 μm total reflection plate; 4--Right-angle total reflection prism; 5--Beam splitter; 6, 11--Laser energy meters; 7--RS-I frequency shifter; 8--Pellin-Broca prism; 9--Variable aperture diaphragm; 10--Focusing lens

The Pellin-Broca prism is used for beam splitting and for deflecting the output beam by 90°. The energy meter is a calibrated NJ-J1 laser energy meter. By rotating the Pellin-Broca prism fixed on a model QJG grating platform, the various order Raman beam and the residual pumping beam consecutively pass through diaphragm 9 and lens 10 accurately enter the energy meter 11. The purity of the hydrogen gas is 99.99 percent and the entire experiment is conducted at an ambient temperature of 18°C.

At a pumping laser energy of 26 mJ and a hydrogen pressure in the frequency shifter ranging from 20-2 atm, the energies of the first order Stokes line (S_1) and the first through the third anti-Stokes lines (AS_1-AS_3) are shown respectively in Figures 2 and 3.

When the H_2 pressure is 13 atm, the output energies of S_1 and AS_1 measured by changing the incident pumping light energy are shown in Figure 4 as functions of the pumping energy.

For a pump energy of 26 mJ and a H_2 pressure of 8 atm, the measured output energies of S_1 and AS_1-AS_7 are compared with the pump energy in Figure 5.

At a pump energy of 26 mJ and a H_2 pressure of 20-2 atm, the order of the anti-Stokes frequency shift is observed on the fluorescent paper screen. The distribution is shown in Table 1.

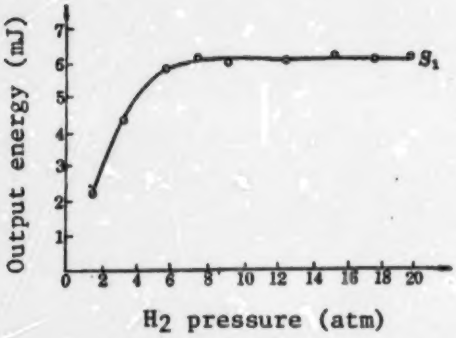

Figure 2. S_1 output energy versus H_2 pressure.
(Pumping laser has an energy of 26 mJ)

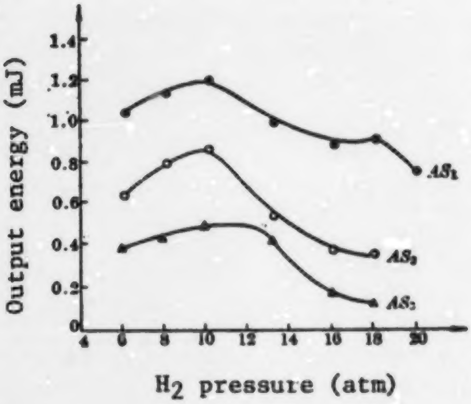

Figure 3. Output energies of AS_1, AS_2, and AS_3 versus H_2 pressure.
(Pumping laser energy = 26 mJ)

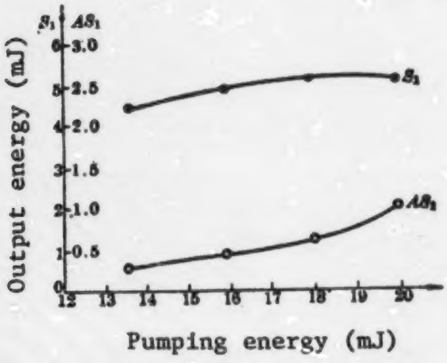

Figure 4. S_1 and AS_1 output energies versus the pumping energy.
(H_2 pressure = 13 atm)

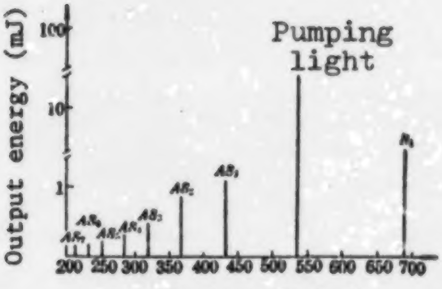

Figure 5. Output energies of S_1 and AS_1-AS_7 as compared to the pump energy. (H_2 pressure = 8 atm, pump energy = 26 mJ)

Table 1. Order of the Anti-Stokes Frequency Shift Observed Under Different H_2 Pressure

H_2 pressure (atm)	20	18~13	8~6	4	2
Orders of the light spots	AS_1 ~AS_3	AS_1 ~AS_5	AS_1 ~AS_8	AS_1 ~AS_7	AS_1 ~AS_6

In the visible and ultraviolet region, the wavelengths of the various order frequency shifted light are measured with a model AAS_1 atomic absorption spectrophotometer and a model AC 15/5 complex projection galvanometer. The accuracy of the AAS_1 is ±0.1 nm. The H_2 pressure is 8 atm and the pump energy is 26 mJ during the measurements. The results are shown in Table 2.

Table 2. Detected Wavelengths at 8 atm H_2 Pressure

Order of the frequency shifted light	S_1	AS_1	AS_2	AS_3	AS_4	AS_5	AS_6	AS_7	AS_8
Center wavelength (nm)	683	435.7	368.9	319.8	282.3	252.7	228.6	208.8	192.1

For higher orders of Stokes lines, their energies were not measured because the spot position could not be accurately determined due to the lack of an upper conversion material. For the S_4 line, we used a model TGS infrared camera and monitor with a Ge window. The camera tube was equipped with a Ge lens, the short wavelength limit was 1.8 μm, and the S_3 (with a wavelength of 1.579 μm) could not pass through. After the camera captured the light spot by rotating the Pellin-Broca prism, the camera was moved back and forth and no noticeable spot size changes were observed, indicating that the spot was coming from a laser. We believe it is a $S_4(\lambda = 4.59\ \mu m)$ spot. Moreover, we measured the infrared transmissivity of the quartz material in the optical path; a small transmission was observed at 4.5 μm. It was therefore possible to have some transmission at a high light intensity, which lent further support to our assessment.

III. Discussion

The energy conversion efficiency is an important technical parameter of a frequency shifter. The energy conversion efficiency is defined as the energy ratio of the frequency shifted light to the imput pump light. Our tests show that the conversion efficiency is affected by the following factors:

1. Quality of the shifter

Commonly used shifters may be divided according to their construction into type A that requires an external focusing lens and type B with a lens window. Under the same conditions a type A suffers about 20 percent more light energy loss than a type B shifter and costs about 30 percent more to operate. The RS-I shifter is a type B shifter and it has good transmissivity and efficiency.

2. Purity of the H_2 gas

The conversion efficiency was low in earlier experiments because of insufficient outgassing. The efficiency has been substantially improved by increasing the purity of the H_2 gas in the gas cell.

3. Pump energy and H_2 pressure

The relationships between the conversion efficiency and the pump energy and the H_2 pressure are very complex. The pump energy and the gas pressure must be determined based on the desired output wavelength.

4. Length of the shifter

Generally speaking a longer shifter has a lower threshold for the same H_2 pressure and pump conditions. A longer shifter in general has a higher efficiency but there is a limit to the length.

5. Sealing of the shifter

How good a shifter is sealed not only affects the safety of the operation but also the conversion efficiency. The RS-I shifter employs a new sealing technique and has been continuously operated for 18 months at 20 atm H_2 pressure without leaking.

6. Temperature

The conversion efficiency is improved by using low temperature cooling gas. It was reported in Ref. 2 that the use of liquid nitrogen coolant improved the AS_7 energy by a factor of 2. Our experiment results on liquid nitrogen cooling will be reported elsewhere.

The authors acknowledge the assistance and support of Liu Songhao [0491 7313 6275], Gu Zhiyu [7357 0037 3768], Zhu Jingyi [2612 2529 3015], Shi Lun [4259 0178], Ji Chunhui [1323 2504 2264], Hua Chungui [5363 2504 6311], Yang Lishu

[2799 4539 2579], Dong Chenggong [5516 2052 0501], Li Guangmao [2621 0342 5399], Zhan Heying [6124 0678 5391], Cao Xiaowen [2580 2400 2429], Hu Xiangkui [5170 6272 7608], Chen Wenzhuo [7115 2429 3820], and Qian Jun [6929 6511].

REFERENCES

1. Guo Yili, et al., WULI XUEBAO [ACTA PHYSICA SINICA] Vol 34, No 1, p 24, 1985.

2. D.J. Brink and D. Proch, Laser and Optoelektronik, No 3, pp 41-48, 1982.

9698/6091
CSO: 4008/79

DISORDER AND LOCALIZATION OF ELECTRONIC STATES IN METALLIC SUPERLATTICES

Nanjing NANJING DAXUE XUEBAO (ZIRAN KEXUE) [JOURNAL OF NANJING UNIVERSITY (NATURAL SCIENCES)] in Chinese Vol 21, No 1, Mar 85 pp 37-39

[English abstract of article by Xiong Shijie [3574 6108 2638]; paper received 14 May 1984]

[Text] The position of the mobility edges in disordered metallic superlattices has been calculated by studying the electronic states for a simplified Hamiltonian model using Anderson's localization theory.

REFERENCES

[1] T.Jarlborg and A.J. Freeman, Phys. Rev. Lett. 45 (1980) 653.

[2] 熊诗杰，蔡建华，物理学报，31 (1982) 474.

[3) P.W.Anderson, Phys.Rev. 109 (1958) 1492.

[4] J.M.Ziman, J.Phys. C2 (1969) 1230.

/6091
CSO: 4009/1116

RESEARCH ON OPTIMUM DESIGN OF MACHINE TOOL STRUCTURES

Nanjing NANJING GONGXUEYUAN XUEBAO [JOURNAL OF NANJING INSTITUTE OF TECHNOLOGY] in Chinese Vol 15, No 4, 20 Oct 85 pp 27-37

[English abstract of article by Tan Li [6223 0500], Ge Qiaoqin [5514 1564 3830], Wen Wenyuan [3306 2429 3293], and Pan Xinlu [3382 2450 7120] of the Department of Mechanical Engineering; paper received 11 November 1984]

[Text] An approach to combine the mathematical programming method with mechanical approximation to optimize the machine tool structures is presented in this paper. In our case, the problem of structure optimization is converted into a nonlinear programming problem with dynamic and static characteristical constrains.

An approximation technic is employed to generate a sequence of mathematical programming for sub-problems with explicit constrains which is easy to solve.

Therefore, the amount of computation work for structure analysis by finite element method is reduced greatly.

The usefulness of this procedure is shown from the optimized results of several structure models and realistic lathe beds.

REFERENCES

[1] 钱令希：《工程结构优化设计》，水利电力出版社，1983年。

[2] Fleury. C. and Schmit. L. A.: ACCESS3. Approximation concepts codes for efficient structural synthesis user's guide, NACA CR-195260, 1980.

[3] 温文源、葛巧琴、虞尔九、潘新陆：机床结构件振动特性的有限元法计算研究，第二届机床设计与研究年会论文集，1980年。

[4] James A. Bennett and Mark F. Nelson: An optimization capability for automative structures, SAE, 1980, 3236—3244。

[5] 谭　力，葛巧琴，温文源，潘新陆：机床结构件优化设计的初步研究，第三届机床设计与研究年会论文集，1984年。

/6091
CSO: 4009/1114

LARGE-CORE DOUBLY CLAD SINGLE-MODE OPTICAL FIBERS

Nanjing NANJING GONGXUEYUAN XUEBAO [JOURNAL OF NANJING INSTITUTE OF TECHNOLOGY] in Chinese Vol 15, No 4, 20 Oct 85 pp 76-81

[English abstract of article by Jiang Shijun [5592 2514 6511] and Lin Zhiyuan [2621 1807 3850] of the Department of Electronic Engineering; paper received 13 October 1984]

[Text] This paper presents the propagation characteristics of double clad single-mode fibers having core with α power index distribution and discusses the effect of the central dip in the refractive index caused in MCVD method. According to the theoretical calculations we have first fabricated some large-core doubly clad single-mode fibers. Their diameters reach 14-17 μm which are about two times that of the conventional single clad single-mode fiber. In addition, their bending loss is very small.

REFERENCES

[1] Unger, H. G.: Planar Optical Waveguides and Fibers, Clarendon, Oxford, 1977, 467.

[2] Gambling, W. A. et al.: Propagation in radially-inhomogeneous single-mode fibre, Opt. Quant. Elect., Vol. 10, 1978, 31.

[3] Cohen L. G. et al.: Tailoring the shapes of dispersion spectra to control bandwidths in single-mode fibers, Opt. Lett., Vol. 7, 1982, 183.

[4] 盛嘉茂：用高斯近似计算单模α光纤的色散参数，《光通信研究》1982年，第4期。

[5] Andreer, A. T. et al.: Experimental study of single-mode W-type optical fiber, Elect. Lett., Vol. 17, 1981, 416.

/6091
CSO: 4009/1114

THE PREPARATION AND CRYSTAL STRUCTURE OF TRINUCLEAR MOLYBDENUM CLUSTER COMPOUND $(Me_4N)[Mo_3(\mu_3\text{-}O)(\mu\text{-}Cl)_3(\mu\text{-}O_2CH)_3Cl_3]$

Beijing HUAXUE XUEBAO [ACTA CHIMICA SINICA] in Chinese Vol 43, No 8, Aug 85 pp 718-723

[English abstract of article by Lin Xianti [2651 6343 2748], Huang Jinling [7806 6855 7117] of Fujian Institute of Research on the Structure of Matter, Chinese Academy of Sciences, Fuzhou, and Huang Jianquan [7806 1696 0356] of the Department of Chemistry, Fuzhou University, Fuzhou; paper received 22 May 1984]

[Text] The title compound was prepared through oxidation of $MoCl_3$ in the liquid phase. The crystal belongs to the orthohombic system with space group D_{2h}^{16}-Pmnb and unit cell parameters: a = 11.403(1), b = 12.345(2), c = 14.292(2)Å, V = 2011.8(8)Å^3; Z = 4, D_c 2.396 g/cm^3. The 2303 independent reflections were collected on a CAD4 four-circle diffractometer with Mo Kα radiation in a range $2<\theta<27$. The crystal structure was solved by heavy-atoms method and refined by a full matrix least-squares technique to final discrepancy factors R = 0.050 and R_w = 0.056 for 1513 reflections of $I>8\sigma(I)$. The configuration of cluster anion was characterized to have the same M1 type structure as presented in a previous paper. The average bond lengths Mo--Mo is 2.577Å, Mo--O-μ_3 is 1.982Å. In addition, relation of Mo--Mo bonds with the bridging atom, bond order, and other lignds coordinated to the Mo atom is discussed briefly.

REFERENCES

[1] 林贤梯, 黄金陵, 黄建全, *科学通报*, 1984, *29*, 1216.
[2] 黄金陵, 商茂虞, 黄建全, *有机化学*, 1983, 326.
[3] (a) Cotton, F. A., *Inorg. Chem.*, 1964, *3*, 1217; (b) Müller, A.; Jostes, R.; Contton F. A., *Angew. Chem., Int. Ed. Engl.*, 1980, *19*, 875.
[4] (a)Scavnicar, S.; Brown, C. J., *Acta Cryst.*, 1966, *21*, 151; (b) Herceg, H.; Scarnicar, S., *Croat. Chem. Acta*, 1967, *39*, 187; (c) Grdonic, D.; korpar-Colig, B., *Proc. Chem. Soc.*, 1963, 308
[5] Bino, A.; Cotton, F. A.; Dori, Z., *J. Am. Chem. Soc.*, 1978, *100*,. 5252.
[6] Bino, A.; Cotton, F. A.; Dori, Z., *J. Am. Chem. Soc.*, 1979, *101*, 3842.
[7] Müllor, A.; Ruck, A.; Darttmann, M.; Rcinsch-Vogell, U., *Angew. Chem. Int. Ed. Engl.*, 1981, *20*, 483.
[8] (a) McCarroll, W. H.; Katz, L.; Ward, R., *J. Am. Chem. Soc.*, 1957, *79*, 5410; (b) Ansell, G. B., Katz, L., *Acta Cryst.*, 1966, *21*, 482.
[9] Bino, A.; Cotton, F. A.; Dori, Z., *Inorg. Chem. Acta*, 1979, *33*, L133.
[10] 吴鼎铭, 庄鸿辉, 郑建基, 黄金陵, 卢嘉锡, 黄建全, *中国科学*, *B* 辑, 待发表.
[11] Wu. D. -M.; Zhuong, H. -H.; Zheng, J-J.; Huang J. -L; Lu, J. -X.; Huang, J. -Q., *J. Struct. Chem.* 1984, *3*, 51.
[12] 商茂虞, 黄金陵, 卢嘉锡, *中国科学*, *B* 辑, 1984, 375.
[13] 吴鼎铭, 庄鸿辉, 郑建基, 黄金陵, 卢嘉锡, 黄建全, *中国科学*, *B* 辑, 待发表.
[14] 吴鼎铭, 黄金陵, 黄建全, 待发表.
[15] 卢绍芳, 商茂虞, 黄金陵, 黄建全, *中国科学*, 待发表.
[16] 庄鸿辉, 黄金陵, 黄建全, 郑建基, 待发表.
[17] 林贤梯, 林玉辉, 黄金陵, 黄建全, *科学通报*, 待发表.
[18] 卢绍芳, 黄金陵, 黄建全, *中国科学*, 待发表.
[19] Müller, A.; Beinsch-Vogell, U., *Angew.Chem., Int. Ed. Engl.*, 1980, *19*, 72.
[20] Vergamini, P. J.; Vahrenkamp, H.; Dalrl, L. F., *J. Am.Chem. Soc.*, 1971, *93*, 6327.

/6091
CSO: 4009/1118

CATALYTIC SYNTHESIS OF LITHIUM HYDRIDE UNDER MILD CONDITIONS

Beijing HUAXUE XUEBAO [ACTA CHIMICA SINICA] in Chinese Vol 43, No 8, Aug 85 pp 752-756

[English abstract of article by Liao Shijian [1675 0013 0256], Kong Wei [1313 1550], Liu Hezhong [0491 0735 5883], Li Jingkui [2621 4737 1145], and Xu Yun [1776 4596] of the Dalian Institute of Chemical Physics, Chinese Academy of Sciences, Dalian; paper received 28 June 1984]

[Text] A method for the catalytic synthesis of lithium hydride under mild conditions is presented. The catalyst is composed of titanium tetrachloride and naphthalene or its methyl derivatives and has a very high activity.

$$Li+\frac{1}{2}H_2 \xrightarrow[25\sim50^\circ C,\ \text{atm. pressure}]{TiCl_4\text{—naphthalene}} LiH$$

Metallic lithium can be quantitatively hydrogenated to lithium hydride at 25-50°C under atmospheric pressure within 2-5 h according to various catalyst compositions. The catalyst stability has been investigated and the relationship between catalyst compositions and reaction controlling step has been established also.

REFERENCES

[1] Sullivan, E. A.; Wade, R. C., "*Kirk-Othmer Encyclopedia of Chemical Technology*", Vol. 12, 3rd Ed, 1980, p. 772.

[2] Bogdanovic, B.; Liao, S. T.; Schwickardi, M.; Sikorsky, P.; Spliethoff, B., *Angew. Chem.*, 1980, *92*, 845; idem, *Angew. Chem.*, *Int. Ed. Engl.*, 1980, *19*, 818.

[3] Bogdanović, B.; Liao, S. T.; Schlichte, K., "*Abstr. of the 3rd. Int. Symp. on Homogeneous Catalysis*", Milano-Italy, 1982, p. 104.

[4] 刘和众, 廖世健, 化学通报, 1984, *4*, 27.

[5] 廖世健, 徐筠, 刘和众, 化学通报, 1983, (*12*), 25.

[6] Martin, H.; Stedefeder, J., *Justus Liebigs Ann. Chem.*, 1958, *618*, 17.

/6091
CSO: 4009/1118

RESEARCH ON COLOR REACTION BETWEEN BISMUTH(III) AND THIAZOLYLAZO-DERIVATIVE

Beijing HUAXUE XUEBAO [ACTA CHIMICA SINICA] in Chinese Vol 43, No 8, Aug 85
pp 771-774

[English abstract of article by Gao Jialong [7559 1367 1727], Bai Hao [4101 4110] of the Institute of Urban Construction and Environmental Protection, Suzhou, Wang Xiaoming [3769 2556 2494], and Chen Tongyue [7115 0681 1471] of the Department of Chemistry, Lanzhou University, Lanzhou; paper received 19 April 1983, finalized 28 December 1984]

[Text] A new chromogenic reagent, 2-(4,5-dimethylthiazolylazo)-5-diethyl aminophenol, DMTAE, has been synthesized by coupling of 2-amino-4, 5-dimethylthiazole with m-dialkylaminophenol. The blue complex formed between Bi(III) and DMTAE at pH 2.8 (potassium biphthalate buffer solution) has been investigated. Molar absorptivity is $1.0 \times 10^5 L \cdot mol^{-1} \cdot cm^{-1}$ at λ_{max} 590 nm. The analytical specificity is $K_{a1} = 7.6 \times 10^{-2}$, $K_{a2} = 1.0 \times 10^{-7}$. The composition of complex as determination by a variety of methods is Bi(III): DMTAE (1:2). The apparent stability constant calculated is 2.9×10^9. A highly sensitive method for spectrophotometric determination of microquantity of bismuth has been developed, which is suitable for the determination of microamounts of bismuth in tool steel, bronze, copper alloy, waste water and tap water.

REFERENCES

[1] Sproull, R. C.; Getter, A. O., *Ind. Eng. Chem. Anal. Ed.*,**1941** *13*, 462; Nielsch, W.; Böltz, G.,*Z.Anal. Chem.*, **1954**, *142*, 321.
[2] Yamane, T.; Suzuki, T.; Mukoyama, T., *Anal. Chim. Acta*, **1972**, *62*, 137.
[3] Танаев, О. А.; Шахабудинов, Щ., *Химия и Хим. Технол.*, **1973** *16* (1), 29.
[4] Шестидесятная, Н. Л.; Миляева, Н. М.; Котелянская, Л. И., *Ж. аналит. химии.*, **1975**, *30*, 522; 徐其亨，许秀君, 化学学报, **1962**, *40*, 419.
[5] Киш, П. П.; Балот, Й. С.; Спиваков, Б. Я.; Золотов, Ю. А., *Ж. аналит. химии.*, **1976**, *31*, 1114.
[6] Антонович, В. П.; Суворова, Е. Н.; Шелихина, Е. И., *Ж. аналит. химии.*, **1982**, *37*, 429.
[7] Саввин, С. Б.; Розовску, Ю. Г.; Прописцова, Р. Ф.; Ливонина, Е. А.; *Татже*, **1970**, *25*, 423.
[8] 刘锡林,顾钢,陈同岳,高家隆,分析化学,**1984**, *12*, 246.
[9] Inczédy, J., "*Analytical Application of Complex Equilibria*", Wiley, New York, 1976.
[10] Smith, A. E., *Analyst*, **1975**, *100*, 300; 郭小伟，杨密云，分析化学，**1980**, *8*, 466
[11] Щербов, Д. П.; Астафьева, И. Н.; Плотникова, Р. Н.; *Ж. аналит. химии.*, **1978**, *33*, 13.

/6091
CSO: 4009/1118

A GC METHOD TO MEASURE SOME ORGANIC POLLUTANTS IN THE SEDIMENTS ON THE BOTTOM OF THE CHEMICAL INDUSTRY WASTE WATER DRAIN

Dalian SEPU [CHINESE JOURNAL OF CHROMATOGRAPHY] in Chinese Vol 4, No 4, Jul 86 pp 252-254

[English abstract of article by Zhao Deren [6392 1795 0088] of Changchun College of Optics and Fine Mechanics, Long Fengshan [7893 7685 1472], and Lang Peizhen [6745 0160 3791] of the Institute of Environmental Science of Northeast Normal University, Changchun; paper received June 1985]

[Text] In this method, FID and ECD are used for measuring 49 organic pollutants in the sediments on the bottom of the chemical industry waste water drain. The retention data, response factors and calibration curves of the 49 compounds are reported. The 49 pollutants are effectively separated on a SP-2250 packed column with a length of 3 m.

An extraction and clean-up procedure for measuring these 49 compounds in sediments by GC is also described. The procedure is simple, convenient and applicable to analysis of complicated sediments which are contaminated by chemical industry waste water.

From the sediment sample 31 organic pollutants are quantitatively measured. And the concentration of these compounds in the sediment are as 10^2-10^4 times as in the waste water in the same drain.

Particularly, in the sediment, many organic compounds possess of toxicity and persistency.

REFERENCES

(1) 樊德方主编．《农药残留量分析与检测》．上海科学技术出版社．1982.
(2) 赵德仁等．第五次全国色谱学术报告会文集．上册246页．1985年10月．成都．
(3) 吉林化学工业公司研究院编．《气相色谱实用手册》．化学工业出版社．37[illegible]页．1980

/6091
CSO: 4009/1122

THE SEARCHING OF X-RAY POWDER DIFFRACTION PATTERN ON MICROCOMPUTER

Nanjing NANJING DAXUE XUEBAO (ZIRAN KEXUE) [JOURNAL OF NANJING UNIVERSITY (NATURAL SCIENCES)] in Chinese Vol 21, No 1, Mar 85 pp 139-145

[English abstract of article by Chen Guanghui [5400 0342 5478], Wu Jianguo [0702 1696 0948], and Qiu Dirong [8002 4574 2837]; paper received 25 June 1984]

[Text] The searching of X-ray powder diffraction pattern on the CROMEMCO microcomputer is presented. The COBOL language is used for coding our program. About 700 JCPDS cards have been stored up for geology. We have searched some samples (including man-made samples and natural samples). We find that there are few misses and a few errors among the phases searched out. The consequences are satisfactory.

REFERENCES

[1] L. K. Frevel, Anal. Chem.37, 471, (1965) L.K.Frevel, C.E.Adams, Anal, Chem. 40, 1335, (1968)

[2] G.G.Johnson. Jr. V. Vand, Ind, Eng. Chem, 59, 19, (1967)

[8] L.K.Frevel, Adv,.in X-ray Anal. 20, 15, (1977); Anal. Chem. 54, 691, (1982)

[4] P.F.Dismore, Adv. in X-ray Anal. 20, 113, (1977)

[5] 马礼敦、许自省、王博义，应用科学学报第一卷第4期353页(,1983)

[6] 林少凡、卢桂章、王祖陶、刘月季、关栋云，南开大学学报第1期51页(1978)

[7] 林天辉、张赛珠、陈丽君、蔡新兴，J. Appl. Cryst. 16. 150, (1983)

/6091
CSO: 4009/1116

A SIMPLE ADAPTIVE BLOCK PICTURE CODING

Beijing TONGXIN XUEBAO [JOURNAL OF CHINA INSTITUTE OF COMMUNICATIONS] in Chinese Vol 6, No 3, Jul 85 pp 67-70

[English abstract of article by Zhang Minli [4545 3046 4539] and Xu Mengxia [1776 1322 0204] of Peking University; paper received 9 February 1984]

[Text] In this paper a simple adaptive block picture coding is discussed, which is based on block coding of (4x4) pels, and is adaptively switched to block coding of (2x2) pels, when contours exist within the block and the root mean square error of the processed block exceeds a given threshold value.

Experiments with test pictures (sampling frequency 10 MHz) by computer simulation show that, if the threshold value TH = 4, then the average bit-rate is less than 3.2 bit/pel, the signal to noise ratio is greater than 36 dB, and the processed pictures show no visible difference in subjective quality when compared with the original.

REFERENCES

[1] A. Habibi, Survey of Adaptive Image Coding Techniques, IEEE Trans. Com., Vol. COM-25, No. 11, 1977, pp. 1275～1284.
[2] 安田靖彦等，利用分层次编码逐步由粗到细地进行图象的传输和显示，信学志，Vol. 63-B, No. 4, 1980, pp. 379～386.
[3] M. Kunt and O. Johnsen, Block Coding of Graphics: A Tutorial Review, PIEEE, Vol. 68, No. 7, 1980, pp. 770～785.
[4] 姚庆栋等编著，图象编码基础，人民邮电出版社，1984年，第9章，静态图象编码。
[5] CCIR Recommendation 500, Method for the Subjective Assesment of the Quality of Television Pictures, CCIR 13 th Plenary Assembly, Vol. 11, pp. 65～68, 1974.

/6091
CSO: 4009/1120

DISCUSSIONS WITH THREE SCHEMES OF ADAPTIVE DPCM INTRAFRAME PICTURE CODING

Beijing TONGXIN XUEBAO [JOURNAL OF CHINA INSTITUTE OF COMMUNICATIONS] in Chinese Vol 6, No 3, Jul 85 pp 55-61

[English abstract of article by Xu Mengxia [1776 1322 0204] of Peking University; paper received 12 April 1984]

[Text] Comparisons and discussions are made between three schemes of adaptive DPCM intraframe picture coding from Jing Donghan et al.[1], Zhang Chuntian[2,3] and the author of this paper[4]. Results of calculations (histograms, entropy values, root mean square values and peak values of prediction errors) and subjective tests (using Pirsch's 15-level quantizer) with four sets of test picture sequences (sampling frequency 10 MHz) show that: The subjective picture quality of these three schemes are similar with "Boy with Toys (Sequence)" and "RMA Test Chart (Sequence)", while the calculation results of Jing's scheme are better. With "Resolution Chart (Sequence)" and "Resolution Chart (Sequence) (mirror)", the subjective picture quality and calculation results of Zhang's scheme are better. As for hardware realization, the author's scheme is relatively simple in algorithm, and then Zhang's scheme, while Jing's scheme is relatively complex.

REFERENCES

[1] 金东瀚，安田靖彦，按邻近象素自适应的非线性预测图象编码，通信学报，第3卷(1982年)，第1期，第1~9页.

[2] Zhang Chuntian, Ein neuer Adaptiver Prediktor für die DPCM-Codierung von Fernseh-Signalen, Frequenz, Bd. 36, A. 6, Juni 1982, S. 161~168.

[3] 张春田，轮廓自适应预测的帧内 DPCM 图象编码，通信学报，第4卷 (1983年)，第1期，第1~7页.

[4] 徐孟侠，开关型自适应帧内 DPCM 图象编码，通信学报，第5卷 (1984年)，第1期，第7~18页.

[5] Cohen, P., Adoul, J. P., Adaptive Differential Coding of Picture Signals based on a Local Contour Prediction, NTC 76, Vol. 1, 6.1~1~5, Dec. 1976.

[6] Zschunke, W., DPCM Picture Coding with Adaptive Prediction, IEEE Tran. Commun., Vol,. COM-25 (1977), No. 11, pp. 1295~1302.

[7] Yamada (山田), K., Kinukaba, K., and Sasaki, H., A DPCM Coder Using Adaptive Prediction for TV Signals, ICC 77, Conference Record, Vol 1, 4 B. 1, pp. 76~80, 1977.

[8] Girod, B., Adaptive Prediction for DPCM Coding of TV Signals, IEEE Trans. ASSP, Vol. ASSP-29 (1981), No. 6, pp. 1142~1147.

[9] Heiss, R., Vorstellung eines neuen Adaptiven Intraframe-Pradtionsverfahrens, Forschungsbericht Nr. 112, Inst. f. Über-tragungstechnik und Electroakustik, Technische Hochschule Darmstadt, April 1983.

[10] 赵新验，图象信号的自适应变系数 DPCM 编码，通信学报，第4卷 (1983年)，第4期，第75~79页.

[11] 徐孟侠，帧内二维 DPCM 图象编码的一次实验，通信学报，第5卷 (1984年)，第4期，第58~61页.

[12] Pirsch, P., A New Prediction Design for DPCM Coding of TV Signals, ICC 80, Conference Record, Vol. 2, 31.2.1~5, June 1980.

[13] Connor, D. J., Pease, R. F. W., Scholes, W. G., Television Coding Using Two Dimensional Spatial Prediction, Bell Syst. Tech. J., Vol. 50 (1971), No. 3, pp. 1049~1061.

[14] CCIR Recommendation 500, CCIR 13 th Plenary Assembly, Vol. 11, pp. 65—68, 1974.

[15] 姚庆栋、顾伟康、徐胜荣、章守苗，电视信号的自适应全数字化综合高频编码，通信学报，第3卷 (1982年)，第2期，第8~16页.

[16] 王兆华，用二维 Walsh 函数分析彩色全电视信号，通信学报，第2卷 (1981年)，第2期，第50~57页.

[17] Wang Zhaohua, Theoretical Analysis and Experimental Investigation of the Two-Dimensional Spectrum of a PAL Composite Video Signal, ntz Archiv, Band 5 (1983), H. 5, S. 143~149.

[18] 王兆华，H. Amiri，二维低通列率重叠数字滤波器的研究，通信学报，第6卷 (1985年)，第2期，第84~88页.

[19] 郑树懋、范树香、毕厚杰，线性 DPCM 的误码响应分析，通信学报，第5卷 (1984年)，第4期，第47~53页.

[20] 肖自美，一种自适应压扩量化的电视信号帧内 DPCM 编码方法，1984年中国通信学会第五次图象通信年会论文集.

A FFT ALGORITHM FOR WIENER IMAGE RESTORATION

Beijing TONGXIN XUEBAO [JOURNAL OF CHINA INSTITUTE OF COMMUNICATIONS] in Chinese Vol 6, No 3, Jul 85 pp 74-79

[English abstract of article by Ding Xiaoqing [0002 2556 7230] of Qinghua University; paper received 27 June 1983, finalized June 1984]

[Text] An algorithm using FFT for fast Wiener Image restoration by replacing the signal Teoplitz correlation matrix with circulant matrix is presented. This algorithm provides a computational reduction nearly from 4 to 1 as compared to that in (1). The restoration error of approximation has been evaluated and this Wiener Image restoration method has been studied experimentally.

REFERENCES

[1] William K. Pratt and Faramarz Davarian. Fast Computational Techniques for Pseudoinverse and Wiener Image Restoration, IEEE Trans. on Computers, Vol. C-26, No. 6, June 1977, pp.571—580.

[2] Andrews, H. C. and Hunt, B. R. (1977), Digital Image Restoration, Prentice-Hall, Englewood Cliffs New Jersey.

[3] Gonzalez, R. C. and Wintz, P. (1977) Digital Image Processing, Addison-Wesley, Reading, Massachusetts.

/6091
CSO: 4009/1120

SINGLE BOARD COMPUTER BASED OPTIMIZATION OF SINGLE OUTPUT COMBINATIONAL LOGIC FUNCTIONS

Nanjing NANJING GONGXUEYUAN XUEBAO [JOURNAL OF NANJING INSTITUTE OF TECHNOLOGY] in Chinese Vol 15, No 4, 20 Oct 85 pp 88-97

[English abstract of article by Yan Zhenxiang [0917 2182 4382] of the Department of Automatic Control Engineering; paper received 8 November 1984]

[Text] This paper discusses implementation of optimization of single output combinational logic functions using single board computers. Features of the developed program are less superfluous items by improving the covering method and less memory capacity requirement by using machine-language and careful programming. The firmware of this program is able to solve many practical problems so that it can be used as a useful tool for logic design or an interesting practice for teaching purpose.

REFERENCES

[1] 刘明业：《数字系统计算机辅助设计》，国防工业出版社，1980年12月，第31～53页。

[2] 沈嗣昌：《计算机辅助逻辑综合》，高等教育出版社，1982年7月，第28～60页。

[3] Carroll, C. C.: A Fast Algorithm for Boolean Function Minimization, Technical Report. No. AU—T—3 AD680305. Dec. 1968.

/6091
CSO: 4009/1114

A PROGRAMMING TOOL TO SUPPORT STEPWISE REFINEMENT

Nanjing NANJING GONGXUEYUAN XUEBAO [JOURNAL OF NANJING INSTITUTE OF TECHNOLOGY]
in Chinese Vol 15, No 4, 20 Oct 85 pp 98-106

[English abstract of article by Dong Yisheng [5516 6654 3932] and Wang Jing [3076 0513] of the Department of Computer Science and Engineering; paper received 24 November 1984]

[Text] An interactive programming tool, SPA, was presented. With the help of the tool, the stepwise refinement method can be applied easily to develop a program and generate a program text. The generated text is clear and readable with the comments which consist of development history and with the indentation format. A note facility contained in the SPA can be used to declare any entity which appears in the development process, so that the resulted program is executable immediately.

This tool, written in C, has been implemented in the MC68000 system on the UNIX. It is applicable to generate any program written in C, PASCAL and other structured programming languages.

REFERENCES

[1] Wirth. N.: Program development by stepwise refinement, Communications of the ACM, 14(4), 1971, 221—227.

[2] INCE, D. C.: A software tool for top-down programming, Software, 13(8),1984, 687—695.

[3] Teitelbaum, T. and Reps, T.: The cornell program synthesiser: A syntax-directed programming environment, Communictions of the ACM, 24(9),1981, 563—573.

[4] Bassett, P. and Giblon, J.: Computer aided programming, proceedings of the Conference on Software Development Tools, Techniques, and Alternatives, 1983, 9—20.

/6091
CSO: 4009/1114

A UNIFIED SOLUTION OF CL FORMULA FOR INTERSECTION POINTS AND ITS APPLICATION TO MICROCOMPUTERS

Nanjing NANJING GONGXUEYUAN XUEBAO [JOURNAL OF NANJING INSTITUTE OF TECHNOLOGY] in Chinese Vol 15, No 4, 20 Oct 85 pp 107-120

[English abstract of article by Shen Kangle [3088 1660 2867] and Zhou Guangsheng [0719 1639 3932]; paper received 7 January 1985]

[Text] CL formula is established on the basis of circle beam transformation theory. It is applied to the calculation of intersection point co-ordinates for two dimensional pattern. The problem which was previously solved with a special technology can be transformed into a general solution only by a couple of normal vectors. It employs a unified CL hexagonal mode in order to favour memorization and computation. It can automatically operate in microcomputers as a mathematic model of dialogue NC auto-programming system. The sub-program can fully be used in its software system, thus decreasing storage capacity.

It is characterized by analyzing input parameters and determining the location of normal vector. This method fully conforms to CL hexagonal mode and can greatly enhance the speed of calculation, for its operation is simple and easy.

REFERENCES

[1] 沈康乐：*CL*公式的理论基础，《南京工学院学报》，1983年第 4 期。
[2] 沈康乐、周广生：*CL*二元公式在 CROMEMCO微型机上的使用，《广东机械》，1983年第 2 期。
[3] 沈康乐、周广生：*CL*三元公式在微型机上使用，《机械开发》，1984年第 2 期。
[4] 沈康乐、周广生：*CL*非圆公式在微型机上的使用，《机械开发》，1984年第 3 期。

/6091
CSO: 4009/1114

Electronics

BOUNDARY ELEMENT METHOD (BEM) IN ELECTROMAGNETIC POTENTIAL FIELD

Beijing TONGXIN XUEBAO [JOURNAL OF CHINA INSTITUTE OF COMMUNICATIONS] in Chinese Vol 6, No 3, Jul 85 pp 1-10

[English abstract of article by Wu Wanchun [0702 8001 2504] and Liang Changhong [2733 2490 3163] of Northwestern Telecommunication Engineering Institute; paper received 20 February 1984]

[Text] Boundary Element Method (BEM) is a new numerical analysis method presented recently by C.A. Brebbia et al. and it has been applied in elasticity and other mechanical problems. The BEM is generally regarded as a special case of weighted residual method (WRM), thus both accurate and stable numerical results are expected. The BEM has the principle advantages, namely smaller computation contents and more flexible for application over subdomain method, such as finite element method, etc.

The BEM in electromagnetic potential field is considered. Various solutions of Dirichlet, Neumann and Mixed boundary value problems are discussed. It is seen that [H] in the BEM equation is a singular matrix. Hence the solution of Neumann problem has an undetermined constant, it is known to be reference potential.

Analytic formulations of matrix elements for constant elements and linear elements are derived. More computation time is saved than a 4-point Gauss quadrature rule by Brebbia.

Some examples showing the application of the BEM to two-wire transmission line and a set of general computer programs are given.

REFERENCES

[1] M. A. Jaswon, Integral Equation Methods in Potential Theory I, Proc, Royal soc, (a), p. 275, 1963.
[2] J. L. Hess and A. M. O. Smith, Calculation of Potential-Flow about Arbitrary Bodies, In Progress in Aeronautical Sciences, Vol. 8, Pergmon Press, 1967.
[3] T. A. Cruse, Mathematical Foundations of the Boundary-Integral Equation Method in Solid Mechanics, Pratt and whitney Aircraft Group, Special Scientific Report, 1977.
[4] C. A. Brebbia, The Boundary Element Method For Engineers, Pentech Press, 1978.
[5] C. A. Brebbia, Boundary Element Techniques in Engineering, Newnes Butterworths Press, 1980.
[6] R. F. Harrington et. al, Computation of Laplacian Potentials by an Eguivalent Source Method Proc IEE, Vol. 116, No. 10, Oct. 1969. pp. 1715～1720.
[7] 杨乃恒，矩量法求解任意截面TEM传输线的特性阻抗，1983年南京微波会议论文。
[8] 哈林登，正弦电磁场，上海科技出版社，1961。
[9] M. A. R. Gunston, Microwave Transmission-Line Impedance Data, VNR, London, 1972.
[10] 林为干，曾令儒，椭圆外导体—矩形内导体同轴线的特性阻抗，物理学报，第30卷，第1期，1981.
[11] 吴万春等，解任意截面形状传输线的边界元法，西北电讯工程学院院刊，第三期，1984。

/6091
CSO: 4009/1120

FAULT DETECTION AND DIAGNOSIS OF T-S-T DIGITAL SWITCHING NETWORKS

Beijing TONGXIN XUEBAO [JOURNAL OF CHINA INSTITUTE OF COMMUNICATIONS] in Chinese Vol 6, No 3, Jul 85 pp 19-28

[English abstract of article by Chen Junliang [7115 0193 0081] of the Beijing Institute of Posts and Telecommunications; paper received 2 March 1984]

[Text] Algorithms for fault detection and diagnosis of T-S-T digital switching networks are devised. The main idea is to partition the whole network into basic modules and perform fault detection or diagnosis for a single basic module while the remaining part of the network is still able to perform switching functions normally. This paper assumes that there is only one faulty T switch or S module in a basic module, but multiple faults of different types are allowed to occur simultaneously within the faulty switch or module. The location of the faulty T switch or S module can be precisely determined by using the algorithm presented in the paper. The cost of fault detection in a basic module is $(3\ (2+\lceil(\log_2 N)/b-1\rceil),\ 12\ N + 4\ r)$, and the cost of fault location is $(5\ (2+\lceil(\log_2 N)/b-1\rceil),\ 14\ N + 4\ r)$. The first term in the formula represents the number of frames of test signals while the second term represents the number of words in the control memories necessarily to be rewritten during fault detection or location. N is the number of time slots, r is the number of T switches in the first stage of the T-S-T network and b is the number of binary digits in a time slot.

REFERENCES

[1] J. C. Bellamy, Digital Telephony, John Wiley & Sons, 1982.
[2] 顾重威，FETEX-150 程控数字电话交话机，电信快报，No, 4, 1982, pp 25～31.
[3] T. Yasui, T. Egawa, T. Sato, System Architecture of Digital Local Switching System, Review of the Electrical Communication Laboratories, Vol. 31, No. 1, Jan. 1983, pp. 16～23.
[4] 陈俊亮，数字交换网络中T及S接线器的模型与分析，«通信学报»第6卷第3期，第11～18页。
[5] 鲁刚，时分接线器的一种测试算法，北京邮电学院 1983 年学术讨论会论文，1983.

/6091
CSO: 4009/1120

ANALYSIS OF ANALOGOUS SIGNALS AND SYSTEMS BY USING GENERALIZED FUNCTIONS

Beijing TONGXIN XUEBAO [JOURNAL OF CHINA INSTITUTE OF COMMUNICATIONS] in Chinese Vol 6, No 3, Jul 85 pp 85-91

[English abstract of article by Luo Yongguang [5012 3057 0342] of the Changsha Institute of Technology; paper received 23 August 1982]

[Text] In this paper a method for analysis of analogous signals and systems by using generalized functions is proposed. Signals are expressed by using a generalized basis. Convolutional operation is converted to formal algebraic operation. Electrical elements and systems are described by using convolution equations and generalized equivalent circuits. Both zero-state solution and zero-input solution are derived directly. This proposed method is more systematized and profound than the popular time domain method and has wider applicability than the transformation method.

REFERENCES

[1] J. Mikusiński, Operational Calculus, Pergamon Press., 1959. (算符演算，王建午译，上海科学技术出版社，1964).

[2] A. Erdélyi, Operational Calculus and Generalized Functions Holt, Rinehart & Winston, New York, 1962.

[3] N. Balabanian, T. A. Bickart, Electrical Network Theory, John Wiley & Sons, Inc. 1969.

/6091
CSO: 4009/1120

RESEARCH ON FOUNDRY COKE AND IMPROVEMENT OF CUPOLA MELTING QUALITY

Shenyang ZHUZAO [FOUNDRY] in Chinese No 6, Nov 85 pp 8-15

[English abstract of article by the Cast Iron Melting Research Section, Shenyang Research Institute of Foundry]

[Text] The authors have studied the regularity of bed coke combustion and melting process in cupola by using foundry coke developed recently in China, gas coke, and furnace coke respectively. In this paper, the characteristics of bed coke combustion and cupola melting effectiveness resulting from cokes of different qualities are compared. Influences of some coke properties, such as ash content, fixed-carbon content, sulfur content, strength, porosity, and reactivity etc. on the bed coke combustion and melting result are especially investigated in detail. The causes of obtaining high quality, high temperature molten iron by using foundry coke are analysed. It is indicated that Zhenjiang foundry coke is rather good and applicable to cupola melting process. The results show that Zhenjiang foundry coke improves the bed combustion process in the cupola, i.e., both the temperature and CO_2 distribution curves move towards the right and the high temperature region moves downward, the temperature and CO_2 content go down gently after reaching the maximum value, and CO_2 content at the charging opening is high whereas CO content is low. Thus, high quality, high temperature molten iron can be obtained with significantly economical benefit.

REFERENCES

[1]沈阳铸造研究所《开发铸造用焦论证方案》1983年2月
[2]鞍山热能研究所、无锡柴油机厂"铸造焦研制及应用的初步试验"《铸造》1983年第2期
[3]铸造焦试验小组（天津拖拉机厂）《铸造焦试验总结》1983年2月.
[4]沈阳铸造研究所 刘幼华"冲天炉测试方法"《铸工》1978年第1期。
[5]南京工学院周重光《倒置大排距双层送风冲天炉》
[6]西安交大陆文华主编《铸铁及其熔化》1981年
[7]东北工学院等校编《铸铁及其熔化》
[8]马利雅巴赫（苏）《冲天炉工作的强化》1958年
[9]《炼焦化学》1982年第1期.
[10]《铸研报告》（日）1962年 №16.
[11]J.E.Rehdor "冲天炉燃料述评"《Faundry M.T.》1981.2。
[12]J.P.Graham等"焦炭块度和性能对冲天炉操作的影响"《The British Foundryman》1982年5月

/6091
CSO: 4009/1121

DEVELOPMENT OF TYPICAL CASTING TECHNOLOGY DESIGN USING COMPUTER

Shenyang ZHUZAO [FOUNDRY] in Chinese No 6, Nov 85 pp 16-18

[English abstract of article by Zhao Jian [4392 0256], Zhang Yi [1728 3015], and Zhang Jiaqiu [1728 0163 4428] of Shenyang Research Institute of Foundry]

[Text] Technology design plays an important part in foundry production. For many years, a lot of foundry researchers have been eager to find a method to make it accurately and quickly. Based on the experiences of practical production, the authors have developed a software of designing casting technology by using computer. This paper describes in detail the general principle and the operating method of this software.

/6091
CSO: 4009/1121

ANALYSIS OF LASER SCANNING SYSTEM

Shanghai YINGYONG JIGUANG [APPLIED LASER] in Chinese Vol 6, No 3, Jun 86
pp 97-100

[Article by Qiu Jinhui [6726 6930 6540], Institute of Lasers, Fujian Normal University]

[Abstract] This paper analyzes the parameter relations of a scanning system, the distortion property of the scanning lens, and the performance of mechanical deflectors using gaussian light-beam theory in order to solve problems in system design. A laser-scanning system placed in front of an objective lens is used in research involving planar scanning of a large visual field. The basic components of the system are a mechanical deflector and a scanning lens; its main requirements are high resolving power (the number of light spots distinguished) and a uniform scanning rate. The system's general index is the product of velocity and capacity, the resolving power. Three figures show the laser-scanning system, distortion property of the scanning lens, and a rotating multifacet lens deflector. A total of 23 mathematical equations are derived in describing the distortion property and two types of mechanical deflectors. The paper was received for publication on 3 February 1986.

10424/6091
CSO: 4009/102

THREE-PHASE CURRENT STABILIZING, CHARGING PULSED POWER SUPPLY FOR SOLID STATE LASERS

Shanghai YINGYONG JIGUANG [APPLIED LASER] in Chinese Vol 6, No 3, Jun 86 pp 107-110

[Article by Yang Weirong [2799 5898 2837], Yin Hua [3009 7520], and Zhang Zhaodi [1728 2156 1229], Shanghai Institute of Laser Technology]

[Abstract] The paper describes a new pulsed power supply, using a three-phase current-stabilizing charging device for solid state lasers with an efficiency of 50-80 percent and a charging accuracy of higher than 99 percent. The power supply system can withstand an output short-circuit current of about 1 A. Its output voltage can be varied from zero to the maximum required value and a storage condenser can be easily changed at the operator's discretion. Its size is about 0.4 m^3, with a maximum power output of 3 kW. Composed of three-phase type E reactors, the power supply system applies the LC transformer technique to convert a constant-voltage power source to a constant-current power supply. Six figures show the system's operating principle, circuits of the three-phase LC transformer, the transformer's input-output property test arrangement, its AC and DC output performance curves, and its current input performance curve. The paper was received for publication on 21 January 1986.

10424/6091
CSO: 4009/102

EXPERIMENTAL RESEARCH ON STIMULATED RAMAN EFFECT--SOURCE OF ULTRAVIOLET LIGHT FOR VITAMIN D SYNTHESIS

Shanghai YINGYONG JIGUANG [APPLIED LASER] in Chinese Vol 6, No 3, Jun 86
pp 111-113, 110

[Article by Zhao Zhensheng [6392 7201 5116], Anhui Institute of Optics and Fine Mechanics, Chinese Academy of Sciences, and D. Proch, Max-Planck-Institut fur Quantenoptik, Gauching, West Germany]

[Abstract] To obtain a UV-optical source for vitamin D synthesis, the authors studied stimulated Raman scattering (SRS) of different media with Raman wavelength varying between 280 and 300 nm and calculated the related parameters by using a discharge-pumped TEA KrF excimer laser (248 nm). As shown in a figure, the KrF laser has a discharge volume of 60 x 5 x 3 cm^3 and a concentrated capacitance of about 50 nF. When discharged to 30 kV, the thyratron-controlled (pre-ionization) TEA device begins to discharge. The resonant cavity is composed of aluminum-coated completely reflected and quartz planar lenses; the laser's output pulse energy is 250 mJ. Three other figures show the experimental arrangement, energy relationship between pumped laser and the Stokes displacement, and the increase in SRS intensity with an increase in CH_4 gas pressure. Two tables show the selected Raman media pumped wavelengths for vitamin D synthesis and Raman scattering cross-sections of some molecules. The paper was received for publication on 20 December 1985.

10424/6091
CSO: 4009/102

MYCOFLORA IN NATURALLY FERMENTED CHINESE SAUCES IN BEIJING AND THEIR ASSAY OF AFLATOXIN B_1

Beijing ZHONGHUA YUFANG YIXUE ZAZHI [CHINESE JOURNAL OF PREVENTIVE MEDICINE] in Chinese Vol 20, No 3, 25 May 86 pp 143-146

[English abstract of article by Zhang Guozhu [1728 0948 2691], Kong Huazhong [1313 5478 1813], Qi Zutong [7871 4371 0681], Ding Xiuying [0002 4423 5391], and Jia Xiuwen [6328 4423 2429] of Beijing Institute for Cancer Research; paper received 30 October 1984, finalized 26 February 1986]

[Text] The distribution of mycoflora in naturally fermented sweet flour paste, and salted fermented soya paste, in Beijing region were surveyed. A total of 12 genera, 30 species of fungi were isolated from the sweet flour paste. The predominant fungi were Chlamydomucor sp., Aspergillus flavus and Penicillium chrysogenum. In salted soya paste 18 genera, 37 species of fungi were isolated, in which Aspergillus flavus predominated.

Aflatoxin B_1-producing ability of the strains of Aspergillus flavus were assayed. In fermented sweet flour paste among the 128 strains of Aspergillus flavus, only one was found to be positive. Among the 19 strains of Aspergillus flavus isolated from salted soya paste one positive strain was encountered also. But no aflatoxin B_1 was detected in mature pastes.

REFERENCES

1. 冀鹤鸣．西北酱曲中曲菌之研究．黄海发酵与菌学特辑 1948，10:40.
2. 刘守初．北京酱曲中曲霉的检究．黄海发酵与菌学特辑 1950，11:150.
3. Hara S, et al. Aflatoxin-producing strains of *Aspergillus flavus* detected by fluorescence of agar medium under ultraviolet light. Microbiol Appl 1974，27:1118.
4. 张国柱，等．发酵菌种黄曲霉毒素B_1的测定和AS 3.870菌株的鉴定．微生物学通报 1981，8:216.
5. 孟昭赫，等．真菌毒素研究进展．北京：人民卫生出版社，1979:156—173.
6. 一島英治．麹菌類に関する研究からみた日本の醸酵学(II) マイコトキシンの生化学．醸酵協会誌 1970，28:482.
7. 真鍋勝ろ．醸酵食品中の螢光成分関する研究(第2報) みそおよびみそ麹のアフラトキシン汚染の有無について．日本食品工業学会誌 1972；19:76.
8. 居乃琥．黄曲霉毒素．北京：轻工业部出版社，1980:219—294.

/6091
CSO: 4009/1107

SYNTHESIS OF THE HIGHLY POTENT ANALGESIC, BUPRENORPHINE

Shanghai SHANGHAI YIKE DAXUE XUEBAO [ACTA ACADEMIAE MEDICINAE SHANGHAI] in Chinese Vol 13, No 4, Jul 86 pp 301-303

[English abstract of article by Wan Weiqin [8001 4856 0530], Qiu Zhuibai [0092 4856 4102], Zhou Youjun [0719 2589 7486], and Huang Qiang [7806 1730] of the Department of Medicinal Chemistry, School of Pharmacy, Shanghai Medical University, Shanghai]

[Text] The highly potent analgesic, "buprenorphine," has been successfully synthesized with a new improved method which eliminates N-methyl and O-methyl simultaneously, replacing Bentley's two-step reaction. In addition to simplification of procedures, this new method also raised the total yield from 5.06 percent to 20 percent, making industrial production of buprenorphine possible.

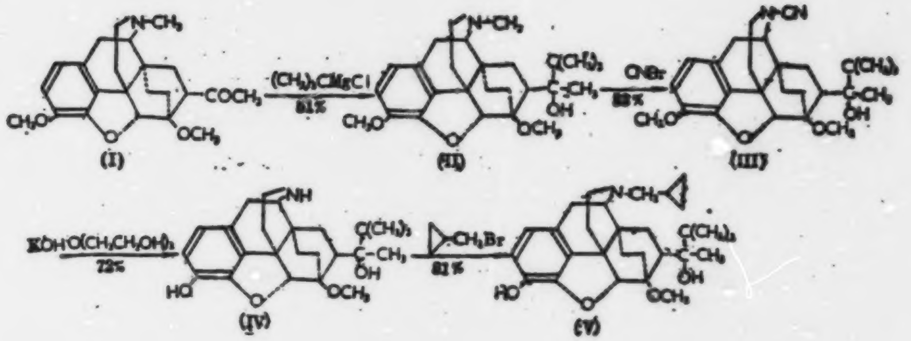

REFERENCES

[1] Mogens K, et al: A Compartive study of intramuscular Buprenorphine and Morphine in the treatment of chronicpain of malignant origin. *Br J Clin Pharmacol* 1982 13:487
[2] Bentley KW: Thebaine and oripavine derivatives. *Br Patent* 1968:1136214
[3] 张明立等: 强效镇痛药 Buprenorphine 的合成。医药工业 1983(2):6
[4] 万维勤等: 阿片受体拮抗剂特培诺啡的研制。上海第一医学院学报 1985 12(1):25
[5] 刘思勤等: 吗啡拮抗剂——纳洛酮的合成。医药工业 1980(3):1
[6] Bentley KW, et al: Novel analgesics and molecular rearrangements in the morphine-thebaine group III. Alcohols of the 6,14-endo-ethenotetrahydrooripavine series and derived analogs of N-allylnormorphine and norcodeine. *J Am Chem Soc* 1967 89:3281
[7] Michael PK, et al: Analgesic narcotic antagonists I. 8β-alkyl, 8β-acyl, and 8β-(tertiary alcohol) dihydrocodeinones and dihydromorphinones. *J Med Chem* 1980 23(2):173

/6091
CSO: 4009/1113

DESIGN CRITERIA OF PWR FUEL ASSEMBLY

Chengdu HE DONGLI GONGCHENG [NUCLEAR POWER ENGINEERING] in Chinese Vol 7, No 3, Jun 86 pp 27-32

[Article by Tian Sheng [3944 4141] and Cheng Rongzhen [4453 5554 3791]]

[Abstract] The article presents the design criteria of fuel assemblies for a pressured water reactor (PWR) in a nuclear power plant; the criteria (design standards) are briefly explained. The functioning, use conditions, and properties of the fuel assembly should be considered in specifying the design criteria, which are only adaptable to the fixed-type PWR fuel assembly using a zirconium-tin alloy to make shell-enclosed tubes and uranium dioxide for the fuel cores. The criteria only stress which design requirements should be satisfied, not how to satisfy these requirements. The criteria serve only for design problems related to nuclear, heat-power, and hydraulic aspects. In addition, an appendix lists the design working conditions of PWR power plants with four levels of possible accidents described. Three tables list the limits of allowable-stress values and austenite (and zirconium-tin alloy) components.

10424/6091
CSO: 4009/104

RELIABILITY ANALYSIS OF A NEW PROTECTION SYSTEM FOR THE SWIMMING POOL REACTOR

Chengdu HE DONGLI GONGCHENG [NUCLEAR POWER ENGINEERING] in Chinese Vol 7, No 3, Jun 86 pp 39-47

[Article by Meng Fanshu [1322 4907 3219]]

[Abstract] The paper presents a new protection system for the swimming pool reactor; the system consists of HTL integrated circuits. The system has redundancy in its design, characterized by a coincidence logic two-out-of-four (2/4). A fault tree analysis is used to evaluate system reliability. The analysis is examined to the extent of "low flow of primary coolant" relying on logic circuits. The author constructed two fault trees: "failure to scram" and "spurious scram." System reliability is higher than the allowable safety indexes. Ten figures show the protection system, LD logic circuits for protective passages for scram events, an electromagnetic driving circuit, fault trees for system (and module M) scram, a simplified scram fault tree, and a simplified sub-fault tree. Two tables list the system's minimum cutoffs and data on fault rates.

10424/6091
CSO: 4009/104

INVESTIGATION AND TESTS FOR CONTINUOUSLY IRRADIATING SHORT-LIVED ISOTOPES IN HFETR

Chengdu HE DONGLI GONGCHENG [NUCLEAR POWER ENGINEERING] in Chinese Vol 7, No 3, Jun 86 pp 61-66

[Article by Shan Runhua [0830 3387 5478], Zhang Dehe [1728 1795 3109], Zhao Xihou [6392 6932 0230], Li Manchang [2621 3341 2490], Lu Changlong [7627 7022 7893], and Li Yinsheng [2621 6892 3932]]

[Abstract] The grid elements of the high flux engineering test reactor (HFETR) are utilized to install ϕ63 pressured tubes filled with ion-free water. MoO_3 irradiating powder (sealed in glass tubes) is placed in pressured tubes to produce short-lived isotopes. This is a new application of HFETR utilization. Using MoO_3 irradiation as an example, the paper describes the continuous irradiation test with the production of ^{99m}Mo-^{99m}Tc isotope. Also described are the installation types, test results, and production capacity. Seven figures show an irradiating assembly, its lateral cross-section, changes in the ^{99m}Mo scale with irradiation time and reactor output power, the correlation between reactor output power and irradiation days by irradiating 3-C/g molybdenum isotopes, and the lateral cross-section of irradiation layouts with different isotope target pieces. Six tables show changes in irradiation time (and reactor output power) with ^{99m}Mo, irradiation days required for different reactor power ratings in producing a 3-C/g molybdenum isotope, irradiation times required at different operating power ratings (of the reactor) for producing a 3-C/g molybdenum isotope, effective cross-section areas of filling with the MoO_3 powder in three layouts, and the total filling capacity of molybdenum in the three layouts.

10424/6091
CSO: 4009/104

STRESS MEASUREMENT OF TiN THIN FILMS

Beijing WULI [PHYSICS] in Chinese Vol 15, No 3, Mar 86 pp 173-174

[Article by Wang Yinghua [3769 5391 5478] and You Yinjuan [1429 1714 1227] of Engineering Physics Department, Qinghua University]

[Abstract] For the case of a TiN ionic coating layer, approximately 0.2-0.3 μm thick, no x-ray diffraction curves can be detected using conventional diffraction instruments. The authors employed the baseline-segment method and the edge inclination method to determine stresses in the above-mentioned coating layer. Two figures show the principle of stress measurement in the edge inclination method and determination results for Cu crumb-samples. Two tables list stress data for the TiN coating layer determined with the edge inclination method and results from using the baseline-segment method. From these data, the authors drew the following preliminary conclusions: (1) For thin films not exhibiting x-ray diffraction curves, the baseline-segment method can be applied to estimate the stress variation law of thin films; and (2) for thin films with a low-incidence angle, stress determination is feasible using the edge inclination method and stress estimation--with the baseline-segment method. Zhang Chun [1728 4783] of Nuclear Energy Institute, Qinghua University, provided samples used in the experiments; Xu Kesheng [6079 0668 0524] and Chang Baoliang [1603 0202 5308], both students at the university, conducted much of the work in setting up the stress-testing methods. The authors are grateful to these individuals.

10424/6091
CSO: 4009/81

IMPROVED K VALUE METHOD IN MULTIPHASE QUANTITATIVE DIFFRACTION X-RAY ANALYSIS

Beijing WULI [PHYSICS] in Chinese Vol 15, No 3, Mar 86 pp 175-176

[Article by Yang Zhuanzheng [2799 0278 6927] and Zhong Fumin [6945 4395 3046] of Shanghai Institute of Metallurgy, Chinese Academy of Sciences]

[Abstract] F.H. Chung proposed the K value method in the x-ray quantitative analysis method in ADVANCED X-RAY ANALYSIS, Plenum Press Vol 17 (1973), p 106, and J. APPL. CRYST. No 7 (1974), p 519. The method has been widely used; this paper presents its principle. The only table in the paper lists the relative errors of the experimental results. A larger deviation appears only in the Si relative errors in one of three test specimens. The error depends on the random orientation and heterogeneity of the original and reference specimens as well as on the precision of the strength determination. Compared with the internal index method and increment method, the K value method is much simpler in experimental procedures, not requiring that standard specimens be added to the unknown specimen. The K value ratio can be derived from a reference specimen of a known weight fraction. Thus, the error sources are fewer.

10424/6091
CSO: 4009/81

RESEARCH FRONTIER IN ATOMIC PHYSICS--DYNAMICS OF EXCITED ATOMS AND MOLECULES

Beijing WULI [PHYSICS] in Chinese Vol 15, No 4, Apr 86 pp 204-210

[Article by Li Jiaming [2621 1367 2494], Institute of Physics, Chinese Academy of Sciences]

[Abstract] Collisions of atomic nuclei lead to submicroscopic energy transfers owing to the production of excited atoms or molecules with prolific species and combinations. These excited atoms or molecules can be regarded as intermediate complexes of the atomic collision processes. Exploring the structure of the excited state of atoms and molecules is a problem in the quantum multibody dynamics of long-range coulombic interaction. Progress in experimental techniques has made it more convenient to observe the excited states; in addition, the effects of magnetic and electric fields on the excited atoms and molecules can be explored. Six figures show a high-resolution laser spectrum of excited atoms, electron energy-loss spectrum of HF molecules, ionized energy spectrum of the vacuum ultraviolet wave band, absorption spectrum of threshold values and its atomic neighborhood, the relationship between orbital energy and interatomic distance, and the near-threshold structure of electrons. The author is grateful to the support of the Chinese Academy of Sciences and China Natural Science Fund for this research.

10424/6091
CSO: 4009/93

PROGRESS IN HIGH-ENERGY PHYSICS

Beijing WULI [PHYSICS] in Chinese Vol 15, No 4, Apr 86 pp 220-225

[Article by Zhu Hongyuan [2612 3163 0337], Institute of High-Energy Physics, Chinese Academy of Sciences]

[Abstract] Since the accelerator energy exceeded 1 GeV in the early 1950's, it has been feasible to study the phenomena of high-energy physics systematically. In atomic studies, quantum mechanics and quantum electromechanics laid the foundation for the quantum field theory, the basis of present-day particle physics, another name for high-energy physics. Both quantum mechanics and quantum field theory have the following fundamental principles: (1) the values of a physical quantity can be discontinuous, and (2) the physical state obeys a statistical law. Physical phenomena still obey the fundamental law of quantum theory, though experimentally the submicroscopic exploration has advanced from 10^{-8} cm to 10^{-16} cm, and energy has been increased from several electron volts to hundreds of billions of electron volts. The wealth of experimental data can lead to theoretical breakthroughs only with profound understanding such as Niels Bohr's insight in pioneering the quantum theory. Two tables show the regularity of particle properties and the total cross-sections of three high-energy collision processes, determined by strong and weak interactions, as well as by electromagnetic interactions.

10424/6091
CSO: 4009/93

CONDENSED-MATTER PHYSICS IN THE EIGHTIES

Beijing WULI [PHYSICS] in Chinese Vol 15, No 4, Apr 86 pp 248-258

[Article by Xie Xide [6200 1585 1795], Fudan University]

[Abstract] In recent years, a diversity of research entities is one of the features of advances in condensed-matter physics: from simple to complex crystal structures. Three other features are: use of modern experimental apparatus (ultra-low temperatures, high pressures, high-power lasers, magnetic resonance, electron beams, and ion beams), penetrating theoretical research, and a close relationship with computational physics. The advent of the computer is pushing theoretical and experimental analyses to a new stage. The physical phenomena and research areas stressed in the eighties are: quantum Hall effect and fractional quantum Hall effect, energy-gap engineering, polyethine and other electrically conductive polymers, organic superconductors, heavy fermions, and five-axis symmetry--quasi-periodicity (or quasi-crystal). Fifteen figures show the quantum Hall effect, the effect obtained by varying the magnetic field, the effect observed in a heterogeneous junction with a very high magnetic field and at a very low temperature, the relationship between electron transfer rate and temperature in a hetero-potential well, bias photoelectrons and cavity ionization doubling of avalanche diodes, the parabola-type effective well potential of the elongation of molecular beams, the relationship between photoconductivity and time of super-crystal lattice, A and B phases in trans- and cis-polyethine, transitions between A and B phases (and vice versa) in polyethine, attraction and rejection between electrons, comparison of resistivity-temperature relationship of organic superconductors and other materials, the basic elements that make up organic conductors and organic superconductors, the structure of $(TMTSF)_2PF_6$, the relationship between resistivity and temperature for heavy fermions, an electron diffraction diagram of Al_6Mn alloy particles, and a brick-laying diagram after Penrose. Two tables list data for heavy fermion parameters and its Wilson ratio.

13424/6091
CSO: 4009/93

NEW NONLINEAR OPTICAL CRYSTAL KTP

Beijing WULI [PHYSICS] in Chinese Vol 15, No 5, May 86 pp 281-284

[Article by Huang Zhao'en [7806 2600 1869], Institute of Artificial Crystals, State Bureau of Construction Materials Industry]

[Abstract] The recently discovered nonlinear optical crystal $KTiOPO_4$, KTP for short, exhibits valuable properties for use with lasers: a high nonlinear coefficient, phase matching at room temperature, insensitivities to changes in temperature and angle, transparency in the range between 0.35 and 4.5 μm, high threshold value (greater than 300 MW/cm^2) to damage, good machinability, stability of chemical properties (such as immiscibility with moisture and tolerance of high temperature), and capability of growing large crystals with satisfactory (optical) homogeneity. Rarely does a crystal exhibit simultaneously as many advantages as KTP does; it has good strategic significance in its applications in bluish green lasers, which in turn may initiate nuclear fusion and is a basic weapon in the SDI (Strategic Defense Initiative) program. KTP's importance in peace and war led to strict controls on its export from the United States. Currently there are two KTP growth methods: water-heating method and fused-salt method. The structure of KTP is explained in the projection of an ATP crystal cell along the [010] direction shown in a figure. Three other figures show the relationship between refractive index and wavelength of KTP, the stereographic projection of phase-match loci caused by a second harmonic wave due to interaction of two KTP types, and the relationship between incident power density and an energy conversion efficiency of double frequency.

10424/6091
CSO: 4009/97

MAGNETIC FLUIDS AND THEIR APPLICATIONS

Beijing WULI [PHYSICS] in Chinese Vol 15, No 5, May 86 pp 295-298

[Article by Guo Huacong [6753 5478 5115], Institute of Nuclear Science and Technology, Sichuan University]

[Abstract] A magnetic fluid is a highly magnetic colloid with a stable distribution of magnetic particles (for example, Fe_3O_4). The colloidal fluid does not aggregate and settle despite the action of gravity and magnetism. A magnetic fluid can be applied in a wide range of fields: sealing, separation by employing differences in specific gravities, jet printing, magnetic separation, lubrication, and magnetic recording as well as in bearings and attenuators. The paper goes on to describe the properties and production of magnetic fluids. Some banks in the United States utilize checks printed with magnetic ink in computer processing. Magnetic fluid can also be used to convert heat energy directly into mechanical energy as well as be used in waste water treatment. Recently in Japan, a patent was granted for a cobalt-iron magnetic fluid with saturated magnetizability intensity as high as 2,460 gauss. Two figures show potential-energy curves of two magnetic particles and the properties of a magnetic fluid. One table lists properties of magnetic fluids.

10424/6091
CSO: 4009/97

Semiconductors

STUDY OF THE LASER ANNEALING OF THE BORON-DIFFUSED SILICON SINGLE CRYSTALS

Nanjing NANJING DAXUE XUEBAO (ZIRAN KEXUE) [JOURNAL OF NANJING UNIVERSITY (NATURAL SCIENCES)] in Chinese Vol 21, No 1, Mar 85 pp 40-45

[English abstract of article by Fan Depei [5400 1779 1014], Zhu Bing [2612 0365], and Chen Nandou [7115 0589 2435]; paper received 11 April 1983]

[Text] Laser annealing of (111) and (001) Si single crystal wafers by an electro-optically Q-switched Nd^{3+}:YAG laser were studied by X-ray divergent beam diffraction method and Van der Pauw method of Hall effect measurement. It is found that lattice constants contract about 2.2×10^{-3} and the concentrations of surface carriers have risen about an order of magnitude after laser annealing.

REFERENCES

[1] C.W.White. et al, Science 204, 461 (1979)
[2] R. T. Young. Appl. Phys.. Lett. 33, 14 (1978)
[8] B. C. Larson. Appl. Phys. Lett. 32, 801 (1978)
[4] 张杏奎等 激光 6, 23 (1979)
[5] H. Yakowitz. "The Divergent Beam X-ray Technique" Advances in Electrons and Electron Physics suppl 6 p361 (1969)
[6] G. L. Pearson. J. Bardeen. Phys. Rev. 75, 865 (1949)
[7] 丘第荣、范得培、激光与红外 3, 9 (1981)

/6091
CSO: 4009/1116

APPLICATION OF A MICROPROCESSOR IN TEMPERATURE CONTROL

Nanjing NANJING DAXUE XUEBAO (ZIRAN KEXUE) [JOURNAL OF NANJING UNIVERSITY (NATURAL SCIENCES)] in Chinese Vol 21, No 2, Jun 85 pp 271-277

[English abstract of article by Ying Zhaomin [2019 2507 2404], Li Zhihua [2621 2535 5478], Ji Hong [1323 4767], and Ji Jiaben [1518 1367 2609]; paper received 2 September 1983]

[Text] Software and hardware of the microprocessor used for temperature control is described. The temperature control system operates in the liquid nitrogen temperature range from 70K to 90K. The stability of temperature control is better than 10mK.

REFERENCES

[1] R.B. Strem, B.K.Das and S. C. Greer Rev, Sci instrum. Vol, 52, No11, Nov. (1981).

[2] J. P. Eisenstein, G. W. Swif and R. E Packard Cryogenics Nov. (1979) 666.

[3] A. Sawade, T. Mamiya, H. Fukuyama and Y. Masuda Cryogenics July (1982) 354.

/6091
CSO: 4009/1115

END

JPRS-CST-86-043

14 OCTOBER 1986

China Report

SCIENCE AND TECHNOLOGY

FBIS FOREIGN BROADCAST INFORMATION SERVICE

NOTE

JPRS publications contain information primarily from foreign newspapers, periodicals and books, but also from news agency transmissions and broadcasts. Materials from foreign-language sources are translated; those from English-language sources are transcribed or reprinted, with the original phrasing and other characteristics retained.

Headlines, editorial reports, and material enclosed in brackets [] are supplied by JPRS. Processing indicators such as [Text] or [Excerpt] in the first line of each item, or following the last line of a brief, indicate how the original information was processed. Where no processing indicator is given, the information was summarized or extracted.

Unfamiliar names rendered phonetically or transliterated are enclosed in parentheses. Words or names preceded by a question mark and enclosed in parentheses were not clear in the original but have been supplied as appropriate in context. Other unattributed parenthetical notes within the body of an item originate with the source. Times within items are as given by source.

The contents of this publication in no way represent the policies, views or attitudes of the U.S. Government.

PROCUREMENT OF PUBLICATIONS

JPRS publications may be ordered from the National Technical Information Service, Springfield, Virginia 22161. In ordering, it is recommended that the JPRS number, title, date and author, if applicable, of publication be cited.

Current JPRS publications are announced in Government Reports Announcements issued semi-monthly by the National Technical Information Service, and are listed in the Monthly Catalog of U.S. Government Publications issued by the Superintendent of Documents, U.S. Government Printing Office, Washington, D.C. 20402.

Correspondence pertaining to matters other than procurement may be addressed to Joint Publications Research Service, 1000 North Glebe Road, Arlington, Virginia 22201.

JPRS-CST-86-043

14 OCTOBER 1986

CHINA REPORT

SCIENCE AND TECHNOLOGY

CONTENTS

NATIONAL DEVELOPMENTS

Scientific Research Fund Reforms 'Going Slowly'
(Xu Yuanchao; CHINA DAILY, 15 Aug 86) 1

Reform of Research Fund Appropriation Urged
(XINHUA Domestic Service, 24 Aug 86) 3

First Science-Technology White Paper Published
(Chen Zujia; RENMIN RIBAO, 10 Sep 86) 4

Problems With Middle-Aged Scientists Revealed
(XINHUA, 13 Sep 86) 6

S&T Information Institutions, Services Expand
(XINHUA, 13 Sep 86) 7

Yan Dongshan on Policymaking Role of CAS
(CHINA DAILY, 15 Sep 86) 8

Reform of Guangxi Research Organizations Discussed
(Guangxi Regional Service, 26 Jun 86) 9

Briefs
Gains in Jiangsu S&T Reform 11

APPLIED SCIENCES

Design of New Wideband Microstrip 3 dB Hybrid Ring
(Wang Shulian; DIANZI XUEBAO, No 1, Jan 86) 12

Environmental Effects on Computer-Controlled Feeding System
(Tong Suqin, et al.; ZIDONGHUA YIBIAO, No 5, 20 May 86) 17

Research on High-Gain Broadband Backfire Antenna
(Song Ximing; DIANZI KEXUE XUEKAN, No 3, May 86) 21

PMR Type Amide-Imide Polymer, Composites (Zhu Wenjiang, et al.; GAOFENZI TONGXUN, No 3, Jun 86) ... 27

Synthesis of Polybutadiene by New Catalyst System Studied (Xu Ling, et al.; GAOFENZI TONGXUN, No 3, Jun 86) 35

LIFE SCIENCES

DDC-Enhanced Killing Effect of HPS-Laser on Tumor Cells (Mo Jian, et al.; ZIRAN ZAZHI, No 5, May 86) 41

Evolution Sites in Ribosomal 5S RNA Structure (Qi Guorong, et al.; ZIRAN ZAZHI, No 5, May 86) 43

Synthesis of Polynucleotides by PNPase Studied (Wang Qisong, Shang Jinbao; ZIRAN ZAZHI, No 5, May 86) ... 46

ABSTRACTS

LASERS

ZHONGGUO JIGUANG [CHINESE JOURNAL OF LASERS] Vol 13 No 8 20 Aug 86 48

SEMICONDUCTORS

BANDAOTI XUEBAO [CHINESE JOURNAL OF SEMICONDUCTORS] Vol 7 No 5, Jul 86 54

NATIONAL DEVELOPMENTS

SCIENTIFIC RESEARCH FUND REFORMS 'GOING SLOWLY'

HK150252 Beijing CHINA DAILY in English 15 Aug 86 p 1

[Report by staff reporter Xu Yuanchao]

[Text] China is to speed up nationwide reforms in the way funds are given to scientific research institutes as the key to restructuring the scientific and technical research system.

The reform is expected to be completed by the end of the year. Starting next year, the growth rate of funds allocated to research institutes throughout the country would exceed the growth of the national income, a conference held this week by the State Science and Technology Commission heard.

A commission official said the Ministry of Finance would allocate 1.4 billion yuan (excluding military appropriations) to research institutes (not including those in social sciences) in this fiscal year. Already, in the first half, about 800 million yuan had been granted.

The budget for research institutes this year had increased 6 percent over last year, compared with a 7.8 percent growth in the nation's revenue, he said.

Following a State Council decree early this year, the Ministry of Finance is to shift its power of fund allocation to the commission so as to make effective use of the limited funds.

But the official said the funds were enough only for small-scale researches. Large research projects would be "contracted by the state to research institutes through competitive bidding."

The research institutes will be divided into three categories.

--Technology development, pure research [word indistinct] welfare, which includes public health, labour protection, family planning, environment protection and disaster control.

Operating expenses for research institutes in technology development will be cut down during the current five-year plan (1986-90) to encourage them to bid for larger projects, the official said.

The projects are designated by the State to meet the current needs of the national economy. The funds saved from operating expenses will be used to make up investment in the country's priority projects, the official said.

The official said the reform was going slowly. About 50 percent of research institutes in local areas had not started the work and some were even taking a wait-and-see attitude.

But in the first half of this year, the reform had been basically accomplished among research institutes subordinate to central ministries and commissions.

/9604
CSO: 4010/2020

REFORM OF RESEARCH FUND APPROPRIATION URGED

OW251112 Beijing XINHUA Domestic Service in Chinese 0704 GMT 24 Aug 86

[Excerpt] Beijing, 24 Aug (XINHUA)--To speed up reforming the system of appropriating funds for scientific operations, the State Scientific and Technological Commission [SSTC] and the Ministry of Finance [MOF] have urged all provinces, regions, municipalities and counties that the transfer of such funds should be carried out simultaneously and completed by the end of this year. They say that beginning 1 January next year, funds for scientific operations should be placed under the management of various scientific and technological commissions, and in accordance with the new format of the MOF's new budgetary plan.

Reforming the system of appropriating funds for scientific operations is an important part of reforming the management of science and technology. So far, this reform has already been carried out in departments under the State Council. The funds for scientific operations of 53 departments have been transferred to the SSTC management, and the categorization of research projects of these departments' research organs has also been basically completed. However, the progress of reform is uneven in various localities. While some have started or are about to start, some others are still waiting. The SSTC and the MOF maintain that the time is ripe for reforming the appropriation system, and that tardiness will affect reforming the management of science and technology as a whole.

In a circular, the SSTC and the MOF have defined the scope of transferring local research funds to the management of local scientific and technological commissions, stating that research and operation funds (including operation funds for various scientific and technological associations) should be defrayed by the operation funds of various departments.

The SSTC and MOF circular points out that reforming the system of appropriating funds for scientific operations is key to reforming scientific and technological management and that all localities must intensify their leadership over the project. They say that scientific and technological commissions and financial departments at all levels should provide meticulous guidance on the basis of conducting investigation and study.

/9604
CSO: 4008/2131

FIRST SCIENCE-TECHNOLOGY WHITE PAPER PUBLISHED

HK111551 Beijing RENMIN RIBAO in Chinese 10 Sep 86 p 1

[Report by Chen Zujia [7115 4371 3946]: "China Publishes First White Paper on Policies Concerning Science and Technology"]

[Text] "A Guide to China's Policies on Science and Technology--The First White Paper on Science and Technology," the first publication on China's principles and policies concerning science and technology and the implementation of these principles and policies, has come off the press and will go on sale across the country.

On 9 September, Wu Mingyu, vice minister of the State Science and Technology Commission, introduced the white paper to foreign scientific and technological officials, representatives of the United Nations offices in Beijing, representatives of foreign companies set up in China, and foreign and Chinese reporters and answered their questions.

A white paper is a government publication used by many countries to make public their major principles and policies of a certain period. With the approval of the State Council, China's white paper on science and technology gives an elaborate account of the main points, basis, and implementation of the principles and policies on science and technology formulated since the Third Plenum of the 11th CPC Central Committee. It carries important speeches made by party and state leaders during this period and the important documents and regulations promulgated by the CPC Central Committee and State Council.

The white paper consists of 6 sections and 26 chapters. Of this, the results of the 1985 national survey of science and technology, including the figures of the scientific and technological activities and personnel of the country's research and exploitation institutes, the preliminary plan for the statistical system of China's science and technology, and the technological policies for 12 fields including energy, communications, and transportation have been made public for the first time.

Wu Mingyu said that the publication of the first white paper by the State Science and Technology Commission with the approval of the State Council is the outcome of the policies of reform and opening up to the outside world.

China attaches great importance to policies, Wu continued, but we have seldom compiled the state policies of a period and made them public. By publishing the white paper, the masses can understand the policies and turn them into action. Moreover, the masses can take part in supervision and the state can obtain feedback. Furthermore, we can help friends of all countries understand China's policies and develop mutual cooperation.

It has been reported that the State Science and Technology Commission will regularly publish white papers in the days to come. The English-language version of the first white paper is expected to be available in the spring of 1987.

/9604
CSO: 4008/2131

PROBLEMS WITH MIDDLE-AGED SCIENTISTS REVEALED

OW130917 Beijing XINHUA in English 0631 GMT 13 Sep 86

[Text] Beijing, 13 Sep (XINHUA)--China has failed to take full advantage of the skills of one-ninth of its four million middle-aged scientists, according to a report in today's overseas edition of the PEOPLE'S DAILY.

The Communist Party paper urged that "effective measures" be taken to better use the scientists' abilities.

It quoted the results of a recent survey by an unnamed source of 30,000 scientists between 36 and 55 years old in 500 work units. China has more than four million scientists of this age group.

The paper blamed the problem on "poor working conditions," such as inadequate books and reference materials, out-of-date instruments and equipment and inadequate support staff.

Lacking assistants, the paper said, more than 12 percent of the senior scientists surveyed said they do work that could be done by less qualified technicians.

Unequal distribution of household responsibilities also impairs the work of some scientists, it said.

"Those who are women routinely have to spend atleast 3 hours a day on household chores--in addition to helping their children with their homework," according to the report. "Combined with the long commuting time many people have, the household situation has prevented many women scientists from having time to study on their own."

The paper called for more in-service training. More than two-thirds of the scientists surveyed said they had had no refresher courses for at least 2 years.

/9604
CSO: 4010/2020

S&T INFORMATION INSTITUTIONS, SERVICES EXPAND

OW131425 Beijing XINHUA in English 1409 GMT 13 Sep 86

[Text] Beijing, 13 Sep (XINHUA)--China now has 3,883 scientific and technical information institutions of various sizes, employing 68,000 people, a senior Chinese official disclosed here today.

Wang Tingjun, director of the Scientific and Technical Information Department of the State Science and Technology Commission, said, as affiliates of government departments, colleges, factories, enterprises and various localities, these information institutions have in the past 3 decades provided valuable services for the country's science and economy.

Information scientists and technicians of the Chang Jiang Transport Department provided 102 research findings in a 10-year period for China's largest water-conservancy project on the Chang Jiang--Gezhouba.

Their service helped save some 100 million yuan of investment and 900 tons of rolled steel, and was very valuable for selecting a correct plan for damming the river and protecting the sturgeon, a freshwater fish.

Scientific and technical information projects, institutions and individuals who have distinguished themselves in this regard will be commended at a national conference on information work slated to be held in mid-October, Wang Tingjun announced.

Beginning in 1956, Wang recalled, the Chinese Government formulated as a national policy the development of scientific and technical information indispensable to the social, economic, scientific and technical development of the nation.

With the implementation of the policy of economic restructuring and opening to the outside world, scientific and technical information institutions extended their services to fields other than science and technology.

More flexible forms and means of service have been introduced, and computerization has been much improved. Moreover, there has been an unprecedented growth of Sino-foreign exchanges in this regard.

Wang Tingjun expressed the hope that scientific and technical information institutions and libraries would coordinate their efforts and make the best use of the country's limited information personnel, financial resources and materials.

/9604
CSO: 4010/2020

YAN DONGSHAN ON POLICYMAKING ROLE OF CAS

HK150242 Beijing CHINA DAILY in English 15 Sep 86 p 3

[Text] The Chinese Academy of Sciences will be more active in organizing China's top scientists to contribute to the democratic and scientific policy-making sought by the Chinese leadership, said Yan Dongsheng, vice-president of the academy, at a meeting of the Technical Science Academic Division that opened yesterday.

He said that as the members of the academy are the most outstanding specialists and experts in China, they should participate in State policy-making as special counsellors.

So, for the first time, over 90 well-known academics from different fields, 40 government officials and 20 technical experts from local enterprises gathered together to compare notes on the current social, economic and scientific developments.

"We've invited officials from major government departments to report and join discussions at the meeting. We believe this will help our scientists know more about the level and needs of national development," Yan said.

According to Shi Changxu, director of the Technical Science Division, the academy will propose four main subjects for its members to deliberate on and provide advice for the government.

The subjects include the allocation and utilization of resources; development of infrastructure; high-tech research, urban and rural construction and environmental protection.

The academy expects the scientists will form special subject groups and raise their research projects during the 4 days of reports and discussions. After the meeting, the groups will set out on study and field inspections.

"We hope the scientists will bring out some valuable reports in a couple of years. Because we are at an experimental stage so far, we'll focus on a few subjects at present. In future, we'll expand the counselling into more fields," Yan said.

/9604
CSO: 4010/2020

REFORM OF GUANGXI RESEARCH ORGANIZATIONS DISCUSSED

HK271359 Nanning Guangxi Regional Service in Mandarin 1000 GMT 26 Jun 86

[Text] The regional CPC Committee Standing Committee has recently made a decision on consolidating and readjusting scientific research institutes of all categories throughout the region with the aim of overcoming the malpractices of the old scientific and technological systems. The goal is for scientific research to be closely linked with production and better serve economic construction.

In the consolidation and readjustment work, we must begin by reforming the system of appropriation of funds and thoroughly change the stage of eating out of the same big pot. In accordance with the orientation of their own work and with the characteristics of their own activities, the existing scientific research organizations will be divided into four categories:

The scientific research institutes of the technological development type must organize their income through the transfer of technology. During the Seventh Five-Year Plan period, each year they must gradually reduce their operating expenses appropriated by the state until they can completely stand on their own feet.

The scientific research institutes of the technology foundation type can mainly solve the problem of their funds by applying for funds for science.

Regarding the operating expenses of the scientific research organizations which belong to the type of technology foundations in the public interests and the type of scientific research in agriculture, the contract system will be implemented and the state will encourage them to vigorously organize income from other enterprises and regions.

Scientific research institutes in many categories can solve the problem of funds through different channels.

In the course of consolidating and readjusting scientific research organizations, regarding those scientific research units whose conditions are very poor and technological ability weak and which do not meet the requirements for a research institute, we must take resolute measures to abolish those that should be abolished and to amalgamate those which should be amalgamated. At the same time, in the light of the needs of the development of the national economy of our region, we must suitably set up some scientific research organizations. All newly established scientific research organizations of the technological development type must, in the future, take the road of standing on their own feet in regard to funds.

/9604
CSO: 4008/2131

BRIEFS

GAINS IN JIANGSU S&T REFORM--From January to July this year, Jiangsu conducted a large-scale, general scientific and technological survey, the first ever since the founding of the PRC. At a provincial briefing on the survey on 18 August, Wu Xijun, member of the provincial party committee standing committee and chairman of the Provincial Scientific and Technological Committee, announced: Since the central authorities' decision on scientific and technological structural reform, Jiangsu's scientific and technological structural reform has healthily developed. Reform has enabled research and development organizations to promote increasingly closer lateral ties with enterprises. Various scientific research and production associations have sprung up like mushrooms. Reform has steadily invigorated research and development organizations. As a result, their incomes have greatly increased. Incomes in 1985 increased by 300 percent over 1983, amounting to 2.9 times the operating expenses allocated by the state in 1985. Reform has also promoted the rational circulation of scientific and technical personnel and readjusted and improved the structure of scientific and technical ranks. [Excerpt] [Nanjing Jiangsu Provincial Service in Mandarin 2200 GMT 18 Aug 86] /9604

CSO: 4008/2131

APPLIED SCIENCES

DESIGN OF NEW WIDEBAND MICROSTRIP 3 dB HYBRID RING

Beijing DIANZI XUEBAO [ACTA ELECTRONICA SINICA] in Chinese Vol 14, No 1, Jan 86 pp 120-122

[Article by Wang Shulian [3769 2885 6647], National Fu Jiang Machinery Plant; Paper received April 1984, revised June 1985]

[Text] Abstract: A new structure of the phase-moved network and a simple method for designing a wideband 3dB hybrid ring circuit are presented. The circuit has better electrical performance over 40 percent frequency band and can withstand higher power. It is easier to fabricate and has a wider field of applications.

1. Introduction

The wideband hybrid ring shown in Figure 1 has its prominant strength.[1, 2] However, the reversed-terminal short-circuit coupling-line width designed from the existing design scheme is quite narrow, having a small slot and low tolerance for power. Thus it is fairly difficult to realize in terms of architecture. Therefore, a new circuit design approach has to be explored.

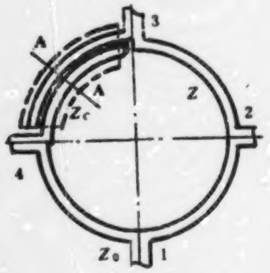

Figure 1. Circuit Diagram of a Wideband Hybrid Ring

At the present time, the reentry coupling theory has enjoyed extensive applications.[3, 4] Strong coupling 3dB wideband hybrid rings can be readily designed using this theory. The design presented in this article is a new design method combining the original hybrid ring design equations and the reentry coupling-line design theory.

2. Design Theory

The characteristic impedance of a λ/4 reversed-terminal short-circuit coupling line in the circuit shown in Figure 1 is:

$$Z_c = \frac{2Z_{0e}Z_{0o}\sin\theta}{[(Z_{0e} - Z_{0o})^2 - (Z_{0e} - Z_{0o})^2\cos^2\theta]^{1/2}} \tag{1}$$

In order to maintain the overall phase move in the circuit at $180° + \theta = 270°$, let $\theta = 90°$. Then equation (1) is simplified as:

$$Z_c = 2Z_{0e}Z_{0o}/(Z_{0e} - Z_{0o}) \tag{2}$$

To have a matching transmission line between the coupling line and the other portions of the ring whose characteristic impedances are Z_r, we must make:

$$Z_c = Z_r = \sqrt{Z_{0e}Z_{0o}} \tag{3}$$

The following is obtained when equations (2) and (3) are solved:

$$Z_{0e} = (\sqrt{2} + 1)Z_r \tag{4}$$

$$Z_{0o} = (\sqrt{2} - 1)Z_r \tag{5}$$

where $Z_r = 1.46Z_0$, and Z_0 is the input-output characteristic impedance.

For the 180° phase-moved network in Figure 1, the circuit width W and coupling slot S designed using equations (4) and (5) are particularly small. For instance, when the medium material $\varepsilon_r = 9$ and the board height H = 1mm, a ring width W = 0.12 mm and slot S = 0.04 mm are derived. This kind of hybrid ring can only be obtained using relatively advanced technology.

It is well known that the odd- and even-mode phase velocities for a microstrip coupling line are different, especially in the case of tight coupling where there is a drastic difference between the odd-mode impedance and the even-mode impedance. This is the primary reason why the aforementioned circuit architecture is difficult to realize. In order to solve the conflict whereby the odd-mode phase velocity is different than even-mode, phase velocity[5], a non-ground contact conductor (called suspension conductor for short) is introduced between the two coupling lines and the ground. The construction is as shown in Figure 2. The equivalent circuit odd and even mode impedance relationship of such coupling line is:

$$Z_{0o} = Z'_{0o} \tag{6}$$

$$Z_{0e} = Z_{01} + 2Z_{02} \tag{7}$$

where Z_{01} is the even-mode impedance corresponding to the odd-mode impedance Z_{00} at selected coupling slot S/H value; Z_{02} is the even-mode impedance formed between the suspension conductor and the ground. The familiar coupling-line impedance approximation equation can be of assistance in the solving for Z_{01}. The computation equation[6] is:

For odd-mode impedance $Z_{0o}=\frac{\eta}{\sqrt{\varepsilon_r}}\cdot\left(C'_{0o}/\frac{\varepsilon_r}{c\eta}\right)^{-1}$ (8)

For even-mode impedance $Z_{0e}=\frac{\eta}{\sqrt{\varepsilon_r}}\cdot\left(C'_{0e}/\frac{\varepsilon_r}{c\eta}\right)^{-1}$ (9)

where

$$C'_{0o}=C_{PP}+\frac{1}{2}(C_{PPV}+C_F+C'_F+C'_{PPV}),\quad C_F=\frac{\varepsilon_r}{c\eta}\cdot 2.7/\lg\frac{4H}{t}$$

$$C'_{0e}=C_{PP}+\frac{1}{2}(C_{PPV}+C_F+C''_F+C''_{PPV}),\quad C'_F=\frac{\varepsilon_r}{c\eta}\cdot 2.7/\lg\frac{4S}{\pi t}$$

$$C''_F=\frac{\varepsilon_r}{c\eta}\cdot 2.7/\lg\frac{4H}{t}\left(\frac{W}{S}+1\right)^{-1},\quad C_{PP}=\frac{\varepsilon_r}{c\eta}\cdot\frac{W}{H}$$

$$C_{PPV}=\frac{\varepsilon_r}{c\eta}\cdot\frac{2}{3\sqrt{\varepsilon_r}}\left[\frac{W}{H}-\left(\frac{W}{H}+1\right)^{-2}\right]$$

$$C'_{PPV}=\frac{\varepsilon_r}{c\eta}\cdot\frac{8}{3\sqrt{\varepsilon_r}}\cdot\left(\frac{S}{W}+1\right)^{-1},\quad C''_{PPV}=\frac{\varepsilon_r}{c\eta}\cdot\frac{2}{3\sqrt{\varepsilon_r}}\cdot\frac{W}{H}\cdot\left(\frac{W}{S}+1\right)^{-1}$$

When the S/H value has been selected, Z_{01} can be obtained using equations (8) and (9). However, it is fairly cumbersome to arrive at the result. To deal with the calculation, a computer-aided design is used. Programs (omitted here) are written for expressions (8) and (9) which represent the microstrip odd- and even-mode impedances for various media and various coupling slots S. The results are printed on a table (only the sample design Table 1 is given in this article). In doing so, the geometric size of the coupling line can be obtained very conveniently. The value for the impedance Z_{02} between the suspension conductor and the ground can be obtained from equation (7), and the geometric size of the suspension conductor can be further looked up using the table for single microstrip.

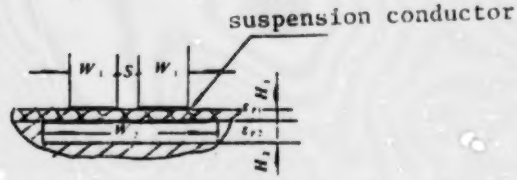

Figure 2. A-A Cross-sectional View from Figure 1

3. Design Computation and Experimental Results

A wideband microstrip 3dB hybrid ring is to be signed. The substrate material used is polytetrafluorethyiene whose εr = 2.55, H = 1.5 mm, t = 0.05 mm, and Z_o = 50 Ω. The design steps are as follows:

(1) Compute the odd- and even-mode impedances according to equations (4) and (5)

$$Z_{0o}=(\sqrt{2}-1)Z_r=30.24\Omega$$
$$Z_{0e}=(\sqrt{2}+1)Z_r=176.24\Omega,\quad Z_r=1.46Z_0$$

(2) Calculate the coupling line size.

Select S/H = 0.5. Let H_1 = 1.5 mm, then S = 0.75 mm. When Table 1 is looked up, as W_1/H_1 = 4.25 corresponding to Z_{00} = 30.24 Ω, and as H_1 = 1.5 mm, then W_1 = 6.38 mm. In addition, the even-mode impedance Z_{01} corresponding to Z_{00} is looked up as 39.3 Ω.

(3) Compute the suspension conductor to ground impedance Z_{02} from equation (7).

$Z_{02}=(Z_{00}-Z_{01})/2=68.46\Omega$, from Table 1, suspension conductor width W_2/H_2 = 3.13. Pick H = 6 mm, then W_2 = 18.78 mm.

(4) Compute λs/4 and the diameter of the ring

$\lambda_s/4=\lambda_0/4\sqrt{\varepsilon_e}$, λ_0 is the space wave length, λg is the medium wave length, and ε_e is the equivalent dielectric constant.

Table 1. Coupling-line Characteristic Impedance (ε_r = 2.55)

S/H	W_1/H_1	Z_{00}	Z_{01}	Z_{02}	W_2/H_2
0.4	4.14	30.24	40.32	67.96	3.17
0.5	4.25	30.24	39.3	68.46	3.13
0.6	4.32	30.24	38.54	68.84	3.10

Figure 3 shows the following: signals fed into opening no. 1, output amplitude A from opening nos. 2 and 4, interval I at opening no. 3, the voltage standing wave ratio (VSWR) for the four openings, and equiphase input and reversed phase input into opening nos. 2 and 4 as well as the output phase ϕ.

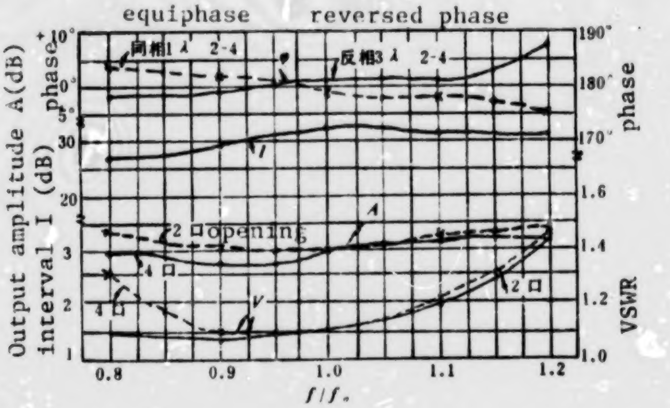

Figure 3. Curve of Output Amplitude A, Interval I, VSWR V and Phase φ Against Changing Frequency

4. Conclusion

The circuit described in this article has a better electrical performance compared with the hybrid ring whose circumferential length is 1.5 wavelength. Approximately over 40 percent of the frequency band, the voltage standing-wave ratio at each opening is less than 1.5, output amplitude $A = -3 \pm 0.5$ dB, interval $I > 27$ dB, the output phase in equiphase case is less than ± 5°, and the output phase in reversed phase case is less than ± 10°.

As a result of the innovation in architecture and circuit design approach which overcomes the fatal weakness in the original circuit having a small line width, narrow slot, and low tolerance for power, the new microstrip hybrid ring enables a wider application for the original hybrid ring.

Appreciation is extended to two very helpful comrades, Luo Yuping [5012 3768 1627] and Lai Xiaoya [6351 1420 7161].

REFERENCES

1. Harlan Howe, Jr., "Stripline Circuit Design," Artech House, Inc., 1974, pp 85-94;
2. S. March: IEEE TRANS, Vol MTT-16, 1968, p 361.
3. Lin Weigan [2651 3634 1631], "Microwave Network," National Defense Industry Publishing House, 1978, pp 211-219, 271-276;
4. Yin Liansheng [3009 6647 3932], "Analysis and Design of a Reciprocal Recoupling Microstrip 3dB Electric Bridge," Transmission Line Edition, by the Radar Information Editing and Translation Group of the Nanjing Electronic Technology Institute, 1978, pp 34-40;
5. Chen Zhencheng [7115 2182 2052], "Microstrip Serial Fed Power Distributors/-Synthesizers," ACTA ELECTRONIC SINICA, 1984, No 3;
6. Gu Qizheng [7357 0366 6154] et al., "Microwave Integrated Circuit Design," People's Posts and Telecommunications Publishing House, 1978, pp 45-64.

13042/7358
CSO: 4008/1088

APPLIED SCIENCES

ENVIRONMENTAL EFFECTS ON COMPUTER-CONTROLLED FEEDING SYSTEM

Shanghai ZIDONGHUA YIBIAO [PROCESS AUTOMATION INSTRUMENTATION] in Chinese
Vol 7, No 5, 20 May 86 pp 30, 38

[Article by Tong Suqin [0157 4790 5367], He Suzhi [0149 4790 5347], and Lin Lu [2651 0712], Anshan Ion Smelting Plant]

[Text] In October 1983, the Shanghai Process Automation Instrumentation Institute successfully developed a computer-controlled feeding system for the No 10 blast furnace in our plant. Ever since it has been in operation, this system has demonstrated steady performance, realizing precision coke/ore measurement with prominent economic benefits and contributing to a reduction in the rate of coke consumption as well as energy conservation.

1. Basic Function of the System

The industrial computer used in the No 10 blast furnace is used to control the ore in the blast furnace such as the loading amount and pre-load amount and to compute the ore and coke weight compensation and coke moisture compensation. The computed results are passed to the sequence controller by the computer, loading the coke and ore into the blast furnace using loading carts.

If there were fluctuations in the blast furnace, the blast furnace foreman would modify the predetermined value, the compensation value, and the pre-load amount relating to loading on the computer's keyboard, bringing the blast furnace to a stable state. (Generally, the loading of the furnace could be brought to a stable state primarily by adjusting the pre-load amount.) The printer provides data regarding shift and daily accumulations, coke moisture value, batch weight, and so on.

2. Environmental Effects on the System and the Solutions

The environment in which the blast furnace instruments are used is extremely unfavorable. The signal input to the computer is delivered from the transducer which is installed under the furnace ditch and is subject to high temperature, vibration, and electroconducting dust as well as the interference magnetic field influence that arises from the frequent turning on of large-scale electric machinery. In the case of a computer into which micro-signals are fed, a significant fluctuation can result from very small interference and will directly affect the operation of the computer.

(1) Influence from Environmental Temperature and the Solution

The device used in our plant is a LGA-high precision transducer manufactured by the Hangzhou Measuring Instrumentation Plant with the following specifications. The operating temperature is -10 - + 40°C, internal resistance is 350 Ω, the rated non-iterations for both the nonlinear and the lag are less than +0.03 percent, with an error of less than 0.05 percent for the three combined, and the responding plate is made of a cobalt-nickel alloy.

An illustration is presented as follows using the transducer in the ore scale as an example. In July 1984, the blast furnace foreman discovered that the ore-loading amount accumulated by the computer was much higher than the theoretical amount based on the furnace ion yield computation. The cost of pig ion would increase when this phenomenon occurred. Initially, we suspected damage in the transducer which turned out all right after the diagnosis. The working temperature of the transducer during that period was 65°C (due to the high temperature caused by thermal radiation from heating the ore). Because the temperature exceeded the specified temperature for the transducer, the transducer's temperature self-compensated resistance failed. The sensitivity coefficient of the responding plate changed with the fluctuation in temperature, resulting in an increase in the load for the transducer. The output signals from the transducer followed the increased load which was not a linear increase.

We covered the transducer with a square box we made from metal sheeting. Compressed air at a constant temperature was passed into the box. (In case conditions did not permit it, the transducer was relocated far from the middle bin where ore is loaded, as well as far from the conveyor on which the ore is transported, as a measure against thermal radiation.) In doing so, not only can it be assured that the transducer will be working under constant temperature, but the electro-conductive dust can also be avoided. Practical experience has proved that it is a better approach.

(2) Influence from Vibration and the Solution

The No 10 blast furnace is a relatively large blast furnace with a feed of 12-14 tons per load from the cart. Fierce vibrations would result when the scale was loading the feed. Because of the influence of vibration, the output signals from the transducer were unstable, the useful lifetime of the transducer could be shortened, and measurement errors could increase. Therefore, a certain amount of time has to be reserved in software programming regarding sample collection so that signals can only be read into the computer after the output signals from the transducer have been stabilized.

In order to assure accuracy in the measurements, the prolonged useful life of the transducer, and stable output signals from the transducer, as well as to minimize the computer's operating time, we employed the following measures:

a) The machine's zero weight must be accurate. Minimize when at all possible the pre-tension of the transducer at empty load;

b) Add a stage mechanical drive lever to achieve the buffering against the scale (as shown in Figure 1);

c) Output the data from the computer after the output signals from the transducer have been stabilized; and

d) Add anti-vibration padding to the transducer's steady voltage supply.

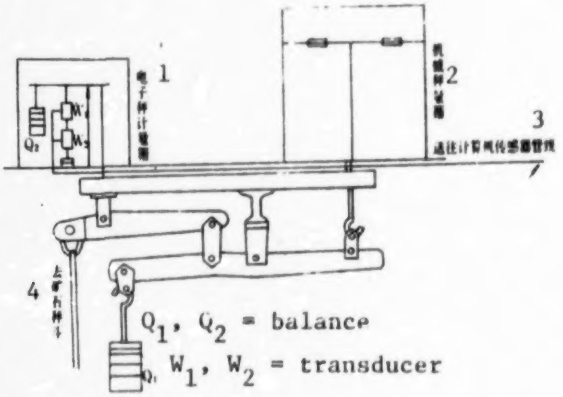

Figure 1

Key:

1. Electronic balance measurement box
2. Mechanical balance measurement box
3. Line feeding to the computer transducer
4. To the ore scale

(3) Electromagnetic Influence and the Solution

(a) Method to eliminate space induction interference

The frequent on and off of large-scale electric machinery is the primary factor producing space induction. To solve this problem, when the utility room for our plant was built, shielding screens were installed, and the ground contact points for such equipment as the transducer, steady voltage supply, and sequence controller were installed as far as possible from the ground contact point of the computer. Practical experience has proved that the result was very good.

(b) Method to eliminate interference from current supply system

A steady AC voltage supply source and an isolating transformer were employed to prevent the influence on the computer from electrified wire netting. The steady voltage current supply for the transducer was provided by the steady

AC voltage supply, as shown in Figure 2. In so doing, electrified wire netting was basically radicated.

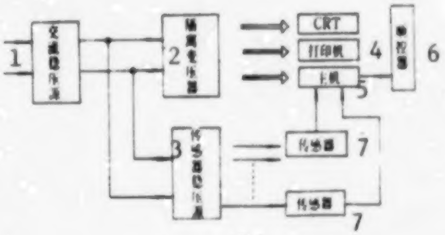

Figure 2

Key:

1. Steady AC voltage supply
2. Isolating transformer
3. Steady transducer voltage supply
4. Printer
5. Computer
6. Sequence controller
7. Transducer

13042/7358
CSO: 4008/1103

APPLIED SCIENCES

RESEARCH ON HIGH-GAIN BROADBAND BACKFIRE ANTENNA

Beijing DIANZI KEXUE XUEKAN [JOURNAL OF ELECTRONICS] in Chinese Vol 8, No 3, May 86 pp 223-227

[Article by Song Ximing [1345 6932 2494] of the Huanghe Machine Building Plant; received 18 September 1984, revised 6 September 1985]

[Text] I. Brief Review

Recently, there have been various theoretical analyses and physical explanations regarding the high-gain radiation characteristics possessed by a backfire antenna. However, the schools are different. This article is based on the basic theory given in Reference [1]: the backfire antenna is approximately equivalent to the antenna of a concaved reflector. In addition to the "equivalent focal point" and "equivalent focal distance," it also has the following relational equation:

$$\left.\begin{aligned} f &= n\lambda, \\ R &= \sqrt{n + \frac{1}{4}}\,\lambda, \end{aligned}\right\} n = 1, 2, 3, \cdots\cdots, \qquad (1)$$

where f is focal distance and R is the radius of the surface wave reflector. Optimal gain is obtained when the phase center of the feeding source is at the equivalent focal point. The following corollaries can be obtained from Equation (1):

Corollary 1. For different values in n:

$$\begin{array}{lll} n = 1, & f = \lambda, & R \approx 1.12\lambda; \\ n = 2, & f = 2\lambda, & R \approx 1.50\lambda; \\ n = 3, & f = 3\lambda, & R \approx 1.80\lambda; \\ n = 4, & f = 4\lambda, & R \approx 2.10\lambda; \\ \vdots & \vdots & \vdots \end{array}$$

then for a given n value, the optimal radiation characteristic can only be obtained under the corresponding f and R.

Corollary 2. There are n "equivalent focal points/distances" for the backfire antenna. However, corresponding to the surface wave reflector having the above given radius, the optimal radiation characteristics can only be obtained when the phase center of the feeding source is at the corresponding focal point.

Corollary 3. The "equivalent focal point/distance" of the backfire antenna is a function of frequency, changing with the frequency. Assume the presence of a feeding source whose phase center is also a function of frequency and whose functional format is the same as or similar to the functional format of the "equivalent focal point/distance," then a broadband backfire antenna can be obtained when such a feeding source is taken as the backfire antenna's feeding source.

Based on the above corollaries, we design several backfire antennas to perform experimental research.

II. Experimental Results

1. High-gain backfire antenna

For the backfire antenna experimental model (please refer to Figure 1 of Reference [1]), the radii of the surface wave reflectors are 1.12λ, 1.5λ, 1.8λ, and 2.1λ, respectively; the rim height can be adjusted continually from 0-2λ; the radius of the small reflector is 0.5λ - 1.0λ; and the feeding source is a half wave oscillator. In addition, a transfer equipment of slot-eqioaxle balance-imbalance is employed. The experiment is conducted in an open outdoor field.

(1) Antenna performance at different values of n

An experiment is performed on antennas of different sizes. Their typical directional diagrams under the optimal radiation states are shown in Figures 1, 2, 3, and 4, respectively. At this point, their corresponding measured gains are 17.5 dB, 19.2 dB, 20.8 dB, and 23 dB, respectively.

It can be seen from the experimental results that the antenna's radiation characteristics is in closer agreement with Corollary 1. As the measured gains are reviewed, if one is to use $G = 4\pi S_A/\lambda^2$ to do the estimate, the effective aperture area S_A of the antenna exceeds the actual geometric area in some cases (such as n = 1 and 4). (Of course, the influence from the rim is not taken into consideration here. As for the function of the rim, i.e., the discussion on "effective aperture radius gain," please refer to Reference [1].) It is an indication that the efficiency of the antenna is pretty high.

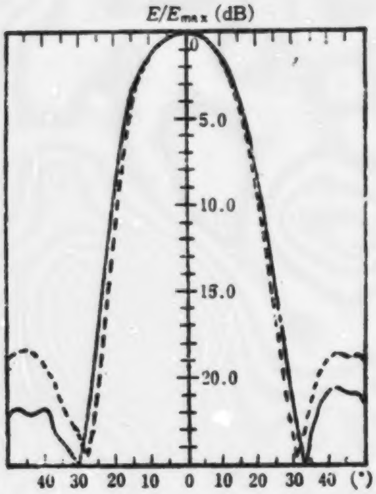

Figure 1. Experimental Direction Diagram at n = 1

----- Vertical polarization

..... Horizontal polarization

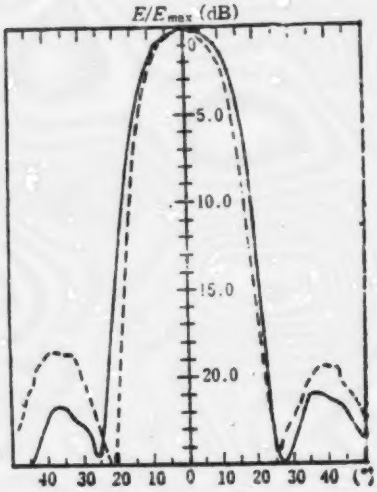

Figure 2. Experimental Direction Diagram at n = 2

----- Vertical polarization

..... Horizontal polarization

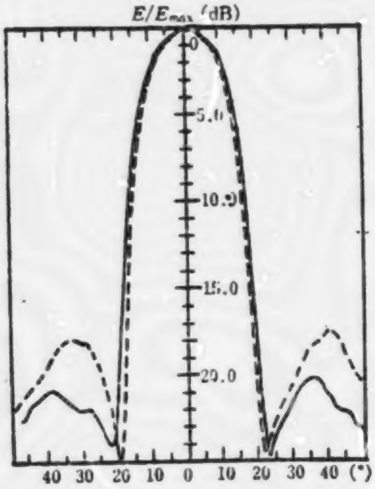

Figure 3. Experimental Direction Diagram at n = 3

----- Vertical polarization

..... Horizontal polarization

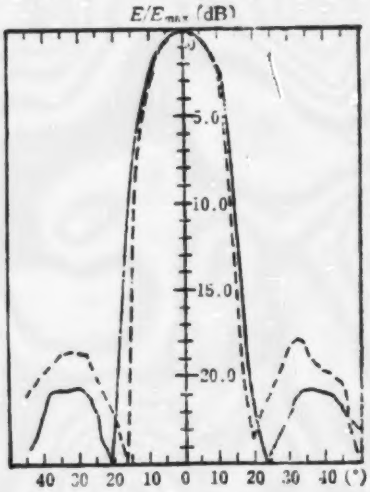

Figure 4. Experimental Direction Diagram at n = 4

----- Vertical polarization

..... Horizontal polarization

(2) Relationship between the feeding source and radiation characteristics

According to Corollary 2, if n = 1, 2, and 3 are taken respectively, the radii of the surface wave reflectors are 1.12λ, 1.5λ, and 1.8λ, respectively. The longitutional position of the feeding source can change continually within a certain range; then the relationship curve representing the received power of the designed antenna and the position of the feeding source can be seen as shown in Figure 5. It can be seen from the figure that the way the curve changes is in agreement with Corollary 2.

This type of antenna is insensitive to polarization and capable of resulting in linear polarization and oval polarization (circular polarization). If a cross-shaped oscillator is used as the feeding source and is placed at the optimal position, then at the direction on which the value of the wave beam is the greatest, the measured axle ratio when frequency is f_0 is less than 0.3 dB. However, a poorer axle ratio will result if a cylindrical spiral wire is used as the feeding source.

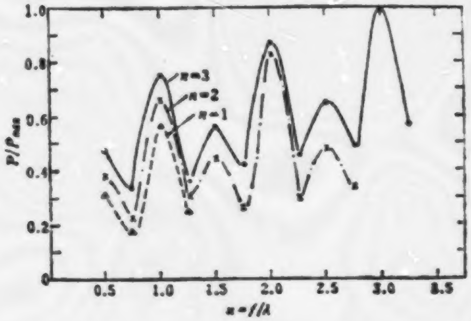

Figure 5. Effect of Position of Feeding Source on Gain

2. Broadband backfire antenna

It is well known that one of the major drawbacks of the backfire antenna is its relatively narrow working band, with a band width only reaching to 10 percent, approximately. Based on Corollary 3, and using a cone-shaped spiral antenna as the feeding source, we design a broadband backfire antenna which has better radiation characteristics with a 50 percent relative bandwidth.

We understand that the cone-shaped spiral wire is formed with a group of coils (about 3.5-4 wraps). The length of each round in the coil approximately equals the wave length at the center frequency (varying within the range of 0.8-1.3λ, where λ is the wave length in free space). These coils work under the state similar to the cylindrical spiral-axle radiation state. Inside this group of coils, the T_1 wave is the most significant. At the high-frequency end of the frequency band, those coils located at the smaller radius spiral wire are contributing, whereas at the low-frequency end of the frequency band, those coils located at the larger radius spiral wire are contributing. In the middle of the frequency band, it is those coils located at the center of the spiral wire that contribute. Thus, the antenna is capable of working inside a fairly wide frequency band. Of course, although the rest of the coils do not contribute significantly, however, there is still some weak radiation which has some influence on the shape of the radiation direction diagram.

The frequency band we experiment with is 1,600-2,900 MHz, with a relative band width of 50 percent, approximately. The spiral antenna is constructed using red copper pipe whose diameter is 3 mm.

The experimental direction diagram inside the working frequency band is shown in Figure 6. It can be seen from the figure that the antenna has better radiation characteristics inside the frequency band; the width of the half-power point on the direction diagram shrinks with increasing frequency. In addition, the corresponding axle ratio is given in the figure. The input voltage standing-wave coefficient of the antenna inside the frequency band is less than 2.5, and is less than 1.50 in 25 percent of the band width.

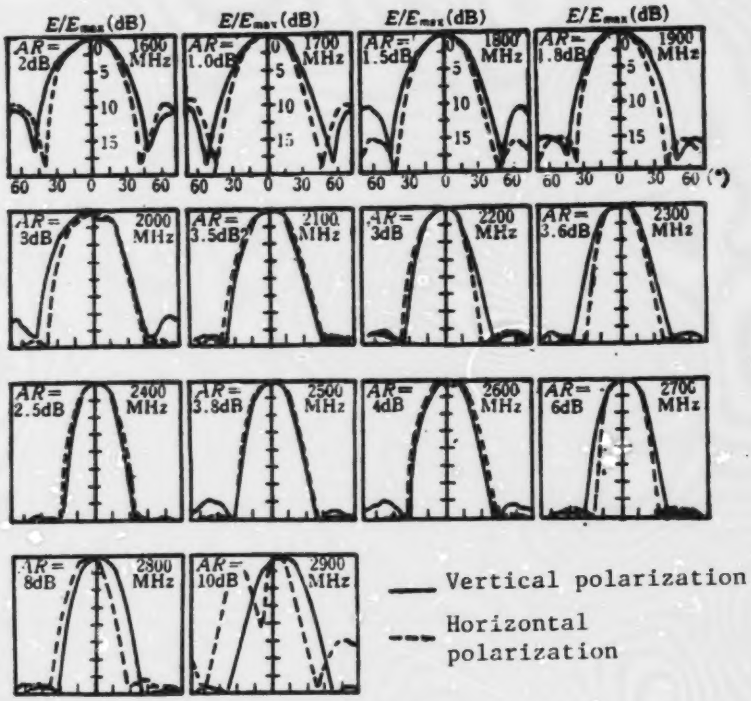

Figure 6. Experimental Direction Diagram

P_{max} is the maximum receiving power at n = 3.

It is noted in the experiment that the height of the rim has an effect on the antenna's radiation characteristics, and such an effect is more significant on the auxiliary amella electricity level. The size and the position of a smaller reflector have more significant influence on the performance of an antenna. In general, better radiation characteristics can be obtained when the diameter of a smaller reflector is set at 0.5λ.

If a disk of proper size is introduced between the surface wave reflector and the cone-shaped spiral wire, and after fine tuning, it can improve the antenna's performance significantly, especially in the enhancement in axle ratio. However, at the same time, the working frequency band would become much narrower.

III. Conclusion

(1) An "equivalent focal point/distance" indeed exists for the backfire antenna. The optimal radiation characteristics of the antenna can be obtained when the phase center of the feeding source is located at the equivalent focal point.

(2) The backfire antenna designed from the theory proposed in Reference [1] possesses the best radiation characteristics.

(3) A broadband backfire antenna can be designed based on the theory given in Reference [1].

(4) This article is an experimental support verifying the theory regarding the backfire antenna given in Reference [1].

This project received the dedicated guidance from Associate Professor Lin Changlu [2651 2490 4389] of the Chengdu Telecommunication Engineering College. In addition, a great portion of the experiment work was completed with the assistance from Comrades Rao Boliang [7437 0130 5328], Li Ruihua [2621 3843 5478], and Zhang Yufeng [1728 3768 1496]. Our appreciation is extended to all of them.

BIBLIOGRAPHY

1. Lin Changlu [2651 2490 4389] and Song Ximing [1345 6932 2494], DIANZIXUE TONGXIN [ELECTRONICS BULLETIN], No 4, 1982 p 331.

2. Lin Changlu [2651 2490 4389] and Song Ximing [1345 6932 2494], "1983 International IEEE/APS Symposium and National Ratio Science Meeting at the University of Houston," pp 138-141.

3. Lin Changlu [2651 2490 4389], CHENGDU DIANXIN GONGCHENG XUEYUAN XUEBAO, [CHENGDU TELECOMMUNICATION ENGINEERING COLLEGE JOURNAL] No 10, 1979 pp 97-102.

4. A.Z.Fradin, "Superhigh Frequency Antenna," translated by Chen Bingchun [7115 4426 6874] and Xiao Duchi [5135 4648 1062], International Industry Publishing House, 1962, Chapter 11.

13042/7358
CSO: 4008/1101

PMR TYPE AMIDE-IMIDE POLYMER, COMPOSITES

Beijing GAOFENZI TONGXUN [POLYMER COMMUNICATIONS] in Chinese No 3, Jun 86 pp 219-225

[Article by Zhu Wenjiang [2612 2429 3068], Zhang Chongli [1728 1504 4539], and Huang Zhitang [7806 1807 6974], Beijing Institute of Chemistry, Chinese Academy of Sciences; Paper received 27 May 1984; presented at the 1983 Hangzhou Polymer Symposium]

[Text] Abstract: The "PMR" (polymerization of monomer reactants) type polyamide-imide resins were prepared from bicyclo-[2.2.1]-hept-5-ene-2,3-dicarboxylic acid monoethyl ester, 1,2,4-trimellitic acid 2-(or 1-) ethyl ester, and 4,4'-diaminodiphenylmethane in ethanol. The composites fabricated from these resins can be used at 260°C over an extended period. The mechanism of formation of polyamide-imide was studied by using model compounds.

Aromatic polyamide-imides (PAI) are generally prepared by condensation polymerization of trimellitic anhydride 4-acyl chloride and aromatic diamines in highly polar, non-protic solvents (e.g., DMF).[1] Materials made from the polymer are viscosity- and heat-stable and are good insulators. But it is not suitable for composite application because of its high molecular weight. Although efforts have been made in improving molecular weight and in finding better starting materials, no significant results are accomplished.[2] It has recently been reported[3] that the amide-imide polymer prepared by using maleic anhydride as a capping reagent shows good flexural strength. However, the resin preparation process involves a high-boiling, toxic solvent and its high molding pressure limits to a certain extent, has wider applications. Based on our experience with the "PMR" type polyimide capped by bicyclo-[2.2.1]-hept-5-ene-2,3-dicarboxylic anhydride (NA), we studied the "PMR" type polyamide-imide resins. The preparation of the resin solution was carried out again in ethanol, using trimellitic anhydride (TMA) and 4,4'-diaminodiphenylmethane (M) as starting materials. Bicyclo-[2.2.1]-hept-5-ene-2,3-dicarboxylic ethyl ester (N) and 1,2,4-trimellitic acid 2- (or 1-) ethyl ester (T) were prepared in anhydrous ethanol. The "PMR" solutions of polyamide-imide of various "molecular weight" were then rpepared in ethanol. In this paper, we mainly studied the amidation reaction at the 4 position and the imidization and amidation reactions at 1 and 2 positions of 1,2,4-trimellitic acid 2-ethyl ester. The structures of low molecular weight polymer and the technology and properties of composite materials were investigated and discussed.

Results and Discussion

1. Amidation of 4-Carboxyl Group of Compound T

The NA-capped "PMR" type PAI resin solution exists as amine salt and can be written as follows:

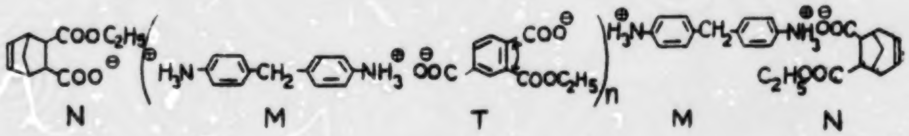

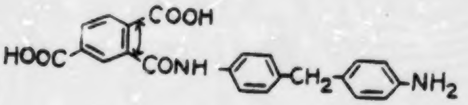

(I)

$$N\text{-}(M\text{—}T)_n\text{—}M\text{—}N$$

In the previous paper,[4] it was pointed out that compound N reacts readily with M. Therefore, the key questions in PAI synthesis are under what condition and by what mechanism different carboxyl and ester groups on compound T react with M. Considering the electronic effect, 4-carboxyl group is much less acidic than 1- and 2-carboxyl groups (two orders of magnitude less). Obviously, 4-carboxyl group is less reactive and less likely to undergo amidation with an amino group. Our experimental results show that no 4-position reaction product formed when compound T, aniline, p-aminobipheny, and compound M were reacted at 150°C for 1-4 hours. All products are 1- or 2-position derivatives. It is also reported in the literature[3] that only 80 percent of 4-position carboxyl group undergo amidation after 28 hours at 200°C. In order to establish the effect of reaction temperature on the amidation of 4-position carboxyl group, we measured the DTA trace of model compound I (Figure 1). The results show that the amidation temperature of 4-carboxyl is around 230°C whereas those of 1- and 2-carboxyls are about 170°C.

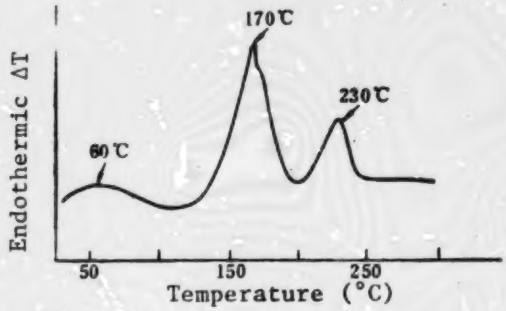

Figure 1. DTA Trace of Compound I

To confirm further the extent of amidation of the 4-carboxyl group, we again use compound I as a model to determine, as an indicator of the extent of amdiation, changes in these carboxyl groups after reacting at different temperatures over a certain period of time. It can be seen from Table 1 that the complete amidation of the 4-carboxyl group of compound I takes 3-4 hours at 250°C or 1 hour at 280°C.

	200°C/1h	230°C/1h	250°C/1h	250°C/2h	250°C/3h	250°C/4h	280°C/1h
Percentage of reacted 4-carboxyl group	24.1	68.9	77.0	95.0	97.9	99.3	99.3

Table 1. Extent of Amidation of Compound I

2. Amidation and Imidization of 1- and 2-position Carboxyl and Ester Groups of Compound T

As pointed out earlier, when compound T is treated with such aromatic amines as aniline at 150°C, 1- and 2-carboxyl groups react completely. How are amide and imide formed from this ester ammonium salt? On the one hand, the salt can be dehydrated at a high temperature to form amide ester, which then forms imide by ethanol elimination (Equation 1), namely by the nucleophilic addition of amino group through its line pair electrons to the carbonyl carbon of the carboxyl group. On the other, the carboxyl and ester groups at positions 1 and 2 can form anhydride upon heating by losing a molecule of ethanol through a cyclic intermediate, an endothermic process. It then forms amide acid and imide (Equation 2).

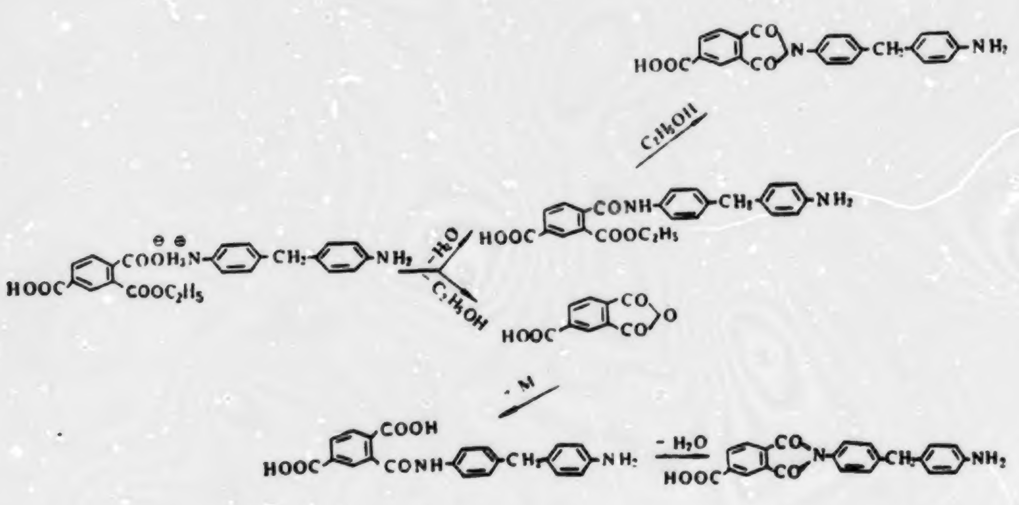

(1)

(2)

It is well known that the dehydration reaction in Equation 1 to form amide can only be accomplished at high temperature and the resulting amide ester requires an even higher temperature to form imide through the elimination of ethanol. This contradicts the experimental observation that imide can be formed at below 150°C. If the reaction follows Equation 2, we try to confirm it by the heating experiment on compound T. But the results show that after heating compound T at 150° and 200°C, the yields of anhydride are 2 and 18 percent, respectively. Obviously, this also does not agree with the above observation that imidization occurs readily. So both mechanisms (1) and (2) cannot account for the experimental results. For this reason, we prepared compound II, m.p. 113°C, and measured its TGA/DTA diagram (Figure 2) by thermal analysis. The results show that there appear three weight loss regions a, b, and c in the TGA diagram. The region b is located in the 140°-170°C range, not far from the m.p. A large endothermic peak and a higher weight loss rate (10.8 percent) occur within this region. The weight loss rate is very close to the theoretical value for the loss of one ethanol molecule (10.13 percent).

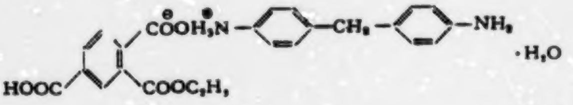

(II)

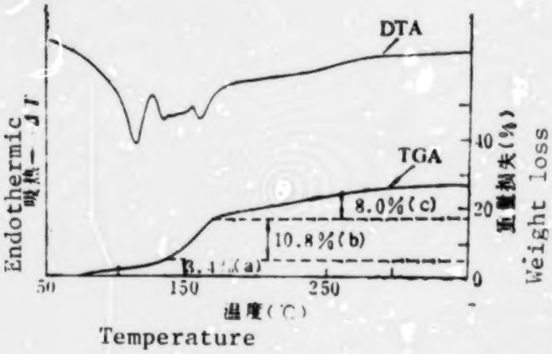

Figure 2. TGA/DTA Traces of Compound II

Therefore, we believe that the amidation reaction probably follows the intramolecular nucleophilic addition-elimination of the carboxylate anion to its neighboring carbonyl group. Because this is a faster reaction than the intramolecular nucleophilic addition in Equation 1 and the endothermic reaction in Equation 2, the amidation can be accomplished within minutes. As to the 3.4 percent (below 140°C) of region a and 8.0 percent (170°-250°C) of region c, they correspond to the loss of one molecule of crystalline water of compound II (3.96 percent) and the sum of the weight loss due to the elimination of water from acid amide to form imide and the weight loss of one molecule of water from 4-carboxylate to form amide bond (7.93 percent).

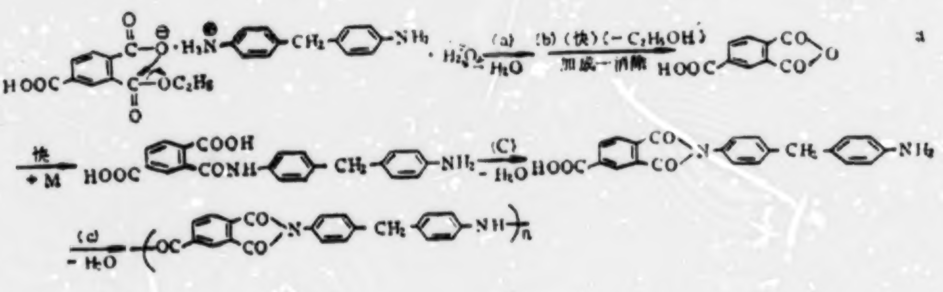

Therefore, it can be seen that, in the "PMR" type PAI, the amidation of 1 and 2 positions occurs through the reaction of the ammonium salt of ester acid. At temperatures beyond the m.p., it follows the fast reaction of ethanol elimination to form anhydride. However, the reaction does not follow the simple intramolecular endothermic mechanism, but rather the intramolecular nucleophilic addition-elimination mechanism between the carboxylate anion and the carbonyl carbon atom.

3. Structure of Low Molecular Weight Polymer

Since the "PMR" type PAI solutions exist as the ammonium salt of ester acid, we carried out a preliminary study of the solid-phase reaction of the resins with n=1 in order to understand, as composite material, the structure of the resin on fabrics after the removal of solvent. The reaction conditions were 120°, 140°, and 160°C for 1 hour. The products were then subjected to liquid chromatography. The results show only the formation of low molecular weight products such as N-M, T-M, T-M-N, and N-M-N. Because no product, N-M-T-M-N, is formed, this agrees with the results of 4-carboxyl amidation of compound T. It can be concluded that for the "PMR" type PAI resins, no large molecule with the structure of $N\text{-}M\text{-}(\text{-}T\text{-}M\text{-})_n\text{-}N$ is produced in the solid-phase reaction at 120°-160°C, whatever the n value. Only such small molecules as N-M, T-M, T-M-N, and N-M-N are generated. The further elongations of the chain and cross-linking reactions occur during the molding process at still higher temperature.

4. Properties

Experimental results show that the formula molecular weight (FMW) of PAI resin has an obvious impact on the breakdown temperature and the flexural strength of the glass cloth-reinforced plastics (Table 2).

N/M/T	FMW	Break-down (°C) temperature	Flexural strength (kg/cm²)	
			Room temperature	300°C
2/2/1	845	460	5760	4640
2/3/2	1198	478	6290	4640
2/4/3	1552	479	6630	—
2/5/4	1902	488	7070	4430
2/10/9	3676	496	4870	1680
2/20/19	7218	—	4360	1400
0/1/1		500	2040	400

Table 2. Correlation of Formula Molecular Weight with Breakdown Temperature and Flexural Strength

The results also show that FMW also has significant impact on their isothermal aging properties (Figure 3).

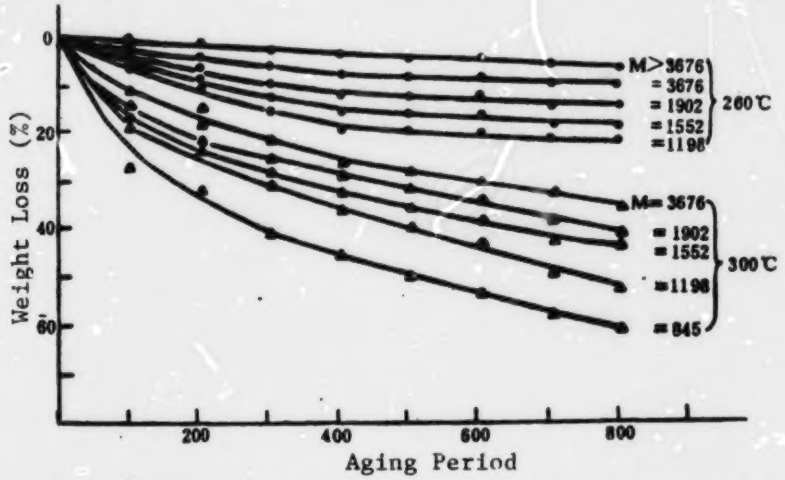

Figure 3. Formula Molecular Weight and Isothermal Aging Behavior

Taking flexural strength and isothermal aging properties into consideration, we believe it is more appropriate to select those PAI with n=3-4 and whose FMW is between 1552-1902.

We ended up choosing a PAI resin with n=3 and FMW=1552 for the fabrication of a glass cloth-reinforced plastic, which was aged for 800 hours at 260°C. The data are shown in Table 3. It can be seen that the flexural strength drops only a little after subjecting to high temperature for 800 hours. Therefore, PAI composites can be used for an extended period of time at 260°C.

1 测试温度 (℃)	2 260℃ 下热老化后的抗弯强度 (kg/cm^2)					
	0	100h	200h	400h	600h	800h
3 室　温	6300	6020	7080	5440	5230	4450
260℃	4130	4590	4640	4360	4130	3800

Table 3. Flexural Strength of Glass Cloth Reinforced Plastic After Isothermal Aging

Key:

1. Temperature (°C)
2. Flexural Strength After Aging at 260°C
3. Room temperature

In summary, we believe that the "PMR" type PAI resin synthesized in ethanol has the advantages of easy preparation, low cost, and low pressure molding. It is recommended for use as a heat-resistant composite.

Experimental

1. Preparation of Compound I

Trimellitic anhydride (2.84 grams) was dissolved in DMAc (20 ml). A solution of MDA (3.96 grams in 10ml of DMAc) was added dropwise with stirring. The overnight reaction solution was diluted by ethanol (30 ml) and quickly decanted into water (200 ml). The precipitate formed was filtered, washed and dried to get an isomeric mixture of compound I. The neutralization equivalent is 195.0 (Calcd 195.3).

IR spectrum (KBr pellet), cm^{-1}: 3150-3420, broad, (OH, NH); 1705 (carboxylic C=O); 1655 (amide C=O).

Elemental Analysis for $C_{22}H_{18}N_2O_5$: Calcd: C: 67.68; H: 4.65; N: 7.18. Found: C: 67.94, 67.86; H: 4.22, 4.32; N: 7.12, 7.13.

2. Preparation of Compound II

With reference to the method in the document[4]: 1,2,4-trimellitic 2-ethyl ester (m.p. 206 C; neutralization equivalent 119.0, calcd 119.5; chromatographically homogeneous, 11 g) was dissolved in ethanol (45 ml) by heating and quickly poured into a suspension of MDA (9.15 grams) in hot water (30 ml). After complete dissolution by stirring, the solution was kept at 0°C overnight to obtain light yellow solids, which were filtered, washed with petroleum ether-benzene, and dried. The product, compound II, has a m.p. of 111-113°C and a neutralization equivalent of 227.0 (calcd 227.2).

IR spectrum (KBr pellet), cm^{-1}: 3400-3450 (OH, NH); 2600 ($-NH_3$); 1722 (ester C=O); 1705 (carboxylic C=O); 1515 (COO-).

Analysis for $C_{24}H_{24}N_2O_6 \cdot H_2O$: Calcd: C: 63.42; H: 5.77; N: 6.17. Found: C: 63.77, 63.84; H: 5.75, 5.76; N: 5.86, 5.75.

3. Thermal Analysis

Differential thermal analysis (DTA) were done by a Mettler Model TA 2000 DTA instrument. The range was 5 μV and temperature gradient was 10°C/min. Sample size was 2-3 mg. The thermal gravity analysis/differential thermal analysis (TGA/DTA) were recorded on a Model 41 differential thermobalance manufactured by Beijing Optical Instruments Factory. The scales of TGA and DTA were 25 mg and 25 μV, respectively. The temperature gradient was 10°C/min and sample size was 11-12 mg.

4. Preparation of Resin

Compounds N, T, and M were weighed according to a precalculated ratio. Ethanol was added to make a 40-45 percent (w/w) solution of PAI. For example, compounds N (2.80 grams) and T (4.76 grams) were placed in a flask. Ethanol (15.5 grams) was added. After dissolution by heating, compound M (5.28 grams) was added, which was dissolved by stirring to make a 45 percent (w/w) resin solution.

5. Preparation of Reinforced Plastic

Resin solution was applied to the KH 550 pre-treated base-free glass cloth (0.1 mm thick), which was then dried at 80°C. High temperature treatment resulted in a pre-treated fabric. The resin content of the fabric is 30-35 percent. It was then fabricated under a pressure of 10 kg/cm^2 at 300-310°C for 1 hour. The resin content in the final product varies somewhat with molecular weight.

FOOTNOTES

1. Lavin, E., Markhart, A.H., Santer, J.O., USP, 3, 260, 691, 1966.

2. Freeman, J.H., Frost, L.W., Bower, G.M., Traynor, E.J., Burgman, H.A., Ruffing, C.R., POLYM. ENG. SCI., 1969, 9(1), 56-72.

3. Krun, D., Jablenski, R.J., J. POLYM. SCI., POLYM. CHEM. ED., 1979, 17, 1945-51.

4. Wang Dong [3769 2639], Wu Yaoman [0702 3852 2581], Li Jiaze [2621 1367 3149], Zhang Chongli, Yu Shangying [0827 0794 5391], Jin Yirong [6855 6965 3310], and Huang Zhitang, GAOFENZI TONGXUN [POLYMER COMMUNICATIONS], 1980 (3), 152.

12922/7358
CSO: 4008/1099

APPLIED SCIENCES

SYNTHESIS OF POLYBUTADIENE BY NEW CATALYST SYSTEM STUDIED

Beijing GAOFENZI TONGXUN [POLYMER COMMUNICATIONS] in Chinese No 3, Jun 86
pp 236-240

[Article by Xu Ling [1776 3781], Zhao Senkun [6392 2773 2492], and Tang Xueming [0781 1331 2494], Qingdao College of Chemical Technology; Paper received 17 February 1985; Research financed by Science Fund administered by Chinese Academy of Sciences]

[Text] In the previous paper,[1] we reported the synthesis of polybutadiene by the catalyst system $MoCl_n(OC_8H_{17})_{4-n}$-$(i\text{-}Bu)_2AlOPh$. It is observed[2] that $MoCl_n(OC_8H_{17})_{4-n}$ dissolves better than $MoCl_4$ in hydrogenated gasoline and displays better catalytic activity. Based on these previous works, we investigated in this paper the correlation of the solubility of $MoCl_n(OR)_{4-n}$ in hydrogenated gasoline and their catalytic behavior with the functional group R by choosing different OR groups. We studied the effect of the dosage and ratio of main catalyst and cocatalyst on the catalysis of polymerization, polymer mean molecular weight, and molecular weight distribution. The microscopic structure of large polymers were studied by IR spectroscopy.

Purifications of butadiene (Bd) and hydrogenated gasoline and the preparation of catalyst and condition of polymerization are as described.[1]

The polymer molecular weight distributions were determined in THF by a Model NJ-762 gel permeation chromatograph. The microscopic structures were determined by IR spectroscopy (Shimadzu model IR-408) following the literature procedure.[3]

1. Solubility of $MoCl_n(OR)_{4-n}$

Various alkyl, cycloalkyl, and benzyl alcohols and phenols with R ranging from C1-10 were chosen to react with $MoCl_4$. The results show that the reaction goes faster with a smaller R. The products from those with an alkyl group of less than four carbons are insoluble in hydrogenated gasoline. The product with isobutyl group has better solubility than that with n-butyl group and those with an alkyl group of more than five carbons have good solubility. When R is cycloalkyl, benzyl, or phenyl, their products dissolve poorly. In the reactions of cyclohexyl alcohol and benzyl alcohol with $MoCl_4$, a small amount of ethyl acetate was added. The solubility and catalytic activity were improved in the former and there was very little difference in the latter.

The results show that temperature also affects the solubility. Higher temperature results in higher solubility. White precipitates appear when dissolving $MoCl_n(OC_{16}H_{33})_{4-n}$ at room temperature which can be redissolved by applying heat.

2. Correlation Between the Catalytic Activity of $MoCl_4(OR)_{4-n}$ and the R Group

Soluble $MoCl_n(OR)_{4-n}$ (abbreviated as Mo) as a main catalyst and $(i\text{-}Bu)_2AlOPh$ (abbreviated as Al) as a co-catalyst were used to catalyze the polymerization of butadiene. The results show that for all R groups, the conversion rate reaches a maximum at a certain Al/Mo value (molar ratio), which varies with R (see Figures 1 and 2).

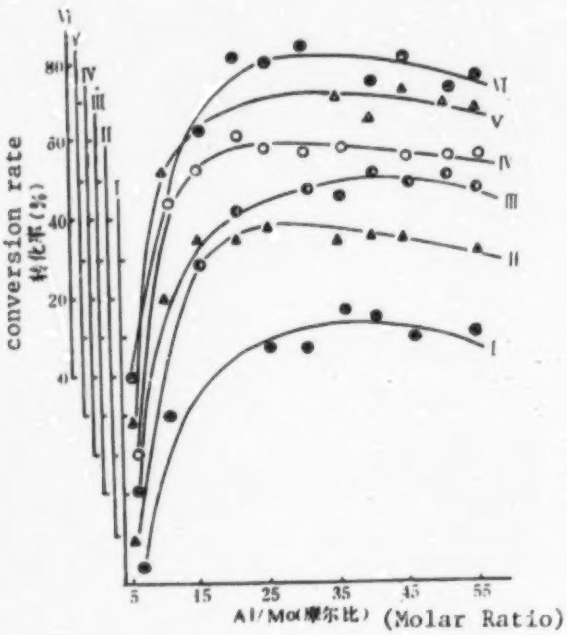

I. $MoCl_n(OC_4H_9)_{4-n}$; II. $MoCl_n(OC_5H_{11})_{4-n}$
III. $MoCl_n(OC_8H_{17})_{4-n}$; IV. $MoCl_n(OC_9H_{19})_{4-n}$
V. $MoCl_n(OC_{10}H_{21})_{4-n}$; VI. $MoCl_n(OC_{16}H_{33})_{4-n}$
ROH/Mo = 8; Mo/Bd = 2.0×10^{-4}; 50°C;
7 小时
hours

Figure 1. Effect of Al/Mo Ratio on Conversion Rate

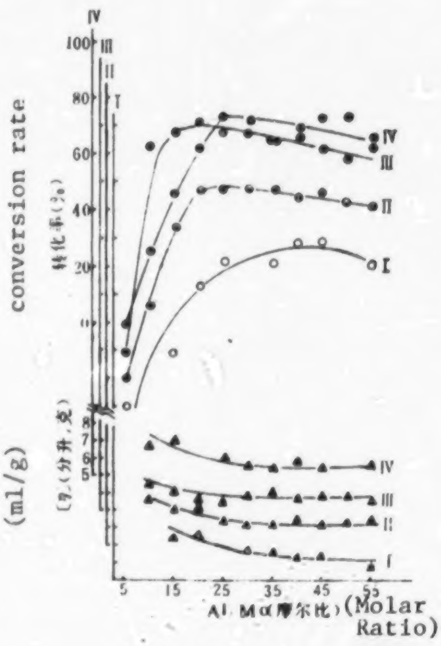

I. $MoCl_n(t\text{-}OC_7H_{15})_{4-n}$;
II. $MoCl_n(S\text{-}OC_5H_{11})_{4-n}$
III. $MoCl_n(i\text{-}OC_5H_{11})_{4-n}$;
IV. $MoCl_n(i\text{-}OC_4H_9)_{4-n}$

Figure 2. Effect of Al/Mo Ratio on Conversion Rate and Inherent Viscosity

It can be seen from Figures 1 and 2 that the catalytic activity of $MoCl_n(t\text{-}OC_7H_{15})_{4-n}$ is lowest and that of $MoCl_n(s\text{-}OC_5H_{11})_{4-n}$ is next to lowest. The $MoCl_n(OR)_{4-n}$ has a level of higher activity when the R is n-alkyl or i-alkyl. Thus, the order of activity is primary > secondary > tertiary alcohol. What is different from the pentavalent Mo system[4] is that i-alkyl R group gives better activity than n-alkyl group does in this system and that whether the carbon number of R group is odd or even has no effect on the solubility and catalytic activity. The conversion rates for all R groups are better than that with the Mo(V) system alone. It takes a smaller amount of Al than Mo(V) to achieve the same conversion rate. The Al/Mo value range that is appropriate for this system is broad.

The R group has little effect on the polymer mean molecular weight and molecular weight distribution (see Figures 2 and 3 and Table 1).

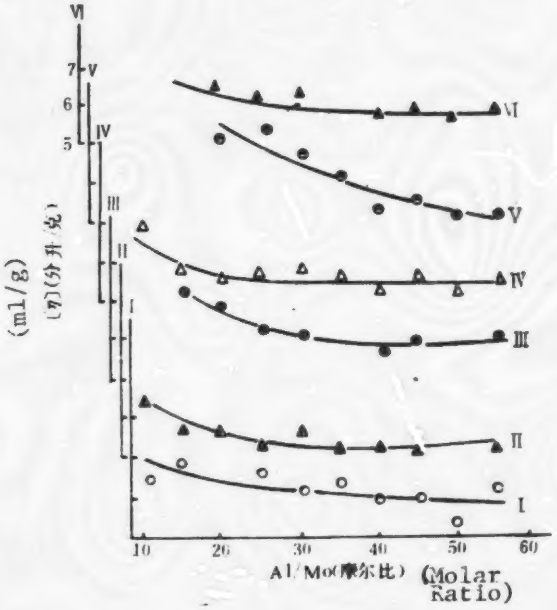

Figure 3. Effect of Al/Mo Ratio on Inherent Viscosity

R Group	Al/Mo* (Molar Ratio)	$\overline{M}_w \times 10^{-4}$	$\overline{M}_n \times 10^{-4}$	$\overline{M}_w/\overline{M}_n$
n-C_4H_9	35	1.83	5.9	3.09
i-C_4H_9	25	1.86	6.9	2.69
n-C_5H_{11}	30	1.81	4.7	3.81
i-C_5H_{11}	20	1.57	5.3	2.97
t-C_7H_{15}	40	1.94	6.9	2.79
n-C_8H_{17}	50	1.75	5.7	3.10
n-C_9H_{19}	20	1.48	4.6	3.19
n-$C_{10}H_{21}$	45	1.69	6.2	2.69
n-$C_{16}H_{33}$	30	1.86	6.4	2.94

* The Al/Mo value for maximum conversion; Mo/Bd = 2.0×10^{-4}

Table 1. Effect of R Group on Molecular Weight Distribution

It can be seen from Figures 2 and 3 that Al/Mo also has little effect on the polymer mean molecular weight. The [η] decreases slightly with an increase in the Al/Mo value when the latter is small. After the Al/Mo value reaches 30, [η] is basically constant. This suggests that there is less chain transfer toward Al in this system.

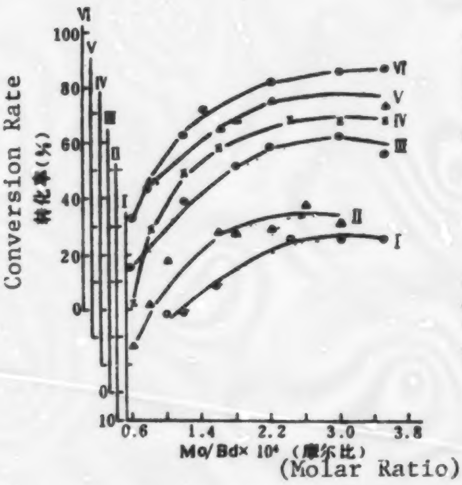

Al/Bd = 4.0×10^{-3}
(see Figure 1 for details.)

Figure 4. Effect of Mo Dosage on Catalytic Activity

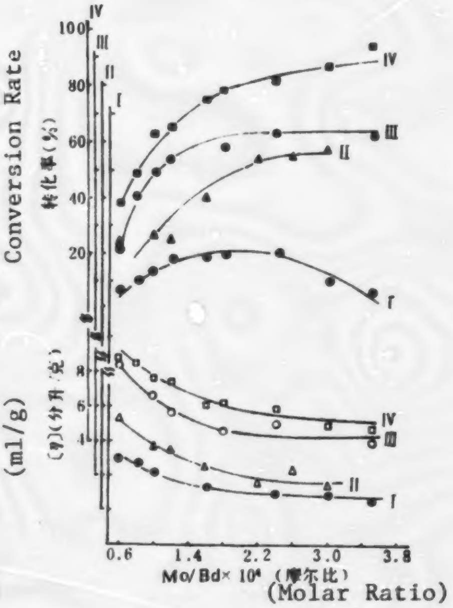

(see Figure 2 for details.)

Figure 5. Effect of Mo Dosage on Conversion Rate and Inherent Viscosity

3. Dosage and Catalytic Activity of $MoCl_n(OR)_{4-n}$

It can be seen from Figure 4 that the conversion rate increases with an increasing Mo dosage regardless of the R group. When R are n-alkyls, the conversion rates all reach over 80 percent at the Mo/Bd ratio of 2.0×10^{-4} (molar ratio). The catalytic activity increases slightly with the increasing R group.

Figure 5 shows the catalytic activities of several catalysts with the branched R group. It can be seen that the catalytic activities of primary, secondary, and tertiary alcohol-substituted $MoCl_n(OR)_{4-n}$ are different. This is consistent with the results in Figures 1 and 2.

The Mo dosage has a greater effect on molecular weight. [η] decreases with the increasing Mo/Bd (see Figures 5 and 6). When R is n-alkyl, [η] value is slightly smaller.

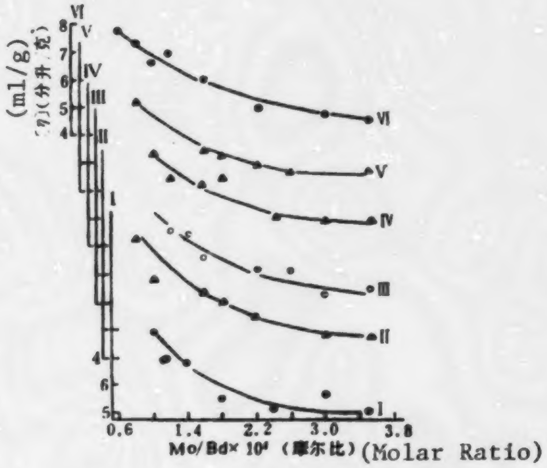

(See Figure 1 for details.)

Figure 6. Effect of Mo Dosage on Inherent Viscosity

4. Microscopic Structures of the Polymers

The microscopic structures of the polymers with different R groups are listed in Table 2. It can be seen that changes in the R group have little effect on the microscopic structure. There are almost no 1,4-trans linkage and about 10 percent of 1,4-cis linkages. The content of the 1,2-linkage is constant, over 80 percent.

R Group	Al/Mo* (Molar Ratio)	Microscopic structure (%)		
		trans 1,4-	1,2-	cis 1,4-
n-C_4H_9	35	0	91	9
i-C_4H_9	25	0	89	11
n-C_5H_{11}	30	0	88	12
i-C_5H_{11}	20	1	82	17
s-C_5H_{11}	25	1	88	11
t-C_7H_{15}	40	0	91	9
n-C_8H_{17}	50	0	90	10
n-C_9H_{19}	20	0	93	7
n-$C_{10}H_{21}$	45	0	91	9
n-$C_{16}H_{33}$	30	1	90	9

* The Al/Mo ratio for maximum conversion.

Table 2. Effect of R group on Microscopic Structure

FOOTNOTES

1. Xu Ling, Yan Chunzhen [7051 2504 3791], and Tang Xueming, HECHENG XIANGJIAO GONGYE [SYNTHETIC RUBBER INDUSTRY], 1985, 1, 21.

2. Yan Chunzhen and Tang Xueming, "The Collected Papers of Changchun Institute of Applied Chemistry," Chinese Academy of Sciences, 1982, 2, 56.

3. Zeng Huanting [2582 3562 1656], HECHENG XIANGJIAO GONGYE [SYNTHETIC RUBBER INDUSTRY], 1978, 2, 56.

4. Ni Shaoru [0242 1421 0320] and Tang Xueming, HECHENG XIANGJIAO GONGYE [SYNTHETIC RUBBER INDUSTRY], 1982, 5, 444.

12922/7358
CSO: 4008/1099

LIFE SCIENCES

DDC-ENHANCED KILLING EFFECT OF HPD-LASER ON TUMOR CELLS

Shanghai ZIRAN ZAZHI [NATURE JOURNAL] in Chinese Vol 9, No 5, May 86 pp 395-396

[Article by Mo Jian [5459 4675], Wang Duoning [3769 1122 1337], Sun Shufen [1327 3219 5358], Li Aiqun [2621 1947 5028], Luo Wenbo [7482 2429 0590], Guo Youchi [6753 0645 3069], and Liu Yaohua [0491 1031 5478], PLA Fourth Military Medical College; paper received 20 May 1985]

[Text] The treatment of tumors by the combination of hematoporphyrine derivative (HPD) and a laser has shown promising clinical results. Its mechanism may involve damaging the cancer cells by reactive oxygen ($^1O_2$) and lipid peroxidation. We suggested that its therapeutic effect could be raised if the cancer cells' ability to withstand the damage of reactive oxygen species and lipid peroxidation is reduced.[1, 2] DDC (sodium diethylaminodithiocarboxylate) inhibits the activity of superoxide dismutase and glutathione peroxidase,[3] which in turn reduces the ability of cancer cells to withstand the damage caused by reactive oxygen species and lipid peroxidation. Therefore, we carried out the DDC-HPD-laser experiments on cancer cells. Five different experiments were done in 3.5-cm (inner diameter) weighing bottles. Each contained $2x10^6$ Ascites tumor cells, 1 ml of 10 percent calf serum-RPMI 1640 medium (pH 7.4), and other ingredients (see Table 1). The concentration of DDC was $1.5x10^{-2}$M when present. There were kept at 37°C immediately after the DDC addition. HPD, 10 ul of a 5-mg/ml solution (manufactured by the Beijing Institute of the Pharmaceutical Industry), was added 4.5 hours later. Laser irradiation was then carried out 1.5 hours after the addition of HPD. The laser output power is 7mW (He-Ne laser model ZN-450, Xingping Radio Factory). Samples were placed 86.5 cm from the source and the laser light was dispersed into a spot of 3.8 cm in diameter. The irradiation time was 10 minutes. The viable cells, determined by their exclusion of Trypan Blue, were counted 1, 3, and 5 hours after irradiation. Each experiment was repeated 12 times and the results were shown in Table 1.

It can be seen from the cell counts after 5 hours that the HPD-laser combination has an obvious killing effect on cancer cells, the cell death rate being raised from 6.7 to 31.2 percent. DDC shows a clear enhancement of the effect and further raises the death rate from 31.2 to 100 percent ($P < 0.01$). The results of cell counts after 3 hours are as follows: in experiment 1, where DDC, HPD, and a laser were used together, the death rate of cancer cell reached 92.9 percent; in experiments 2, 3, and 4, when DDC, HPD, or a laser was omitted, the death rates were below 30 percent and the sum of any two of them was still far lower than that of experiment 1. This shows that DDC, HPD, and a laser contribute synergistically to the killing of cancer cells.

Experiment No.	Death percentage ($\bar{X}$±SD)		
	1hr	3 hr	5hr .
Ⅰ. **DDC+HPD+**Laser	89.1± 9.8	92.9± 5.2	100± 0
Ⅱ. **HPD+** Laser	10.6± 7.1	15.9± 15.8	31.2± 9.3
Ⅲ. **DDC+** Laser	25.1± 10.6	25.2± 21.2	
Ⅳ. **DDC+HPD**	21.3± 11.6	28.2± 16.7	
V. Control	6.5± 4.4	5.8± 6.9	6.7± 4.8

Table 1. Killing Effect of HPD-laser on Cancer Cells and Enhancement by DDC

Use of the DDC-HPD-laser approach to treat tumors in animal is currently underway. Preliminary results show that DDC also enhanced the therapeutic effect of HPD-laser under certain conditions.

FOOTNOTES

1. Mo, Jian, "Progresses in Biochemistry and Biophysics," 5, (1984) 11.

2. Nathan, C.F., FED. PROC., 41 (1981) 2206.

3. Smith, M.J., et al., BIOCHEM. PHARMACOL., 31 (1982) 19.

12922/7358
CSO: 4008/1084

EVOLUTION SITES IN RIBOSOMAL 5S RNA STRUCTURE

Shanghai ZIRAN ZAZHI [NATURE JOURNAL] in Chinese Vol 9, No 5, May 86 pp 396-397

[Article by Qi Guorong [4359 0948 2837], Cao Gongjie [2580 0501 2638], Jiang Peng [3068 7720], Feng Xiaoli [7458 2556 7812], and Gu Xiangrong [6581 4382 2837], Shanghai Biological Chemistry Institute, Chinese Academy of Sciences; paper received 18 October 1985]

[Text] The earliest studies of evolution and developmental biology at the molecular level were done on protein molecules such as hemoglobin and cytochrome C. In recent years, there is a widespread use of small pieces of nucleic acid to study the evolution of molecules. 5S rRNA exists in all forms of life and is the direct product of gene expression. Its biological functions do not vary among species. Thanks to the revolutionary breakthrough in DNA sequence analysis methodologies and the fact that 5S rRNA does not contain modified bases, the primary structure of over 250 5S rRNA's has been determined by 1984.[1] This makes it even more appropriate to study biological evolution through the structure of 5S rRNA. Osawa and Hori have established a molecular evolution tree model for 5S rRNA[2] through comparisons of the base compositions of various 5S rRNA's. But they have not examined the correlation between base change in each position of the 5S rRNA and evolution.

Since 1979, we have determined the primary structure of six 5S rRNA's from different sources, including the highest invertebrate lancelet (branchiostoma belcheri, subphylum cephalochordata), the lowest vertebrate lamprey (lampetra reissneri, subphylum vertebrata, class cyclostomata), three kinds of silkworm (castor silkworm,[3] tussah, and hybride), and cottonseed.[4] We compared our results with the published sequences of eucaryotic 5S rRNA's[1] and observed some significant phenomena. Comparisons were made at the secondary structure level. Using the generally accepted secondary structure model of De Wachter, et al.,[5] we examined the structural features of over 170 eucaryotic 5S rRNA's and made the graphic presentations of their structures. As shown in Figure 1, there are four kinds of sites in the structure: (1) conserved, (2) semi-conserved, (3) random mutation, and (4) evolution. We find that these evolution sites within the 5S rRNA structure are closely related to biological evolution. This discovery provides further insight into the study of molecular evolution. Take, for example, the animal kingdom. In the evolution of species, there are sequential changes in these evolution sites. Some of them occur at the early stage of the evolution and others later. Once the change takes place, it is conserved throughout the subsequent evolutions (Table 1). If more sequences of 5S rRNA are determined, particularly those of the species that occupy unique places in the evolution, the results in the table can be expected to be improved and the classification of these sites further refined. Though we do not understand the cause and biological significance of these "ordered" changes, at least the phenomenon can be used as a marker, i.e., the classification of a species and its place in the evolution can be determined from the primary structure of its 5S rRNA by following the rules of evolution site we proposed.

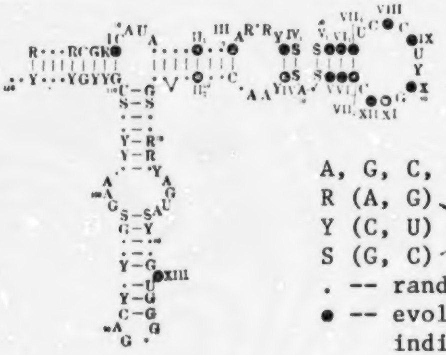

A, G, C, U -- conserved sites
R (A, G)
Y (C, U) --- semi-conserved sites
S (G, C)
. -- random mutation sites
● -- evolution sites (Roman numerals indicate site numbers)

Figure 1. Structural Features of Eucaryotic 5S rRNA's

		Evolution site #	I	II	III	VI₁-VI₂	VII	VIII	XI	IX	V₁-V₂	II₁-II₂	IV₁-IV₂	X
		Base position #	9	42	21	31—46	35	83	43	37	30—47	18—60	27—52	40
Protozoa			C	C A	U,A G	C-G G-C	C	G	A U	A G	G-C	G-C	A-U	C
Parazoa			C	A	G	G-C	U	C	C	A	C-G	G-C	A-U	C
Metazoa		Other vertebrates (porifera→ Echinoderms)	C	A	G	G-C	U	A	U	G	G-C	G-C	A-U	C
	Protochordate	Hemichordate	C	A	G	G-C	U	A	U	G	G-C	G-C	A-U	C
		Tunicate	C	A	G	G-C	U	A	U	G	C-G	A-U	A-U	C
		Cephalochordate	C	A	G	G-C	U	A	U	G	C-G	G-C	A-U	C
	Vertebrate	Class cyclostomata	C	A	G	G-C	U	A	U	G	C-G	C-G	G-C	C
		Class Osteichthyes	C	A	G	G-C	U	A	U	G	C-G	C-G	G-C	C U
		Class Amphibia→Class Maxmalia	C	A	G	G-C	U	A	U	G	C-G	C-G	G-C	U

Table 1. Evolution Sites in Animal 5S rRNAs

* Only those occurring over 90 percent of the time are included.

FOOTNOTES

1. Erdmann, V.A., et al., NUCL. ACIDS RES., 13 (1985), suppl. r105.

2. Osawa, S., and Hori, H., "Ribosomes--Structure, Function, and Genetics," Chambliss, G., et al., eds., University Park Press, Baltimore (1980) p 333.

3. Cao, Gongjie, et al., SHENGWU HUAXUE YU SHENGWU WULI XUEBAO [JOURNAL OF BIOCHEMISTRY AND BIOPHYSICS], 15, 5 (1983) p 406.

4. Qi, Guorong, et al., ZHONGSHAN DAXUE XUE BAO (ZIRAN KEXUE BAN) [JOURNAL OF ZHONGSHAN UNIVERSITY (NATURAL SCIENCES EDITION)], 2 (1985) p 65.

5. De Wachter, et al., BIOCHEM., 64 (1982) p 311.

12922/7358
CSO: 4008/1084

LIFE SCIENCES

SYNTHESIS OF POLYNUCLEOTIDES BY PNPase STUDIED

Shanghai ZIRAN ZAZHI [NATURE JOURNAL] in Chinese Vol 9, No 5, May 86 p 398

[Article by Wang Qisong [3769 0796 2646] and Shang Jinbao [0794 6855 1405], Shanghai Biochemistry Institute, Chinese Academy of Sciences, and Dai Dingming [2071 1353 2494], Shanghai Chemical Reagents Plant No 2; paper received 26 April 1985]

[Text] The authors have reported the 3'-end phosphorylation of oligonucleotides by polynucleotide phosphatase (PNPase).[1] In this article, the method is applied to the synthesis of polynucleotides. The principle is that nucleoside diphosphate and 7-methyl guanosine diphosphates (^{m7}GDP) are polymerized by PNPase in the presence of a premier. The 7-methyl guanine residues in the polymer are then selectively removed. In this fashion, a limited number of nucleotides can be introduced at the 3'-end of the primer. The number of nucleotides introduced can be controlled by the ratio of nucleoside diphosphates and ^{m7}GDP. For example, we used 120 O.D. (A260) of the trinucleotide CpUpC as a primer and reacted them with 16 mg of GDP and 8 mg of ^{m7}GDP in the presence of PNPase. The ^{m7}G residues in the polymer were then selectively removed.[1] The resulting products CpUpCpGp, CpUpCpGpGp, and CpUpCpGpGpGp were separated by DEAE-Sephadex A25 column chromatography. The chromatogram is shown in Figure 1. Peaks III, V, VII, and VIII are homogeneous with both solvent systems I and II. Peak III is identified as CpUpCp and peak V CpUpCpGp by comparison with the standards. Peaks VII and VIII are identified as CpUpCpGpGp and CpUpCpGpGpGp, respectively, by spectral measurement and base composition determination after calf pancreatic ribonuclease digest. Peaks IV and VI are heterogeneous. Their spectra show the peaks of guanylic acid and are possibly the oligo(G)'s from the hydrolysis of the polymer CpUpCp(Gp)n-(^{m7}Gp)m. Such data as the spectral radio, Rf value, base composition, and yields for peaks III, V, and VII are listed in Table 1.

When the ratio was changed to GDP:^{m7}GDP = 3:1, the result was the increased yield of longer chains CpUpCp(Gp)n(n >4.5) while the yields of CpUpCp and CpUpCpGp were lowered. When using $^{m'}$IpΨ and Cp$^{m'}$Ψ as a primer to copolymerize with a certain ratio of GDP and ^{m7}GDP, results similar to the chromatogram shown in Figure 1 were obtained, suggesting the general applicability of the method. This method is particularly suitable for synthesizing those oligonucleotides with stretches of a particular base, a common occurrence in mRNA, 5S rRNA, and tRNA.

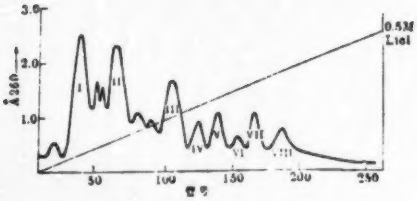

Figure 1. Column Chromatography Profile of CpUpCp(Gp)n

Column: DEAE-Sephadex A25 HCO_3 type (1x30 cm).
Initial eluant: 0.02M Tris·HCl (pH 7.2), 7M urea.
Final gredient: 0.02M Tris·HCl (pH 7.2), 7M urea, 0.5M LiCl.
Flow rate: 5 ml/15 min; 5 ml/tube.

a 样品	光谱比值 b A250/A260		光谱比值 b A280/A260		R_f 值		d 碱基组成	产率 e (%)
	pH2	pH7	pH2	pH7	溶剂I c	溶剂II c	U_p:C_p:G_p	
峰III	0.66	0.90	1.09	0.69	0.97*	0.94*	1.0:2.1 :0	~30
f 峰V	0.77	1.03	0.91	0.70	0.97**	0.99**	1.0:2.07:1.02	13~16
峰VII	0.84	1.02	0.89	0.70	0.50*	0.09*	1.0:1.98:2.1	~9
峰VIII	0.93	1.01	0.85	0.71	0.22*	0.05*	1.0:2.05:2.9	~5

Key:
a. sample
b. spectral ratio
c. solvent system
d. base composition
e. yield
f. peak

Table 1. Spectral Ratio, Rf Value, Base Composition and Yield of Samples

* The Rf of the standard CpUpCp = 1.
** The Rf of the standard CpUpCpGp = 1.
Solvent I: 95% ethanol : 1 M ammonium acetate = 6 : 5 (v/v)
Solvent II: 2-butanoic acid : 1M ammonium hydroxide : 0.1M EDTA = 100 : 60 : 0.6 (v/v).

FOOTNOTES

1. Wang, Qisong, SHENGWU HUAXUE YU SHENGWU WULI XUEBAO [JOURNAL OF BIOCHEMISTRY AND BIOPHYSICS], 11, 3 (1979) p 207.

12922/7358
CSO: 4008/1084

INVESTIGATION OF STIMULATED BRILLOUIN SCATTERING SPECTRA IN LASER-PLASMA INTERACTIONS

Shanghai ZHONGGUO JIGUANG [CHINESE JOURNAL OF LASERS] in Chinese Vol 13 No 8, 20 Aug 86 pp 449-456, 461

[English abstract of article by Tang Yonghong [0781 3057 4767] and Xu Zhizhan [1776 5267 1455] of Shanghai Institute of Optics and Fine Mechanics, Chinese Academy of Sciences]

[Text] Equations describing Brillouin backscattering are obtained in one-dimensional inhomogeneous plasma. Based on the equations, the scattering spectra are calculated both for linear and nonlinear multimode instability. For a thermal noise source, the spectral shape is dependent on the ion-acoustic wave damping, the plasma inhomogeneity and the incident light depletion. The resultant spectra, including these effects, are in agreement with experimental observations.

LASER PULSE COMPRESSION AND AMPLIFICATION BY STIMULATED BRILLOUIN SCATTERING

Shanghai ZHONGGUO JIGUANG [CHINESE JOURNAL OF LASERS] in Chinese Vol 13 No 8, 20 Aug 86 pp 457-461

[English abstract of article by Yang Jingguo [2799 4842 0948], et al., of the Department of Physics, Sichuan University]

[Text] A 30 ns ruby laser pulse is compressed to about 6 ns with acetone (C_3H_6O) by SBS. The Stokes pulse is then amplified again in a laser amplifier, with the energy gain being greater than 5 and the total power gain about 60. The characteristics and applications of the technique are discussed.

TUNABLE LASER SOURCE AT WAVELENGTH DOWN TO 218.3 NM

Shanghai ZHONGGUO JIGUANG [CHINESE JOURNAL OF LASERS] in Chinese Vol 13 No 8, 20 Aug 86 pp 466-469

[English abstract of article by Yang Xiangchun [2799 7449 2504] and Zhang Xinnan [1728 2450 8189], et al., of Shanghai Institute of Optics and Fine Mechanics, Chinese Academy of Sciences]

[Text] Calculation results of frequency doubling and frequency summing phase matching parameters for different wavelengths using KDP-type crystals are given. Experimental verification has been performed, nad a tunable wavelength down to 218.3 nm has been obtained.

SECOND HARMONIC GENERATION WITH UREA CRYSTAL BY Ar$^+$ LASER LIGHT

Shanghai ZHONGGUO JIGUANG [CHINESE JOURNAL OF LASERS] in Chinese Vol 13 No 8, 20 Aug 86 pp 478-481

[English abstract of article by Zeng Yongjian [2582 3057 0256], et al., of Shanghai Institute of Laser Technology; Su Genbuo [5685 2704 0590], et al., of Fujian Institute of Material Structure]

[Text] Characteristics of the second harmonic generation at three lines, 514.5, 496.5 and 488.0 nm, with a urea crystal by Ar$^+$ laser light is reported in detail for the first time. The phase mismatch at the azimuthal angle due to the thermal effect has been found. The dependence of frequency-doubling efficiency upon other parameters is given.

OUTPUT AND MEASUREMENT OF RADIATION IN FREE-ELECTRON LASER BASED ON STIMULATED RAMAN SCATTERING

Shanghai ZHONGGUO JIGUANG [CHINESE JOURNAL OF LASERS] in Chinese Vol 13 No 8, 20 Aug 86 pp 482-484, 481

[English abstract of article by Chu Cheng [5969 2052], et al., of Shanghai Institute of Optics and Fine Mechanics, Chinese Academy of Sciences]

[Text] The authors have succeeded in obtaining laser action in a free-electron laser based on stimulated Raman scattering. This paper presents a brief account of the output and measurement of the free-electron laser radiation in the Ka band. The design method of the drift tube, emitting and receiving horns and filters are summarized together with radiation measurement results.

LASER HETERODYNE BIAS FREQUENCY-LOCKING FOR COHERENT OPTICAL COMMUNICATION

Shanghai ZHONGGUO JIGUANG [CHINESE JOURNAL OF LASERS] in Chinese Vol 13 No 8, 20 Aug 86 pp 489-492

[English abstract of article by Liao Shiqiang [1675 0013 1730], et al., of Shanghai Institute of Optics and Fine Mechanics, Chinese Academy of Sciences]

[Text] A new frequency modulation system for lasers by heterodyne bias frequency-locking is proposed and developed. The technique can be used in heterodyne or coherent single mode optical communication. Experiments on the grating-tuned CO_2 laser system and Zeeman He-Ne laser system are described. A radio broadcast has been relayed successfully in the locked system. The conditions for practical optical fiber communication with a semiconductor laser and the heterodyne bias frequency-locked system are discussed.

9717
CSO: 4009/112

NOVEL DEFECT IN LEC In-DOPED GaAs SINGLE CRYSTALS

Beijing BANDAOTI XUEBAO [CHINESE JOURNAL OF SEMICONDUCTORS] in Chinese Vol 7 No 4, Jul 86 pp 341-345

[English abstract of article by He Hui [0149 2547], et al., of the Institute of Semiconductors, Chinese Academy of Sciences]

[Text] A novel defect has been found in LEC In-doped GaAs single crystals. It is a rectangular area in which longer edges are parallel to one of two <110> directions and have a high density of dislocations. Its In content is higher than that of the matrix. Its crystallographic and chemical properties have been studied by SEM-CL, EPMA, CTEM, HREM and XRT techniques. A possible explanation for its origin is suggested, i.e., the formation of this defect is related to the cellular growth under composition supercooling, and it is inherent in continuous solid solution systems, such as $In_xGa_{1-x}As$. (Paper received 5 September 1985.)

REFERENCES

[1] Masamichi Ohmori, "Gallium Arsenide Integrated Circuits", 11th Int. Symp. on GaAs and Related Compounds, Biarritz, 1984.
[2] M. Duseaux and S. Martin. "Growth and Characterization of Large Dislocation-Free GaAs Crystals for Integrated Circuits Appilations", 3rd Conf. on Semi-Insulating III-V Materials, pp. 118—125 (1984).
[3] H. M. Hobgood, *et al.*, "Large Diameter, Low Dislocation In-Doped GaAs: Growth, Characterization and Implications for FET Fabrication", *ibid.*, pp. 149—156 (1984).
[4] 林兰英等,"低位错密度的 LEC-SI-GaAs 单晶", 砷化镓及有关化合物会议, 峨眉, 1985.
[5] 闵乃本, "晶体生长的物理基础", 第五章第二节 (1982).

LOW DOSE B^+ AND P^+ IMPLANTATION ASSOCIATED DEFECTS IN n-Si AND THEIR ANNEALING BEHAVIORS

Beijing BANDAOTI XUEBAO [CHINESE JOURNAL OF SEMICONDUCTORS] in Chinese
Vol 7 No 4, Jul 86 pp 363-373

[English abstract of article by Chen Jianxin [7115 1696 2450], et al., of the Graduate School, University of Science and Technology of China]

[Text] Detailed information of hole (H) as well as electron (E) traps produced by low dose (10^{11} cm^{-2}) B^+ and P^+ ion implantation in n-Si and their annealing behavior is reported. The hole traps are investigated for the first time. For B^+ implantation, five hole traps are produced: two B related acceptor levels, $H_2(0.62)$, $H_3(0.49)$, of huge concentrations, and three other hole traps, $H_4(0.37)$, $H_1(0.63)$, $H_5(0.15)$. H_4 is probably a C related acceptor. For P^+ implantation, four hole traps are produced: H_2'' (0.15) of huge concentration, and $H_4(0.37)$, $H_1(0.63)$, H_5''. Electron traps are also reported. For B^+ implantation, seven electron traps are produced: B related acceptor $E_3(0.35)$ with huge concentration at 280°C annealing temperature (AT), E_6, E_7 with small concentrations and shallow levels which are hard to test precisely, but they anneal out drastically above 320°C. The other three E traps, $E_2(0.41)$, $E_4(0.25)$ and $E_5(0.15)$, are detected in both B^+ and P^+ implantation, and are consistent with previous reports for ion, neutron and electron irradiation induced defects of V_{2-} (P.V), $V_{2-}{}^{6}$, and (O.V) centers respectively. Another low concentration, $E_1(0.45)$, is also detected for B^+ implantation. Annealing behavior of E and H traps are reported. At 800° AT, all traps diminish to average concentrations of less than 10^{12} cm^{-3}. (Paper received 9 May 1985.)

REFERENCES

[1] 北京师范大学："离子注入原理与技术"，北京出版社，1982.
[2] 罗晋生："离子注入物理"，国防工业出版社，1980.
[3] L. C. Kimerling and J. M. Poate: Defect and Radiation effects In semiconductors, 1974 (Inst. Phys. Conf. Ser. no. 23. London, 1975) p. 126.
[4] K. Masuda, Radiation effects In Semiconductors. 1976. Ed. N. B. Urli and J. W. Corbett (Inst. Phys. Conf Ser. no. 31. London, 1977) p. 174.
[5] J. R. Troxell, *Solid State Electronics*, 26, 539(1983).
[6] J. W. Corbett and J. C. Bourgoin, Point Defects in Solids, Vol. 2, Ed, J. H. Crawford Jr and L. M. Slifkin (Plenum, New York, 1975) p. 1.
[7] J. W. Corbett *et al.*, Radiation effects in semiconductors 1976, Ed. n. b. urli and J. W. Corbett, (Inst. Phys. Conf. Ser. no. 31, London, 1977) p. 174.
[8] W. M. Penney, L. Lau, Mos integrated circuits, (Van Nostrand, New York, 1972).
[9] G. G. Qin (秦国刚). M. F. Li (李名复) and C. T. Sah. *J. Appl. Phys.*, 53, 4800(1982).
[10] D. V. Lang, *J. Appl. Phys.*, 45, 3023(1974).
[11] A. Wang and C. T. Sah, *J. Appl. Phys.*, 56, 1021(1984).
[12] S. M. Sze. Physics of semiconductor de vices, (Wiley, New York, 1969)
[13] O. Engstrom and A. Alm, *Solid State Electronics*, 21, 1571(1978).
J. E. Lowther, *J. Phys. C. Solid State Phys.*, 13, 3681(1980).
秦国刚，姚秀琛，中国科学，A(1984) No.5, 432
[14] J. M. Meese, Defects in Semiconductors, Ed.J. Naravan and T. Y. Tan. (North Holland, New York, 1981), p. 225.
[15] 杜永昌、张玉峰、秦国刚，半导体学报，5, 7(1984),
[16] L. C. Kimerling, Radiation effects in Semiconductors. 1976, Ed. N. B. Urli and J. W. Corbett, (Inst. Phys. Conf. Ser. No. 31. London, 1977) p. 221.

[17] K. L. Wang, *Appl. Phys. Lett.*, 36, 48(1980).
[18] 张玉峰，张丽珠，吴书祥，杜永昌、半导体学报 3，251(1982).
[19] G. D. Watkins and J. W. Corbett, *Phys. Rev.*, 121, 1001(1961).
[20] J. W. Walker and C. T. Sah, *Phys. Rev.*, 7, 4587(1973).
[21] G. D. Watkins and J. W. Corbett, *Phys. Rev.*, 134, A1359(1964).
[22] J. Krynicki and J. C. Bourgoin, Defects and Radiation effects in Semiconductors, 1978 (Inst of Phys. Conf. Ser. No. 46. London, 1979), p. 482.
[23] P. M. Mooney et al., *Phys. Rev.*, B15, 3836(1977).
[24] A. Mitic, T. Sato, M. Nishi and H. Hashimoto, *Appl. Phys. Lett.*, 37, 1727(1980).
[25] D. B. Jackson and C. T. Sah, J. Appl. Phys., 58, 1270(1985).
[26] D. B. Jackson and C. T. Sah, J. Appl. Phys., 59, 459(1986).

CALCULATIONS OF COMPOSITIONAL VARIATIONS OF ENERGY GAPS FOR ALLOYS BY CPA METHOD USING LCAO

Beijing BANDAOTI XUEBAO [CHINESE JOURNAL OF SEMICONDUCTORS] in Chinese
Vol 7 No 4, Jul 86 pp 380-386

[English abstract of article by Lu Fen [7120 1164] of the Modern Physics Institute, Fudan University]

[Text] Compositional variations of energy gaps for A_xB_{1-x}-type alloys, such as $GaAs_xP_{1-x}$, are calculated by the coherent-potential approximation method based on a tight-binding approximation using LCAO. Zero-order approximation is taken from the virtual-crystal approximation. The results obtained for $GaAs_xP_{1-x}$ agree well with the experimental results and the theoretical results from Chen and Sher. It is possible that the method can be used for studying other A_xB_{1-x}-type alloys. In addition, the energy bands and densities of state can also be calculated by this method. (Paper received 14 May 1985.)

REFERENCES

[1] Chen A. B. and Sher A., *Phys. Rev. Letters*, 40, 902(1978).
[2] Chen A. B. and Sher A., *Phys. Rev.*, B17, 4726(1978).
[3] Chen A. B. and Sher A., *Phys. Rev.*, B23, 5360(1981).
[4] Mariette H., Chevallior J. and Leroux-Hugon P., *Phys. Rev.*, B21, 5706(1980).
[5] Bugajski M. and Kontkiewicz A. M. and Mariette H., *Phys. Rev.*, B28, 7108(1983).
[6] Ehrenreich H. and Hass K. C., *J. Vac. Sci. Technol.*, 21, 133(1982).
[7] Chen A. B. and Sher A., *J. Vac. Sci. Technol.*, 21, 138(1982).
[8] Slater J. C. and Koster G. F., *Phys. Rev.*, 94, 1498(1954).
[9] Economou E. N., Green's Function in Quantum Physics, Spring-Verlag Berlin Heidelberg New York 1979.
[10] Yuan Li and Lin-Chung P. J. 未发表
[11] Ley L., Pollak R. A., Mcfeely F. R., Kowalczyk S. P. and Shirley D. A., *Phys. Rev.*, B9, 600 (1974).
[12] Eastman D. E., Grobman W. D., Freeouf J. L. and Erbudak M., *Phys. Rev.*, B9, 3473(1974).
[13] Thompson A. G. and Woolley J. C., *Phys. Rev.*, 146, 601(1966).

PLACEMENT SUBSYSTEM OF THE LSIS-II LAYOUT AUTOMATED SYSTEM

Beijing BANDAOTI XUEBAO [CHINESE JOURNAL OF SEMICONDUCTORS] in Chinese
Vol 7 No 4, Jul 86 pp 412-418

[English abstract of article by Cheng Kexing [4453 0668 5887], et al., of the Institute of Semiconductors, Chinese Academy of Sciences]

[Text] The modular placement subsystem for a standard cell with a macrocell is presented. The design can be in the batch or interactive way. In order to regulate the process of the placement, every module is reenterable. As macrocells are introduced, the layout of the circuit with RAM, ROM, PLA and gate matrix will be feasible, and the hierarchical design will be realized. The multiple objective function and multilevel iterative method are adopted in improvement placement. (Paper received 16 April 1985.)

REFERENCES

[1] 程可行，庄文君，半导体学报 5，422(1984).
[2] G. Persky, D. N. Deutsch and D. G. Schweikert, 13th D. A. Conf., pp399—407 (1976).
[3] S. Horiguchi, et al., IEEE Int. Solid-State Circuits Conf., 54(1982).
[4] B. T. Preas and C. W. Gwyn, 15th D. A. Conf., pp. 206—212 (1978)
[5] G. Persky et al., 18th D. A. Conf., pp. 22—29 (1981).
[6] H. Beke and W. Sanser, 16th D. A. Conf., pp. 102—108 (1979).
[7] 庄文君，计算机学报 7，217(1984).
[8] 庄文君，李玉兴，LSI/VLSI 布图设计自动化，上海交通大学出版社(将出版).

APPLICATION OF B SPLINE FUNCTION DEVICE INTERPOLATION MODELING IN CIRCUIT SIMULATION PROGRAM SPICE

Beijing BANDAOTI XUEBAO [CHINESE JOURNAL OF SEMICONDUCTORS] in Chinese
Vol 7 No 4, Jul 86 pp 419-426

[English abstract of article by Yan Zhixin [0917 1807 2450] of the Department of Physics, Shanghai University of Science and Technology; Wang Bijuan [3769 4310 1227], et al., of Shanghai Institute of Metallurgy, Chinese Academy of Sciences]

[Text] A new device interpolation modeling is added to SPICE (simulation program with integrated circuit emphasis) circuit simulation program by introducing into it a one to three-dimensional second-order B spline function. Therefore, the device simulation function in SPICE is extended and the circuit simulation accuracy in SPICE is enhanced. The characteristic simulation results of the tunnel diode oscillator and the 3 μm E/E NMOS circuit when using this modified SPICE program demonstrate the above-mentioned superiority of this new device modeling. Shanghai Computing Institute's IBM 370/148 was used in this work. (Paper received 29 April 1985.)

REFERENCES

[1] A. Vladimirescu and S. Liu, ERL Memo No. ERL M80/7, Electronics Research Laboratory, Univ. of California, Berkeley, Feb. 1980.
[2] [美]阿・弗拉吉米列斯科等，"SPICE 通用电路模拟程序用户指南",清华大学出版社(1983).
[3] 严志新,半导体学报，6,113(1985).
[4] L. W. Nagel, ERL Memo No. ERL-M520, Electronics Research Laboratory, Univ. of California, Berkeley, May 1975.
[5] A. Vladimirescu, K. H. Zhang *et al.*, SPICE 2G.5 源程序版本附例，Aug. 1981.
[6] 孙家昶,"样条函数与计算几何",科学出版社(1982).
[7] Z. X. Yan and H. C. Lin, Presented at the Joint SIAM, IEEE Conference on Numerical Simulation of VLSI Device, Boston, Nov. 1982.

PHOTOELECTRON SPECTROSCOPY OF OXYGEN ADSORPTION ON a-GaAs(:H) SURFACE

Beijing BANDAOTI XUEBAO [CHINESE JOURNAL OF SEMICONDUCTORS] in Chinese
Vol 7 No 4, Jul 86 pp 433-436

[English abstract of article by Wang Zhaoping [3076 0340 1627] of the Institute of Semiconductors, Chinese Academy of Sciences]

[Text] The photoelectron spectroscopy of a-GaAs(:H) films after being exposed to excited oxygen is presented for the first time. The samples are prepared in situ by d.c. sputtering in a mixture of Ar and H_2. Two oxygen induced structures, a peak at 4.7 eV and a weak structure at 7-9 eV below the valence band maximum, are observed. Comparing these with the results of oxygen adsorption on the crystalline GaAs surface we presume that only dissociated oxygen is adsorbed on the surface of a-GaAs(:H). (Paper received 15 April 1985.)

REFERENCES

[1] W. Ranke and K. Jacobi, *Surf. Sci.*, 81(1979) 504.
[2] W. Ranke, Y. R. Xing and G. D. Shen, *Surf. Sci.*, 122(1982) 256.
[3] P. Pianetta, I. Lindau, P. E. Gregory, C. M. Garner and W. E. Spicer, *Surf. Sci.*, 72(1978), 298.
[4] C. Y. Su, I. Lindau, P. W. Chye, P. R. Skeath and W. E Spicer, *Phys. Rev.*, B25(1982) 4045.
[5] L. Ley, H. Richter, R. Kärcher, R. J. Johnson and J. Reichardt, *J. Physique*, 42(1981) C4-753.
[6] R. Kärcher, Z. P. Wang and L. Ley, J. Non-Gryst. Solids, 59/60(1983), 629.

9717
CSO: 4009/1123

END